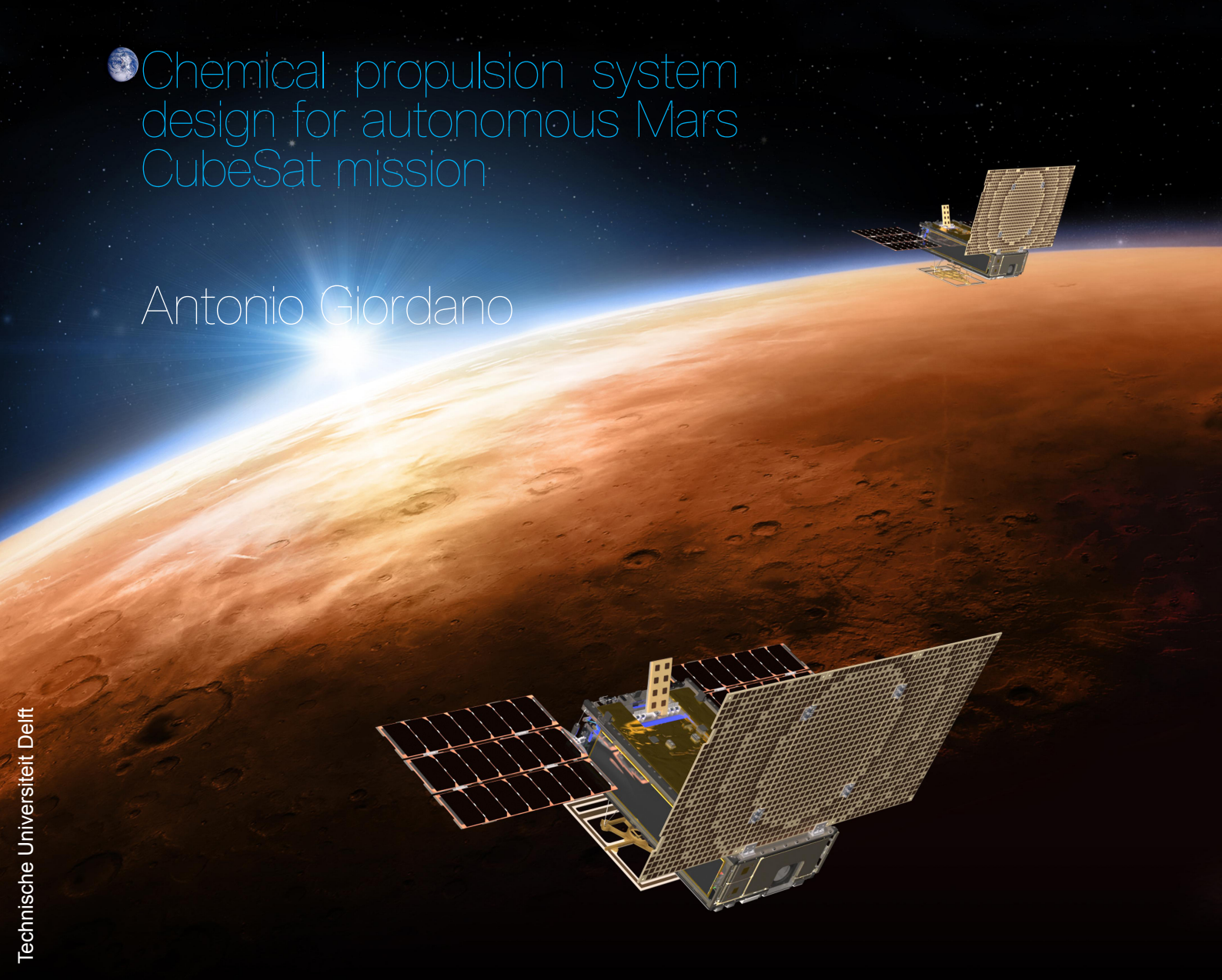


 Chemical propulsion system
design for autonomous Mars
CubeSat mission

Antonio Giordano



Technische Universiteit Delft

Chemical propulsion system design for autonomous Mars CubeSat mission

by

Antonio Giordano

to obtain the degree of Master of Science
in Space Engineering
at the Delft University of Technology,
to be defended publicly on Friday January 28, 2022 at 09:00 AM.

Student number: 4746325

Thesis committee: Dr. A. Cervone, TU Delft - LR-SPE-SSE, supervisor
Dr. B.V.S. Jyoti, TU Delft - LR-SPE-SSE
ir. R. Noomen, TU Delft - LR-SPE-AS

Preface

The research pursued in this thesis work represents the culmination of my studies at TU Delft for the Master of Science in Aerospace Engineering. Even during tough times caused by the COVID pandemic in the past two years, I have been surrounded by professors, colleagues and friends that kept me motivated throughout my studies, allowing me to reach this objective I am proud of.

Thanks to my professor Angelo Cervone for having supported me during the writing of the thesis as the daily supervisor. I have really appreciated the availability and support that I was given throughout these months, whenever I requested, even if the meetings could not take place in person.

This journey wouldn't have been the same without all the friends that have been with me. Friends I met from Milan in the residenza: Giuliano, Lorenzo (thanks for the CAD tips!), Mariateresa and Gabriele. Thanks to old and new friends that were with me while I lived in Delft and Friedrichshafen: Samuele, Benedetto and Isabella. Last but not the least, I need to mention the place in which I have written most of my thesis: thanks to Lucrezia, Francesco, Alessia, Paola and Domenico for being with me during the Erasmus Venafro. I was not expecting to find new friends in the same place I grew up, but I am really grateful to have met all of you. Thanks for all the time spent together, crazy or not, that we have tried to live at our best despite the pandemic.

Thanks to all of my friends from Dynamo Camp: Federica, Serena and Sofia. With you I have kept the good vibes from that magical place throughout these years of studies. It has been a pleasure to meet (almost) all of you during the past summer, and I hope we can finally meet again in the most beautiful place in the world.

Thanks to my sister, my mom and my dad: Maria Assunta, Michela and Giampiero. Since when the COVID pandemic started, I knew that I could always rely on you. Being used to living far from home for many years, I really appreciated the time we could spend together in these past two years. I could not have done it without your support and all of the possibilities that you made available for me. I will always be grateful. In particular, thanks to my parents for all the sacrifices they have made to help me reach this objective, I will never forget them. Thanks to my sister who was able to make this journey funnier everyday: I wish you maintain your enthusiasm through all of the experiences of your life.

Finally, thanks to the person that has been one of the closest to me since the start of my thesis work. The beginning was a difficult period for me and I felt that I was missing something from the life I would have wanted, far away from the country I used to live in. Thank you for being close to me even in the toughest of times, when I wanted to give up, but you were there to support me no matter what. We have spent a lot of good days together in which the distance did not make a difference, visited beautiful cities, and I am grateful to have shared all these moments, the good and the bad ones, together with you. *a Silvia.*

*Antonio Giordano
Delft, January 2022*

Abstract

In recent years, the advent of the so-called "New Space" has opened the perspective of using smaller scale spacecrafts for a broad horizon of space missions, ranging from low-earth-orbit (LEO) to interplanetary ones. The most common standard used throughout the space industry for small satellites is the CubeSat, which can be composed on the several units (U) where to allocate the subsystems, determining its dimension. These platform are mostly to be utilized for LEO missions, but it is envisioned that such small platform could play a game-changing role in the exploration of solar system. For this matter, having a propulsion system scaled to a smaller satellite can increase the manifold of different mission such a small satellite (or a constellation) can achieve.

The Thesis work hereby presented is focused on the analysis and design of a propulsion system that can open the horizons to a new level of interplanetary missions to Mars, without the need of adopting a launcher that puts the spacecraft on a direct trajectory towards the sphere of influence of Mars: it is envisioned to use a parking orbit around Earth and use the propulsion system of the spacecraft itself to escape the gravitational attraction of the Earth and reach Mars. The methodology used for this scope starts from the research performed in the literature studies on the state-of-the-art propulsion systems adapted to CubeSats, in order to understand the current available performance parameters from commercial-off-the-shelf units. These are used, together with the research on other interplanetary CubeSats mission proposal to generate a list of requirements that the mission, and therefore the propulsion system itself, must adhere for a successful operation. Between these requirements, particular emphasis is put on the Δv budget required by the mission and the trajectory it can follow between the two planets, to show that CubeSat propulsion system can render interplanetary travel for small spacecraft safely achievable.

Once the subsystem requirements are listed, the focus is shifted towards the propulsion system itself: several trade-offs are performed with systems engineering tools to determine which type of propulsion system can better fit to the proposed mission and its requirements. Afterwards, a detailed design of the chosen propulsion system type is executed: the most optimal propellant is chosen by analysing its chemical properties that will affect the size and shape of the system, as well as simulating the performance of each propellant using the "Rocket Propulsion Analysis" (RPA) tool. The full system is designed to reach the performance levels described by the requirements. Once the design is closed, a CAD drawing of the system is created to complete the project and to showcase the possibility of complying to severe constraints given by interplanetary missions with a small propulsion system that can fit in the reduced volume of the CubeSat standard.

This Thesis work is intended to be a first step towards the definition of fully chemical propulsion system requirements for autonomous CubeSat missions that intend to travel from Earth towards deep-space, in this case the planet Mars: the assessment of propulsion systems currently available and/or under development has allowed an overall understanding on the topic and the available levels of performance of the variables at play. This has led to modifications on the most common designs of part of a propulsion system that would better fit the needs of such an total high-impulse high-thrust mission, with the assessment of the most optimal propellants that will enable this technology. This work has the goal of assessing the possibility of reaching the planet Mars even with small spacecrafts with a single chemical propulsion system of their own, drastically reducing travel time and increasing the availability of scientific missions that would be feasible without relying on direct insertion towards deep-space.

Contents

List of Figures	ix
List of Tables	xiii
1 Introduction	1
1.1 Context	1
1.2 Research objectives and questions	2
1.3 Literature Study summary	2
1.4 Thesis outline	5
2 Mission and propulsion system requirements	7
2.1 Motivation	7
2.2 Requirements and constraints definition	9
2.2.1 Mission requirements.	9
2.2.2 Propulsion system requirements.	11
2.3 Conclusions.	12
3 Preliminary mission analysis	15
3.1 Interplanetary flight assumptions	15
3.2 Interplanetary transfer	16
3.3 Earth escape	18
3.3.1 Simulation procedure.	18
3.3.2 Earth escape simulation results	24
3.3.3 Conclusions.	30
3.4 Arrival at Mars	31
3.4.1 Simulation procedure.	31
3.4.2 Mars stabilization simulation results	35
3.4.3 Conclusions.	38
3.5 Total propellant budget	38
4 Propulsion system trade-off	41
4.1 Chemical propulsion basics and classification	41
4.1.1 Solid propulsion systems.	42
4.1.2 Liquid propulsion systems	43
4.1.3 Conclusions.	44
4.2 Green mono-propellant options	45
4.2.1 Propellant trade-off	47
4.3 Conclusions.	55
5 Propulsion system detailed design	57
5.1 Initial assumptions	57
5.1.1 Preliminary thruster design.	57
5.1.2 Pressurization system	58
5.1.3 Pressure drops causes and estimation	60
5.2 Pump selection	61
5.2.1 Pump performance estimation.	61
5.2.2 Pump power usage estimation.	65
5.2.3 Pump dimensions	67
5.3 Tank design	67
5.3.1 Pressurization level.	68
5.3.2 Tank shape	70
5.3.3 Conclusions.	74

5.4	Feed system	75
5.4.1	Preliminary design	75
5.4.2	Feed system pressure drop estimation	78
5.4.3	Injector design	81
5.4.4	Conclusion	82
5.5	Thruster design	83
5.5.1	Catalyst bed	83
5.5.2	Combustion chamber and nozzle	89
5.5.3	Conclusion	92
5.6	Preliminary design	92
5.6.1	Pressure budget	92
5.6.2	Power budget	93
5.6.3	Mass budget	94
5.7	Design finalization	95
5.7.1	Effects of initial spacecraft mass M_0	95
5.7.2	Trajectory analysis	97
5.7.3	Final design dimensioning and CAD drawing	101
5.7.4	Conclusion	106
5.8	Conclusion	106
6	Conclusions	109
6.1	Research objective	109
6.2	Recommendations and future work	110
	Bibliography	113
A	Earth escape single variable simulations	119
B	Mars stabilization budget estimation	123
C	Candidate pumps data-sheet performance graph interpolation	127

List of Figures

1.1	MARIO mission phases [38]	5
2.1	Orbit raisings from LEO to an high earth orbit using eletrical and chemical propulsion [61]	8
3.1	Hyperbolic escape trajectory from a parking orbit around Earth [77]	15
3.2	Hohmann transfer between Earth (planet 1) and Mars (planet 2) around the Sun [17]	16
3.3	Geometry of powered flight and a definition of the flight path angle γ , and the thrust angle δ [77]	20
3.4	Example of orbit raising strategy	21
3.5	Successful Earth escape sample trajectory, showing the manoeuvres performed after the orbit raisings	22
3.6	Comparison between Earth escape orbits to validate the results from the MATLAB/Simulink script	25
3.7	Δv budget needed for Earth escape: initial satellite mass $M_0 = 25$ kg, propellant specific impulse $I_{sp} = 230$ s	27
3.8	Δv budget needed for Earth escape. Initial satellite mass $M_0 = 30$ kg, propellant specific impulse $I_{sp} = 230$ s	29
3.9	Δv budget needed for Earth escape. Initial satellite mass $M_0 = 35$ kg, propellant specific impulse $I_{sp} = 230$ s	29
3.10	Example of correct stabilization around Mars	33
3.11	Example of failed stabilization around Mars	34
3.12	Comparison between Δv outpputs of the MATLAB/Simulink tool and the bitangential transfers Δv for different initial peri-apsis of Mars orbit	35
3.13	Mars stabilization Δv budget for case 1C (initial satellite mass of 25 kg) and specific impulse level of $I_{sp} = 260$ s	37
3.14	Propellant mass required for a initial satellite mass of 30 kg, calculated with the Δv budget from Table 3.13 and Δv_{miss} .	39
4.1	Schematic of a solid propulsion system [69]	42
4.2	Ideal and estimated specific impulse level of FLP-106 with varying expansion ratio.	52
4.3	FLP-106 volume intake for the mission with varying specific impulse, given an initial spacecraft mass of $M_0 = 30$ kg.	52
4.4	Ideal and estimated specific impulse level of AF-M315E with varying expansion ratio.	54
4.5	AF-M315E volume intake for the mission with varying specific impulse, given an initial spacecraft mass of $M_0 = 30$ kg.	54
5.1	Table comparison of GR-1 thrust generation vs feed pressure. [59] [60]	57
5.2	Pump 2212-M04C49/C50/C51 performance values for different fluid viscosities [29]	62
5.3	Pump 2212-M04X01/X03/X04 performance values for different fluid viscosities [30]	63
5.4	Maximum pressure differential values interpolated among the working fluid viscosity range	64
5.5	Maximum pressure differential values interpolated among the working fluid viscosity range	64
5.6	Lunar Flashlight pump performance and power requirement at different speeds [11]	66
5.7	Pump model 2212-M04X01 dimensions in mm [30].	67
5.8	Initial to final pressure ratio of pressurant gas and internal tank volume increase for blow-down ratio varying between 1 to 10.	69
5.9	Mass and height of cylindrical tank with emispherical enclosure on internal radius R_t .	71
5.10	Integrally forged flat head [75]	71
5.11	Tank mass and total height based on internal radius R_t .	72
5.12	Sketch of pressure vessel of non-circular cross section	73

5.13	Total stresses in point N (mid-line of short side of the tank), point M (mid-line of long side of the tank) and maximum yield stress of tank material.	74
5.14	Propulsion system sketch.	76
5.15	VACCO F1D10807-02 filter data sheet [73]	77
5.16	VACCO V8E10580-01 latch valve data sheet [74]	77
5.17	VACCO V0D10898-01 thruster valve data sheet [72]	78
5.18	Pressure drop occurring for water and AF-M315E orifice calibration [67]	78
5.19	L/D ratio for different tubing components [82]	79
5.20	Tubing pressure drop estimation for varying tube diameter D_t	80
5.21	Thruster valve pressure drop graph [72]	81
5.22	Monopropellant thruster sketch, with catalyst bed highlighted [82]	83
5.23	Plots of void fraction profile for : (a) spherical pellets, using $\epsilon_{min} = 0.24$, $\epsilon_0 = 0.41$, $b = 0.876$, $c = 10$ and for (b) cylindrical pellets, using $\epsilon_{min} = 0.275$, $\epsilon_0 = 0.375$, $b = 0.876$, $c = 2$	86
5.24	Radial void fraction ϵ_{loc} for cylindrical pellets of diameter ratio 7. Cylinder length set equal to diameter.	87
5.25	Catalyst bed loading for state-of-the-art H_2O_2 and N_2H_4 thrusters [23]	87
5.26	Pressure profile simulation of HAN-Methanol propellant over catalyst bed for different bed porosity values [27]	89
5.27	Pressure profile simulation of HAN-Methanol propellant over platinum barium pellets, with pre-heating to 350° [31]	89
5.28	Chamber cylindrical and convergent part sketch [82]	90
5.29	Conical nozzle sketch [82]	91
5.30	Mass budget available for the spacecraft subsystems and payload for initial spacecraft mass values of 25, 30 and 35 kg, choosing a cylindrical tank with semi-spherical or flat enclosure. A fit of the values is presented.	96
5.31	Volume budget available for the spacecraft subsystems and payload for initial spacecraft mass values of 25, 30 and 35 kg, choosing a cylindrical tank with semi-spherical or flat enclosure. A fit of the values is presented.	97
5.32	Earth escape optimization for an initial spacecraft mass of $M_0 = 28 \text{ kg}$ and propellant specific impulse $I_{sp} = 262.865 \text{ s}$	98
5.33	Successful Earth escape trajectory	98
5.34	Mars capture Δv budget for an initial spacecraft mass (at Mars) of $M_{0M} = 19.7225 \text{ kg}$ and a propellant specific impulse value of $I_{sp} = 262.865 \text{ s}$	99
5.35	Successful Mars stabilization trajectory	100
5.36	Zoomed-in particular of the final orbit, showing the burn arcs in red.	100
5.37	Isometric view of the CAD model	103
5.38	Bottom view of the CAD model	103
5.39	Front view of the CAD model	104
A.1	Results of Earth escape simulation using the constant input values of $M_0 = 25 \text{ kg}$, $I_{sp} = 240 \text{ s}$, $t_b = 600 \text{ s}$	120
A.2	Earth escape trajectories using the constant input values of $M_0 = 25 \text{ kg}$, $I_{sp} = 240 \text{ s}$, $t_b = 600 \text{ s}$	121
A.3	Orbit energy variation during Earth escape manoeuvres, using the the constant input values of $M_0 = 25 \text{ kg}$, $I_{sp} = 240 \text{ s}$, $t_b = 600 \text{ s}$	122
B.1	Ideal Δv budget required to stabilize around Mars, entering the sphere of influence with the hyperbolic orbit parameters defined in Chapter 3.4. On the x-axis the initial periapsis of the orbit is varied. Values are shown for final target orbit eccentricities of 0, 0.3, 0.6, 0.9.	124
C.1	Extrapolated and real operating graph of pump 2212-M04C49/C50/C51 for a fluid of viscosity 1 cP [29]	128
C.2	Extrapolated and real operating graph of pump 2212-M04C49/C50/C51 for a fluid of viscosity 2 cP [29]	128
C.3	Extrapolated and real operating graph of pump 2212-M04C49/C50/C51 for a fluid of viscosity 1 cP [29]	128

C.4	Extrapolated and real operating graph of pump 2212-M04C49/C50/C51 for a fluid of viscosity 1 cP [29]	129
C.5	Extrapolated and real operating graph of pump 2212-M04X01/X03/X04 for a fluid of viscosity 1 cP [30]	129
C.6	Extrapolated and real operating graph of pump 2212-M04X01/X03/X04 for a fluid of viscosity 2 cP [30]	129
C.7	Extrapolated and real operating graph of pump 2212-M04X01/X03/X04 for a fluid of viscosity 16 cP [30]	130
C.8	Extrapolated and real operating graph of pump 2212-M04X01/X03/X04 for a fluid of viscosity 70 cP [30]	130

List of Tables

1.1	Results of the survey for state-of-the-art cubesat chemical propulsion (part 1)	3
1.2	Results of the survey for state-of-the-art cubesat chemical propulsion (part 2)	4
2.1	Keplerian elements of the parking SSGTO used as starting orbit of the CubeSat [35] . . .	10
2.2	Preliminary mission requirements	13
2.3	Preliminary chemical propulsion system requirements	13
3.1	Gravitational parameters and mean distance from Sun of Earth, Mars and Sun [77] . . .	16
3.2	Specific energy $\left[\frac{km^2}{s^2} \right]$ of orbit after orbit raising manoeuvres around Earth ($T = 4.1 N$, $M_0 = 25 \text{ kg}$, $I_{sp} = 240 \text{ s}$, $t_b = 600 \text{ s}$)	23
3.3	Specific energy $\left[\frac{km^2}{s^2} \right]$ of orbit after orbit raising manoeuvres around Earth ($T = 6 N$, $M_0 = 30 \text{ kg}$, $I_{sp} = 280 \text{ s}$, $t_b = 500 \text{ s}$)	23
3.4	Specific energy $\left[\frac{km^2}{s^2} \right]$ of orbit after orbit raising manoeuvres around Earth ($T = 41 N$, $M_0 = 25 \text{ kg}$, $I_{sp} = 240 \text{ s}$, $t_b = 60 \text{ s}$)	24
3.5	Specific energy $\left[\frac{km^2}{s^2} \right]$ of orbit after orbit raising manoeuvres around Earth ($T = 60 N$, $M_0 = 30 \text{ kg}$, $I_{sp} = 280 \text{ s}$, $t_b = 50 \text{ s}$)	24
3.6	MARIO mission parameters for orbit raising and Earth escape	24
3.7	Earth escape Δv budget for $M_0 = 25 \text{ kg}$	27
3.8	Earth escape Δv budget for $M_0 = 30 \text{ kg}$	28
3.9	Earth escape Δv budget for $M_0 = 35 \text{ kg}$	30
3.10	Braking manoeuvre sample performed around Mars: the final orbit specific energy after stabilization is higher than the ideal case, using the same applied Δv	34
3.11	Samples of stabilization manoeuvres, with increased available thrust and reduced burn- ing time: manoeuvres are performed near the peri-apsis of the orbit	35
3.12	Mars stabilization optimal Δv budget result for initial satellite mass of 25 kg, case 1C . .	36
3.13	Mars stabilization optimal Δv budget result for initial satellite mass of 30 kg, case 2B . .	37
3.14	Mars stabilization optimal Δv budget result for initial satellite mass of 35 kg, case 3B . .	38
3.15	Mission requirements	40
3.16	Chemical propulsion system preliminary requirements, assuming an initial satellite mass of $M_0 = 30 \text{ kg}$	40
4.1	Preliminary design trade-off comparing propulsion system options.	46
4.2	Hydrazine physical and performance characteristics. f) Parameters dependent on the amount of ammonia dissociation, usually ranging between 30 to 70% [25]	46
4.3	Physical, performance and thermochemical properties of the propellant candidates. Con- ditions for specific impulse estimation: a): $P_c = 0.7 \text{ MPa}$, $A_e/A_t = 50$, b): $P_c = 2 \text{ MPa}$, $A_e/A_t = 50$	48
4.4	Physical, performance and thermochemical properties of the propellant candidates. Con- ditions for specific impulse estimation: c): $P_c = 2 \text{ MPa}$, $A_e/A_t = 50$, d): $P_c = 2 \text{ MPa}$, A_e/A_t $= 50$,	49
4.5	Chemical structure, molecular weight and standard heat of formation of propellant com- ponents used for RPA simulation between the propellant candidates. [49]	50
4.6	AF-M315E estimated properties	51
4.7	AF-M315E specific impulse and mass/volume given an expansion ratio of $\varepsilon = 200$ for an initial spacecraft mass of $M_0 = 30 \text{ kg}$ and $\Delta v = 2045 \text{ m/s}$	55

4.8	Chemical propulsion system preliminary requirements, assuming an initial spacecraft mass of $M_0 = 30 \text{ kg}$.	55
5.1	Thrusters propellant mass flow and thrust parameters	58
5.2	Pump models, with nominal voltages, speed constant and max continuous current values for pump 2212-M04C49/C50/C51 [29]	65
5.3	Pump models, with nominal voltages, speed constant and max continuous current values for pump 2212-M04X01/X03/X04 [30]	65
5.4	Pump operating conditions at the end of the transfer conditions.	67
5.5	Tank, propellant and pressurant volume and mass budget.	75
5.6	Injector design values.	82
5.7	Feeding system mass and pressure drop estimation.	82
5.8	Spherical and cylindrical pellets constants ϵ_{min} , ϵ_0 , b and c investigated by Bey and Eigenberger [47].	84
5.9	Thruster (chamber + nozzle) dimensions.	92
5.10	Propulsion system power budget.	93
5.11	Preliminary propulsion system mass budget.	94
5.12	Mass and tank dimensions iteration based on the Δv obtained with the I_{sp} from Chapter 4. Tank radius of 98 mm .	96
5.13	Mission parameters for Earth orbit raising and escape.	99
5.14	Mission parameters for Mars capture.	101
5.15	Pressurant, propellant and pressurant volume and mass budget for the final design, considering an initial spacecraft mass of $M_0 = 28 \text{ kg}$.	102
5.16	Final design of feeding system mass and pressure drop estimation.	105
5.17	Final propulsion system design mass budget.	105
5.18	Final design propulsion system power budget.	106
B.1	Output Δv results for Mars capture [km/s], used for validation with [66], by using as input values: $M_0 = 30 \text{ kg}$, $I_{sp} = 240 \text{ s}$, $t_b = 20 \text{ s}$ and $T = 500 \text{ N}$. The infinite velocity $v_{\infty M}$ values at Mars for the H1-H4 cases are: 3.388 (H1), 2.090 (H2), 3.163 (H3), 1.881 (H4) [km/s]	125
C.1	Pump models maximum pressure differential for four different fluid viscosities, in psi.	127

Nomenclature

List of acronyms

- ADN : Ammonium dinitramide
- BOL : Beginning of life
- COTS : Commercial off-the-shelf
- ECSS: European Cooperation for Space Standardization
- EIL : Energetic ionic liquid
- EOL : End of life
- GEO : Geostationary orbit
- GPIM : Green propellant infusion mission
- HAN : Hydroxylammonium nitrate
- LEO : Low earth orbit
- LUMIO : Lunar Meteoroid Impact Observer
- MARIO : Mars Atmospheric Radiation Imaging Orbiter
- MEO : Medium earth orbit
- MEOP : Maximum expected operating pressure
- NPSH: Net Positive Suction Head
- RPA : Rocket propulsion analysis
- SCAPE : Self-contained atmospheric protective ensemble
- SSGTO : Super synchronous geostationary transfer orbit
- TBD : To be determined
- TRL : Technology readiness level

List of symbols

- a : orbit semi-major axis
- e : orbit eccentricity
- i : orbit inclination
- Ω : orbit longitude of the ascending node
- ω : orbit argument of periapsis
- θ : orbit true anomaly
- g_0 : mean Earth gravitational acceleration
- I_{sp} : propellant specific impulse
- t_b : propulsion system continuous burn time
- Δt_b : waiting time in-between manoeuvres
- μ : gravitational parameter

- ρ : propellant/material density
- γ : specific heat ratio
- Γ : Vandekerckhove function
- η : efficiency
- ε : area ratio
- \dot{m} : mass flow
- \dot{V} : volumetric flow
- B_R : tank blow-down ratio
- σ : material yield strength

Introduction

This chapter serves as a presentation of the thesis work research objectives, providing an early description to the state-of-the-art of the topic of interest and a summarized review of the literature study previously pursued.

1.1. Context

The thesis work hereby presented is pursued with the objective of developing an innovative propulsion system that may unlock new possibilities in terms of low-cost deep-space exploration for small satellites. In recent years, in fact, industries, agencies and universities have started to develop more interest towards small satellites and their applications. This wishful thinking has led to an exponential increase of small satellites launches in the past years, as well as newly discovered opportunities for scientific missions allowed by small satellites flying in close formation or working together as a constellation. A CubeSat is formed by one or more cubes of $10 \times 10 \times 10$ cm dimensions, each one called a unit (or U), in which to allocate each of the subsystems needed for its scientific scope. Compared to much larger spacecrafts, the cost/time to manufacture and develop a readily available system is much smaller, and the mass, which poses a severe constraint for launches, is greatly reduced: most of the CubeSat applications until now have seen opportunities mostly around Earth, with few exceptions that will be introduced later. A crucial step towards enabling more variety in CubeSat applications is the availability of on-board propulsion: in this way the spacecraft would not be fixed in the insertion orbit that the launcher will send it to, but more diversity in the orbital position can be achieved by performing autonomous manoeuvres. This would allow spacecrafts to autonomously manoeuvre and guide themselves towards their scientific goal of interest, which might be an higher altitude with respect to Earth. These application, though, are only related to propulsion systems that provide small levels of power: if it is envisioned to autonomously propel a spacecraft in deep-space, which means beyond the common altitudes of Earth orbits (LEO, MEO, GEO) and away from the Earth's sphere of influence, there is the need for propulsion systems that provide high levels of Δv to the current velocity of the spacecraft. When talking about propulsion, there are three different domains at play: chemical, cold gas and electric. Chemical propulsion systems use the chemical energy stored in a propellant to generate thrust, breaking the molecular bond and producing energy, therefore increasing the propellant temperature and causing the reaction products to be accelerated through a nozzle: they are characterized by an higher level of thrust and smaller specific impulse levels with respect to their electric counterparts. Cold-gas propulsion system generate low levels of thrust by the expulsion of an inert, non-toxic propellant which can be stored in high pressure gas. They are suitable for small buses due to their low grade of complexity and are relatively inexpensive and robust. Their main application include small impulse bits for attitude control. Electric propulsion systems, generally use electrical and/or magnetic fields to change the velocity of the spacecraft. They can provide thrust for longer time, not being highly constrained on the mass of propellant that can be carried on board of the spacecraft, but the thrust levels are considerably lower.

Chemical propulsion can provide a spacecraft system with high-thrust manoeuvres compared to the other two cases: this can be advantageous in the cases in which the energy of the orbit needs to be

increased or decreased quickly, as for orbit raising manoeuvres around the Earth in which the travel time needs to be minimized. If a propulsion system providing a lower amount of thrust is used, the spacecraft orbiting Earth would follow a spiralling trajectory with much longer waiting times, which are not optimal in case the radiation incoming from Van Allen belts passes need to be reduced. High thrust is also useful in the case of orbit stabilization around a celestial body: during a fly-by, a chemical propulsion system might be used to quickly brake around the celestial body and obtain a closed orbit of the spacecraft around it, without the need of slowly spiralling in, which is the case for lower thrust-generating systems. The goal of this thesis is to investigate the level of maturity of chemical propulsion systems for small spacecrafts currently available for commercial use or under development, and the envisioned CubeSat missions in which chemical propulsion systems are employed. Mission requirements that will benefit the most from chemical propulsion will be produced, or taken as reference from literature, and the most efficient design of a propulsion system that satisfies such requirements will be performed, in order to provide a new option or application of this type of propulsion for CubeSat systems.

1.2. Research objectives and questions

The following research questions and sub-questions need to be answered throughout the project, in order to reach the master thesis goal.

1. What are the Cubesat mission requirements that will most benefit from the application of chemical propulsion?
 - (a) What are the propulsion system requirements of this mission?
 - (b) What are the constraints acting on the propulsion system?
2. What is(are) the best propellant(s) option(s) that are more efficient for the Cubesat mission?
 - (a) What are the available options of propellant for the chosen kind of propulsion system?
 - (b) What is the technology readiness level and flight heritage of this propellant?
 - (c) What are the maximum thrust and specific impulse provided by this propellant option?
3. What is the architecture of the propulsion system that can better satisfy the mission requirements?
 - (a) What is the optimum volume and material of the tanks to contain the propellant?
 - (b) What is the best configuration for the thrusters?
 - (c) Which system elements shall be present in order to ensure correct functioning of the system?

The main research objective and sub-goals of this thesis are:

1. "Designing a chemical propulsion system to be employed for a deep-space Mars mission".
 - (a) Research or generate a set of requirements for the propulsion system of a deep-space Cube-sat mission.
 - (b) Perform a design trade-off between the different kind of chemical propulsion systems to determine which one better meets the need of the mission.
 - (c) Perform thrust chamber simulations in order to determine which propellant(s) is(are) better suited for the mission.
 - (d) Design the complete architecture of the propulsion system, comprehensive of tanks, feed lines, injectors and thrusters.
 - (e) Provide a final CAD work of the propulsion system designed.

1.3. Literature Study summary

The purpose of the literature study has been to investigate the current available technologies and the on-going research for chemical propulsion for CubeSat applications, analysing both the developed liquid propulsion systems (mono- and bi-propellant) and solid propulsion systems. The main factors that are taken into account for the analysis of the differences between the available technologies will be

their TRL, their flight heritage, their performance values, the greenness of the propellant(s) used and their compliance with the currently available standards for CubeSat propulsion systems. Afterwards, a research on the available literature for the ECSS (European Cooperation for Space Standardization) standards that have been developed for CubeSat chemical propulsion system has been undertaken: the standards defined to these days are relative to spacecrafts with bigger size than standard CubeSats, and these would put a high constraint on the low-cost propulsion system for a generic smaller spacecrafts. Therefore, some of the defined standards for chemical propulsion systems have been tailored to be partially applied for CubeSat chemical propulsion system. An extensive overview on which standards have been kept applicable and which other has been modified/removed has been performed, ranging from design, to verification and constraints. Finally, a general overview of missions where chemical propulsion systems is envisioned to be adopted was presented: as explained earlier, these propulsion system provide high-impulse manoeuvres within a short amount of burn time, and are optimal for missions which require fast manoeuvring. The research performed on the state-of-the-art chemical propulsion system for Cubesats currently in development at university and industry level are summarized in Table 1.1 and Table 1.2. Each propulsion system type is categorized between Mono-prop, Bi-prop and Solid, along with the manufacturer and the product name. The main parameters investigated are thrust levels, specific impulse, technology readiness level (TRL), the total mass (or divided between dry and wet, if listed), the total impulse the occupied volume.

Table 1.1: Results of the survey for state-of-the-art cubesat chemical propulsion (part 1).

Propulsion type	Manufacturer	Product Name	Propellant	Thrust [mN]	Isp [s]	TRL 1-9	Mass [kg]	Total Impulse [N*s]	Volume
Mono	VACCO	MIPS	LMP-103S/LT or AF-M315E	400	190	6	3.0 Dry (max) 5.0 Wet (max)	3320	3U
Mono + ColdGas	VACCO	Argomoon Hybrid MIPS	LMP-103S & R134a	100 & 4*25	190	6	1.43 Dry (max) 2.065 Wet (max)	783 & 72	1.3U + tuna can
Mono	VACCO	Integrated Propulsion System	LMP-103S	3970	220	6	9 Dry 14.7 Wet	12000	-
Mono	AeroJet Rocketdyne	MPS-130-1U	AF-M315E	250-1000 per thruster	240	-	1.1 Dry 1.7 Wet	>1130	1U
Mono	AeroJet Rocketdyne	MPS-130-2U	AF-M315E	250-1000 per thruster	240	-	1.4 Dry 2.8 Wet	>2720	2U
Mono	AeroJet Rocketdyne	MPS-135-4U	AF-M315E	250-1000 per thruster	-	-	3.5 Dry 7.2 Wet	>7290	4U
Mono	AeroJet Rocketdyne	MPS-135-6U	AF-M315E	250-1000 per thruster	-	-	4.3 Dry 11.2 Wet	>13740	6U
Mono	AeroJet Rocketdyne	MPS-135-8U	AF-M315E	250-1000 per thruster	-	-	5.1 Dry 14.7 Wet	>19360	8U
Mono	AeroJet Rocketdyne	MPS-120-1U	Hydrazine	250-1000 per thruster	206-217	-	1.2 Dry 1.6 Wet	>810	1U
Mono	AeroJet Rocketdyne	MPS-120-2U	Hydrazine	250-1000 per thruster	206-217	-	1.5 Dry 2.5 Wet	>1960	2U
Mono	AeroJet Rocketdyne	MPS-125-4U	Hydrazine	250-1000 per thruster	-	-	3.6 Dry 6.2 Wet	>5240	4U
Mono	AeroJet Rocketdyne	MPS-125-6U	Hydrazine	250-1000 per thruster	-	-	4.4 Dry 9.3 Wet	>9890	6U
Mono	AeroJet Rocketdyne	MPS-125-8U	Hydrazine	250-1000 per thruster	-	-	5.1 Dry 12.1 Wet	>13930	8U
Mono	AeroJet Rocketdyne	GR-1	AF-M315E	400-1100	235	6	-	23000	-
Mono	AeroJet Rocketdyne	GR-22	AF-M315E	8000-25000	250	5	-	74000	-
Mono	Busek	BGT-X1	AF-M315E	100	214	-	-	-	-
Mono	Busek	BGT-X5	AF-M315E	500	220-225	5	1.5 Wet	565	1U + external

Table 1.2: Results of the survey for state-of-the-art cubesat chemical propulsion (part 2).

									tuna can volume occupied by the ejector spring of a 3U Cubesat launcher
Mono	Busek	BGT-5	AF-M315E	5000	>230	-	-	-	-
Mono	Busek	AMAC	AF-M315E	425	225	5	-	565	1U
Mono	ECAPS	HPGP	LMP-103S	250-1000	204-231	9	0.48		
Mono	Nanoavionics	EPSS C1 (1U)	ADN Blend	100	200	7	0.8 Dry 1.2 Wet	650	1U (available also 2&3U)
Bi-prop	Tethers Unlimited	HYDROS-M	Liquid water (electrolyzed)	>1200	>310	6+	6.4 Dry 12.6 Wet	>18000	381 diam x191 mm
Bi-prop	Tethers Unlimited	HYDROS-C	Liquid water (electrolyzed)	>1200	>310	6+	1.87 Dry 2.61 Wet	>251	190x130x92 mm
Bi-prop	Hyperion	PM200	Nitrous Oxide + Propane	500	285	-	1.1 Dry 0.31 Prop	>850	1U
Bi-prop	Hyperion	PM400	Nitrous Oxide + Propane	1000	>285	-	<1.4 Dry 0.625 Prop	>1750	2U
Hybrid	Utah State University	Green hybrid	Solid 3D printed acrylonitrile butadiene styrene (ABS) and oxidizer (60% nitrogen, 40% oxygen)	8000	215	6	-	-	-
Solid	DSSP	CDM-1	AP/HTPB	76500 (max 186800)	235	-	-	226.4	64 diam * 47 mm
Solid	DSSP	CAPS 3	HIPEP-501A	300	900	8	0.0233	0.125	0.5U
Solid	DSSP	MPM-7	HIPEP-H15	-	200	-	<0.75	1.5	<0.75 U
Solid	Industrial Solid Propulsion	ISP 30 sec	HTPB/AP	36900 (max 66700)	249 or 187	6	0.95 Motor 0.544 Prop	996	57.2 diam * 249 mm
Solid	Northrop Grumman Innovation Systems (former Orbital ATK)	STAR 4G	Al + Ammonium Perchlorate	258000	277	6	-	-	-
Solid	PacSci EMC	MAPS	-	-	210	9	-	-	380*10.5 cm

The previous tables provided several insights on the state-of-the-art for CubeSat chemical propulsion systems, summarized below:

- Thrust levels increase when moving from mono-propellant to bi-propellant and finally solid propulsion: this is expected, since the energy of their propellants and the chamber temperature reached is higher, therefore most of the enthalpy of the system can be transformed into thrust. Furthermore, to generate lower thrust, smaller systems need to be employed: this becomes more complex when higher temperatures need to be managed, which is the case of bi-propellant and solid propulsion systems.
- Specific impulses are still much below the levels provided by means of electric propulsion (in the order of thousands). In any case, the highest levels of I_{sp} for chemical propulsion are obtained from solid propulsion (around 200 s) to mono-propellant (around 250) to bi-propellant (around 300).
- The complexity of the systems is different between the three branches: while solid propellant technologies are the simpler in terms of architecture, they are more difficult to control. The bi-propellant systems are the most complex ones in terms of architecture, since they need double the number of feed systems and pumps, compared to mono-propellant.
- In general the TRL of all the levels is medium, around 6 or 7, with small exceptions of TRL 9.

- All the number of systems currently in development in universities and companies suggest that there is an interest towards this "older-fashioned" type of technology, since in many cases it is the only available solution to perform rapid orbit variations that are not quickly obtainable by electric/cold-gas propulsion means.

Finally, the mission that has been chosen to be taken as an initial reference is MARIO (Mars Atmospheric radiation Imaging Orbiter) [38] proposed by Politecnico di Milano and is a 16-U CubeSat mission that is intended to demonstrate autonomous deep-space cruise from Earth and position itself in a stable orbit around Mars where it will be operational. The proposed propulsion system is composed by both a chemical and an electrical propulsion system, separated and not operating in dual-mode, which are used for different parts of the interplanetary travel during the phases in which each one is most adapt to: the chemical propulsion system is expected to be operated when high-thrust and fast manoeuvres are predicted, while the electrical propulsion system will be operated during the interplanetary voyage and after Mars stabilization.

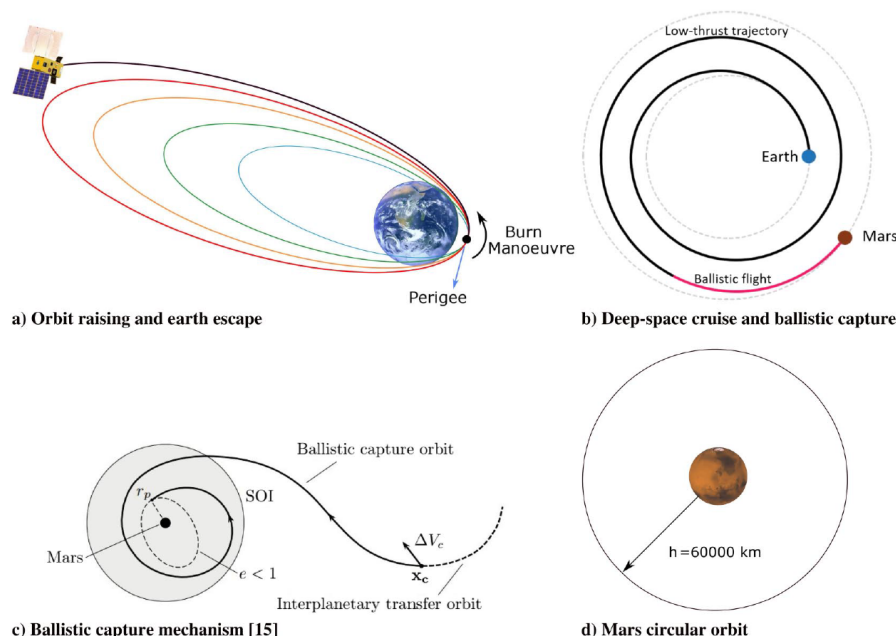


Figure 1.1: MARIO mission phases [38]

This thesis project takes the starting points of this interplanetary mission as a reference to define their own missions requirements that would be characteristic of a similar deep-space mission, but adopting only one of the two propulsion systems, therefore reducing considerably the complexity of having two different propulsion systems on-board, and nullifying issues caused by eventual interactions between the two systems. This will improve the time required for such a mission to be fully operative, not having to rely on a slower deep-space cruise adopting electric propulsion, but will also show the downsides of adopting a large amount of propellant for an high Δv budget. The work is intended to push the boundary of what type of missions chemical propulsion systems can be the enabler for CubeSat, by trying to generate as much Δv as possible, in a reliable way, considering the power, volume and several other constraints that place a burden on CubeSat propulsion systems.

1.4. Thesis outline

After the Literature Study, it has been proposed to investigate the mission and propulsion system requirements that a deep-space autonomous CubeSat mission shall adhere to. These requirements will pose the base of the Thesis work: a first set of requirements is derived based only on the actual limitations derived from the state-of-the-art for CubeSat chemical propulsion systems, in order to not end up with a viable solution on paper that might not be reflective of what can be manufactured and designed at this point in time. Furthermore, an initial set of mission requirements is used as a baseline for an

autonomous Mars mission, similarly to the proposed MARIO mission, such as the initial spacecraft parking orbit, the maximum number of manoeuvres before leaving Earth and the final orbit parameters of the orbit around Mars.

Following this first set of requirements, an analysis on the amount of Δv , given the starting orbit of the CubeSat, is afterwards performed to show the feasibility of the mission with the propulsion system constraints. Once all of the requirements are defined and derived, a first trade-off based on the available literature and performance parameters is performed in order to choose which type of chemical propulsion system better fits the requirements. A selection between the best available propellant option is afterwards performed, by using both literature values and numerical simulations, to verify that the performance parameters fit the mission.

Once the propellant has been chosen, the complete design of the architecture of the system is undergone, taking into account tanks, thrusters, injector and the main components that will ensure the correct functioning of the propulsion system. Finally, a CAD model of the design is presented.

2

Mission and propulsion system requirements

This chapter serves as the first step towards the design of a chemical propulsion system for CubeSat deep-space mission: with this intention, preliminary Mars mission requirements are displayed, derived from assumptions or from relevant literature. The same is done for the constraints acting on the propulsion subsystem capabilities, obtained from other missions adopting chemical propulsion and from the current available performance parameters of this technology, adapted to CubeSats.

2.1. Motivation

Interplanetary exploration has always been performed with large spacecrafts, but recent years have seen the rising usage of CubeSats with the advent of the so-called "New-Space" era: these interplanetary spacecrafts that have served for mission beyond the Earth sphere of influence have been launched towards deep-space directly with their launcher. It is envisioned that in the future fast deep-space cruising might be achievable by using autonomous CubeSats that are able to direct themselves with their own propulsion system, exiting Earth's sphere of influence and reaching other celestial objects of interest. In order to do this, it is crucial to adopt a propulsion system capable of providing high impulse levels to the spacecraft in motion around Earth, in order to minimize the time orbiting around the planet and begin its interplanetary voyage: this will lead to lower transfer times and will also reduce the impact of radiation onto the spacecraft. Electric propulsion systems are capable of providing large amounts of Δv to a spacecraft at the cost of very low propellant mass, due to their very high specific impulse levels. This comes at the cost of very high power consumption levels, and very long burn times: in fact, an electric propulsion system is able to provide large changes in total impulse but over a long active time of the propulsion system, therefore increasing the time spent before reaching the operational orbit for a given mission. On the other hand, chemical propulsion systems provide much higher thrust, in the levels of newtons and therefore are able to provide a large amount of impulse change in a shorter activation time of the thrusters: this comes at a cost for a very high propellant mass required, increasing the volume to be carried on board just to reach the operational phase of a mission.

In recent years, the trend of propulsion system has shifted towards an higher interest for electric propulsion system, due to their capability of providing high Δv budgets with low propellant mass, occupying less volume on-board and potentially enabling deep-space cruise with smaller spacecrafts. This is desirable for missions that are already launched towards exiting the sphere of influence of the Earth with their own launcher, using most of the propellant mass to perform manoeuvres in the heliocentric system of reference without disturbance from the sphere of influences of other planets. In the case of autonomous departure from Earth's sphere of influence, adopting electrical propulsion might be able to save a lot of propellant mass as per its characteristic, but the amount of time needed to perform orbit raisings will be very high, since the motion of the spacecraft will be much resembling of a spiral with increasing semi-major axis: each branch of the spiral will correspond to two passes through the Van Allen belts, which increase the amount of radiation that the spacecraft (and each subsystem or payload) will experience.

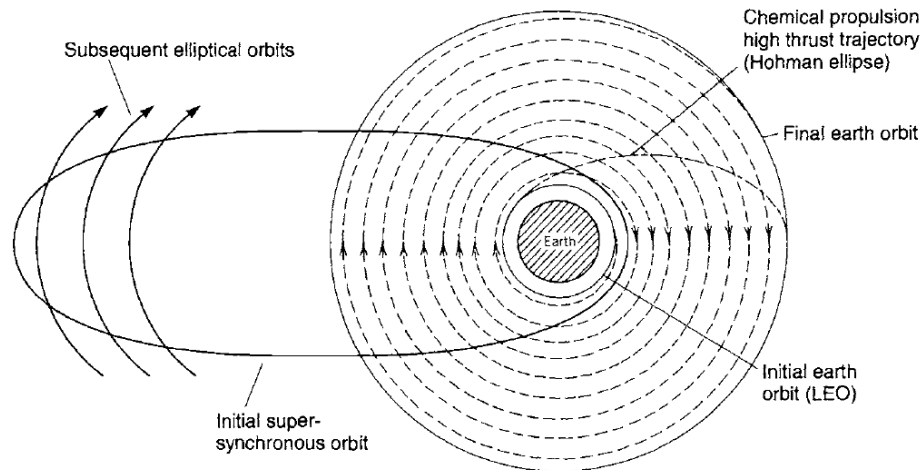


Figure 2.1: Orbit raisings from LEO to an high earth orbit using electrical and chemical propulsion [61]

Figure 2.1 shows a simplified diagram of trajectories for a spacecraft that moves from low earth orbit (LEO) to an high earth orbit using electrical or chemical propulsion. As discussed before, using electrical propulsion will save the amount of propellant needed for the manoeuvre, but the spiralling trajectory that the spacecraft will follow will take much longer than the one that can be achieved by using chemical propulsion. The latter only needs one (or several) perigee manoeuvres to move among the optimal Hohmann transfer orbit and reach the operating orbit quicker: of course, this comes at a cost of a higher propellant mass requirement.

Adopting electric propulsion for the orbit raising manoeuvres around Earth is not only time consuming, but it also increases the possibility of damages to the electronics of the spacecraft. Each time the spacecraft revolves around Earth, it will pass through the Van Allen belts twice, accumulating radiation that might damage the on-board data handling (OBDH) system of the spacecraft and its payload. In the case an electric propulsion system is adopted, the passes through the Van Allen belts will be numerous since the spiral will slowly raise its perigee around the Earth. In the case of chemical propulsion, instead, the damages to electronics would be less probable since the insertion in the heliocentric phase of the interplanetary trip will be obtained with fewer passes through the Van Allen belts. For these reasons, it is reasonable to adopt a chemical propulsion system for this phase of the mission, as it will help save time before reaching the operational orbit and limit damages coming from radiation.

For the interplanetary part of the trajectory, the MARIO mission proposal decides to adopt an electric propulsion system, separated from the chemical one. Earth escape is achieved by using a chemical propulsion system that increases the energy of the orbit up to a small enough positive value and become open (hyperbolic), such that the spacecraft is directed towards the edges of the Earth's sphere of influence on its own. After reaching that theoretical limit, the interplanetary phase begins where an electric propulsion system is adopted in order to minimize the total Δv required for the interplanetary transfer and enter the sphere of influence of Mars, minimizing the propellant mass requirement of this phase. Finally, both the electric and chemical propulsion systems are adopted once Mars is reached, in order to stabilize around a circular orbit and start operations. Designing the propulsion system of a spacecraft by having two separate kind of propulsion systems increases the flexibility of the missions that can be achieved with a small spacecraft: it can use high-thrust manoeuvres to propel itself around the Earth or stabilize around the final orbit, and also utilize the advantages of electric propulsion system to perform the interplanetary travel with minimum propellant mass. In this case they are two separated propulsion systems, but there have been several proposal of multi-mode propulsion systems, where the two systems actually share part of the subsystems and can be activated in one mode or another. Achieving this feat will highly benefit the possibilities of space missions performed with smaller spacecrafts, since sharing parts of the same system might lead to a considerable reduction in dry mass.

Nevertheless, for this thesis work it has been decided to try and simulate how a single chemical propulsion system might be able to perform in such a mission compared to the proposed chemical/electrical

ones. Adopting different propulsion systems might lead to an higher total volume required for propulsion, by taking into account dry mass for example. Furthermore, the compatibility of the two systems needs to be carefully assessed, since they should not influence each other when one is active and the other is not: the reliability of such a system needs to be carefully assessed since multiple interaction with other subsystems increase the possibility of failures, as can be the case for the electrical power system (EPS) for electric propulsion systems. For these reasons, as a first step towards enabling autonomous CubeSat interplanetary mission, an high level design of a chemical-only propulsion system to meet the high Δv budget requirements is performed in this thesis work.

2.2. Requirements and constraints definition

The first stepping stone in this thesis work will be the definition of the preliminary requirements and constraints that need to be met in order to achieve an autonomous interplanetary flight from Earth to Mars by adopting a satellite of CubeSat scale. At first, high-level requirements on the trajectory of the satellite around the Earth and Mars will be used as a baseline for the analysis of the path followed by the spacecraft around the two planets. Afterwards, the constraints acting on the propulsion system will be imported from the data obtained in the literature study, providing an early estimation of the thrust and specific impulse levels that a state-of-the-art chemical propulsion system is capable of achieving.

2.2.1. Mission requirements

The spacecraft taken as a baseline of the mission is a $12U$ CubeSat, made of 12 cubes arranged in a $2 \times 2 \times 3$ fashion to form its prismatic shape. This is chosen since it is considered a standard dimension for CubeSat with higher volume needs, as one will also be used for the Lunar mission LUMIO. It is also expected that providing autonomous flight from Earth to Mars might require higher level of volumes, therefore a CubeSat up to $24U$ is considered, with two $12U$ stacked on top of each other. Once all of the requirements have been fixed, most importantly the Δv and therefore the mass and volume budget, the CubeSat size most favourable to the propulsion system will be considered for the rest of the design. The total mass of the spacecraft, considering a range from $12U$ to $24U$, will be associated with 25 to 35 kg total: this is due to the fact that the propulsion system is going to take most of the volume inside the spacecraft due to the nature of chemical propulsion, therefore the payload to be carried on board is assumed to be small enough to not compromise the mass budget. If the initial mass increases too much, the propellant mass to be carried on-board increases proportionally and could require more than total CubeSat volume considered and the mission would be considered unfeasible under such conditions, therefore the maximum wet mass of the CubeSat is limited at 35 kg. As a baseline, a single camera is considered as payload.

The purpose of this hypothetical mission is to reach a stable orbit around Mars starting from a parking orbit at Earth: for this purpose, several requirements need to be defined in order to fix the initial and final parameters of the orbits that the spacecraft will follow at the start of the mission and at the start of operation. These requirements will only be high-level, since only a first estimate of the Δv budget needed for such a mission is needed. In fact, several simulations will be later be performed in order to check the most optimal strategy to adopt when departing Earth and stabilizing around Mars, but it is assumed to be working with orbit in the 2-dimensional plane: therefore, the parameters most relevant for this case will be the eccentricity (e) and the semi-major axis (a) of the orbits. The interplanetary flight will be simulated by adopting the patched conics method, which will assume an Hohmann transfer from Earth to Mars in the heliocentric system of reference, and two separate two-body problems around the Earth and Mars to simulate the departure from the parking orbit and the arrival on the operative orbit. As it will be thoroughly described in the next chapter of the thesis work, it is assumed that the thrusters will mainly perform manoeuvres around the planets, and the heliocentric phase of the flight will not be simulated: while such assumption is not very realistic, an additional mass budget percentage will be considered in order to take into account other manoeuvres that will be needed to complete the trip from Earth to Mars. For these reasons, the mission requirements have been split into two different sections: one regards the departure phase of the mission, while the second is reserved to the arrival on Mars.

Earth escape The parking orbit is chosen to be an eccentric super synchronous geostationary transfer orbit (SSGTO), taken from the proposed MARIO mission. It is characterized by a very low perigee and high apogee, and is commonly used from geostationary satellites that need to circularize their or-

Table 2.1: Keplerian elements of the parking SSGTO used as starting orbit of the CubeSat [35]

Keplerian elements	Value	Unit
a	51526	km
e	0.8705	-
i	0.01	deg
ω	0	deg
Ω	0	deg
θ	0	deg

bit to GEO. The Falcon 9 v1.1 rocket launched Thaicom 6 in January 2014 into this specific orbit and Thaicom 8 in May 2017 into an orbit with 350 km and 90226 km as the respective perigee and apogee [36]. This choice is made in order to reduce the amount of Δv needed to escape Earth, since being a very eccentric orbit it can become hyperbolic with low amount of impulse and allow the CubeSat to perform the mission on its own, without relying on bigger satellites. Its parameters are shown in Table 2.1, and the requirement derived from this rationale is named "MISS-E01":

- MISS-E01: the starting orbit is the SSGTO defined by parameters in Table 2.1.

As anticipated before, the reason why chemical propulsion is crucial for this phase of the mission is since it allows faster orbit raising compared to electric propulsion, thereby reducing the total amount of residence time around the radiation belts. From the MARIO trajectory analysis, Earth escape is achieved within 6 manoeuvres around the orbit perigee, accounting for a total of 13 belts crossings. The same number of manoeuvres has been chosen to be the maximum allowable for the manoeuvres for orbit raising around Earth, defined in requirement MISS-E02.

- MISS-E02: the number of orbit raising manoeuvres around the Earth shall be at most 6.

It needs to be clarified that MARIO only uses the chemical propulsion system to reach a positive level of the orbit around Earth, such that the spacecraft is afterwards able to move on its own towards the edges of the Earth's sphere of influence. In this case however, to successfully complete Earth escape, the final orbit of the spacecraft shall not only be characterized by a generic positive specific energy value: the final specific energy of the orbit shall be high enough to comply to the patched conics method hypothesis. Therefore, the number of manoeuvres around Earth mentioned in requirement MISS-E02 is only referred to the number of manoeuvres before the orbit of the spacecraft becomes hyperbolic: it is already predictable that several other manoeuvres shall be performed once the spacecraft will be on its way towards the boundary of the sphere of influence of the Earth, but these will not increase the total number of passes through the Van Allen belts. The exact value for the specific orbit energy will be discussed in the next section, therefore the requirement MISS-E03 will be a place-holder until the value is found.

- MISS-E03: the specific energy of the orbit before leaving Earth's sphere of influence shall be TBD.

These few high-level requirements will be used in the next chapter of the thesis work, where the two-body problem will be numerically solved taking into account the continuous thrust that will be applied on the spacecraft when manoeuvring. Setting this early requirements will allow for an estimation of the overall Δv needed for the Earth escape phase of the mission.

Mars stabilization Once the spacecraft enters the sphere of influence of Mars, it will follow an hyperbolic trajectory around the planet. If no braking manoeuvres are performed, the spacecraft will just fly-by the planet and exit its sphere of influence. Therefore, braking manoeuvres need to be executed to stabilize on a closed orbit around Mars. Since the scope of the thesis work is to assess the capabilities of a full chemical propulsion system for CubeSats, and the limits of propellant mass and volume to be carried on-board are going to be the worst burden between the constraints, it has been decided to not have a strict requirement on the final Keplerian values to be obtained around Mars. This is due

to the fact that performing a full circularization around the planet is presumably going to be very mass-consuming, since the orbit shall transform from an hyperbolic one to a circular one. Therefore, since this thesis work has the intention to show the capabilities of current chemical propulsion systems for CubeSats, the main requirement that the final orbit of the spacecraft shall comply to is a maximum value of eccentricity: as resumed in requirement MISS-M01, the final orbit shall at maximum have an eccentricity of 0.92. This value has been chosen such that there is not the need to decrease the energy (and eccentricity) of the orbit since it will be an additional Δv cost, but at the same time the period of the orbit shall not be too long or the passes near the planet might be too scarce, and values close to 1 for the eccentricity cause the orbit to have very long periods.

- MISS-M01: the final orbit eccentricity after stabilization shall be less than 0.92.

A second parameter to be fixed for the final orbit is one between the semi-major axis or its the peri/apo-apsis. It has been decided to put a requirement on the minimum distance from Mars, expecting it to be used for an hypothetical camera for a payload, where the minimum distance is crucial when calculating its field of view. Taking into account all of these motives, as well as the benefits of having a window for the camera or any other eventual payload in which the spacecraft orbits very close to Mars, the peri-apsis of the orbit is chosen to be low, contrary to the final orbit of MARIO. The "Mars Express" orbiter from ESA is currently flying around Mars on an highly elliptical orbit having peri-apsis and apo-apsis altitudes of 330 km and 10500 km respectively [20]: considering that the radius of Mars is The radius of Mars is $R_{mars} = 3389 \text{ km}$, the peri-apsis of the orbit is 3719 km. A slightly higher maximum value for the peri-apsis is chosen for this thesis work to allow for higher flexibility, and is summarized in MISS-M02.

- MISS-M02: the peri-apsis of the martian operational orbit shall be less than 5000 km.

This set of 5 requirements serves the purpose of defining the baseline of the Δv budget estimation, which will be highlighted in the following chapter of the thesis work.

2.2.2. Propulsion system requirements

The main requirements to which the chemical propulsion system shall comply to are related to its performance levels and safety. Values as the minimum level of Δv provided, minimum level of thrust and specific impulse need to be specified. The first values will be crucial in the first phase of the trajectory and Δv budget estimation for the mission, since different values of thrust and manoeuvre burn time will lead to different trajectories. The specific impulse will play an important role on the amount of propellant that will be carried on board, given the budget Δv : furthermore, it will be important for the propellant(s) choice to be made at the start of the propulsion system design, since minimizing volume (and consequently mass) occupied by the wet part of the propulsion system is especially important in small satellite design like CubeSats. The first requirement is related to the Δv required for Earth escape and stabilization around Mars: the propulsion system shall be able to deliver this Δv value by carrying enough propellant on-board. At this stage, since the exact value is not known, the specific Δv value is put as "To Be Determined" (TBD).

- PROP-01: the chemical propulsion system shall provide at minimum $\Delta v = TBD$

The exact value for this requirement will be obtained in the next section, together with the trajectory analysis. The objective of the latter will be an optimization of the Δv budget given the performance values of the propulsion system and the initial and final orbits requirement, such that the minimum level of propellant will be carried on-board, reducing the volume impact of the propulsion system on the CubeSat.

One important performance parameter to characterize a propulsion system is the level of thrust (T) it can provide, measured in Newtons: for chemical propulsion systems, as it has been described during the literature study in Tables 1.1 and 1.2 it varies between 0.25 to 5 N. For the MARIO mission, the maximum allowable value for the chemical propulsion system has been set to 3 N, based on torque misalignment, and adopts two 1.5 N thrusters. Given these considerations, it is expected that an higher level of thrust is required for the mission currently being studied, since the propulsion system shall be able to provide a faster Earth escape due to the energy requirements of the orbit. Given the state-of-the-art of current propulsion system, it is expected that values over 6 N are difficult to be achieved at this current stage of time, and is therefore used as the maximum thrust level to be adopted for the

mission. The results from the MARIO mission analysis have shown that 3 N are enough to reach the end of the sphere of influence starting from the same parking orbit, therefore it is expected that with double the amount of thrust the correct orbit energy can be reached in fewer orbit raising manoeuvres. Thus, a requirement on maximum thrust is set:

- PROP-02: The maximum thrust level of the system shall be 6 N.

Another performance parameter that influences the amount of mass of the propulsion system is the specific impulse (I_{sp}): it is related through the Tsiolkovsky equation to the amount of propellant mass to perform a manoeuvre with a given Δv , as follows:

$$M_p = M_0 \left[1 - \exp\left(-\frac{\Delta v}{g_0 I_{sp}}\right) \right] \quad (2.1)$$

The higher the specific impulse of the propulsion system, the lower propellant mass needs to be expelled to provide a Δv impulse, given the same initial spacecraft mass M_0 . It is therefore a very crucial parameter when designing propulsion systems for CubeSats, since it impacts directly the volume of propellant needed for the mission. Looking at Table 1.1 and Table 1.2, it is seen how for chemical propulsion systems the values of I_{sp} range from 230 to 300, depending on the propellant used and on the type of chemical propulsion system adopted: solid, mono-propellant and bi-propellant have the lowest to highest specific impulse values, in this order. Since the specific impulse is directly linked with the amount of Δv budget by the mission already set in requirement PROP-01, an additional requirement on the specific impulse is not included, but the consideration of having an higher specific impulse in order to be minimize the total Δv budget is recommended.

Another requirement is set on the thrusting time t_b : for the MARIO mission, a maximum value of 600 s is chosen in order to limit the gravity losses that can occur in the Earth escape phase. This has shown in the MARIO mission analysis to only produce a 1% increase over the ideal Δv required to escape from the same parking orbit and is considered to be acceptable for this application: it is expected, though, that higher gravity losses will occur in the orbit manoeuvres of this mission since the chemical propulsion system will need to accelerate the spacecraft to an orbit characterized by an higher energy compared to the MARIO case. Furthermore, this limit needs to be taken into account since state-of-the-art systems have shown a continuous pulse mode in the order of minutes to hours, and therefore it can not be chosen to be arbitrarily too high. For these reasons, the maximum burn time of the propulsion system is set to be equal to the requirement from the MARIO mission:

- PROP-03: The maximum burning time t_b shall be 600 s for each time the propulsion system is activated.

Lastly, a requirement is set to ensure the usage of non-toxic propellants: chemical propulsion systems have always been adopting propellants that are too dangerous to be conserved or handled without severe precautions, just like hydrazine. In recent years, a trend towards the usage of green propellant blends has risen and is replacing the old-fashioned propellants that need higher restrictions for handling, storage and filling of tanks. For this propulsion system, the same considerations are adopted:

- PROP-04: The propulsion system shall utilize non-toxic "green" propellant.

This set of 4 requirements for the propulsion system will at first serve in order to perform trajectory simulations for the spacecraft flight, checking the feasibility of the mission and extrapolating the amount of Δv budget for the mission. Afterwards, the same requirements need to be met when the particular propulsion system design will be performed in detail: the specific impulse level will mainly determine the type of propellant(s) to be used and the thrust values will define the shape and dimensions of the thrusters. It has to be noted that no requirement or limit has been put to the mass and volume of the propulsion system: this is because the exact configuration of the spacecraft is still not known and will be fixed after the Δv budget value is obtained, while the initial mass will be guessed based on common total mass values for CubeSat standards.

2.3. Conclusions

This chapter of the thesis work has been dedicated to the definition of the main requirements for a Mars mission that will rely on autonomous navigation from a parking station on Earth, adopting only chemical propulsion. They have been divided between "Mission" requirements, which define the trajectory

that the spacecraft will follow during its flight, and "Propulsion" requirements which are related to the performance of the latter. Their purpose is to provide an indication of what type of flight the satellite must follow, specifically an Earth escape with high impulsive manoeuvres to minimize the time spent orbiting around Earth and a stabilization around Mars, having the peri-apsis of the final orbit within a certain distance from the surface of the planet. Their preliminary formulation is highlighted below in Table 2.2:

Table 2.2: Preliminary mission requirements

ID	Rationale
MISS-E01	The starting orbit is the SSGTO defined by parameters: [51526 km, 0.8705, 0.01°, 0°, 0°, 0°]
MISS-E02	The number of orbit raising manoeuvres around the Earth shall be at most 6.
MISS-E03	The specific energy of the orbit before leaving Earth's sphere of influence shall be at least TBD .
MISS-M01	The final orbit eccentricity after stabilization shall be less than 0.92.
MISS-M02	The peri-apsis of the martian operational orbit shall be less than 5000 km.

On the other hand, the propulsion system requirements need to fix the margins for the performance parameter values of the chemical propulsion system: they are based on the specific mission, as the Δv budget will be dependent on the trajectory followed by the spacecraft, but also from other considerations as minimization of gravity losses and propellant mass. The preliminary chemical propulsion system are shown in Table 2.3.

Table 2.3: Preliminary chemical propulsion system requirements

ID	Rationale
PROP-01	The chemical propulsion system shall provide at minimum $\Delta v = TBD$.
PROP-02	The maximum thrust level of the system shall be 6 N.
PROP-03	The maximum burning time t_b shall be 600 s for each time the propulsion system is activated.
PROP-04	The propulsion system shall utilize non-toxic "green" propellant.

The set of requirements comprises two of them (MISS-E03 and PROP-01) for which the exact values will be completed in the next chapter: specific hypothesis and trajectory estimation for Earth escape and Mars stabilization will check the feasibility of the mission, based on the other mission and propulsion system requirements, and estimate the two parameters that are still unknown. Afterwards, the set of requirements will be complete and the specific chemical propulsion system trade-off and design will begin.

3

Preliminary mission analysis

This chapter is intended to showcase the mission analysis performed to obtain the Δv budget level needed for the CubeSat mission to reach Mars, starting from an orbit around Earth and stabilize around Mars. The mission analysis will be divided into different sections: the departure from the parking orbit around Earth, the Hohmann transfer between Earth and Mars around the Sun and the final brake at Mars in order to reach the target orbit.

3.1. Interplanetary flight assumptions

In order to reach Mars from a parking orbit around Earth, several assumptions need to be used in order to estimate the trajectory of the CubeSat after leaving the sphere of influence of Earth and before the reach of the sphere of influence of Mars. For this matter, the "patched conics" method will serve as a reference for the interplanetary trajectory approximation and the relative Δv required to perform the manoeuvres, which will later be calculated with more precise simulations.

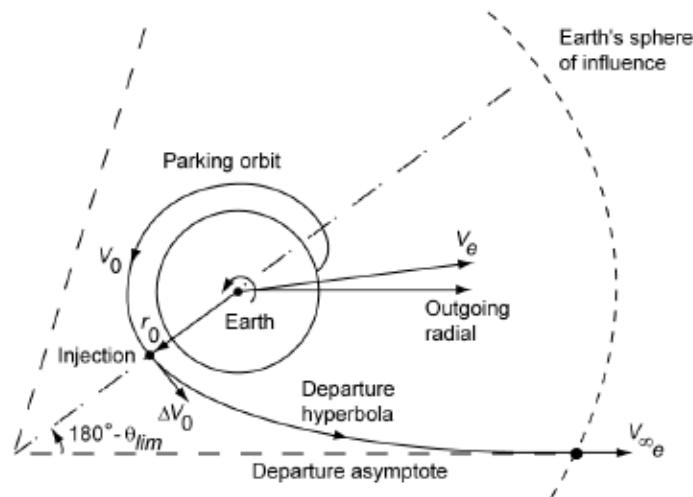


Figure 3.1: Hyperbolic escape trajectory from a parking orbit around Earth [77]

The "patched-conics" method allows for an early estimate of time and required Δv needed for the three phases of the interplanetary flight. Assuming that the spacecraft will perform impulsive boosts for its manoeuvres, the phases are as follows:

1. First manoeuvre boost from the perigee of the parking orbit around Earth, transforming the elliptic orbit into an hyperbolic orbit. This orbit has to be characterized by an "infinite velocity" $v_{\infty E}$ that summed up with the one of the Earth around the Sun, allows for an Hohmann transfer between Earth and Mars.

2. The trajectory of the interplanetary flight around the Sun is then assumed to be an elliptic orbit between Earth and Mars, being in the sphere of influence of the Sun.
3. A braking manoeuvre once arrived near the sphere of influence of Mars, such that the spacecraft brakes from the "infinite velocity" $v_{\infty M}$ with respect to the velocity of Mars around the Sun to an orbit that becomes elliptic and stable around Mars.

The following sections of the chapter will illustrate the calculations made in order to evaluate the amount of Δv required for an interplanetary transfer: at first, ideal values will be obtained from orbital mechanics, using the assumption of the availability of an instantaneous boost of the spacecraft. Afterwards, in order to have a better estimate of the Δv , several simulations taking into account the time needed for each boost will be performed, for both the departure from the Earth's parking orbit and the arrival at the final orbit around Mars.

3.2. Interplanetary transfer

The motion of the spacecraft from Earth to Mars is assumed to be an Hohmann transfer with the two planets, Earth and Mars, on opposite sides with respect to the Sun. This section will serve to evaluate the velocity at which the spacecraft will need to leave and approach each sphere of influence in order to comply to the Hohmann transfer.

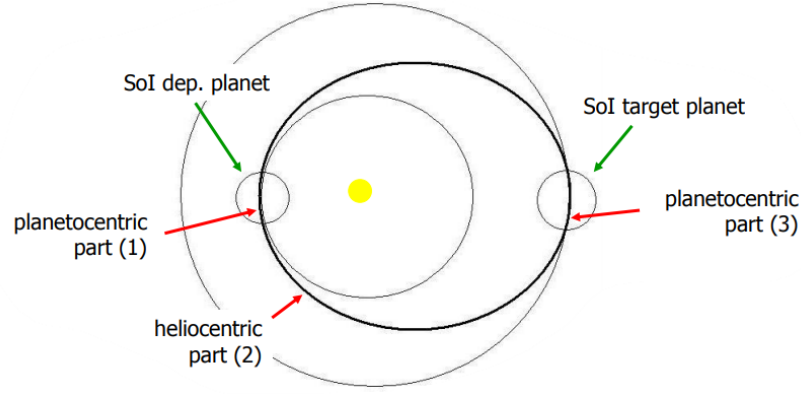


Figure 3.2: Hohmann transfer between Earth (planet 1) and Mars (planet 2) around the Sun [17]

The following table sums up several values that will be used for this purpose: the gravitational parameter (μ) for each planet and the Sun, and the mean distance of each planet from the Sun.

Table 3.1: Gravitational parameters and mean distance from Sun of Earth, Mars and Sun [77]

Celestial object	Gravitational parameter [$km^3 s^{-2}$]	Mean distance from Sun [km]
Earth	$3.986004418 \cdot 10^5$	149600000
Mars	$4.282837 \cdot 10^4$	227900000
Sun	$1.327124400183 \cdot 10^{11}$	-

Assuming equal inclination and circular orbit for the planets, the values of their orbital speed around the sun is obtained using the gravitational parameter of the Sun and their mean distance from it:

$$v_E = \sqrt{\frac{\mu_S}{d_E}} = 29.7844 \text{ km/s} \quad (3.1)$$

$$v_M = \sqrt{\frac{\mu_S}{d_M}} = 24.1314 \text{ km/s} \quad (3.2)$$

These values will be needed for the calculation of the amount of excess velocity (v_{∞}) needed to the spacecraft in order to follow the Hohmann elliptical transfer orbit around the Sun. The semi-major axis and eccentricity of this transfer orbit are:

$$a_{tr} = \frac{d_E + d_M}{2} = 188750000 \text{ km} \quad (3.3)$$

$$e_{tr} = \frac{|d_M - d_E|}{d_M + d_E} = 0.207417 \quad (3.4)$$

The semi-major axis and the eccentricity of the heliocentric orbit to be followed by the spacecraft around the Sun provide information regarding the velocity of the spacecraft itself around the Sun, most notably at the perihelion and at the aphelion, where the two planets are placed with respect to this transfer orbit. The relative velocity of the spacecraft with respect to the Sun at Earth and Mars position is, respectively:

$$v_{sat/S_E} = \sqrt{\mu_S \left(\frac{2}{d_E} - \frac{1}{a_{tr}} \right)} = 32.7279 \text{ km/s} \quad (3.5)$$

$$v_{sat/S_M} = \sqrt{\mu_S \left(\frac{2}{d_M} - \frac{1}{a_{tr}} \right)} = 21.4835 \text{ km/s} \quad (3.6)$$

Finally, these latter values can be used to calculate the relative velocity between each planet and the spacecraft, which will represent the excess velocity of the hyperbolic trajectory that the spacecraft needs to have when leaving Earth and when approaching Mars, respectively:

$$v_{\infty E} = |v_{sat/S_E} - v_E| = 2.94346 \text{ km/s} \quad (3.7)$$

$$v_{\infty M} = |v_{sat/S_M} - v_M| = 2.64792 \text{ km/s} \quad (3.8)$$

These two velocities will play a crucial role in the estimate of Δv for the interplanetary transfer:

- The first value is the "infinite velocity" that the spacecraft must possess when exiting the sphere of influence of the Earth, therefore the propulsion system needs to be able to not only propel the spacecraft just enough to leave Earth's sphere of influence, but it shall also provide additional energy to reach this precise infinite velocity.
- The second value is the "infinite velocity" at which the spacecraft will approach Mars after entering its sphere of influence.

Since they will be used for simulation purposes, it is useful to also calculate the specific (per unit mass) energy of the hyperbolic orbits associated with these "infinite velocities":

$$E_{\infty E} = \frac{v_{\infty E}^2}{2} = 4.332 \text{ km}^2/\text{s}^2 \quad (3.9)$$

$$E_{\infty M} = \frac{v_{\infty M}^2}{2} = 3.5057 \text{ km}^2/\text{s}^2 \quad (3.10)$$

The transfer time between escaping the sphere of influence of the Earth and entering the sphere of influence of Mars is obtained with:

$$T_{sun} = \pi \sqrt{\frac{a_{tr}^3}{\mu_s}} = 258 \text{ d} = 0.71 \text{ y} \quad (3.11)$$

The specific energy value of the hyperbolic orbit used to leave the sphere of influence of Earth completes the mission requirement MISS-E03, that was missing from the earlier chapter. Its complete formulation is shown below:

- MISS-E03: the specific energy of the orbit before leaving Earth's sphere of influence shall be at least $4.332 \text{ km}^2/\text{s}^2$.

This orbit energy value will be important when simulating the trajectory followed by the spacecraft when leaving the sphere of influence of the Earth: since the manoeuvres will not be impulsive, it will not be possible to perform a single boost and follow an orbit characterized by the infinite velocity $v_{\infty E}$ and energy $E_{\infty E}$. The latter value will be used as a reference to check whether, after performing several thrust manoeuvres, the orbit specific energy value is the same as $E_{\infty E}$, allowing for a correct interplanetary transfer. This requirement on the energy departure level is usually referred in literature as the characteristic energy, $C_3 = v_{\infty E}^2 = 2E_{\infty E}$. Based on the year and the relative position of Earth and Mars, a different optimal value for C_3 is required to reach Mars from Earth, which ranges from 7.8 up to $14.8 \text{ km}^2/\text{s}^2$ [34] [13]. For this case, the C_3 value is $C_3 = v_{\infty E}^2 = 8.664 \text{ km}^2/\text{s}^2$.

3.3. Earth escape

In order to establish the value of the Δv required to escape Earth, the initial parking orbit Keplerian values need to be known. The parking orbit of the satellite around Earth is assumed to be the SSGTO (Super synchronous geostationary transfer orbit) characterized by the orbit parameters found in Table 2.1 [35].

The perigee position with respect to the Earth center and the velocity at the perigee of a satellite following this orbit are:

$$r_{perE} = a(1 - e) = 6672.617 \text{ km}$$

$$v_{perE} = \sqrt{\frac{\mu_E(1 + e)}{a(1 - e)}} = 10.5706 \text{ km/s}$$

As a first estimate of the Δv requirement for the first phase of the patched-conics method, it is possible to assume that a single impulsive manoeuvre performed in the perigee of the parking orbit will suffice to vary the orbit of the satellite, such that it reaches the perigee velocity of an hyperbolic orbit characterized by the "infinite velocity" of Equation (3.7). The velocity of the satellite in this hyperbolic trajectory are calculated as follows, by first evaluating the escape velocity (v_{escE}):

$$v_{escE} = \sqrt{2 \frac{\mu_E}{r_{perE}}} = 10.9304 \text{ km/s}$$

$$v_{hypE} = \sqrt{v_{escE}^2 + v_{\infty E}^2} = 11.3198 \text{ km/s}$$

Therefore, the ideal (impulsive) Δv required for this Earth escape manoeuvre is:

$$\Delta v_{idE} = v_{hypE} - v_{perE} = 749.2 \text{ m/s} \quad (3.12)$$

This result is based on the main assumption that the satellite may be able to perform impulsive manoeuvres at the perigee of the parking orbit, and therefore will be the lowest Δv requirement possible for this manoeuvre: since such a result may give only a first estimate of the required Δv needed to reach the chosen hyperbolic orbit, a series of simulation have been performed on the MATLAB/Simulink environment in order to take into account the finite burn time of the manoeuvres, which leads to gravity losses and therefore a higher Δv budget.

3.3.1. Simulation procedure

Problem approach In a real case scenario, departure from Earth is achieved by performing several burns around the perigee orbit perigee to maximize the effect of impulsive boosts. Mass expelled by the thrusters is limited by the performance parameters that the propulsion system can achieve, but most notably by the limited burn time t_b , which poses a severe constraint on how long the thrusters can be active for. Furthermore, the limitation on thrust capabilities of CubeSat propulsion systems further

reduce the amount of Δv that can be delivered with a single manoeuvre. The purpose of this section is to highlight the procedure undertaken to generate realistic Δv values for the Earth escape part of the mission, by taking into account gravity loss effects and continuous time manoeuvres. By doing this, it is possible to have a better estimate of the real Δv budget that needs to be taken into account for the first section of the mission, while respecting the mission requirements for this phase.

Due to the limitations on performance parameters of the propulsion system, it can be expected that the Earth escape phase will be divided into two different phases. In fact, since each single manoeuvre will deliver a limited amount of Δv , the energy of the orbit followed by the satellite will increase in small steps, and two different strategies for two different phases of manoeuvres need to be implemented to achieve Earth escape:

1. A first closed orbit phase, where the satellite will perform boost around the perigee increasing the specific energy of its orbit, which will still remain closed around Earth. In this phase, the energy of the orbit will still be lower than 0, while the eccentricity will be lower than 1.
2. A second open orbit phase, where the orbit of the satellite will reach an orbit energy higher than 1, therefore becoming hyperbolic. During this phase, the satellite shall continue to perform manoeuvres while travelling farther from Earth, in order to obtain an orbit energy characterized by the "infinite velocity" $v_{\infty E}$ calculated in Equation (3.7), before it reaches the sphere of influence of the Earth.

These two different phases of the Earth escape procedure are characterized by different strategies that need to be designed specifically for the two cases: during the closed orbit phase, it will be crucial to evaluate at which true anomaly to start the manoeuvre to maximize the increase of the orbit energy around Earth, while during the second hyperbolic phase several burns will need to be performed as close to the Earth as possible to reach the orbit energy that will allow for the interplanetary transfer described earlier.

Simulation environment description The value for the Δv budget for the two phases of Earth escape will be obtained by simulating the trajectory of the satellite around the Earth, while time-continuous manoeuvres will be performed by its propulsion system: this will steadily increase the energy of the orbit of the satellite, leading to a successful Earth escape characterized by an orbit with "infinite velocity" $v_{\infty E}$ found in Equation (3.7).

The simulations will be performed on MATLAB/Simulink environment: a MATLAB script will be used to initialize the initial parameters of the parking orbit, the satellite position and velocity and the propulsion system parameters. A first Simulink model is used to describe the motion of the satellite around the Earth and perform the orbit raising manoeuvres. The input parameters that can be modified by the user for the simulations are four: the thrust T , the specific impulse I_{sp} , the initial satellite mass M_0 and the burn time t_b . Taking these four values into account, the simulator performs the orbit raising and Earth escape by taking into account the maximum allowable burn time t_b and calculates where to start the manoeuvre before reaching the perigee: in this way, half of the manoeuvre is performed before reaching the perigee and the other half after the perigee.

The orbital equation of motion is integrated over the simulation time:

$$\ddot{\vec{r}} = -\frac{\mu_e}{\|\vec{r}\|^3}\vec{r} + \frac{\vec{T}}{m} \quad (3.13)$$

The equation is written to find the instantaneous acceleration vector of the satellite: the first term of the right side of the equation describes the effect of the gravitational attraction between the Earth and the satellite, while the second term takes into account the effect of the thrust provided by the propulsion system, with the mass of the satellite expressed with the symbol m .

The "actual" mass of the satellite is evaluated by taking the initial satellite mass and subtracting the mass of propellant expelled, which will be dependent on the propulsion system parameters and the total time the propulsion system has been active t_{btot} :

$$M_p = \frac{T}{I_{sp}g_0} \int_0^{t_{btot}} dt \quad (3.14)$$

$$m = M_{in} - M_p \quad (3.15)$$

The thrust acting on the satellite is assumed to be parallel to the current velocity vector of the satellite when in orbit. For this early analysis level, thrust is assumed to be constant when the propulsion system is activated. Therefore the thrust vector can be written as:

$$\vec{T} = T \cdot \frac{\vec{v}}{\|\vec{v}\|} \quad (3.16)$$

If no manoeuvres need to be performed, the value of the thrust is null: $\vec{T} = [0, 0] N$

In order to evaluate the orbit arc in which the manoeuvre shall be performed each time, the input value of the burn time t_b is used. It is best to perform manoeuvres around the perigee of the orbit to minimize the effect of gravity losses, since there is an angular difference between the normal to the position vector and the flight path angle, as shown in the figure below.

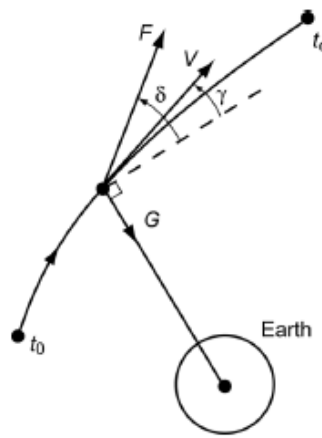


Figure 3.3: Geometry of powered flight and a definition of the flight path angle γ , and the thrust angle δ [77]

For the case analysed in this thesis work, it is assumed that the thrust is aligned with the trajectory followed by the satellite, therefore $\delta = \gamma$. Even with this assumption, there will always be the effect of gravity losses in a real orbital manoeuvre since the angle γ will be always different from 0 in an elliptical orbit (except in the pericenter), with the lowest values appearing around the pericenter of the orbit. The gravity losses will only be null if the thrust vector is continuously perpendicular to the position vector of the satellite, therefore in order to minimize them it is best to manoeuvre around the pericenter of the orbit.

To evaluate where to start performing each manoeuvre when orbiting around the Earth, the input value of the burn time t_b is used: in fact, as can be seen from the following equations, it is possible to calculate at which value of true anomaly of the current orbit the satellite will take half of the burn time $\frac{t_b}{2}$ to reach the perigee. In this way, the manoeuvre can be started at this value θ_{man} of true anomaly of the orbit and will last for t_b seconds, maximizing the effect of the manoeuvre by operating symmetrically with respect to the perigee.

$$E_{man} - e \sin E_{man} = \sqrt{\frac{\mu_e}{a^3}} \cdot \frac{t_b}{2} \quad (3.17)$$

$$\theta_{man} = 2 \arctan \left[\sqrt{\frac{1+e}{1-e}} \tan \left(\frac{E_{man}}{2} \right) \right] \quad (3.18)$$

Equation (3.17) is solved by using the input burn time t_b and the Keplerian parameters of the current orbit a and e , that will vary each time a manoeuvre is performed since the orbit energy will increase

after each manoeuvre. This transcendental equation is solved using the function "fzero" in MATLAB and will output the value of the eccentric anomaly of the manoeuvre E_{man} . Finally, Equation (3.18) is used in order to evaluate the true anomaly at which the manoeuvre shall start: it takes the orbit parameters and the previously calculated eccentric anomaly of the manoeuvre E_{man} and outputs the true anomaly value at which the satellite will take $\frac{t_b}{2}$ time to reach the perigee of the orbit. When the satellite reaches this true anomaly of the orbit, the manoeuvre is then started and lasts for t_b seconds. If the orbit is still closed, which means the energy of the orbit is still negative, the semi-major axis value and the eccentricity of the orbit are used to evaluate the new true anomaly at which it is best to perform the manoeuvre, maintaining the constraint of only lasting t_b seconds.

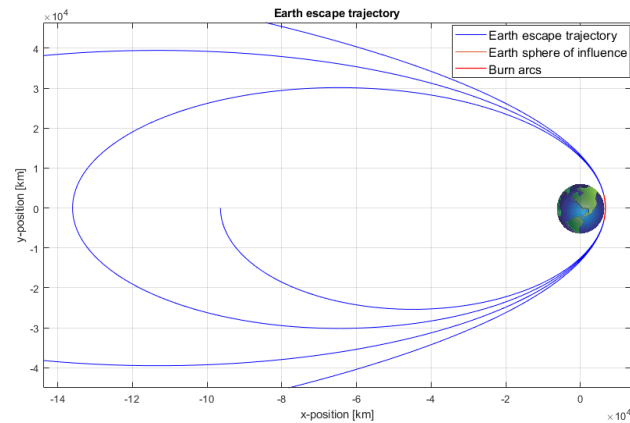
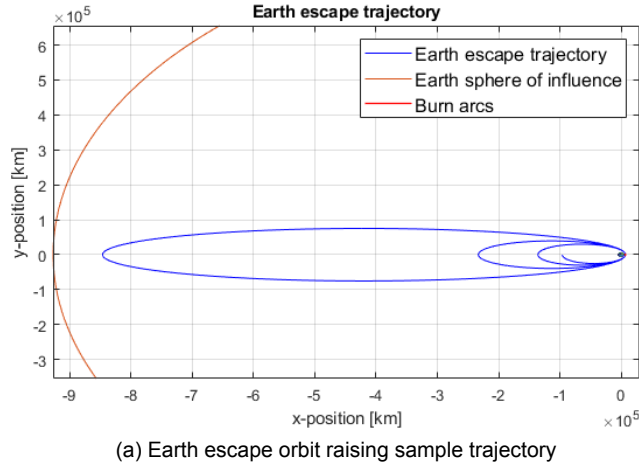
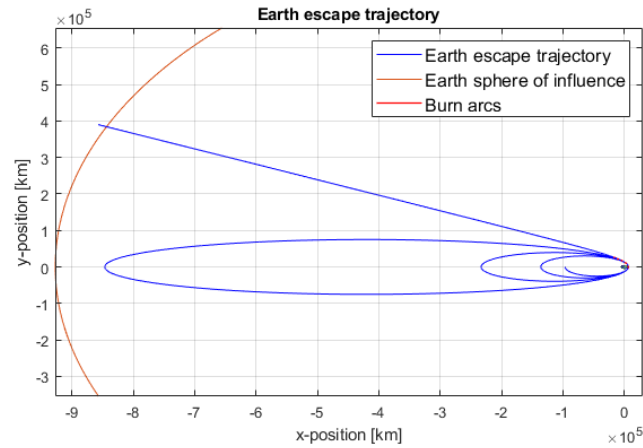


Figure 3.4: Example of orbit raising strategy

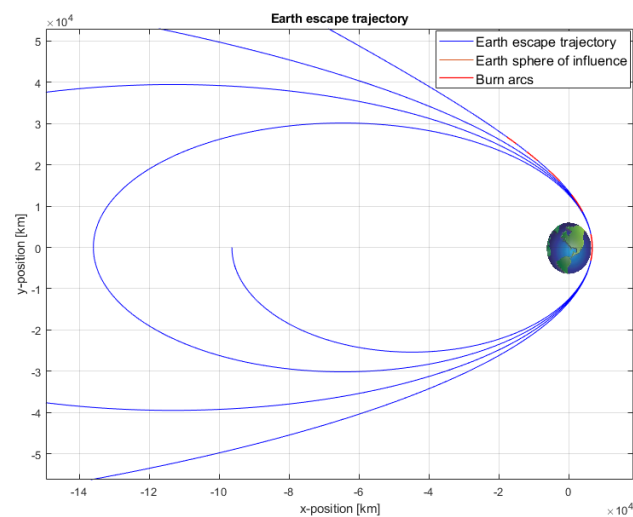
Figure 3.4 shows an example of the orbit raising strategy described: the satellite starts from a generic position in the SSGTO (the true anomaly at which the simulation starts has been chosen to be $\theta_0 = \pi$ without loss of generality) and then it performs several boosts around the perigee lasting for t_b seconds. Each manoeuvre increases the energy of the orbit, meaning that its semi-major axis and eccentricity values rise. In 3.4 (b) it is possible to see that the position at which the manoeuvres start to take place is similar, and close to the perigee of the orbit. This procedure is repeated until the last manoeuvre makes the orbit become hyperbolic.

Once the last manoeuvre using this strategy makes the energy of the orbit become positive, the final values of position and velocity vectors are saved and sent to the second part of the simulation. As it has been described in the previous sections, the satellite does not only need to reach an orbit with a positive value with respect to Earth, but it also need to reach a specific value of energy which is characterized by the "infinite velocity" $v_{\infty E}$ calculated in Equation (3.7). Due to the restricted amount of

burn time available, reaching an higher value of orbit energy will be possible by continuing to perform boosts after the orbit has become hyperbolic. This means that a new strategy has to be implemented since the previous one is not applicable. For this instance, a simpler approach can be used: once the last manoeuvre around the Earth has been performed, the subsequent manoeuvres will be performed along the hyperbolic trajectory of the satellite leaving Earth.



(a) Earth escape sample trajectory



(b) Earth escape sample trajectory zoomed around the perigee

Figure 3.5: Successful Earth escape sample trajectory, showing the manoeuvres performed after the orbit raisings

These manoeuvres will be characterized by the same duration t_b as the previous part of Earth escape, but a new constraint has to be considered: the time between each of the burns, which will be named Δt_b . For the previous part of the Earth escape simulation, this constraint is negligible since each burn is performed after a long time-span from the previous one, since the satellite needs to travel around Earth and reach the new true anomaly θ_{man} for the next manoeuvre. In this case, however, this variable will play a crucial role on the value of Δv that will be needed to reach the required orbit energy, since these manoeuvres will be performed at increasingly higher distance from the Earth. The strategy for the manoeuvres to be executed after the orbit has become hyperbolic is simpler than the previous one, and will be characterized by a square-wave: the satellite will need to wait the set amount of time Δt_b from the previous manoeuvre and then will start a new burn that will last for t_b seconds, parallel to the velocity vector as in the earlier described case. If the orbit energy still does not meet the requirement for the "infinite velocity" $v_{\infty E}$, the same procedure is repeated: again, the Δt_b constraint will

be respected and another burn will be executed. This will be repeated until the orbit energy does not meet the requirement, with the last manoeuvre stopping before exceeding the energy target. Figure 3.5 showcases the result for a full Earth escape simulation using the same inputs as Figure 3.4: the satellite follows an hyperbolic (open) orbit around the Earth and repeatedly activates the propulsion system to increase the energy of its orbit, following the strategy described earlier. It is set to wait Δt_b from the last manoeuvre and then, if the value of set orbit energy is still not reached, it performs a manoeuvre lasting for a maximum of t_b . In Figure 3.5 (b) it is possible to see that the satellite performs other 4 manoeuvres after reaching an hyperbolic orbit, and in Figure 3.5 (a) the full path until the Earth's sphere of influence is reached.

Verification of results From this early stage of development, it is possible to already check that the results obtained by the simulations are indeed realistic and correct. This can be done by checking the ideal Δv that each manoeuvre can provide to the satellite, as well as the change in orbit energy. The mass of propellant can be found by integrating for each burn time duration Equation (3.14), obtaining the mass of propellant burned for each manoeuvre:

$$M_{pi} = \frac{T \cdot t_b}{I_{sp} \cdot g_0} \quad (3.19)$$

If the hypothesis of instantaneous burn is performed, it is possible to estimate the Δv delivered by each manoeuvre:

$$\Delta v_i = -I_{sp} g_0 \ln \left(1 - \frac{M_{pi}}{M_{oi}} \right) = -I_{sp} g_0 \ln \left(1 - \frac{T \cdot t_b}{M_{oi} \cdot I_{sp} \cdot g_0} \right) \quad (3.20)$$

Then, it is possible to estimate the ideal change in specific energy of the orbit, by assuming an impulsive manoeuvre in the perigee: each time an ideal manoeuvre is performed, the Δv_i is obtained in Equation (3.20) and it is assumed that the change in velocity is fully provided to the satellite, and that the perigee altitude does not change. In this way, a good estimate of the effect of each manoeuvre is obtained, and it is possible to confront the ideal results with the ones obtained by the simulations, in order to verify that the simulation environment is providing accurate results. Before and after each manoeuvre, the initial mass of the satellite and the current specific orbit energy can be calculated using:

$$M_{oi} = M_0 - n_{man} \cdot M_p \quad (3.21)$$

$$E_{orb} = -\frac{\mu_E}{r_{perE}} + \frac{(v_{perE} + \Delta v_1 + \dots + \Delta v_{n_{man}})^2}{2} \quad (3.22)$$

Two sample results using propulsion system performance values in the range of chemical propulsion system of interest are shown in the tables below: they prove that the results, in terms of Δv budget, are in the same range as the ideal cases. As expected, after each manoeuvre the orbit energy value is lower than the ideal case: this is due to effects of gravity losses, as already discussed earlier in Figure 3.3, since the manoeuvre times are longer than the ideal instantaneous case.

Table 3.2: Specific energy $\left[\frac{km^2}{s^2} \right]$ of orbit after orbit raising manoeuvres around Earth ($T = 4.1 N$, $M_0 = 25 \text{ kg}$, $I_{sp} = 240 \text{ s}$, $t_b = 600 \text{ s}$)

n_{man}	Simulation	Ideal case
1	-2.8102	-2.8004
2	-1.6950	-1.6744
3	-0.5167	-0.4841
4	0.7315	0.7775

Table 3.3: Specific energy $\left[\frac{km^2}{s^2} \right]$ of orbit after orbit raising manoeuvres around Earth ($T = 6 N$, $M_0 = 30 \text{ kg}$, $I_{sp} = 280 \text{ s}$, $t_b = 500 \text{ s}$)

n_{man}	Simulation	Ideal case
1	-2.7930	-2.7860
2	-1.6660	-1.6513
3	-0.4825	-0.4594
4	0.7626	0.7952

Further verification is obtained by performing simulations of Earth escape with lower burn time t_b available to the satellite: in this way, the results shall be much more similar to the ideal case, in which the

hypothesis of instantaneous burn is chosen. The following tables highlight the results obtained for the same set of parameters shown before, with a burn time divided by a factor of 10 to ensure a quicker manoeuvre and a thrust level of 10 higher, to make sure that the mass of propellant expelled in each manoeuvre is the same, as expected from Equation (3.19):

Table 3.4: Specific energy $\left[\frac{km^2}{s^2}\right]$ of orbit after orbit raising manoeuvres around Earth ($T = 41 N$, $M_0 = 25 \text{ kg}$, $I_{sp} = 240 \text{ s}$, $t_b = 60 \text{ s}$)

n_{man}	Simulation	Ideal case
1	-2.8004	-2.8004
2	-1.6745	-1.6744
3	-0.4842	-0.4841
4	0.7770	0.7775

Table 3.5: Specific energy $\left[\frac{km^2}{s^2}\right]$ of orbit after orbit raising manoeuvres around Earth ($T = 60 N$, $M_0 = 30 \text{ kg}$, $I_{sp} = 280 \text{ s}$, $t_b = 50 \text{ s}$)

n_{man}	Simulation	Ideal case
1	-2.7860	-2.7860
2	-1.6514	-1.6513
3	-0.4595	-0.4594
4	0.7948	0.7952

As expected, lowering the burn time t_b of each manoeuvre causes the orbit specific energy values obtained to be much closer to the ideal case, since the latter is obtained by assuming an instantaneous burn. Therefore, the MATLAB/Simulink results are realistic and will provide a good approximation of the budget Δv needed to escape Earth with a CubeSat from the initial parking orbit, by also taking into account the effects of gravity losses that will be present for realistic continuous burn-time manoeuvres.

Validation of results To validate the results of the Earth escape simulations, the inputs from the MARIO trajectory analysis are investigated [37]. For the MARIO mission, the Earth escape phase of the mission is deemed successful when the satellite manages to reach a level of specific energy of $0 \text{ km}^2/\text{s}^2$, corresponding to an ideal parabolic orbit. Differently from the Earth escape of this thesis work, there are no manoeuvres involved after the orbit of the satellite has become open. Nevertheless, the inputs from [37] are shown in Table 3.6:

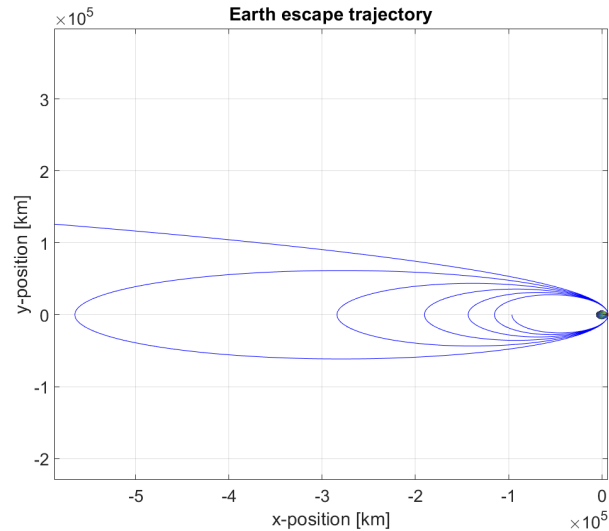
Table 3.6: MARIO mission parameters for orbit raising and Earth escape

Parameter	Value
Initial Mass, m_i	32 kg
Thrust, T	3 N
Specific Impulse, I_{sp}	241.2 s
Burn Time per maneuver, t_b	598.6 s
Orbit raising maneuvers	6
Ideal ΔV_{esc}	359.66 m/s
Real ΔV_{esc}	363.14 m/s
Margined $\Delta V_{esc,mg}$ (10% margin)	396 m/s

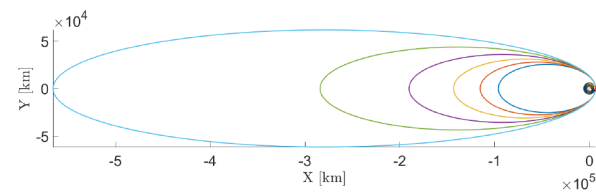
Adopting the same inputs in the MATLAB/Simulink environment developed for the thesis work generates an orbit escape within 6 manoeuvres, in which the Δv budget for Earth escape is $\Delta v = 363.220 \text{ m/s}$, resulting in a relative error of 0.02% with the result from [37] of $\Delta v = 363.14 \text{ m/s}$. This shows that the simulation environment written for the thesis work regarding the Earth escape phase of the mission correctly estimates the amount of gravity losses, being supported by relevant literature in the same topic. Furthermore, the number of orbit raisings are the same (6) to achieve Earth escape, and the orbit dimensions are comparable as can be seen from Figure 3.6.

3.3.2. Earth escape simulation results

This section will be reserved to the showcase of the results of the simulations described earlier in order to estimate the real amount of Δv budget that will be needed for a CubeSat to achieve Earth escape when parked in a SSGTO parking orbit. These results will take into account the available technological advance that is currently under development for propulsion system adapted to a CubeSat level: as described earlier, thrust values range from $0.1 N$ up to $5 N$ for single thrusters, while the I_{sp} values range from 230 to 320 seconds, varying between solid propulsion systems up to bi-propellant systems.



(a) Earth escape simulation adopting inputs from MARIO mission



(b) MARIO Earth escape trajectory analysis [37]

Figure 3.6: Comparison between Earth escape orbits to validate the results from the MATLAB/Simulink script

The previous methods for Earth escape have been implemented to work together, taking the final results of the first phase as inputs to the second phase, where the orbit becomes hyperbolic. The two most important variables for the simulation are shown below, and will be used to represent the Δv budget results on the x-axis and y-axis, respectively:

- Thrust (T): the maximum thrust that the propulsion system can provide to the satellite. At each manoeuvre, the simulation tool will integrate Equation (3.13) using the chosen value of thrust, for both the first and second phase of Earth escape. As mentioned earlier, thrust is assumed to be constant when the propulsion system is activated: throughout the mission, it is expected that the real value of thrust can become lower due to degradation of the nozzle or other propulsion system components. This is not considered at this early stage of mission analysis, but the final Δv budget will be margined.
- Burn time (t_b): the value that dictates for how long the propulsion system can be active to perform a manoeuvre, before needing to shut off.

There are several other inputs that can be modified by the user and will serve to indicate different types of satellite and propellants, and will change the results of the Δv budget needs. When displaying the results, since these variables will not be shown on any axis, will be described earlier to mention their values:

- Initial satellite mass (M_0): the initial wet mass of the satellite at launch. Several simulations are going to be performed for different values of initial mass, to gauge the effect of having a lower mass satellite with a bigger one, and understand the effects of increasing mass on realistic manoeuvring to escape Earth.
- Propellant specific impulse (I_{sp}): one of the most important parameters of the propulsion system, describing how effectively propellant mass is transformed into impulse by the propulsion system.

- Time between burns (Δt_b) : value affecting the second phase of Earth escape. This value will put a severe constraint on how much time needs to be waited to re-start the propulsion system when moving along an hyperbolic escape trajectory.

Two constraints have been chosen for the problem in order to satisfy the mission requirements related to a swift Earth escape manoeuvring:

- The total time spent around Earth with a closed orbit from operation start shall be lower than 1000 hours. A longer residence time would mean that the satellite will pass several times through the Van Allen belts, increasing the risk of electronics malfunction due to ionizing doses.
- The maximum distance point from Earth shall be lower than a 0.9 factor from the sphere of influence of the Earth. The sphere of influence concept is crucial in this simulation since it defines the ideal volume in which the satellite motion can be described as a two-body problem without the effect of third celestial objects. The radius of the sphere of influence of Earth is $R_{SOIE} = 9.2701 \cdot 10^5$ km [77].

The results have been obtained by approaching the problem with one variable being the thrust level (T) while fixing the burn time (t_b) at first, and then moving onto a 2D domain and running simulations for both cases. With this approach, code debugging and verification and validation have resulted to be easier and helped in parallel with the full 2D variable domain solving of the problem. This procedure is described thoroughly in Appendix A. While the first approach to the problem has served as an easier developing step to finding the required Δv budget of the Earth escape part of the mission, the next one will merge these results with another variable to the most optimal burn time t_b allowed by currently available propulsion systems to achieve fast Earth escape. For this reason, the burn time t_b allowed for each manoeuvre will be used as a variable, changing its value within range in order to check what different solutions will be available for the design of the first part of the mission. Differently from the 1-D approach, where only thrust was varied throughout the simulations, the results will be shown having the thrust levels on the X-axis and the burn time on the Y-axis.

The values in which the variables can range is chosen to be:

- Thrust (T) varies between 4 and 6 N, since currently available propulsion systems range between 1 and 1.5 N of thrust: it is expected to remain in these values and have a 4-formation of such thrusters. Furthermore, as seen in the previous 1-D results, the Δv values obtained for Earth escape with thrust lower than 4 N are much higher than the ones between 4 and 6 N.
- Burn time (t_b) varies between 400 and 600 s: lower values do not allow Earth escape given the constraints of time spent orbiting around Earth and low passes through the Van-Allen belts. The same values are also used in [36].
- $\Delta t_b \geq t_b$. In order to be consistent with every manoeuvre, it is expected that the time between each manoeuvre shall at least be t_b .
- Initial satellite mass (M_0) is chosen to be between 25 and 35 kg, since it is expected for the Cubesats units to be at least 12U. The simulations are run for 3 different values of initial satellite mass: 25, 30 and 35 kg.
- Propellant specific impulse (I_{sp}) for chemical propulsion system is, based on the literature, between 230 and 300 s: the simulations are run for 5 different values of propulsion system I_{sp} : 230, 240, 260, 280 and 300 s.

25 kg CubeSat The result for an initial CubeSat mass of $M_0 = 25$ kg is shown below in Figure 3.7. The figure relates to the specific case of I_{sp} of 230 s: the graphic results for all of the specific impulse values are not shown since the shape is almost equal to the one highlighted in Figure 3.7. This reference image is used to identify the "optimal" points of the surface, which have been already highlighted in the figure: the Δv values for such points will be displayed in Table 3.7.

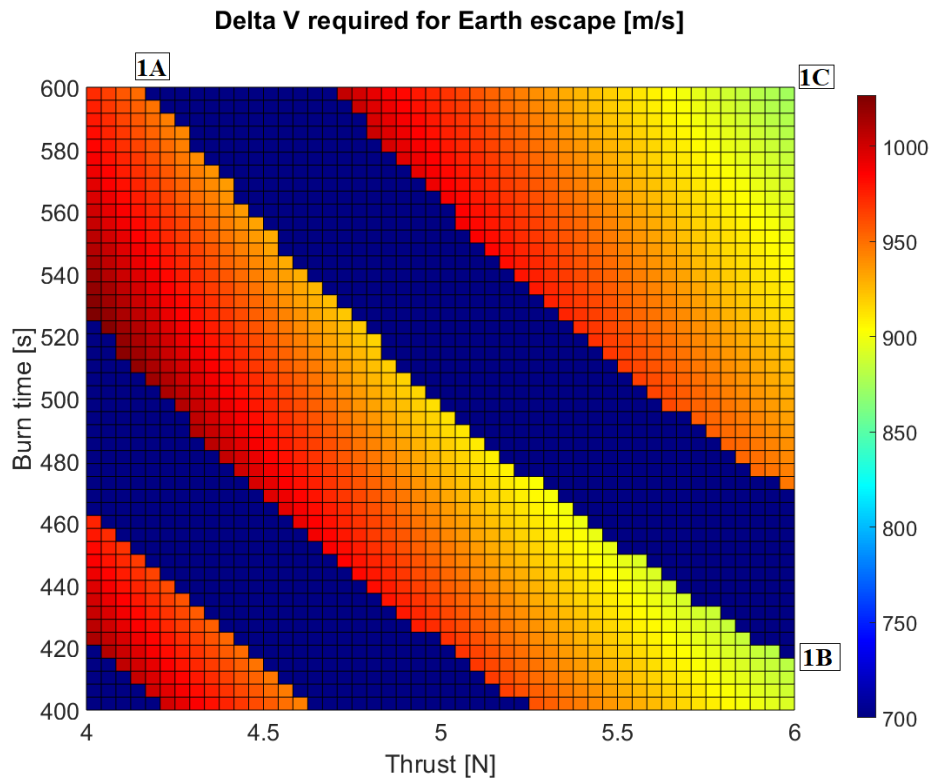


Figure 3.7: Δv budget needed for Earth escape: initial satellite mass $M_0 = 25$ kg, propellant specific impulse $I_{sp} = 230$ s

In Figure 3.7 (and for the following ones), the input values of thrust and burn time which do not allow for Earth escape given the set constraints, are showed with a Δv value in blue, to omit them from the successful ones. It can be noticed that the set of solutions for which Earth escape is successful is similar to 1-D problem approach described in Appendix A: the successful solutions are grouped in "waves", each one representing a different number of orbit raisings needed around Earth. For lower levels of thrust and burn time, more time will be spent orbiting around Earth and more Δv will be needed to complete Earth escape.

The Δv budget for this phase of the mission tends to be minimized when moving towards the bottom-right part of the domain by its nature, but the domain provides optimal solutions also moving in the top-right direction. For all of the five different I_{sp} inputs chosen, 3 points are the most interesting in terms of optimization of Δv . They are shown in Figure 3.7 and are named 1A, 1B and 1C.

Table 3.7: Earth escape Δv budget for $M_0 = 25$ kg

I_{sp}	Point 1A			Point 1B			Point 1C		
	Thrust [N]	Burn time [s]	Δv [m/s]	Thrust [N]	Burn time [s]	Δv [m/s]	Thrust [N]	Burn time [s]	Δv [m/s]
230	4.125	600	948.3	6	408.3	881.8	6	600	868.2
240	4.125	600	951.6	6	412.5	881.2	6	600	871
260	4.167	600	951.2	6	412.5	885.8	6	600	876
280	4.167	600	956.5	6	416.7	886.5	6	600	880.2
300	4.167	600	961.3	6	416.7	889.9	6	600	883.8

The input values for each of these points are shown in Table 3.7, together with the reference I_{sp} used for the simulation set, and the resulting Δv budget for Earth escape by using the relative thrust and burn time corresponding to each point. It has to be noted that each of these points has a relatively optimal Δv , being on the Pareto front for each wave or being on the edge of the domain, therefore it is mostly preferred to work under these propulsion system performance levels. Each of the values show that it is possible to achieve Earth escape with a Δv budget lower than 900 m/s if points 1B or 1C are chosen

and the satellite mass is 25 kg, given the availability of 6 N of thrust. Points 1B and 1C show that with the same amount of thrust and different burn time, a similar Δv budget is needed: this is caused by how the manoeuvres are performed in the second phase of Earth escape. While for the orbit raising part the gravity losses are minimal in both cases, they become much higher when activating the thruster along the hyperbolic orbit. The variable Δt_b has been set to be equal to the burn time t_b : this means that if a propulsion system is able to continuously fire for t_b seconds, then it will need the same amount of time before it can start the thrusters firing again. Along the hyperbolic orbit of the satellite, this means that in case 1B the satellite can activate the thrusters earlier than in case 1C, which leads to lower gravity losses. But when thrusters can be activated again for case 1C, the thrusters can be active for longer time t_b : these two effects counterbalance each other: with lower t_b , the thrusters can be activated for lower time during the hyperbolic earth escape phase, but more frequently, and the opposite for the cases in which the burn time is higher. If 6 N of thrust is a value too high to be obtained by the propulsion system, point 1A shows that Earth escape is possible with a thrust level just lower than 4.2 N, but with an higher Δv budget of around 950 m/s. All of the other points on the edge of the solution "wave" as point 1A allow for a successful Earth escape with lower Δv with respect to point 1A, but with increasing thrust level constraints.

A consideration needs to be made to explain the increase in Δv budget trend with increasing I_{sp} : at first it may seem counter-intuitive, but the reason for this difference lies in the two phases of the Earth escape plan. Given the same values of thrust and burn time, a different amount of propellant is expelled based on the propulsion system I_{sp} : considering a case with higher I_{sp} , the final specific energy of the orbit after all of the manoeuvres around Earth have been performed will be lower since less propellant is expelled, if the I_{sp} is higher. Therefore, to achieve the energy requirement given by MISS-E03, the propulsion system will need to be active for more time in the second phase of Earth escape, during its hyperbolic trajectory. Since this phase of the mission comprehends manoeuvres far away from the perigee of the orbit, they will be less efficient in terms of the amount of energy and momentum increase compared to the first phase: the propulsion system will need to be active for more time compared to a case where the I_{sp} is lower, and more gravity losses will occur. These consideration do not make a propulsion system with higher I_{sp} less preferable than a propulsion system characterized by a lower specific impulse: indeed, the small increase in terms of Δv is highly surpassed by the effect of having an higher specific impulse. The corresponding propellant mass burned for the Earth escape phases are indeed lower for increasing specific impulse, as expected.

30 kg satellite In Figure 3.8 the Δv budget is shown for an initial satellite mass of $M_0 = 30$ kg. The shape of the graph changes, moving further towards the top-right section of the domain: this is reasonable, since satisfying the mission requirements with high-impulsive manoeuvres for an higher initial satellite mass will require more thrust. The overall shape of the results does not change significantly by varying the specific impulse, and once again three relevant points will be highlighted for this case: they are named points 2A, 2B and 2C.

Table 3.8 shows the Δv budget for the three points of interest: as expected, for most of the combinations of thrust and burn time, an higher level of Δv is required with respect to the ones obtained for an initial satellite mass of 25 kg. Point 2B exhibits the lower Δv budget of the three, being characterized by the highest level of thrust available. The other two points provide solutions in which 6 N of thrust are not available, but still the Δv budget is small enough to consider them as optimal solution, given the lower thrust availability scenario.

Table 3.8: Earth escape Δv budget for $M_0 = 30$ kg

I_{sp}	Point 2A			Point 2B			Point 2C		
	Thrust [N]	Burn time [s]	Δv [m/s]	Thrust [N]	Burn time [s]	Δv [m/s]	Thrust [N]	Burn time [s]	Δv [m/s]
230	4.958	600	947.3	6	491.7	912.7	5.5	400	944.3
240	4.958	600	950.6	6	495.8	912.5	5.542	400	943
260	5	600	951.2	6	495.8	917.7	5.542	400	948.6
280	5	600	956.5	6	500	919.1	5.583	400	948.9
300	5.042	600	955.7	6	500	922.9	5.583	400	953

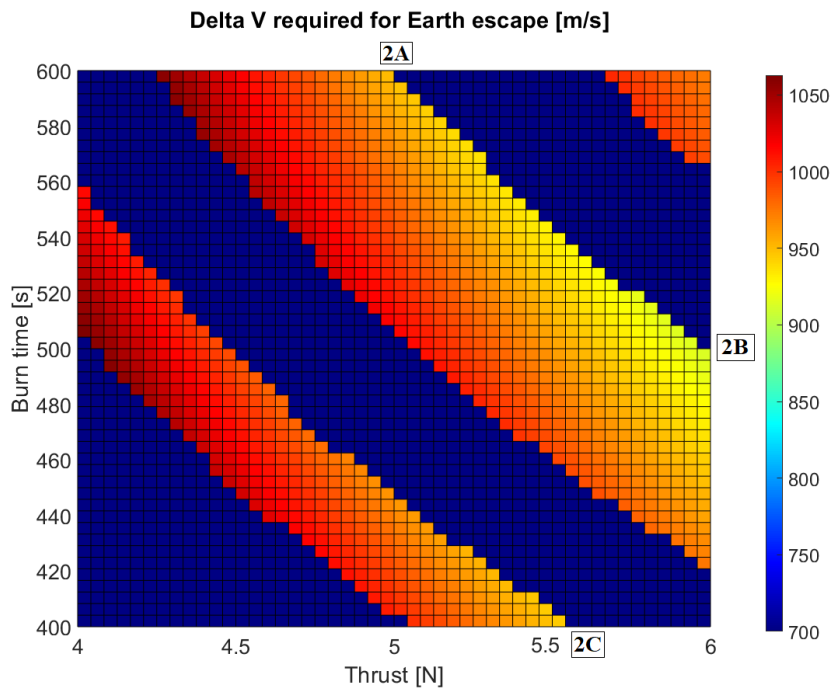


Figure 3.8: Δv budget needed for Earth escape. Initial satellite mass $M_0 = 30$ kg, propellant specific impulse $I_{sp} = 230$ s

35 kg satellite Finally, in Figure 3.9 the Δv budget for an initial satellite mass of $M_0 = 35$ kg is shown: as expected for an higher level of mass, less combinations of thrust and burn time allow for Earth escape, given the chosen constraints. This is indeed represented by only two "waves" of solutions present in the graph, compared to the three available for the previous two cases. Finally, three points can be chosen as the most optimal, given the shape of the solution regions: they are named points 3A, 3B and 3C.

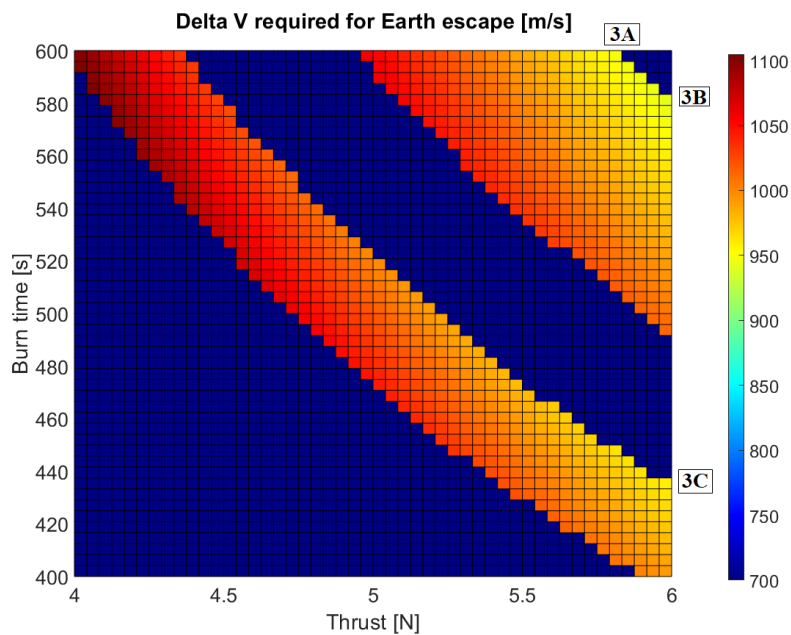


Figure 3.9: Δv budget needed for Earth escape. Initial satellite mass $M_0 = 35$ kg, propellant specific impulse $I_{sp} = 230$ s

Table 3.9: Earth escape Δv budget for $M_0 = 35$ kg

I_{sp}	Point 3A			Point 3B			Point 3C		
	Thrust [N]	Burn time [s]	Δv [m/s]	Thrust [N]	Burn time [s]	Δv [m/s]	Thrust [N]	Burn time [s]	Δv [m/s]
230	5.75	600	951.1	6	575	942.1	6	429.2	957.4
240	5.792	600	949.8	6	579.2	942.4	6	429.2	960.8
260	5.833	600	951.2	6	583.3	945.2	6	433.3	962.2
280	5.833	600	956.5	6	583.3	950.3	6	433.3	967.7
300	5.875	600	956.5	6	587.5	951.8	6	433.3	972.3

Table 3.9 displays the Δv budget result for the three points of interest and the range of values of specific impulse taken into consideration. The Δv budget in the three cases is similar to each other, since the amount of thrust that characterize these 3 points is close to 6 N for each of them. As expected, the Δv budget is increased even more with respect to the optimal points of the two previous cases, given the increased initial satellite mass.

3.3.3. Conclusions

This section described the procedure used to highlight the preliminary trajectory analysis of the Earth escape phase for a CubeSat mission that autonomously flies from the parking SSGTO mentioned in MISS-E01 towards Mars. To do this, the patched-conics method has been used to evaluate the orbit energies and "infinite velocities" that the satellite shall possess when leaving the sphere of influence of the Earth and entering the one of Mars, which has led to the completion of requirement MISS-E03. The patched conics method assumes that the total Δv can be divided between manoeuvres in the sphere of influence of the Earth and Mars, and this section was dedicated to the analysis of the manoeuvres around the Earth. To estimate the first part of the total Δv budget of the mission, given the requirements MISS-E02 which poses a limit on the number of orbit raising manoeuvres, a MATLAB/Simulink environment has been programmed to solve the two-body problem with the addition of satellite thrust, displayed by Equation (3.13). Two different strategies had to be adopted, given the first phase of orbiting around Earth with a closed orbit, and a second phase of hyperbolic flight: the first phase comprehended several orbit raisings with perigee burns that increased the energy of the orbit, until the total specific energy becomes positive. This starts the second phase of the Earth escape phase, where other manoeuvres are performed along the trajectory of the satellite to ensure that the final "infinite velocity" of the CubeSat coincides with v_{infE} calculated with Equation (3.7).

The inputs to the simulation program have been the following:

- Initial satellite mass between 25 to 35 kg, since it is expected to be at least a 12U CubeSat from other autonomous interplanetary missions to Mars.
- Propellant specific impulse I_{sp} between 230 and 300 s, from literature of state-of-the-art chemical propulsion systems developed for CubSats.
- Single burn time duration t_b of maximum 600 s, to align with other currently proposed autonomous missions such as MARIO [35]. Furthermore, current state-of-the-art propulsion systems have proven capability of continuous burns around the same time-duration, therefore an higher value would not be feasible for all types of propellants.
- The time to wait between each burns Δt_b has been chosen to be equal to the burn time t_b of each manoeuvre.

Two constraints have been added, to make sure that the two-body problem approximation is correct and to check that the number of Van Allen belts passing does not surpass the limit given from MISS-E02:

- The maximum distance point from Earth shall be lower than a 0.9 factor from the sphere of influence of the Earth.
- The total time spent around Earth with a closed orbit from operation start shall be lower than 1000 hours.

Under these circumstances it has been noticed how there are several optimal combination of thrust levels and burn times that most effectively propel the satellite outside the sphere of influence of the Earth,

mainly influenced by the initial mass of the satellite. For different values of the latter, the solution graphs have a different shape, which has been characterized by several "waves" of feasible manoeuvres combinations given thrust and burn time levels, with each "wave" corresponding to a different number of orbit raising manoeuvres needed. Each of these graphs have been characterized by choosing the three most optimal points in which the Δv budget is minimized: as expected, the values are lower for higher levels of available thrust and smaller burn times, naturally decreasing towards the hypothetical impulsive manoeuvre combination. In general, it turns out that the lower the initial mass of the satellite, the lower the Δv budget required for the first phase of the mission and more combinations of thrust and burn time allow for a feasible Earth escape, given the previously mentioned conditions. The Δv budget ranges from 870 m/s up to 960 m/s: it is decided to choose only one point of the three analysed for each initial satellite mass case. The thrust level available and the Δv used for the first phase of the mission will be taken from points **1C**, **2B** and **3B** for the respective initial satellite masses of 25, 30 and 35 kg. These points provide the most optimal value of Δv for the first phase of the mission and these values will be used in the stabilization around Mars, since the results from the latter will depend on the initial mass that the satellite will have once it reaches the sphere of influence of Mars.

3.4. Arrival at Mars

Following the patched-conics approach adopted to estimate the Δv budget, in this last phase of the interplanetary trip to Mars the satellite has reached the Martian sphere of influence and enters it following a hyperbolic orbit characterized by the "infinite velocity" found in Equation (3.8). During this phase of the satellite needs to perform braking manoeuvres in order to decrease the energy of its orbit around the planet, resulting in a final closed orbit meeting the requirements established by the mission. The purpose of this section is to obtain the second part of the Δv budget that is needed in order to correctly stabilize around Mars: to do so, a MATLAB/Simulink interface has been programmed, similarly to the previous case, in which the braking manoeuvres will be performed using non-instantaneous burns in order to check the feasibility of this last part of the mission.

3.4.1. Simulation procedure

Problem approach Differently from the previous phase of the mission, the satellite has to now brake in order to reduce the energy of the orbit such that it will not only fly-by the planet, but reach a negative value for the specific energy of its final orbit. This means that the satellite needs to reduce the orbit by the time it flies around the planet, otherwise it would continue to orbit away from the planet and will not have any other chances to brake. Therefore, a different strategy to determine when to perform burns has to be implemented, finding the best possible true anomalies at which to brake. The results will be shown such that for a given Δv of braking, the satellite shall minimize the eccentricity of the final orbit. Another important parameter that will be shown in the results is the minimum distance from the Mars surface that will be reached by the satellite in its stabilized orbit, which will be reached at the peri-apsis of this orbit. The feasibility of the "braking" phase of the mission will be confirmed if the final orbit of the satellite has the following properties:

- Final eccentricity < 0.92 , from MISS-M01.
- Minimum orbit peri-apsis $< 5000 \text{ km}$, to ensure the satellite flies close enough to the planet to obtain surface pictures, from MISS-M02.

The initial semi-major axis of the hyperbolic orbit of arrival is fixed, since the "infinite" velocity of Mars approach is already defined by Equation (3.8). Therefore, the semi-major axis of the hyperbolic orbit of arrival is:

$$a_M^{(i)} = -\frac{\mu_m}{v_{\infty M}^2} = -6108.413 \text{ km} \quad (3.23)$$

where the apex (i) stands for the initial conditions, referred to the orbit properties when entering the sphere of influence of Mars and before starting any manoeuvres. Since the semi-major axis of the initial orbit is fixed, there is one parameter to be chosen in order to fully constrain the initial orbit: it can be either the eccentricity of the hyperbolic initial orbit or its periapsis distance. Since each one of them changes with respect to the other, only one of the two needs to be chosen in order to have a fully defined orbit and the other parameter will be derived. In this thesis work it has been decided to fix

the periapsis distance: this is because "ideally" the periapsis distance should not vary too much during the braking manoeuvres, and can be seen as the intended minimum distance from the planet after the stabilization, while the eccentricity will vary during each manoeuvre.

Theoretical Δv evaluations have been performed in order to check whether it is more optimal to have the periapsis closer or further from Mars in terms of ideal Δv budget to stabilize around Mars. Most of these evaluations are highly dependant on the final eccentricity that the final target orbit needs to achieve, and are thoroughly discussed in Appendix B. It has been found that for a final eccentricity orbit close to 1, assuming that the peri-apsis of the hyperbolic entrance orbit as low as possible reduces the Δv budget for this part of the mission: since the radius of Mars is $R_{mars} = 3389.5 \text{ km}$, it has been fixed to 5000 km . This assumption has also been made in order to comply with requirement MISS-M02, since the difference between the peri-apsis distance and the radius of Mars will be lower than 2000 km , considering the initial hyperbolic orbit. Since this assumption is favourable to the Δv and takes into consideration an overly good case of the initial trajectory, a Δv budget margin will be added to the overall mission, in the end, taking into account any other manoeuvre that should be taken during the interplanetary trip and that has not been addressed in detail.

Assuming an initial (and final) peri-apsis of $r_{pM} = 5000 \text{ km}$ for the hyperbolic orbit when entering the Martian sphere of influence, its eccentricity is found with:

$$e_M^{(i)} = 1 - \frac{r_{pM}}{a_M^{(i)}} = 1.8185; \quad (3.24)$$

The ideal Δv for the Mars stabilization phase, assuming a final orbit eccentricity of $e_M^{(f)} = 0.92$ and an initial (and final) peri-apsis of $r_{pM} = 5000 \text{ km}$, is :

$$a_M^{(f)} = \frac{r_{pM}}{1 - e_M^{(f)}} = 62500 \text{ km} \quad (3.25)$$

$$v_{perM}^{(f)} = \sqrt{\frac{\mu_m [1 + e_M^{(f)}]}{a_M^{(f)} [1 - e_M^{(f)}]}} = 4.0558 \text{ km/s} \quad (3.26)$$

$$v_{escM} = \sqrt{2 \frac{\mu_M}{r_{pM}}} = 4.139 \text{ km/s} \quad (3.27)$$

$$v_{pM}^{(i)} = \sqrt{v_{escM}^2 + v_{\infty M}^2} = 4.9135 \text{ km/s} \quad (3.28)$$

$$\Delta v_{Mid} = v_{pM}^{(i)} - v_{perM}^{(f)} = 858.15 \text{ m/s} \quad (3.29)$$

Simulation environment description To estimate the Δv required to brake around the orbit of Mars, coming from an heliocentric orbit after the interplanetary travel, a new simulation environment has been programmed in MATLAB/Simulink. It will serve the purpose of demonstrating the feasibility of slowing down around a planet during its fly-by, given the current state-of-the-art propulsion system parameters available to CubeSats. This time, it will be crucial to decrease the speed of the satellite rapidly enough, since there will be a window in which the satellite will be close enough to the planet to make the braking manoeuvres and affect more efficiently the specific energy of the orbit. This means that an important parameter to successfully demonstrate the feasibility of this phase of the mission is the true anomaly θ_m at which the braking manoeuvres will begin. Once the true anomaly θ_m is reached, the strategy will be the same as for the second phase of Earth escape, but reversed: a succession of manoeuvres lasting t_b , each separated by Δt_b , will be performed in a square-wave trend.

The setup for the simulation will be the following: the satellite is arriving from an hyperbolic orbit with specific energy found in Equation (3.10), derived from the heliocentric orbit between Earth and Mars. It will perform braking manoeuvres from different values of true anomaly of the orbit, in order to verify

the feasibility of the stabilization around Mars. The simulation is successful if the satellite stabilizes around Mars, satisfying requirements MISS-M01 and MISS-M02.

The equations used to estimate the trajectory followed by the satellite are similar to the ones used for the Earth escape phase, with some small differences. The equation of motion is highlighted in Equation (3.30):

$$\ddot{\vec{r}} = -\frac{\mu_m}{\|\vec{r}\|^3}\vec{r} + \frac{\vec{T}}{m} \quad (3.30)$$

where μ_m is the gravitational parameter of Mars, which can be found in Table 3.1. For this case, the thrust is assumed to be parallel but opposite to the current velocity vector, therefore the thrust and flight path angles shown in Figure 3.3 are related by: $\delta = \gamma + \pi$. The current satellite mass is obtained with Equation (3.31):

$$m = M_{in} - M_{p \ earth} - \frac{T}{I_{sp}g_0} \int_0^{t_{tot}} dt \quad (3.31)$$

in which it has been taken into account the fact that the overall satellite mass will be lower due to the propellant usage for the Earth escape phase of the mission.

Figure 3.10 shows an example of successful stabilization around Mars: the satellite arrives from the open hyperbolic orbit and performs several braking manoeuvres (highlighted in red) in order to stabilize around the planet.

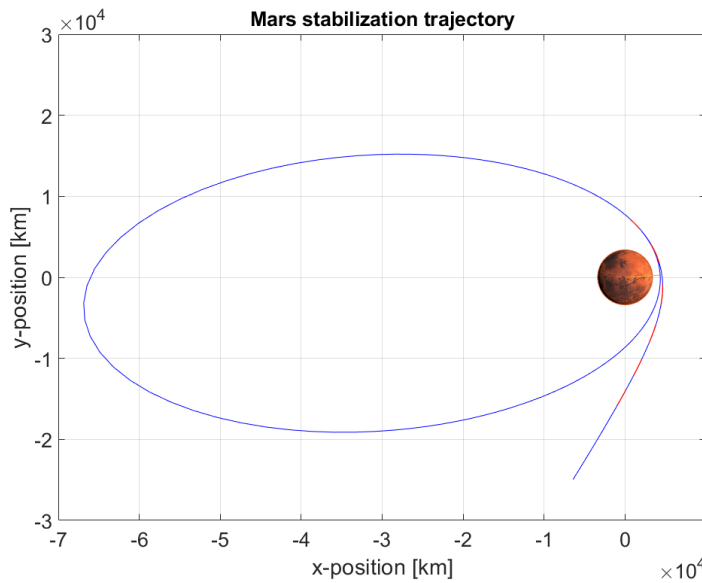


Figure 3.10: Example of correct stabilization around Mars

Figure 3.11, on the other hand, shows an example of unsuccessful stabilization around Mars: the satellite starts the braking manoeuvres from a true anomaly θ_m too close to the periapsis of the hyperbolic orbit. This means that due to the propulsion system parameters limitations, it is not able to lower the energy of its orbit to close it around the planet, and continues flying on an hyperbolic orbit after the fly-by with Mars.

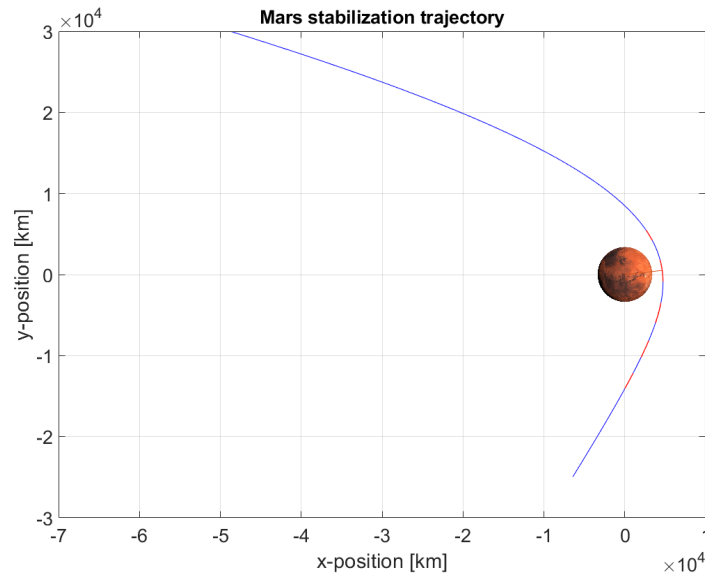


Figure 3.11: Example of failed stabilization around Mars

From the previous two examples, it can be seen how adopting the most optimal strategy for braking highly depends on the true anomaly θ_m at which the manoeuvres are started: braking too early will result in the satellite crashing onto the surface of Mars, while braking too late will make the satellite continue on its hyperbolic orbit. Similarly to what has been done for the Earth escape phase of the mission, a set of simulations has been programmed in order to choose what are the best optimal choices of t_b and θ_m , choosing them as inputs, while obtaining as outputs the feasibility of the stabilization, the Δv budget needed, the final orbit eccentricity and the minimum distance from Mars. An overview of the simulation environment is highlighted in the block scheme below:

Differently from the previous phase, now the check to consider the manoeuvring phase over is done over the eccentricity: if the latter is lower than the 0.92 as required from MISS-M01, the stabilization is successful. Otherwise, it means that the burn time available and the true anomaly of the start of the manoeuvres could not satisfy the mission requirements.

Verification of results Similarly to the Earth escape phase, verification and validation procedures are used in order to check the validity of the results for Mars stabilization: the results will be compared to the effect on the specific orbit energy by an ideal instantaneous manoeuvre used to brake around the peri-apsis of the hyperbolic orbit around Mars.

$$E_{orb} = -\frac{\mu_M}{r_{perM}} + \frac{(v_{perM} - \Delta v_M)^2}{2} \quad (3.32)$$

One example is shown below, which takes into account propulsion system parameters similar to the ones used for this mission. The value of E_{ell} is representative of the final specific orbit energy reached by adopting the finite burn time, while E_{id} represent the ideal orbit energy to be reached with an instantaneous manoeuvre around the perigee for the same Δv applied:

Table 3.10: Braking manoeuvre sample performed around Mars: the final orbit specific energy after stabilization is higher than the ideal case, using the same applied Δv

T [N]	M_{OM} [kg]	t_b [s]	I_{sp} [s]	θ_{man} [deg]	Δv [m/s]	E_{ell} [km ² /s ²]	E_{id} [km ² /s ²]
5	20	600	240	268.9°	1010.9	-0.4659	-0.9504

Table 3.10 shows that, as expected, the energy value of the closed orbit around Mars obtained after the braking manoeuvre is higher than the specific energy of the orbit obtained by Equation (3.32): once again, this is due to the nature of central fields, which cause gravity losses when manoeuvring far

from the peri-apsis of the orbit. In order to verify that these value differences are generated from such phenomenon, and not by software issues, a few examples are shown below where the performance parameters of the propulsion system are increased, to allow for a continuous braking manoeuvre much more resembling of the ideal case:

Table 3.11: Samples of stabilization manoeuvres, with increased available thrust and reduced burning time: manoeuvres are performed near the peri-apsis of the orbit

T [N]	M_{0M} [kg]	t_b [s]	I_{sp} [s]	θ_{man} [deg]	Δv [m/s]	E_{ell} [km ² /s ²]	E_{id} [km ² /s ²]
50	20	326.85	240	350°	1003.7	-0.9194	-0.9221
500	20	32.9	240	359°	1012.1	-0.9550	-0.9550

It can be noted from Table 3.11 that by reducing the burn time and increasing the allowable thrust, the Δv delivered remains almost the same and the results from the final orbit energy coincide with the ideal case.

Validation of results In [66], a comparison between Hohmann bitangential transfers between Earth and Mars and ballistic capture transfer is presented. The 4 options of bitangential transfer between Earth and Mars named H1-H4, result in 4 possible infinite velocity values v_{infM} , since the eccentricities of the orbit of Earth and Mars around the Sun are taken into account. The values obtained in [66] are compared with the result of the MATLAB/Simulink tool, in which the infinite velocities values $v_{\infty M}$ have been used as inputs: the initial satellite mass used is 30 kg, the specific impulse is 240 s, the maximum available thrust is 500 N and the burn time is 20 s, in order to be more representative of impulsive manoeuvres. The results are obtained by varying the initial peri-apsis of the hyperbolic orbit around Mars between 5000 to 2500000 km and the final orbit eccentricity target is 0.99, as analysed in [66]. The comparison between the results of the MATLAB/Simulink program developed in the thesis and the Δv values obtained from [66] are shown in Figure 3.12:

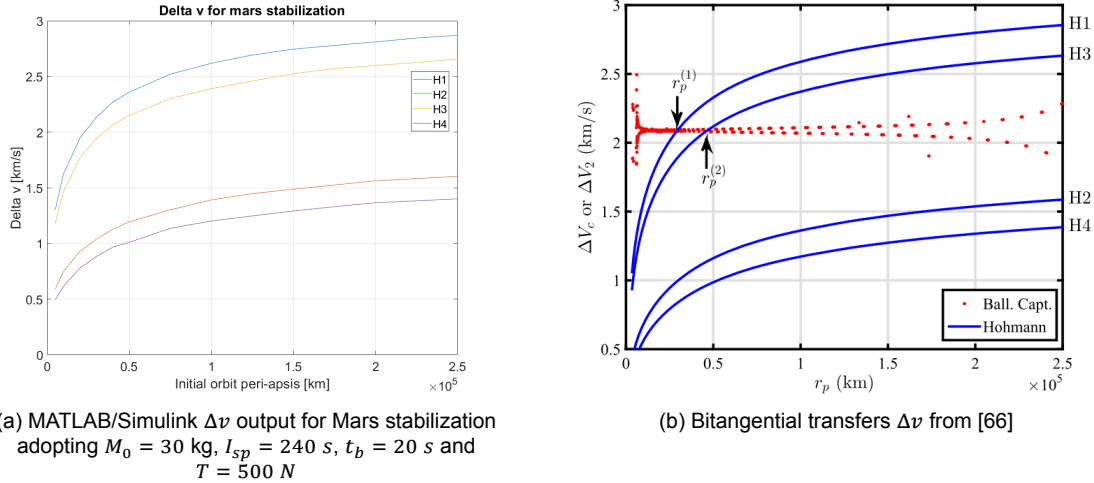


Figure 3.12: Comparison between Δv outputs of the MATLAB/Simulink tool and the bitangential transfers Δv for different initial peri-apsis of Mars orbit

Figure 3.12 shows that the results for all the 4 cases of the Mars stabilization are consistent, validating the output Δv result for the Mars stabilization phase, even for different values of $v_{\infty M}$ considered. The numerical data plotted in Figure 3.12 - (a) is highlighted in Table B.1.

3.4.2. Mars stabilization simulation results

This section is reserved to highlight the results obtained from the trajectory analysis described in detail in the previous section, which will allow the completion of requirement PROP-01 with the second part of the needed Δv for completing the mission.

The input parameters adopted for this phase are the set of parameters of the initial orbit of the satellite entering the sphere of influence of Mars, the thrust (T), specific impulse (I_{sp}) and satellite initial mass at Mars arrival (M_{OM}) that are obtained from the results of the Earth escape phase, namely points **1C**, **2B** and **3B** from Table 3.7, Table 3.8 and Table 3.9. This decision leads to a consideration on the overall minimization of the Δv budget: by choosing the previous three configurations as the starting points for the Mars stabilization and the subsequent Δv estimation, the total Δv budget between Earth escape and Mars will not be necessarily minimized. In fact, a different configuration of thrust and burn time for these three points could eventually lead to a lower Δv budget, or a different configuration for which the Earth escape was not optimal could hold the lowest possible total Δv between Earth and Mars. The scope of this thesis chapter is not to find the exact Δv optimum for the interplanetary trip, but to find a good Δv estimate given the state-of-the-art propulsion system parameters and to show the feasibility of the mission. Looking for the optimum combined Δv requires to take several inputs into account at the same time and would deviate from the scope of the thesis, in which the propulsion system design of a chemical propulsion system for an interplanetary mission between Earth and Mars is the main objective. Further optimization of the Δv would surely benefit the design of the mission by lowering the overall propellant mass to be carried on-board, but confirmation of the feasibility of the mission and an estimate of the Δv budget obtained with the tools mentioned earlier, which also take into account propulsion system parameters and do not only rely on ideal instantaneous manoeuvres, are deemed sufficient for the scope of the thesis work.

The initial satellite mass at Mars arrival is obtained for the relative Δv used for the Earth escape phase, and the resulting propellant mass is subtracted from the initial satellite mass at beginning of operations. The other two inputs given to the algorithm are the two variables that are needed to find the optimized Δv for the stabilization around Mars and to show the feasibility of the mission. They are:

- t_b : the burn time, which once again will serve to understand what will be the most optimized time to hold the thrusters active during the stabilization phase. As constrained before, there will be a Δt_b to be waited after each manoeuvre: just as the previous case, it is chosen to be $\Delta t_b = t_b$ as a first approximation. It is varied once again between 400 and 600 seconds.
- θ_m : the true anomaly of the hyperbolic trajectory at which the braking manoeuvres will begin. This value will be of extreme importance since starting the braking manoeuvres too early would result in the satellite crashing onto Mars, while braking too late would make the satellite fly-by the planet and not closing the orbit around it. By trial and error, its range is chosen to be between 250° to 310° .

The simulations will stop once the eccentricity value of 0.92 from MISS-M01 is achieved, or if that is not the case if the satellite has not successfully stabilized around Mars. The output parameters will be the propellant mass (and Δv) used for the stabilization, the final orbit eccentricity and the orbit peri-apsis, which is also a parameter to be taken into account from MISS-M02. The results obtained are shown below, divided between the different initial satellite masses cases.

Table 3.12 highlights the results obtained for the initial satellite mass of 25 kg, arrived to Mars after the Δv burn sequence described by thrust, burn time and Δv budget of point 1C, described in the previous section in Table 3.7. The same thrust level is shown to render feasible the stabilization around Mars with different values of true anomaly and burn time for each manoeuvre, given the different specific impulse values. In total, the Δv budget for this phase of the mission reaches a maximum of 952.4 m/s in the worst case.

Table 3.12: Mars stabilization optimal Δv budget result for initial satellite mass of 25 kg, case 1C

I_{sp}	θ_m [deg]	t_b [s]	e_{fin} [-]	d_{min} [km]	Δv [m/s]	Δv_{tot} [m/s]
230	280	536.8	0.919	1280	935.4	1803.6
240	280	452.6	0.919	1268	936.9	1807.9
260	280	421.1	0.919	1234	944.2	1820.2
280	280	473.6	0.919	1213	948.7	1828.9
300	275.7	505.3	0.919	1203	952.4	1836.2

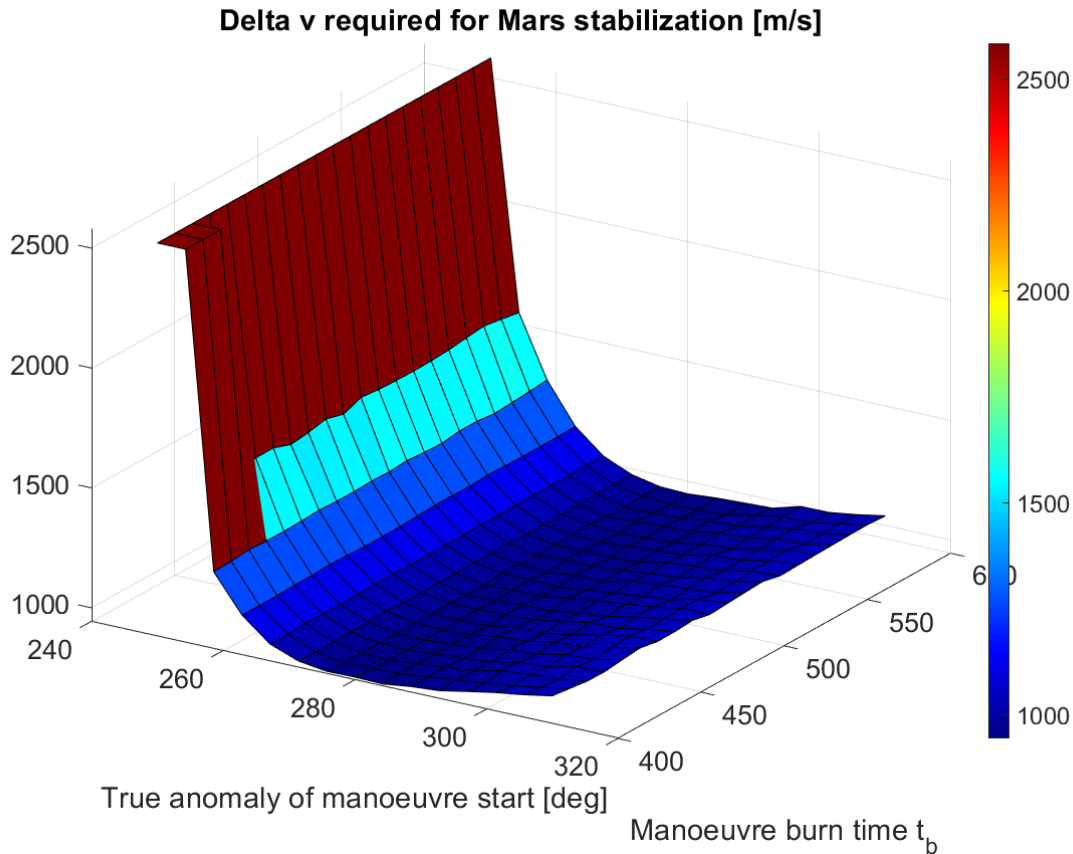


Figure 3.13: Mars stabilization Δv budget for case 1C (initial satellite mass of 25 kg) and specific impulse level of $I_{sp} = 260$ s

An example from the surface of results is given in Figure 3.13, realized for the 1C case and a specific impulse value of 260 s: the values of true anomaly θ_m and burn time t_b for which Mars stabilization is not successful is shown in red.

Table 3.13 highlights the results obtained for the initial satellite mass of 30 kg and with propulsion system parameters shown in Table 3.8. Stabilization around Mars is feasible given the constraint of the mission, and the maximum Δv used for this phase reaches the value of 978 m/s.

Table 3.13: Mars stabilization optimal Δv budget result for initial satellite mass of 30 kg, case 2B

I_{sp}	θ_m [deg]	t_b [s]	e_{fin} [-]	d_{min} [km]	Δv [m/s]	Δv_{tot} [m/s]
230	275.7	473.7	0.919	1177	957.0	1869.7
240	275.7	536.8	0.919	1168	959.2	1871.7
260	271.4	473.7	0.92	1138	965.9	1883.6
280	271.4	589.5	0.918	1113	972.8	1891.9
300	271.4	589.5	0.92	1082	977.7	1900.6

Finally, Table 3.14 shows the results obtained for the initial satellite mass of 35 kg and with propulsion system parameters shown in Table 3.9. Given the higher initial mass, the Δv budget required for this phase of the mission, similarly to the Earth escape case, is the higher amongst the three. Nevertheless, stabilization around Mars is feasible and it reaches a maximum Δv need of 1007 m/s in the worst case.

Table 3.14: Mars stabilization optimal Δv budget result for initial satellite mass of 35 kg, case 3B

I_{sp}	θ_m [deg]	t_b [s]	e_{fin} [-]	d_{min} [km]	Δv [m/s]	Δv_{tot} [m/s]
230	271.4	410.5	0.92	1072	979.4	1921.5
240	267.1	452.6	0.918	1061	984.4	1926.8
260	267.1	557.9	0.919	1032	990.8	1936.0
280	267.1	431.6	0.919	996	997.6	1947.9
300	267.1	600	0.918	959.2	1007.0	1958.8

3.4.3. Conclusions

The results from the trajectory estimation performed in the previous section show that the real amount of Δv needed to stabilize around Mars are increased with respect to the ideal budget found in Equation (3.29). This is once again caused by the gravity losses that affect the braking manoeuvres, since they have to be performed along the hyperbolic trajectory followed by the satellite when it enters the sphere of influence of Mars. The initial conditions of the satellite mass and thrust levels are taken from the most optimal points obtained in the Earth escape analysis: the value of thrust that achieved the best combination (together with the manoeuvre burn time) for the Earth escape phase is used for this case and the resulting Δv from the first phase is needed to estimate the initial satellite mass once it enters the sphere of influence of Mars. The performance values of the propulsion system, together with the available range of burn time combinations, show that correct stabilization around Mars respecting the requirements MISS-M01 and MISS-M02 is feasible: the amount of Δv budget required is slightly higher than the one needed for the Earth escape phase. Different values of burn time are needed for the specific impulse values cases analysed, as well as different true anomaly at which to start the braking manoeuvres.

Given the previous hypothesis for the estimation of the Δv budget for the Mars stabilization phase the Δv value ranges between 935 and 1007 m/s, depending on the initial mass of the satellite and the specific impulse of the propulsion system.

3.5. Total propellant budget

This chapter described the high-level trajectory analysis performed in order to check the feasibility of a small satellite mission, with initial satellite mass ranging from 25 to 35 kg, using chemical propulsion systems with currently available performance parameters. The analysis has comprehended a first approximation of the interplanetary travel between Earth and Mars, which has been assumed to be an Hohmann transfer around the Sun, only influenced by the gravity of the star. It has been assumed that both planets lie on the same plane, and that they have mostly circular orbits. Afterwards, both the planets influences have been prioritized in order to verify that Earth escape and Mars stabilization, respectively, are feasible with the current state-of-the-art chemical propulsion systems. The ideal Δv values obtained from the patched conics method served as a baseline to understand what amount of Δv would be the minimum needed for such mission: further analysis have been performed to showcase the effect of gravity losses on a propulsion system that is not able to achieve impulsive manoeuvres, limited by the smaller amount of thrust that a state-of-the-art propulsion system can provide to a CubeSat. The first approach to the problem for the Earth escape phase is shown in Appendix A. In Appendix B, the Δv estimation based on the peri-apsis hypothesis value for the hyperbolic orbit and the final orbit eccentricity of the satellite is described.

Depending on the initial mass of the satellite, the Δv budget varies for each mission phase: this will affect the propellant mass needed to be carried on-board of the satellite, also depending on the propellant specific impulse. For the continuation of the thesis, a single level of Δv needs to be chosen for the requirement PROP-01 and the start of the propulsion system design: it is decided to use a reference case of a satellite with initial mass of 30 kg, similar to the initial mass of the MARIO satellite which has inspired this thesis work. Since the Δv budget has shown to vary based on the specific impulse values, an average on the Δv obtained from Table 3.13 is used since the exact specific impulse of the propulsion system is still unknown, but it is expected to be in the range between 230 to 300 seconds. This average amounts (taken without the 230 s case since it would not be equally distributed with the

other specific impulse values) to:

$$\Delta v_{30kg} = \frac{\Delta v_{30kg,240s} + \Delta v_{30kg,260s} + \Delta v_{30kg,280s} + \Delta v_{30kg,300s}}{4} = 1886.95 \text{ m/s} \quad (3.33)$$

Since the trajectory analysis approximations do not take into account the different inclinations of the planets around the Sun, as well as the effects of third-bodies or solar wind that may affect the satellite during the interplanetary voyage, a safety margin of 10% on the Δv budget has been chosen. In conclusion, the total Δv that the propulsion system will need to be capable to provide to the CubeSat is:

$$\Delta v_{miss} = 1.1 \cdot \Delta v_{30kg} = 2075 \text{ m/s} \quad (3.34)$$

It is expected that the propellant specific impulse, as well as the overall satellite mass, might differ from the ones used for the Δv_{30kg} estimation. This decision is made in order to progress with the design, since the overall Δv budget will not differ much from this "average" case, as can be seen from Figure 3.14, and corrections by iterating the total satellite mass will be performed at the end of the thesis work. These variations in Δv budget will not change the overall design of the system, but will only affect the sizing of the tanks that will need to be sized and pressurized to fit the correct amount of propellant at the correct amount of pressure. After the specific impulse of the propulsion system is known, the same procedures applied in this chapter will be repeated to find the Δv associated with the newly found I_{sp} .

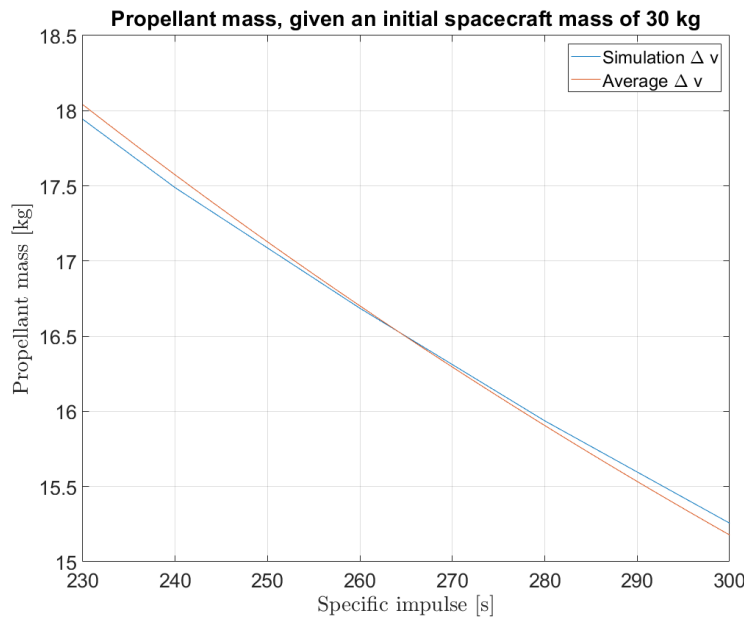


Figure 3.14: Propellant mass required for a initial satellite mass of 30 kg, calculated with the Δv budget from Table 3.13 and Δv_{miss} .

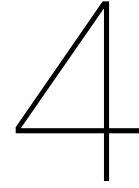
This value of Δv is the one that will be used to gauge the propulsion system mass and volume to be carried on board for the next chapter of the thesis, in which the trade-off between propellant options is performed. The set of mission and propulsion system requirements that will be used in the next chapter of the thesis as a foundation for the baseline design of the propulsion system are shown in Table 3.15 and Table 3.16.

Table 3.15: Mission requirements

ID	Rationale
MISS-E01	The starting orbit is the SSGTO defined by parameters: [51526 km, 0.8705, 0.01°, 0°, 0°, 0°]
MISS-E02	The number of orbit raising manoeuvres around the Earth shall be at most 6.
MISS-E03	The specific energy of the orbit before leaving Earth's sphere of influence shall be at least $4.332 \text{ km}^2/\text{s}^2$
MISS-M01	The final orbit eccentricity after stabilization shall be less than 0.92.
MISS-M02	The peri-apsis of the martian operational orbit shall be less than 5000 km.

Table 3.16: Chemical propulsion system preliminary requirements, assuming an initial satellite mass of $M_0 = 30 \text{ kg}$.

ID	Rationale
PROP-01	The chemical propulsion system shall provide at minimum $\Delta v = 2075 \text{ m/s}$
PROP-02	The maximum thrust level of the system shall be 6 N.
PROP-03	The maximum burning time t_b shall be 600 s for each time the propulsion system is activated.
PROP-04	The propulsion system shall utilize non-toxic "green" propellant.



Propulsion system trade-off

This chapter shows the design trade-off that has been performed to choose which chemical propulsion system type better meets the needs for a deep-space Mars mission, based on the state-of-the-art performance levels of propulsion systems under development and available in the market as COTS. Afterwards, a trade-off between the propellants is performed in order to choose the one that better satisfies the mission requirements: this will underline the differences between each option and lead to the final propulsion system type and propellant choice.

4.1. Chemical propulsion basics and classification

Chemical propulsion systems use the chemical energy stored in a propellant in order to generate thrust. There exist three main families of chemical propulsion systems: cold gas, solid and liquid. For the context of this thesis work, the cold gas option is not analysed since it does not comply to the thrust and specific impulse requirements highlighted in Section 2, and therefore the main focus will be the solid and liquid propulsion systems.

As anticipated earlier, chemical propulsion systems are able to provide high-thrust manoeuvres compared to the electric counterpart. These higher levels of thrust is obtained by combustion of the propellant(s), converting the exhaust gasses energy by accelerating it with a convergent-divergent nozzle. Due to the third principle of dynamics, an exiting mass from a system with a given velocity provides the main system (the spacecraft) with a momentum change, increasing its velocity. Thrust is generated by taking into account the exiting velocity of the exhaust gasses and the pressure difference between the gasses at the exit of the nozzle and the ambient pressure:

$$T = \dot{m}w_{ex} + (P_e - P_a)A_e \quad (4.1)$$

The two terms contribute to the generation of thrust, one caused by momentum change and one by pressure difference. The first term is provided by the product of the mass flow (\dot{m}) of exhaust gasses exiting the nozzle times the exhaust velocity of the jet, while the second one is obtained with the product between the pressure differential at the exit of the nozzle times its area. In space, it is assumed that the ambient pressure is null at vacuum condition, therefore it will be considered the case for $P_a = 0$. Another important parameters is the specific impulse I_{sp} , which is a measure of how much thrust is generated per unit of weight of propellant. If thrust and mass flow are constant over time, it can be obtained with:

$$I_{sp} = \frac{T}{\dot{m}g_0} \quad (4.2)$$

As shown in Section 3, this parameter is of extreme importance when estimating the amount of mass of propellant that needs to be carried on board: it is both related to the total Δv of the mission, and to the amount of mass flow needed to generate a given level of thrust. When tailoring a mission to a CubeSat level, the low allowable volume needs to be taken into account when deciding which propellant to use: since the specific impulse I_{sp} provides an indication on how much propellant mass is needed

for a mission, it has become conventional to use a modified specific impulse parameter that takes into account the density of the propellant itself. This parameter is the volumetric specific impulse, (I_ρ or ρI_{sp}) and is obtained with the product of the propellant specific impulse and its density:

$$I_\rho = \rho I_{sp} \quad (4.3)$$

The usefulness of this parameter comes handy when comparing propellants because it can establish the amount of propellant volume (and not just mass) that will be needed for a mission. For example, a propellant characterized by an high level of specific impulse I_{sp} and therefore requiring a low level of mass to perform a mission, is also characterized by a low density value: this would result in a high volume requirement, even though the mass is lower compared to other cases.

Given these initial principles for chemical propulsion, the rest of the section will be reserved to the description of the chemical propulsion systems classification that are taken into account for the propellant choice: solid and liquid propulsion systems.

4.1.1. Solid propulsion systems

Solid propulsion systems adopt the strategy of burning grains of solid propellants and generate thrust by ejecting the gases that are afterwards formed during combustion. Usually, the propellant grain is held in the combustion chamber itself and an igniter is used to start the combustion process. The propellant comprehends a solid mix that consist of both the oxidizer and the fuel, of which the final resulting mix is called a "grain". The propellant grain can take different shapes and its burn starts from an internal or external surface until the whole grain is consumed. This propulsion system does not need any reserved storage volume or feed lines, since everything happens in the combustion chamber itself. Furthermore, the effects of liquid propellant moving in a tank (sloshing) is not present for a solid propulsion system.

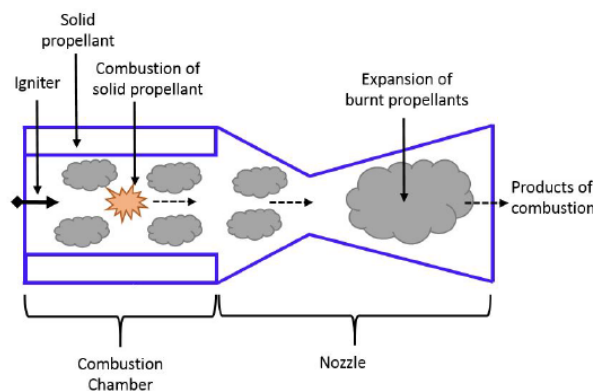


Figure 4.1: Schematic of a solid propulsion system [69]

Even though they consist of a very simple system compared to their liquid counterparts, their lack of control makes it difficult to precisely regulate the thrust levels provided: once the ignition is started and the propellant starts to burn, it is not possible to stop it until the whole grain has been utilized. Furthermore, they achieve moderate specific impulse, typically below 220 s . Chamber design is also a critical process since an optimal combustion needs to be assured in order to avoid the presence of unburned propellant grains. Therefore, if repetitive ignition is required as for this application, several stages would need to be used which highly increases the system complexity.

The current state-of-the-art solid rocket motors developed for CubeSats applications include the DSSP (Digital Solid State Propulsion) "CAPS-3" [53], "CDM-1" [54] and "MPM-7" motors, the Industrial Solid Propulsion "Isp 30 sec" [55], the Northrop Grumman Innovation System "STAR 4g" [83]. All of their performance parameters are highlighted in Table 1.2. They are characterized by relatively low I_{sp} values and very high thrust levels. CAPS-3, the only one possessing a very specific impulse value, is characterized by a burn time of 2 ms . With regards to the specific application of this thesis work, their low performance values in terms of specific impulse I_{sp} and the non-availability of start-stop capabilities

does not make solid propulsion system a consistent choice for the autonomous interplanetary trip of the spacecraft, where each burn shall be precisely tuned for each manoeuvre.

4.1.2. Liquid propulsion systems

In a liquid propulsion system, thrust is generated by ejecting the gases formed during the process of combustion of a liquid propellant. They are characterized by a combustion chamber and a convergent-divergent nozzle as their solid counterparts, but they also require specific tank storage and feed lines to keep the propellant pressurized such that its pressure levels are maintained once it reaches the combustion chamber. Additional thruster valves, as well as injector plates to uniformly distribute the propellant among the chamber area are needed. Liquid engines present more complexity with respect to solid propulsion system due to the presence of much more components, which on the other hand allow for an easier controllability of the manoeuvres, as well as restart capabilities and pulsed cycles. The specific impulse values for liquid engines are considerably higher than the solid propulsion ones, meaning that less propellant needs to be carried on-board, given the same Δv requirement, at a cost of more dry mass of the system.

Due to the need of high chamber pressures, the liquid propellants need to be fed to the combustion chamber with precise pressure levels, which can be achieved in different ways: a system can be pressure-fed, in which a volume of gas is stored at high pressure and when valves are used to activate the flow of the propellant, the pressurant gas pushes the liquid outside of the tank at high pressure. Depending on where the pressurant gas is stored, a distinction can be made between blow-down and regulated systems. A blow-down system comprises of both the propellant and pressurant stored in the same tank: each time the thruster is activated, the pressurant pushes the propellant outside of the tank, but at diminishing pressure since the gas itself is expanding in the tank. In a regulated system, the pressurant gas is stored in a different tank from the propellant, at very high pressures: a pressure regulator is used to push the propellant outside of its tank at constant high pressure. A pump-fed system, on the other hand, does not require high storage pressures since it relies on external pumps that will be used to provide the required pressure differential.

Depending on the number of propellants to be used, this characterization can be further brought to the distinction between mono-propellant systems and bi-propellant liquid propulsion systems. The first one, as the name implies, will require only the use of a single propellant for the gas generation, while the latter uses two different liquids as fuel and oxidizer, that need to be mixed in order to generate thrust and exhaust gasses. There are cases of tri-propellants and other kind of liquid propulsion systems, but the research is focused on these two main ones, since they are the most attractive for CubeSat liquid propulsion.

Mono-propellant propulsion system A mono-propellant liquid propulsion system typically adopts a single propellant to generate thrust and it is usually ignited by passing through a catalyst bed, which helps with the decomposition of the propellant. Most of the times the catalyst bed needs specific pre-heating. The propellant that have been used in the past for this case are most notably hydrazine (N_2H_4) and hydrogen peroxide (H_2O_2). Hydrazine has been used largely in the past as mono-propellant, but the downside to its usage is that it is highly toxic and requires trained personnel for handling and the use of SCAPE (self-contained atmospheric protective ensemble) suits [33]. Therefore, using hydrazine as propellant adds these safety requirement costs to the overall propulsion system manufacture costs. The density of hydrazine is 1000 kg/m^3 and its specific impulse is 240 s [58]. Hydrogen peroxide is mostly available in a solution together with water and for its propellant usage purposes, typical high levels of concentrations are used, giving it the name of "High test peroxide" (HTP). Concentration values can range from 87.5% to 98%, leading to a specific impulse ranging from 160 to 173 s [23] [24].

In recent years, more interest has grown towards the usage of green propellants, where green refers to fewer requirements for safety handling and operation such as low vapour pressure posing no risk of inhalation. There are two main blend families that are the most representative cases of green mono-propellant options: they are either based on ADN (Ammonium dinitramide) or HAN (Hydroxylammonium nitrate).

ADN propellant blends development has started at the Swedish Defence Research Agency (FOI): the main propellant blends are the FLP family, and LMP-103S. The FLP family consists of FLP-103, FLP-

105, FLP-106 and FLP-107 while LMP-103S has been developed by Bradford ECAPS. Each of these propellants blends ADN with water and either Methanol or MMF (monomethylformamide). They can provide theoretical specific impulse values of around 250 s, while their density varies from 1310 to 1405 kg/m^3 [79]. These two ranges of values provide a very high level of volumetric specific impulse I_ρ with respect to the previous alternatives.

The most mature HAN-based propellant blend is known as AF-M315E (recently also named ASCENT) which was invented at the US Air Force Research Laboratory (AFRL) in 1998. Its exact composition is unknown, but it delivers around 50% higher volumetric specific impulse than hydrazine, it poses no health hazard and offers performance comparable to traditional bi-propellant systems [60]. Its theoretical specific impulse level is 266 s, while its density is 1470 kg/m^3 [65].

State-of-the-art mono-propellant thrusters that adopt HAN- blend propellants have a range of thrust that mostly varies between 0.1 N to 1 N: Aerojet Rocketdyne "MPS" thrusters adopting AF-M315E provide up to 230 s of specific impulse and up to 1 N of thrust [57], while Busek's BGT-X5 provides 0.5 N of thrust [14]. The NASA Green Propulsion Infusion Mission (GPIM) employed a set of thrusters also developed by Aerojet Rocketdyne named GR-1 using by AF-M315E, providing up 1.4 N of thrust; a second thruster of higher scale has been developed to provide 26.9 N [40]. Bradford Ecaps has developed a series of LMP-103S based thrusters named "HPGP", which provide thrust levels from 0.1 N to 22 N, with specific impulse levels ranging from 196 s to 255 s [19]. One of these thruster has also flight heritage, with two thrusters adopted for the mission PRISMA [51].

Bi-propellant propulsion system A bi-propellant liquid propulsion system adopts two different propellants, stored in their liquid phase, in order to generate thrust. The two propellants, usually taking the part of oxidizer and fuel, are injected together in the combustion chamber and by reacting with each other, generate high temperature and the reactant gases that are accelerated in the nozzle in order to generate thrust. System-wise, bi-propellant propulsion systems need to use at least double of the amount of system tank and feed lines, since both the propellants need to be stored in their liquid phase and at correct pressurization levels. While not requiring a specific catalyst bed that is needed for the reaction to take place, it is critical to correctly dimension the injector plates, since the two propellants need to properly mix together in order to fully generate the combustion products. The benefit of using a bi-propellant system is the higher I_{sp} that they provide with respect to all of the other chemical propulsion options. The cons come from the low maturity that such systems have with respect to CubeSat applications, since they are the most complex type of chemical propulsion system based on the number of tanks, feeding lines and eventual pumps to be used, taking up most of the allowable volume. The few state-of-the-art options found for bi-propellant systems adapt to CubeSats are manufactured by Hyperion Technologies, namely the PM200 and PM400 [63] [64], and Tethers Unlimited "HYDROS-M" and "HYDROS-C" [70]. The ones from Hyperion adopt Nitrous Oxide+propane, achieving a specific impulse of around 285 s, while the HYDROS family utilizes electrolyzed liquid water, reaching a specific impulse value of 310s. The technology readiness level for such system is around 6, as can be noted from Table 1.2.

4.1.3. Conclusions

This section has been reserved to the description of chemical propulsion systems and what are the main parameters that characterize them. The distinction between solid, liquid-mono and liquid-bi has been discussed and the main advantages and disadvantages of each kind have been addressed. The value of the performance parameters relative to the state-of-the-art propulsion system has served to understand which classification of chemical propulsion system might better fit the needs of an inter-planetary mission to Mars with autonomous Earth escape. An early estimate of the propellant mass required for the mission can be seen in Figure 3.14, which shows the amount of propellant mass in relation with the Δv requirement derived in the previous section and the I_{sp} level of the propulsion system: based on the range of current chemical propulsion systems, the mass of propellant needed to be carried on-board will range between 18 to 15.2 kg, based on the kind of propulsion system utilized and the specific propellant(s). The exact value of propellant mass will be known only when the results from the complete design of the spacecraft, accounting for all the components masses, and the specific impulse of the propellant are known: Figure 3.14 only shows the relation for a fixed initial spacecraft

mass and propellant specific impulse, to gauge the amount of propellant that is expected to be carried on-board.

As expected, an higher I_{sp} value allows for a lower amount of propellant mass to be carried on-board. Based on this information only, one could argue that the best way to save mass (and volume) from the rest of the spacecraft is the adoption of a bi-propellant system, but several other factors, some of which already mentioned previously, come into play before deciding the kind of propulsion system to be adopted. For an early trade-off decision, it has been decided to take into consideration four different parameters: system complexity, technology readiness level (TRL), specific impulse I_{sp} and thrust levels T :

- Thrust levels are important since the trajectory analysis carried out in the previous chapter has produced as result the need of high values of thrust, ranging from 4 to 6 N, to minimize the Δv of the mission. Both mono-propellant and bi-propellant are capable of providing these thrust level, if four different 1 to 1.5 N thruster are use for the case. Solid propulsion, on the other hand, offers very high levels of thrust: while at first it may seem useful, it needs to be remembered that thrust vectoring misalignments may occur and the higher the thrust, the higher the amount of torque is need from the RCS to stabilize the spacecraft, therefore levels of thrust over 30 N are not useful for this application.
- Specific impulse values increase when moving from solid to mono- and then bi-propellant systems. It is useful to have this value as high as possible, in order to minimize the propellant mass to be carried on board.
- The complexity of the system is favourable to solid propulsion systems, since they do not require particular storage volume or feed lines, since everything happens in the combustion chamber itself. The liquid propulsion systems need more components to be operated, with double the amount of complexity for bi-propellant systems, having to manage two liquids, the eventual pressurant, and ensure the correct mixture in the combustion chamber.
- Finally, the TRL levels are an indicator of the qualification status of each system for space operations. Due to their simple architecture, solid propulsion systems have a very high level of TRL. In recent years, the interest towards mono-propellant systems has brought light on the development of many families of propellants and thrusters for CubeSats, of which some have already flight heritage in the past few years. This is expected to increase, with other missions adopting mono-propulsion systems, like MARIO. Finally, fewer are the options currently available for bi-propellants since the management of several propellant is complex, and even harder in the case of limited available volume.

All of the previous considerations are summarized in Table 4.1: the columns represent the 4 different criteria used to perform the trade-off, while the rows show the choices between the three propulsion system options available. Each of the previous considerations has been summarized by using three colours based on the satisfaction of each criterion by using red, yellow and green to characterize the score of each propulsion system classification in the four categories: red is the least preferable option, accounting for 0 points, yellow is the "Ok" case with 1 point and green represent a very good option, providing 2 points. Solid propulsion scored 4 points, bi-propellant scored 5, and mono-propellant scored 6.

Taking into account these results, it has been decided to adopt the mono-propellant option for this chemical propulsion system application, having the highest score of the three options. In the next section, a decision will be made on the exact propellant to be used, based on their physical and chemical properties, as well as their performance levels for this specific application.

4.2. Green mono-propellant options

The previous section consolidated the decision of adopting a mono-propellant system for the analysed mission. This section is reserved to the detailed choice of the propellant to be adopted: while the range of specific impulse and thrust of state-of-the-art thrusters are similar even using different mono-propellants, each individual propellant choice is characterized by different thermochemical and physical values. Density plays an important role, since it defines how much volume is needed to fit a given mass of propellant, as well as the chemical composition that will result in different chamber temperatures to be sustained by the chamber walls. These are just few of the parameters that will be deeply analysed

Table 4.1: Preliminary design trade-off comparing propulsion system options.

Criteria/ choices	Thrust	Specific impulse	Complexity	TRL
Solid	Bad (Over 37 N)	Bad (<240 s)	Good Simplest system	Good 9
Mono-propellant	Good (0.1 to 22 N)	Ok (>240 s)	Ok Easier system to manage with single propellant	Good 6 to 9, with increasing trends
Bi-propellant	Good (0.5 to 1.2 N)	Good (>280 s)	Bad Most complicated system	Ok <6

Meets requirement: 2 points
 Workable solution: 1 point
 Least preferable: 0 points

in this section, together with thermochemical simulations for a fixed thruster geometry, to make the choice on the propellant that will better meet the needs of the mission. The choice of a mono-propellant system has been made based on the performance levels that state-of-the-art mono-propellant thrusters adapted to CubeSats are able to achieve, and are in line with the requirements PROP-01 to PROP-04. The last requirement, PROP-05, states that the propellant to be used has to be non-toxic. This requirement already rules out the possibility of adopting the vastly used hydrazine option: as anticipated earlier, hydrazine is highly toxic when compared to the green propellants derived from ADN and HAN. Its handling and storage does not only increase risks related to safety, but also increases costs for handling and storage.

The two main green propellant option available at this current stage of time are either derived from ADN or HAN. These two energetic ionic liquids (EIL) are salts with melting points below 100°, characterized by high internal nitrogen and oxygen contents, which makes them highly energetic. The rest of the chapter focuses on the detailed description of the chemical composition of both the available ADN- and HAN- type blends currently available or in development for miniaturized propulsion systems. The physical and performance parameters of hydrazine, the mono-propellant that has seen the most usage in space applications, are shown in Table 4.2 for a comparison with the newly developed green propellants:

Table 4.2: Hydrazine physical and performance characteristics. f) Parameters dependent on the amount of ammonia dissociation, usually ranging between 30 to 70% [25]

Hydrazine properties	Value
Density ρ [kg/dm ³]	1.004 [25]
Specific impulse I_{sp} [s]	225-250 ^f [25]
Volumetric specific impulse I_{ρ} [kg · s /dm ³]	225-250 [25]
Flame temperature T_c [K]	1123-1423 ^f [25]
Freezing temperature T_F [°C]	2 [25]
Vapour pressure P_V [mbar]	19 [25]
Acute toxicity LD_{50} oral, dermal [mg/kg]	60,91 [4]

Hydrazine is characterized by a low liquid density, which in return does not provide an high volumetric specific impulse. The flame temperatures can be below 1000°C , a value that is highly surpassed by the newest blends that are more energetic and therefore reach higher temperatures in the chamber. This is in favour of hydrazine, since an higher range of lightweight materials can be used for the chamber design. Finally, the toxicity level is measured based on LD_{50} , which is the amount of mass needed to causes the death of 50% of a group of test animals: a lower value indicates an highly toxic element, while an higher value indicates that more mass needs to be inhaled/touched to concur in a fatality. Anything below 50 mg/kg is considered highly toxic, while being below 500 mg/kg is considered to be moderately toxic: as expected, hydrazine is very close to the first category, and the next pages of the chapter will detail the available options that would better satisfy the greenness of the propellant posed by requirement PROP-05.

ADN-based propellants ADN stands for ammonium dinitramide and is a colourless salt with high solubility in water. Its chemical formulation is $[\text{NH}_4]^+ [\text{N}(\text{NO}_2)_2]^-$. The ADN mono-propellant formulations developed with ADN are either the FLP family (FLP-103, FLP-106 and FLP-107) or the LMP-103S, with the latter being developed by Bradford ECAPS and having flight heritage on the "Mango" spacecraft from the PRISMA mission adopting the High Performance Green Propulsion system (HPGP) [6]. Contrary to the HAN- counterparts, ADN- based propellants can not only be ignited by adopting a pre-heated catalytic bed but also by using thermal ignition, either pyrotechnic or resistive, reducing the amount of power needed to operate the thruster [80]. The main ADN-based mono-propellant options available at the stage of this research are listed below, with the weight percentage composition between brackets [56] [24] [46]:

- **FLP-103:** ADN (63.4%), water (25.3%), methanol (11.2%), urea (0.1%)
- **FLP-106:** ADN (64.6%), water (23.9%), MMF (11.5%)
- **LMP-103S:** ADN (63.0%), ammonia (4.65%), water (13.95%), methanol (18.4%)

HAN-based propellants HAN stands for hydroxylammonium nitrate $[\text{NH}_3\text{OH}]^+ [\text{NO}_3]^-$ is a salt of the non-stable base hydroxylamine and nitric acid. Due to the polar character of the HAN molecule, the solubility in water or other solvents is sufficient enough to form liquid propellants, making technical handling like pumping more feasible. The addition of fuels and water gives the opportunity of changing the propellants' enthalpy, adiabatic combustion temperature and physical-chemical properties, just like for ADN-blends [24]. AF-M315E (which stands for Air Force Mono-propellant 315E) represents the state-of-the-art for HAN-based mono-propellants: it has also been flown on the GPIM (Green Propellant Infusion Mission) with thrusters developed by Aerojet Rocketdyne. It consists of a mixture of HAN, HEHN (hydroxyethyl-hydrazinium nitrate) and water. Another interesting HAN-based mono-propellant is the SHP-163 which has been developed by ISAS (Institute of Space and Astronautical Science) and JAXA: it consist of a blend of HAN, methanol, water and AN (ammonium nitrate) [28]. Compared to the other green propellants listed, it shows the highest adiabatic flame temperature level.

The composition of the two analysed HAN-based mono-propellants is listed below [22] [21] [28]:

- **AF-M315E:** HAN (44.5%), HEHN (44.5%), Water (11%)
- **SHP:** HAN (73.6%), AN (3.9%), Methanol (16.3%), Water (6.2%)

It has to be noted that most of the current literature discussing the possibility of adopting green propellants does not provide the exact chemical composition of AF-M315E, most probably because it is a proprietary propellant from Air Force Laboratory US: the chemical composition shown in this thesis work has been found through a reference dedicated to self-adjusting catalyst [22], in which the example of adopting AF-M315E is described, but the patent is not dedicated in detailing the properties of AF-M315E, like other references used for data acquisition. For this reason, two different methods of estimating the properties of AF-M315E are shown later in the chapter, one adopting the chemical composition and using the RPA (Rocket Propulsion Analysis Tool), and the second one by reverse-engineering some missing values using Ideal Rocket Theory.

4.2.1. Propellant trade-off

Several references have been found during the thesis project for this particular trade-off: it is crucial to understand the correct properties of each propellant that can satisfy the requirements obtained in

Chapter 2 and Chapter 3. Below, in Table 4.3 and Table 4.4 the most relevant physical and performance properties of the five propellant candidates (2 HAN-based and 3 ADN-based) are shown and compared, each with the reference from which the data has been obtained, as well as the experimental/theoretical conditions at which some of them have been measured/estimated. The properties that have been chosen to be the most important to describe the propellants and help with the propellant choice are the following:

- Density ρ
- Specific impulse I_{sp} and Volumetric specific impulse I_ρ : these values describe the capability of generating impulse per unit of mass propellant as well as the volume intake.
- Flame temperature T_c : having a low combustion temperature allows for more variety of lightweight materials to design the combustion chamber. It is a very important parameter since, as it will be seen next, each of these propellants is very energetic and the combustion temperatures reach very high levels, at which only few materials can withstand it.
- Freezing temperature T_F : having a low freezing point is important for the storability of the propellant, reducing tank heating power to be accounted for maintaining the propellant above the freezing temperature during the mission.
- Dynamic viscosity μ : all of the propellant candidates have different dynamic viscosities that affect the pressure drops that will be present in the feed system, as well as in the catalyst bed.
- Vapour pressure P_V : it relates to the capability of the propellant particles to escape from the liquid phase. It is important to have a low vapour pressure for both ground storability and space operations.
- Acute toxicity: referring to requirement PROP-05, the propellant needs to be considered green, and therefore its toxicity effects have to be as low as possible.
- Heritage: having flown in a mission in the recent years is seen as a plus, since it proves the space readiness of the propellant.

Each property is listed below in Table 4.3 and Table 4.4:

Table 4.3: Physical, performance and thermochemical properties of the propellant candidates. Conditions for specific impulse estimation: a) : $P_c = 0.7$ MPa, Ae/At = 50 , b) : $P_c = 2$ MPa, Ae/At = 50

Propellants/properties	SHP163	AF-M315E	FLP-103
Density ρ [kg/dm ³]	1.4 [28], 1.411 [4]	1.47 [65], 1.5 [28]	1.310 [78] [80]
Specific impulse I_{sp} [s]	276 ^a [28] [4]	266 ^a [65] [28] [71]	254 ^b [78] [80]
Volumetric specific impulse I_ρ [kg · s /dm ³]	386 [28] [4]	390 [28]	332
Flame temperature T_c [K]	2401 [28], 2373 [4]	2166 [28] [71]	2033 [80]
Freezing temperature T_F [°C]	<-30 [28], <-37 [4]	<-22 [28], <-20 [71]	-
Dynamic viscosity μ @25 °C [mPa·s=cP]	11.9 [4]	25 [18], 27 [68]	-
Vapour pressure P_V [mbar]	-	140 [65]	-
Acute toxicity LD_{50} oral, dermal [mg/kg]	300-2000, > 2000 [28]	Moderate [65]	-
Heritage	RAPIS-1 [28]	GPIM mission [45]	-

Table 4.4: Physical, performance and thermochemical properties of the propellant candidates. Conditions for specific impulse estimation: c): $P_c = 2$ MPa, $A_e/A_t = 50$, d): $P_c = 2$ MPa, $A_e/A_t = 50$,

Propellants/properties	FLP-106	LMP-103S
Density ρ [kg/dm ³]	1.357 [81] [78]	1.238 [50], 1.24 [65]
Specific impulse I_{sp} [s]	255 ^c [78]	252 ^d [65] [49]
Volumetric specific impulse I_ρ [kg · s /dm ³]	346	312
Flame temperature T_c [K]	2095 ^c [78]	1903 ^d [49]
Freezing temperature T_F [°C]	0 [25]	-7 [25]
Dynamic viscosity μ @25 °C [mPa·s=cP]	3.7 [78] [80]	3 [50]
Vapour pressure P_V [mbar]	< 21 [25]	136 [50]
Acute toxicity LD_{50} oral, dermal [mg/kg]	1270, > 3000 [25]	750-800, - [25]
Heritage	-	PRISMA mission [6]

All of the propellant candidates show several improvements with respect to the hydrazine option: density is considerably higher, as well as the specific impulse, which also causes the volumetric specific impulse to be even higher. The freezing temperatures are lower, as well as a lower acute toxicity value, which ensures the greenness of the propellant. The vapour pressure values are similar, while the combustion temperatures are higher as predicted: ADN- and HAN- based propellants are very energetic and therefore release much more enthalpy in the combustion chamber, which translates higher performance values, at the cost of higher combustion temperatures. Nevertheless, the values for specific and volumetric specific impulse are increased, which means that performance and compactness can be improved by adopting one of these 5 propellant candidates for an interplanetary Mars CubeSat mission.

A preliminary elimination between 3 of the 5 candidates is performed based on the literature data found during the thesis work and shown in Table 4.3 and 4.4. The three propellants option that are not considered for further application are:

- SHP163: this innovative propellant provides the second highest volumetric specific impulse value among the 5, but at the cost of a very high flame temperature of around 2400 K. Such temperature is several hundreds of degrees higher than the other options, restricting the choice of chamber material to a few options.
- FLP-103: one of the two propellants from the FLP-family is excluded since it generally provides a lower volumetric specific impulse with respect to the FLP-106. It achieves combustion at lower chamber temperatures, but provides lower performance parameters. Furthermore, it has currently no flight heritage like FLP-106, but the latter has been investigated majorly during the recent years for space applications.
- LMP-103S: while its theoretical specific impulse is comparable to the other candidates in the list, its lower density does not provide a good enough option for a CubeSat mission that has to minimize the volume impact on the spacecraft. The lower combustion temperatures make this option very promising, but performance-wise it seems to be shadowed by the other propellants taken into account.

The two propellant options that remain available after a preliminary trade-off are AF-M315E and FLP-106. Both candidates have a similar theoretical specific impulse value, as well as combustion temperature. Further analysis is performed via the RPA (Rocket Propulsion Analysis) tool that provides the possibility of obtaining performance values of the propellant starting from the chemical composition and few thruster preliminary parameters. This will allow an easier comparison between the two propellants by matching the performance at every chamber pressure value or expansion ratio, and will not only rely

on propellant performance values obtained by literature. As a general note, Table 4.5 displays most of the major components of the 5 propellant candidates that have been taken into account, together with their chemical formula, molecular weight and heat of formation ΔH_f^0 : all of these values are needed as inputs to the RPA tool and can be used to perform thermo-chemical and rocket simulations for each of these propellants, by using the chemical compositions listed earlier.

Table 4.5: Chemical structure, molecular weight and standard heat of formation of propellant components used for RPA simulation between the propellant candidates. [49]

Component	Chemical structure	Molecular Weight [g/mol]	Heat of formation [kJ/mol]
HAN	$[\text{NH}_3\text{OH}]^+[\text{NO}_3]^-$	96.04	-338.97
ADN	$[\text{NH}_4]^+[\text{N}(\text{NO}_2)_2]^-$	124.06	-134.6
AN	$[\text{NH}_4]^+[\text{NO}_3]^-$	80.043	-365.28
HEHN	$[\text{HO-C}_2\text{H}_4\text{-N}_2\text{H}_4]^+[\text{NO}_3]^-$	139.11	-388.69
MMF	CH_3HNCHO	59.067	-247.4
Methanol	CH_3OH	32.04	-238.77
Urea	$\text{CO}(\text{NH}_2)_2$	60.06	-333.43

Since specific literature for AF-M315E composition is old and sparse, being a proprietary propellant, one other option for estimating its performance parameters has been thought of. From recent literature only few values are available at the time, not comprehending the exact mixture composition of the propellant [49], so it has been decided to also try and reverse-engineer the estimated performance values variation with expansion ratio A_e/A_t by adopting Ideal Rocket Theory equations. Few references provided estimation of AF-M315E, of which most of them presented a constant value with varying chamber pressures: the specific heat ratio γ of the exhaust gasses, which is reportedly estimated to be around values of $\gamma = 1.2$ or $\gamma = 1.21$ [3] [44]. The latter has been chosen, and this allows the evaluation of the Vandekerckhove function as follows:

$$\Gamma = \sqrt{\gamma} \left(\frac{2}{\gamma + 1} \right)^{\frac{\gamma+1}{2(\gamma-1)}} \quad (4.4)$$

The values of the pressure ratio can be estimated by inverting the relation between the area ratio and the pressure ratio, governed by the chemical parameters γ and Γ :

$$\varepsilon = \frac{A_e}{A_t} = \frac{\Gamma}{\sqrt{2 \frac{\gamma}{\gamma-1} \left(\frac{P_e}{P_c} \right)^{\frac{2}{\gamma}} \left[1 - \left(\frac{P_e}{P_c} \right)^{\frac{\gamma-1}{\gamma}} \right]}} \quad (4.5)$$

It is possible to numerically solve this equation and find the pressure ratio $\frac{P_e}{P_c}$ for the assumed operating conditions, knowing the area ratio. From Ideal Rocket Theory, the specific impulse I_{sp} is obtained with:

$$I_{sp} = \frac{w_{ex} + \frac{P_e - P_a}{\dot{m}} A_e}{g_0} \quad (4.6)$$

where w_{ex} is the exhaust velocity of the combustion products, P_e and P_a represent the exit and ambient pressure, \dot{m} is the mass flow rate and g_0 is the gravitational acceleration. The exhaust velocity of the gasses can be found with:

$$w_{ex} = \sqrt{2 \frac{\gamma}{\gamma-1} RT_c \left[1 - \left(\frac{P_e}{P_c} \right)^{\frac{\gamma-1}{\gamma}} \right]} \quad (4.7)$$

where T_c represents the chamber temperature, while R is the gas constant for the combustion products. Finally, the mass flow rate \dot{m} is obtained, with the assumption of nozzle choked throat:

$$\dot{m} = \frac{\Gamma P_c A_t}{\sqrt{RT_c}} \quad (4.8)$$

Since everything takes place in vacuum, in the I_{sp} formulation the ambient pressure term P_a in Equation (4.6) can be eliminated. By using Equation (4.7) and (4.8), and substituting them into Equation (4.6), it can be noted that all of the parameters can be obtained from literature [49], leaving only the gas constant R (and the molar mass of the gas products) to be calculated. By substitution, it is obtained:

$$I_{sp} = \frac{\sqrt{2 \frac{\gamma}{\gamma-1} RT_c \left[1 - \left(\frac{P_e}{P_c} \right)^{\frac{\gamma-1}{\gamma}} \right]} + \frac{\sqrt{RT_c} P_e A_e}{\Gamma P_c A_t}}{g_0} \quad (4.9)$$

$$M = \frac{R_A}{R} \quad (4.10)$$

where R_A is the absolute gas constant: $R_A = 8.31446 \text{ J}/(\text{K} \cdot \text{mol})$ and the area ratio $\frac{A_e}{A_t} = \varepsilon$ is equal to 50, as taken from Table 4.3. Using this procedure, the value for the combustion products gas constant R can be estimated and used for an approximation of the performance parameters of AF-M315E with varying expansion ratio, even without taking into account the propellant chemical composition. The results of this procedure are shown below in Table 4.6 and will be compared with the outputs from RPA simulations, which will use as inputs the exact chemical composition of AF-M315E reported in [22] [21].

Table 4.6: AF-M315E estimated properties

Property	Value	Unit
γ	1.21	-
Γ	0.6504659	-
R	371.91459	$\frac{\text{J}}{\text{kg K}}$
M	22.35567	kg/kmol

RPA performance estimation of FLP-106 and AF-M315E In this paragraph the two propellant candidates are compared by adopting their chemical composition:

- **FLP-106:** ADN (64.6%), water (23.9%), MMF (11.5%)
- **AF-M315E:** HAN (44.5%), HEHN (44.5%), Water (11%)

These values will be used as inputs for the RPA tool, together with the relative Heat of formation ΔH_f^0 of each chemical component from Table 4.5, which will provide an estimate on the real performance of the propellant. The baseline thruster geometry that will be used for these parameter estimations are: conical nozzle with exit semi-half angle of 15° , contraction area ratio of $\varepsilon_c = 50 - 100$ and frozen equilibrium flow at nozzle exit as taken from [37].

The results obtained from the RPA chamber and nozzle simulations by adopting FLP-106 as propellant are hereby described. The chamber pressure is set at $P_c = 2 \text{ MPa}$, and the expansion ratio is varied between 50 and 120. No further increments have been analysed since RPA could not converge to a solution for an higher expansion ratio. The combustion temperature has remained constant at $T_c =$

2132.84 K; the combustion and nozzle efficiencies provided by the RPA tool remained constant at $\eta_b = 0.9716$ and $\eta_n = 0.9721$, for a total efficiency of $\eta_{tot} = 0.9445$. Below in Figure 4.2, it can be seen how the total efficiency affects the specific impulse value of the propellant: for an expansion ratio of $\varepsilon = 120$, the I_{sp} is evaluated to be at around 250 s, taking into account the total thruster efficiency.

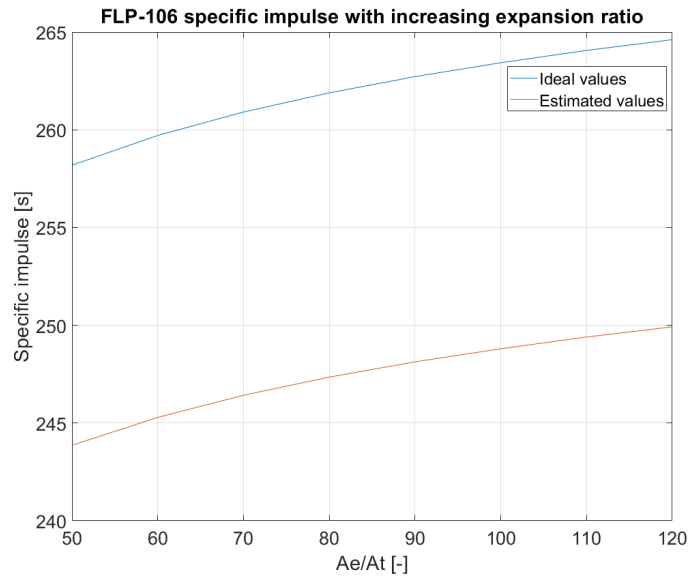


Figure 4.2: Ideal and estimated specific impulse level of FLP-106 with varying expansion ratio.

These values can be used to estimate the amount of propellant volume that will be needed to be carried on-board for the mission, using the Δv budget found in the previous chapter. It can be found with the Tsiolkovsky equation, accounting for the propellant density:

$$V_p = \frac{M_0}{\rho_p} \left[1 - \exp\left(-\frac{\Delta v}{g_0 I_{sp}}\right) \right] \quad (4.11)$$

Using Equation (4.11), the initial mass of the spacecraft and propellant budget from the previous chapter, and the specific impulse values of the propellant found earlier, an estimate of the volume that FLP-106 itself will be needed to be carried for the mission is found, and shown below in Figure 4.3:

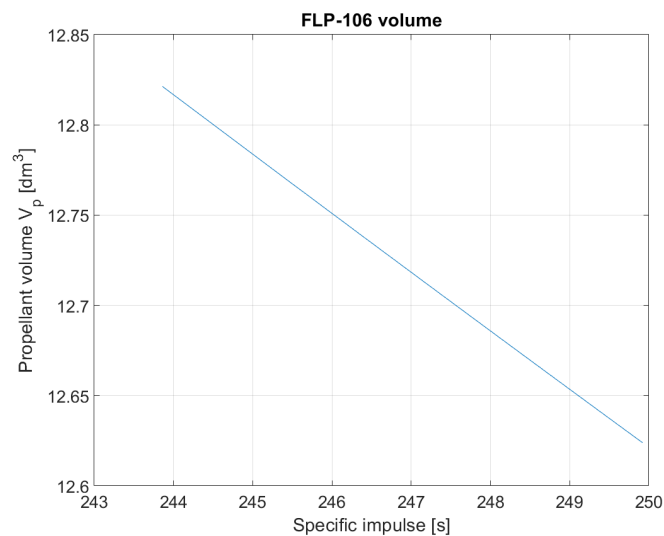


Figure 4.3: FLP-106 volume intake for the mission with varying specific impulse, given an initial spacecraft mass of $M_0 = 30$ kg.

It can be seen how increasing the specific impulse diminishes the amount of total volume occupied by the propellant, since less mass is required. For FLP-106 and the initial conditions defined by the propulsion system requirements, the propellant volume only varies between 12.62 to 12.82 dm^3 or U (spacecraft units).

The same procedure is repeated for AF-M315E composition, adopting the same thruster and chamber approximations used for the FLP-106 case: exit semi-half angle of 15° , contraction area ratio of $\varepsilon_c = 50 - 100$, frozen flow at nozzle exit and chamber pressure of $P_c = 2$ MPa. By adopting the composition mentioned earlier though, the outputs of RPA do not match with the data found from literature shown in Table 4.3. In fact, for an expansion ratio of $Ae/At = 50$ and other inputs mentioned earlier, the outputs of the tool are:

- Theoretical specific impulse $I_{sp} = 274.36$ s
- Chamber temperature $T_c = 2296.26$ K

which are considerably higher than the ones obtained for the same conditions from literature. Referring to Table 4.3, the specific impulse at this condition should be $I_{sp} = 266$ s, while the chamber temperature is $T_c = 2166$ K. Two options have been investigated to estimate the variation of specific impulse of AF-M315E at different expansion ratios: either by modifying the chemical components mass ratio, until values that match the data from literature is obtained and these values are used for the full analysis, or by adopting the previous method adopting Ideal Rocket Theory equations, based on literature data and expanding it to guess the specific impulse at higher expansion area ratios. Between the two, the latter has been adopted for the rest of the chapter.

Ideal rocket theory is adopted by using Equation (4.5) and Equation (4.9): since the case from literature has provided insights on the estimated properties of AF-M315E, shown in Table 4.6, the same equations can be applied using the known values of these parameters to estimate the effect on the specific impulse. Equation (4.5) is solved for a different area ratio to find the resulting pressure ratio, which is used in Equation (4.9) to find the specific impulse at that given area (and pressure) ratio. This method does not provide an estimate on both the combustion and nozzle efficiencies: using RPA with the composition of AF-M315E found in literature shows that the estimated efficiencies results are a combustion efficiency of $\eta_b = 0.9716$ and a nozzle efficiency of $\eta_n = 0.9721$, for a total efficiency of $\eta_{tot} = 0.9445$. These values are going to be adopted for the estimation of the real specific impulse of AF-M315E, which is found as follows:

$$I_{sp,real} = \eta_b \eta_n I_{sp,id} = \eta_{tot} I_{sp,id} \quad (4.12)$$

The estimated specific impulse values and volume intake of AF-M315E for the mission are shown below in Figure 4.4 and Figure 4.5, where the value of density $\rho = 1.47$ kg/dm³ is adopted. The expansion ratio range is chosen to vary between 50 to 200:

It can be clearly seen as for the same expansion ratio value of 120, FLP-106 reaches a specific impulse value of 250s, while the one from AF-M315E at the same conditions is 258 s. As expected, AF-M315E outperforms FLP-106 both in terms of specific impulse generation and volume to be carried on board, due to its higher density (and volumetric specific impulse). Both the propellants are good candidates for a mission that needs to adopt chemical mono-propulsion and has strict volume requirements: even if they are based on two different energetic ionic liquids, most of their properties are similar, as can be seen from Table 4.3 and 4.4. Due to the better performance in terms of both specific impulse and lower volume requirement, it is decided that **AF-M315E (ASCENT)** will be taken in consideration as the propellant of this propulsion system.

Since the specific impulse value of the propellant is now known, the procedure from Chapter 3 can be repeated in order to evaluate the Δv budget required to complete the mission, complying to the mission and propulsion system requirements. The optimal Δv_E for Earth escape amounts to 916.8 m/s, while the Δv_M for Mars capture is 967.7 m/s. The total Δv budget for the mission, margined by 10%, amounts to: $\Delta v_{miss} = 2072.90$ m/s. The specific impulse and mass of propellant to be carried on board are shown in Table 4.7.

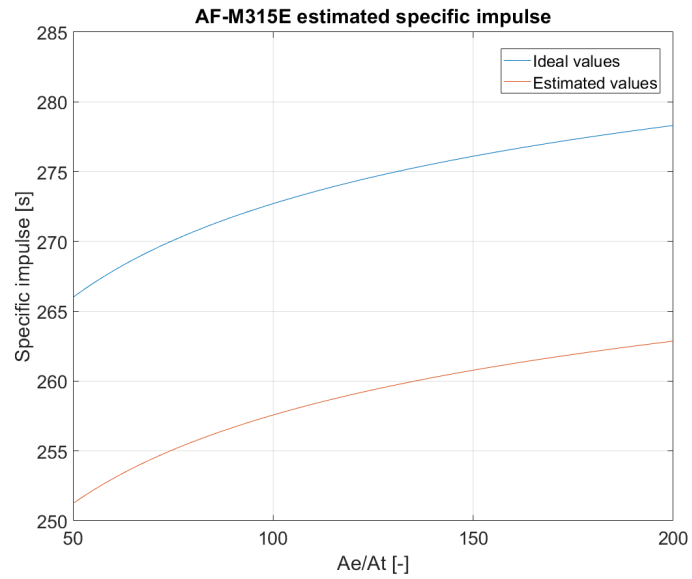


Figure 4.4: Ideal and estimated specific impulse level of AF-M315E with varying expansion ratio.

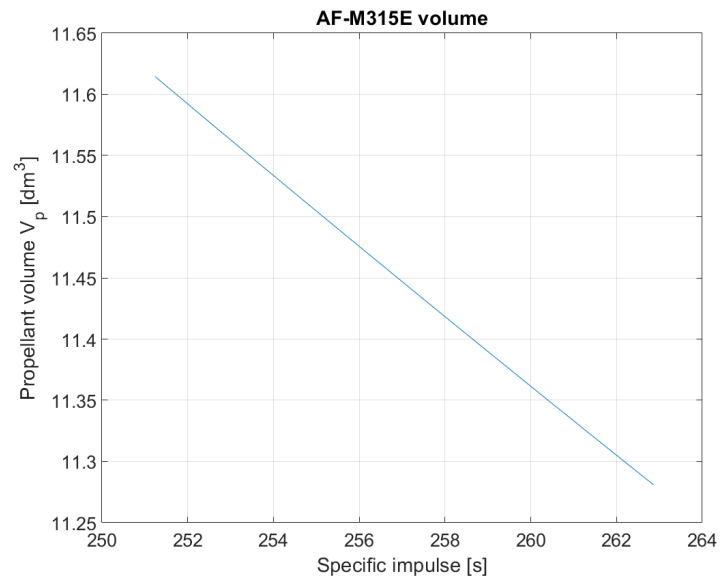


Figure 4.5: AF-M315E volume intake for the mission with varying specific impulse, given an initial spacecraft mass of $M_0 = 30$ kg.

Table 4.7: AF-M315E specific impulse and mass/volume given an expansion ratio of $\varepsilon = 200$ for an initial spacecraft mass of $M_0 = 30$ kg and $\Delta v = 2045$ m/s

Property	Value	Unit
I_{sp}	262.8650	s
Δv_{miss}	2072.90	m/s
M_p	16.5720	kg
V_p	11.2734	dm ³

The propulsion system requirements for an initial spacecraft mass of $M_0 = 30$ kg and specific impulse $I_{sp} = 262.865$ s are shown in Table 4.8.

Table 4.8: Chemical propulsion system preliminary requirements, assuming an initial spacecraft mass of $M_0 = 30$ kg.

ID	Rationale
PROP-01	The chemical propulsion system shall provide at minimum $\Delta v_{miss} = 2072.9$ m/s
PROP-02	The maximum thrust level of the system shall be 6 N.
PROP-03	The maximum burning time t_b shall be 600 s for each time the propulsion system is activated.
PROP-04	The propulsion system shall utilize non-toxic "green" propellant.

4.3. Conclusions

This chapter described the concept of propulsion applied to spacecraft, by mentioning the main performance parameters to take into account which were also anticipated in the preliminary mission analysis performed in Chapter 2. The division between different types of chemical propulsion systems has been highlighted (mono-, bi- and solid) together with the state-of-the-art propulsion system developed for CubeSat applications: this has brought light on understanding which kind of propulsion system is able to better perform in terms of specific impulse, complexity and technology readiness level (TRL). In order to decide which chemical propulsion system type better meets the requirements defined in Chapter 2, a trade-off between the three kinds has been done in order to choose the best option for a Mars autonomous CubeSat mission. Out of this trade-off, a chemical **mono-propulsion** system has emerged as the best option: it is easier to design and develop, its technology readiness level is high and the performance parameters of current mono-propulsion systems for CubeSat are also increasing, with respect to the older fashioned hydrazine-based ones.

Once the kind of chemical propulsion system has been chosen, the decision for which propellant to use is left. Chemical mono-propulsion systems have been currently developed and studied by several universities and companies, and have also been featured in recent missions to demonstrate their space operational capability. Furthermore, the interest has grown towards the adoption of the so-called "green" propellants, which are less toxic than the most commonly used hydrazine and can be used with fewer handling and storage requirements. The two main branches of green mono-propellants are based on ADN or HAN, to energetic ionic liquids (EIL). In total, five different propellants have been chosen as candidates for the mission: SHP-163, AF-M315E (ASCENT), FLP-103, FLP-106 and LMP-103S. Literature for all of the propellants has been carefully studied in order to obtain the most recent and reliable data for both chemical and physical properties, and were summarized in Table 4.3, Table 4.4 and Table 4.5. The different parameters from each propellant have been used to rule out 3 candidates out of 5, leaving only FLP-106 and AF-M315E to be more carefully analysed. This has been done through the use of the Rocket Propulsion Analysis (RPA) Tool for FLP-106, and ideal rocket theory equations for AF-M315E, since the output values of the tool did not match the values found in the literature. The result of this analysis showed how, even if for most characteristics the two propellant are very similar, in terms of specific impulse and volume requirement the **AF-M315E (ASCENT)** option better meets the needs of

this mission, and will therefore be considered the propellant to be used for the mono-propulsion system of the thesis.

Once the propulsion system type and the propellant have been chosen, the detailed chemical propulsion system design needs to be performed in order to carefully size the components that will ensure the correct functioning of the system, starting from storage, feeding lines, injector and catalyst bed. This will be done in Chapter 5.

5

Propulsion system detailed design

This chapter of the thesis work is written to describe in detail the design of the chemical propulsion system, given the kind of chemical propulsion system and propellant options chosen in the chapter before. This comprises the selection and design of most of the parts comprehending the rest of the propulsion system, namely the pressurization system, the feed lines components and the thruster interface.

5.1. Initial assumptions

5.1.1. Preliminary thruster design

Having chosen the propellant, an initial thruster design can be done to check the amount of thrust that the propulsion system can provide. It is crucial to remember that the thesis work shall be representative of the state-of-the-art of chemical propulsion system available for CubeSat, therefore it can not be assumed that very high levels of thrust can be achieved compared to the currently developed chemical thruster. For these reasons, it is decided that the baseline for the thruster design is taken from the most current technological advancements in terms of propulsion systems adopting AF-M315E as their propellant.

Looking at the state-of-the-art thrusters mentioned in the previous chapter, Busek Inc. and Aerojet Rocketdyne both employ AF-M315E as propellants: the first has developed the BGT-X5, a class 0.5 N thruster, while the latter has developed two different class thrusters of 1 and 22 N respectively. Due to the nature of the mission having as requirement PROP-02 a thrust level of 6 N, it is decided to design the thruster based on the Aerojet Rocketdyne thruster which, in combination with other elements, shall generate a total thrust that satisfies the propulsion requirement. These thrusters adopting AF-M315E have been used for the GPIM mission for NASA: originally developed to consist of four 1-Newton thrusters (GR-1) and one 22-N thruster (GR-22) from Aerojet Rocketdyne, in the end managed to consist of five 1-Newton thrusters only [45]. Each of these thrusters had the capability of 1-Newton as nominal values, but from the data-sheet it can be seen how this value can actually increase based on the higher the feed pressure is. There are actually two different references from the same manufacturer that show a slightly different behaviour for the thruster, and are listed below:

GR-1	
Thrust (N)	0.4 - 1.1
Feed Pressure (bar)	6.8 - 27.6
Nozzle Expansion Ratio	100:1
Valve Power (W)	12
Preheat Power (W)	10

(a) GR-1 thrust performance [59]

GR-1	
Nozzle Expansion Ratio:	100:1
Valve Power @ 28VDC, 10 °C (W):	8.3
Feed Pressure (bar):	37.9-6.9
Thrust (N):	1.42-0.26

(b) GR-1 thrust performance [60]

Figure 5.1: Table comparison of GR-1 thrust generation vs feed pressure. [59] [60]

Since [60] is more recent than [59], it is believed that the propulsion system parameters for GR-1 shown in Figure 5.1-(b) are up to date and therefore will be used for the rest of the thesis work. Overall, Figure

5.1 shows that even if the thruster has a nominal value of 1 N, there is data available that reports the possibility of achieving an higher thrust with the same element by adjusting the feed pressure, and therefore the chamber pressure, most probably due to the thrusters being tested in blow-down mode and showing the performances for a range of feed pressure. Requirement PROP-02, derived in the previous chapters and shown in Table 3.16, implies a total thrust level of 6 N: this values has been found by trying to minimize the Δv budget for Earth escape. Therefore, it is decided to adopt 5 thrusters as described before: 4 at the corners of a square and one positioned in the center. Each thruster will be sized to provide up to 1.2 N of thrust, to match the requirement of 6 N. Thrust and specific impulse are directly related to the mass flow of propellant exiting the satellite system, therefore the mass flow of propellant for the propulsion system parameters is obtained with Equation (5.1). The specific impulse value is obtained from Figure 4.4 for an expansion ratio of $\varepsilon = 200$:

$$\dot{m} = \frac{T}{I_{sp}g_0} \quad (5.1)$$

Table 5.1: Thrusters propellant mass flow and thrust parameters

Property	Value	Unit
Total thrust	6	N
Thrust per thruster	1.2	N
Specific impulse	262.865	s
\dot{m}_{tot}	2.3267	g/s
\dot{m} per thruster	0.46535	g/s
\dot{V}_{tot}	94.967	mL/min
\dot{V} per thruster	19	mL/min

As per the chamber pressure value, no data is available from the GR-1 data sheet. Since the specific impulse for the AF-M315E propellant have been obtained by using ideal rocket theory equations starting from the literature value of chamber pressure of 2 MPa, the same value will be needed to be obtained in this chamber design. To be consistent with the current state-of-the-art thruster GR-1, a first approximation on the feed pressure level is made for the pressurization system design: it is expected that high losses are obtained from pressure drops due to the high viscosity of the propellant. These will be estimated more in detail in the next sections, but as a starting point a value of 3 MPa is chosen. It is obtained by linearization of the feed pressure vs thrust values of Figure 5.1: adopting the same feed pressure vs thrust ratio taken by the upper limit of the available thrust and multiplying it for a value of 1.2 N, the first reference provides a value of 3 MPa while using the second reference data provides a feed pressure level of 3.2 MPa: since the latter reference is more recent and also confirmed by [41], the feed pressure value of $P_{feed} = 3.2$ MPa is used and it is assumed to be capable of providing the chamber pressure necessary to generate up to 1.2 N of thrust.

5.1.2. Pressurization system

There are several options for a propulsion system to provide the propellant at the correct mass flow rate and pressure that is needed to generate thrust. Typical satellite propulsion system are the reference pressurized systems: regulated or blow-down.

A regulated system stores the pressurant gas needed to feed the propellant at high pressures in a different tank from the propellant one. The initial pressure of the pressurant gas is usually of several hundred bars, and this is needed in order to make sure that the propellant is fed through the feed system at a constant high pressure, with the means of using a regulator. A regulated system has also been designed for the MARIO mission that has been taken as a reference for the interplanetary trip to Mars, since constant high-level thrust is required in order to escape Earth and stabilize around Mars. Its reliability is lower compared to a blow-down system, due to its complexity, while its cost is higher because of the components that allow for a constant and precise high value of fluid pressure.

In a blow-down system the pressurant is not stored at an high pressure as for the regulated case. For this reason, the pressure at which the propellant will be fed after leaving the tank will decrease after each time the propulsion system is employed since the gas will expand in the tank, lowering the mass flow and thrust. Typical storage pressures for a blow-down system are lower than the pressure at which the pressurant gas is stored in a regulated system, but a larger storage volume will be needed to store the same amount of pressurant mass. For this reason, this option is not considered for this particular application since precise and constant thrust are needed for this particular mission and the way it has been designed: the availability of high level of thrust when reaching Mars is critical for the success of the stabilization. Since the satellite will enter the martian orbit with an hyperbolic trajectory, it has only one chance to fully stabilize around the planet, otherwise it will continue on its open trajectory and exit the martian sphere of influence. A blow-down system would inevitably provide much lower thrust levels in the second phase of the mission compared to the Earth escape phase, considering that half of the pressurant would have already left the tank and the pressure would be critically reduced. Furthermore, the amount of pressurant volume to be stored for a blow-down system increases by a lot the total volume of the tank storing both propellant and pressurant: typical blow-down ratio values for missions range between 2 to 4 [12] [82], meaning that assuming an isothermic expansion of the pressurant the total tank volume has to be considerably higher than respect to the propellant volume, as shown by Equation (5.4). The blow-down ratio B_R is the ratio between the initial and final pressure of the gas inside the tank, which in isothermic conditions is equivalent to the ratio of the initial and final volume of the gas.

$$B_R = \frac{V_g^{(f)}}{V_g^{(i)}} = \frac{V_t}{V_p} \quad (5.2)$$

where the apex (f) refers to the pressurant final condition and (i) to the initial conditions. It is assumed that the final volume of the pressurant will coincide with the total volume of the tank, once all of the propellant is expelled. Therefore, the volume of the tank consisting of both the propellant and the pressurant with respect to the volume of propellant is found as follows:

$$V_t = V_p + V_g = V_p + \frac{V_t}{B_R} \quad (5.3)$$

$$V_t = V_p \left(\frac{B_R}{B_R - 1} \right) \quad (5.4)$$

For blow-down ratios of 2 to 4, the tank volume would increase between 33 % to 100% with respect to the propellant volume. Due to the mission requirements posing an high burden on the Δv budget of the mission, the propellant itself already takes a lot of the available volume of the CubeSat: it is estimated that the amount AF-M315E volume to be carried on-board is already 11.28 U, as shown in Table 4.7, taking most of the space of the hypothetical 16/24 U CubeSat. Increasing this volume by such high factors would render the design of the propulsion system unfeasible for this CubeSat application, since the shape of the tank will surely be sub-optimal in terms of volume containment, ending up taking up even more volume of the spacecraft. For this reason, together with the need of constant thrust which can not be obtained by adopting this option, a blow-down system is not considered feasible for this mission.

The option of adopting a regulated pressure system is therefore not investigated further: a second tank will need to be reserved for the pressurant, and the pressure at the end of operation needs to be at least a factor 2 higher than the pressure in the propellant tank [82]. In the MARIO [36], this resulted in an initial pressure of 28 MPa for the pressurant: for this mission, it is envisioned that the system might be launched with the lowest pressurization possible since it is expected to be launched together with bigger satellites. Having an high pressurized system might increase the risks of the main mission and is also not recommended for CubeSat missions in general. Adding another tank increases the volume required for the propulsion system which is already taking most of the mass and volume of the spacecraft. Hence, it is decided to not further analyse the possibility of adopting a regulated pressure system.

The early designs of both a blow-down system and considerations for a regulated system have shown that each of these solutions is not compatible with the low volume requirement of a CubeSat missions which has to spend half of its available volume in wet propellant only. It is decided to explore a feed system type that has been only recently proposed for applications to CubeSat, which is the use of micro pumps. Pump-fed systems are widely used for larger systems: they consist of one or several pumps that transfer the propellant (or propellants) from their tanks to the distributor and injector. The advantage of using a pump in order to achieve the correct feeding conditions to the chamber is that lower tank pressurization values are allowed: if the pump is used in order to provide the high pressure values required for correct combustion, the propellant can be stored at lower pressure values with respect to regulated and blow-down systems. This comes at the cost of power usage, since the pump will be needed to use electric power in order to correctly function and generate the pressure differential for the fluid. But, compared to the other two solutions, the use of a micro pump for this application is the most optimal for volume saving, which is critical in CubeSats application like this one, where the amount of propellant mass is high and will surely take most of the available units of the satellite.

The preliminary design which will be optimized in the following chapter comprehends a single tank containing both propellant (AF-M315E) and pressurant (gaseous N_2) at a relatively low storage pressure: the proposed application is to have just enough pressure from a small amount of pressurant gas inside the propellant tank in order to obtain, with the pressure differential provided by the pump, the correct mass flow rates and pressures that are defined in literature for AF-M315E and were detailed before, ensuring to have the same operating values reported in reviews.

5.1.3. Pressure drops causes and estimation

Before looking for a pump that meets the needs for the propulsion system, a few clarifications need to be made on the feed system. First, pressure losses need to be taken into account when looking at the whole scheme of the propulsion system: the sum of the tank (current) pressurization level plus the pressure differential provided by the pump does not need to be only equal to the chamber pressure, but it needs to surpass them by a margin given by the pressure losses that will be present in the system, as shown by Equation (5.5).

$$P_{press} + \Delta P_{pump} - \Delta P_{loss} = P_c \quad (5.5)$$

The most relevant pressure losses that occur in the system will be listed below.

Injector The injector is usually designed in order to have an high pressure drop across the injector in order to de-couple the feed system from the combustion chamber, enhancing combustion stability. A common requirement for it is taken from [82], where the pressure drop across the injector needs to be taken as 20% of the chamber pressure. For this case, since the chamber operating pressure is $P_c = 20 \text{ bar}$, the pressure drop across the injector needs to be:

$$\Delta P_{inj} = 0.2 \cdot P_c = 4 \text{ bar} \quad (5.6)$$

Feed lines and components Flowing through the pipes, the propellant will experience pressure drops due to friction. These losses do not contribute highly to the pressure drops of the system like the injector does, but can become relatively high if the diameter of the feed lines is too small. The amount pressure drop also depends heavily on the nature of the fluid, namely its dynamic viscosity: the more viscous the fluid is, the higher the shear stress acting on it when flowing through the pipe and higher losses will be experienced. AF-M315E is considerably more viscous than water (1 cP) and other ADN-based propellants (3 cP), since its viscosity at room temperature is 25 cP. Depending on whether the fluid will follow a laminar or turbulent flow, different models can be used to estimate the friction experienced through a feed line. The same happens for other components such as valves and filters: passing through any of this additional components inside the propulsion system lines will cause an amount of pressure drop. Generally the manufacturer provides a data-sheet with a calibration graph that helps generalizing the amount of pressure drop based on the mass flow and other fluid characteristics. If possible, these manufacturer approximations will be used, otherwise general approaches for typical pressure drop in valves or filters will be analysed.

Catalyst bed The catalyst bed is one of the most critical component when designing of a mono-propellant system, since proper materials and pellet dimensions need to be adjusted to make sure that complete chemical decomposition of the propellant is achieved. During the decomposition process, though, the flow of reacted gas/liquid phase will experience a pressure drop due to friction and inertia of the fluid passing through the catalyst bed particles. These losses are not only defined by the physical properties of the fluid, but the total dimensions of the catalyst bed and its pellets also play an important role in the friction determination.

5.2. Pump selection

In order to provide the necessary pump feed pressure that the system requires, it has been decided to adopt a micro-pump as it is the best solution in terms of volume compactness for a CubeSat application which already requires a lot of propellant wet volume for the mission. While such a solution ends up adding an higher burden on the power usage while it needs to be active, it relieves the propulsion system from a secondary tank to store a pressurant at high pressures, or large volumes of pressurants in a typical blow-down system. An important aspect to be taken into account is also the mass and the volume of such an additional component: while it allows for a lower pressurization of the tanks, it has to be compact enough to fit in the CubeSat size.

The total feed pressure to be provided after the pump has to be at least the feed pressure that has been derived from literature in the earlier section, $P_{feed} = 3.2$ MPa. Since the tank will empty during the mission, the pump needs to be able to vary its operating point to constantly adjust the pressure differential such that it equals the feed pressure requirement. This means that the propellant in the tank will initially be at high pressures and at the end of operations, when most of the propellant is ejected, the pressure after the expansion will be considerably lower depending on the initial to final volume ratio. It is convenient to have the pressure of the tank as low as possible in order to reduce the amount of thickness of the tank needed to withstand the pressure and have the pump provide most of the ΔP to the propellant: the micro-pump needs to be chosen such that it can provide the required feed pressure by itself, considering the end of life operation of the propulsion system. At the beginning of life the pressurant will push the propellant with higher initial pressures and in that case the pump shall adjust its operating point to a lower ΔP to provide a constant mass flow and a similar feed pressure to ensure the correct functioning of the propulsion system as it has been designed for.

The micro-pump shall therefore be capable of providing at least a pressure differential of $\Delta P = 30$ bar to a total flow rate of $\dot{V}_{tot} = 94.967$ mL/min, capable of fitting inside the CubeSat remaining volume and with the lowest possible amount of power requirement.

5.2.1. Pump performance estimation

Products from several companies have been investigated to find a micro e-pump that would provide the correct mass flow and pressure differential to the propellant in use. Pump data-sheets that have been investigated for space application generally provide their working parameters as graphs based on flow rate and pressure differential provided; in some cases, different behaviour based on several viscosity option is also provided, as well as the total torque and power requirement. Between all of the analysed manufacturers, two micro-pumps have been selected as the most performing given the needs of the mission: they are both from the same manufacturer, FlightWorks Inc., and the candidate models are 2212-M04C49/C50/C51 [29] and 2212-M04X01/X03/X04 [30]. The information regarding the mass flow rate with respect to pressure are shown in Figure 5.2 and Figure 5.3 respectively. The C-model pump allows for a maximum pressure differential of 450 psid, which corresponds to 31.02 bar, while the X-model can provide up to 440 psid, matching 30.34 bar of pressure differential and a maximum flow rate of 185 and 190 mL/min: these values are fluid-dependent since performance will vary based on the fluid viscosity and the voltage control applied to the pump, which changes the power input and the speed of the rotors. Both of the components weigh 175 g only and the dimensions consist of a diameter of 22 mm and a total length lower than 10 cm: these values make both of the candidates very promising for this mission, since they can provide a high pressure differential and easily fit in the CubeSat allocated volume. They are both proven to be compatible with AF-M315E (ASCENT), as mentioned from the manufacturer website [2]. As it can be seen from Figure 5.2 and Figure 5.3 the data sheet provides information about the pump operating points at different speeds: the lowest available speed being 5000 rpm, while 15000 rpm is the highest. The graphs are only provided for

four different fluid viscosities, which are reported in $cP = mPa \cdot s$: the y-axis represents the volumetric flow rate [mL/min], while the x-axis the provided pressure differential [psid]. The propellant that has been chosen for this application has, on the other hand, a viscosity value of $25 mPa \cdot s$ for which the performance values are not known. It is therefore decided to recreate the graphical data from the data sheet on MATLAB and interpolate the values in order to obtain an expectations of the performance of this pump for all the range of viscosities: in this way, it can be seen whether the pump would correctly allow for the mass (or volumetric) flow and pressure differential that is needed for the correct thrust generation of the propulsion system.

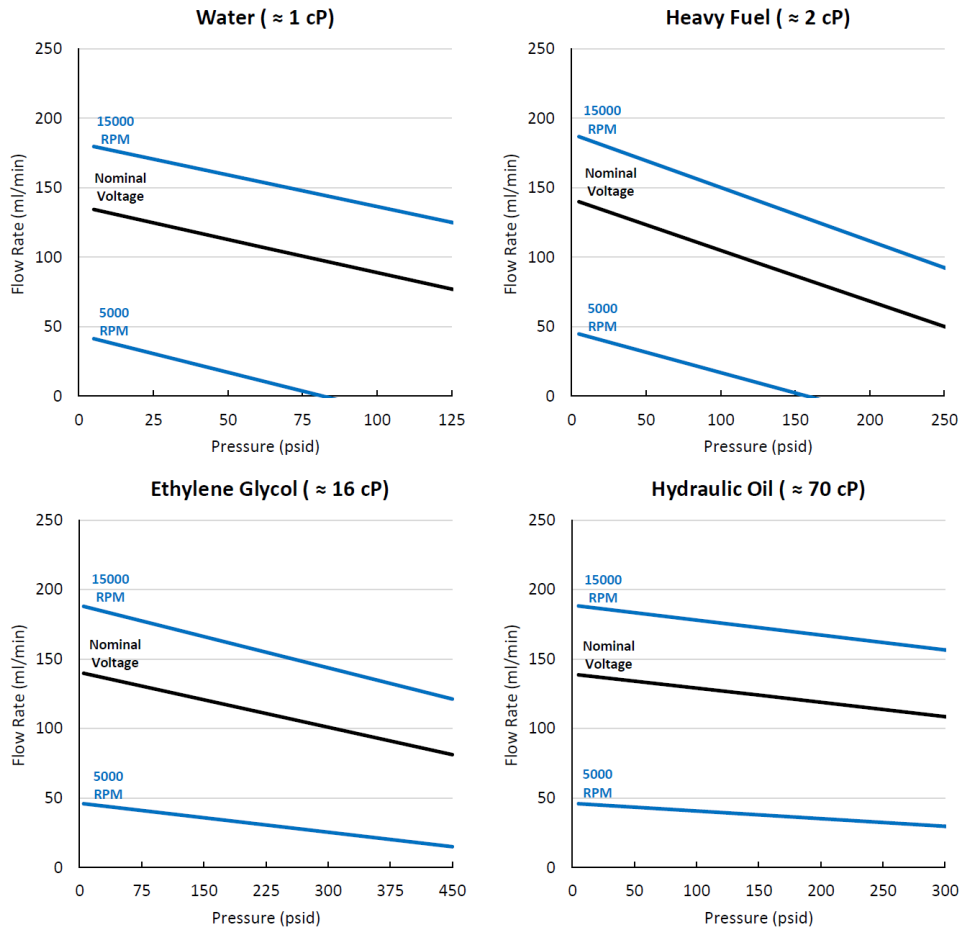


Figure 5.2: Pump 2212-M04C49/C50/C51 performance values for different fluid viscosities [29]

The performance graphs for both the candidate pumps show an increase in the maximum pressure differential at increasing low viscosities and a lower value for the viscosity value of $70 mPa \cdot s$. The maximum value reached is respectively at 450 and 440 psid, which correspond to 31.20 and 30.34 bar. In general, the trend that can be noticed from the pump data-sheets is that for increasing viscosities the three lines representative of lowest, nominal, and highest rotational speed become inclined, tending to horizontal.

The first step towards interpolation of the previous graphs for the viscosity value of AF-M315E is the interpolation of the maximum pressure differential that each pump can provide among the range of viscosity of interest: this operation is performed for the pressure differential values only, since it highly differs from viscosities, while the volumetric flow rates keeps its maximum limit at 185 and 190 mL/min respectively, regardless of viscosity. In this way, it is possible to gauge what is the maximum pressure differential that the pump can provide at each viscosity value, and can be applied for the AF-M315E case which is characterized by a viscosity value of 16 cP. The next step will be the estimation of the performance based on the three available operating lines of 5000 rpm, nominal voltage and 15000 rpm: once the maximum pressure differential has been estimated, the four graphs can be extrapolated from

the data sheet and their mathematical expression can be found. The slope and offset of each line can be then interpolated among the viscosity range, in order to reproduce the behaviour of the pump in each of the three modes.

The interpolation of the maximum pressure differential has been performed using MATLAB: the MATLAB function "pchip" has shown to be the most resembling of the trends hereby discussed, and the results are shown in Figure 5.4. The value of maximum pressure differential is intended as the maximum value for which the data sheet provide an operating point on the graph: theoretically, the maximum pressure differential at a given pump velocity should be reached for a null volumetric flow, which would not provide helpful information. For both the pump components, the maximum pressure differential at each viscosity is chosen as the latest value for which an operating point is found in any voltage configuration. In particular, for pump model 2212-M04X01/X03/X04, the maximum pressure differential at 16 cP is found at 440 psid, as mentioned by its data sheet [30]. The maximum pressure differential is seen increasing for the early range of fluid viscosity, which resembles the increase shown for both data sheet when moving from 1 to 2 to 16 cP of viscosity. Finally, the maximum pressure differential remains stable and drops afterwards for higher viscosity values, until it reaches the final viscosity value reported in the data sheet of 70 cP.

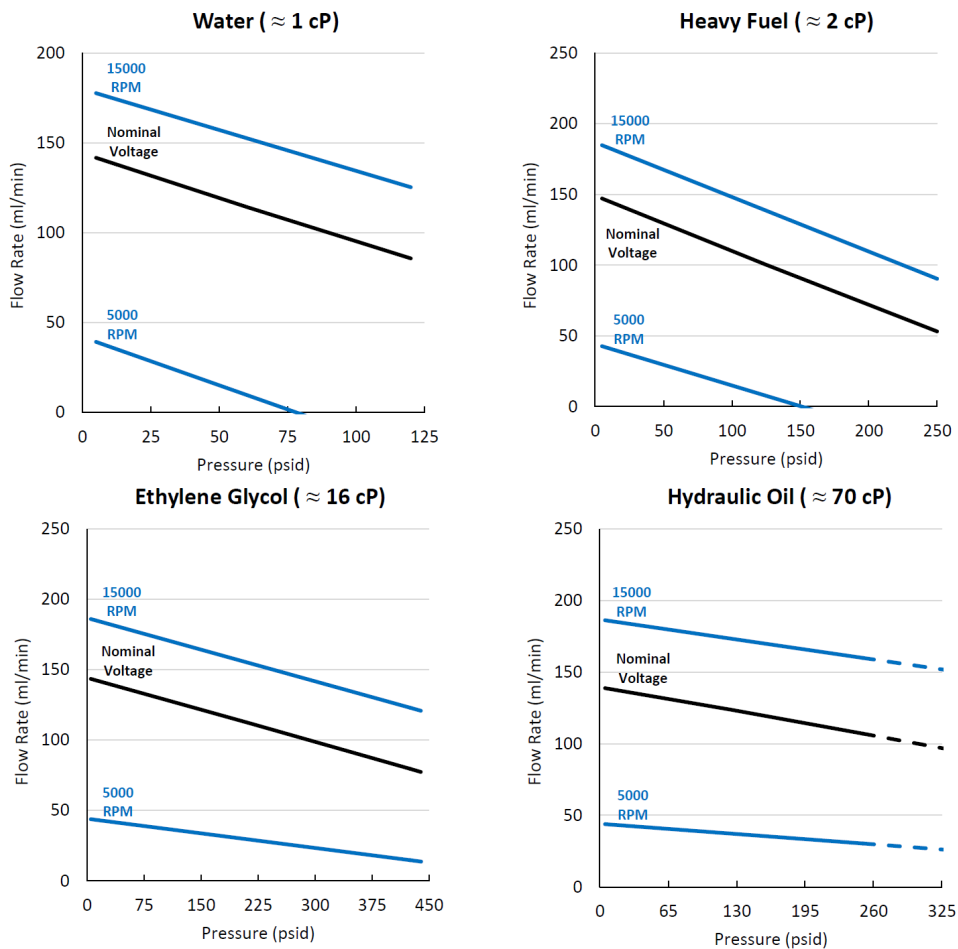
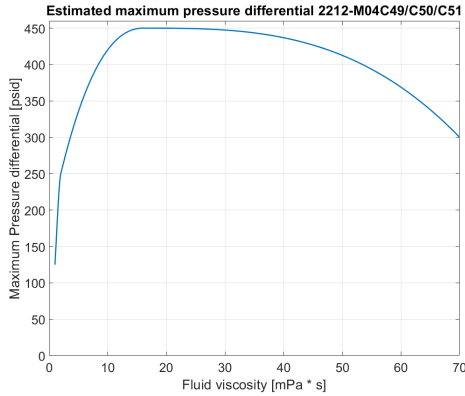
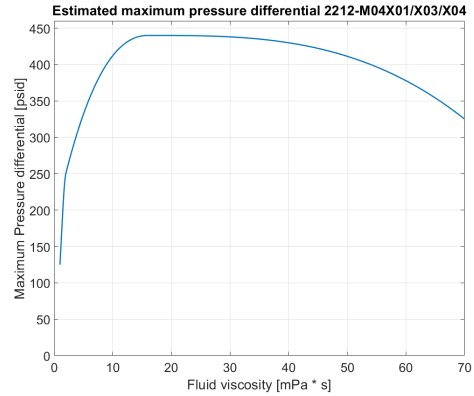


Figure 5.3: Pump 2212-M04X01/X03/X04 performance values for different fluid viscosities [30]



(a) Estimated maximum pressure differential with respect to fluid viscosity for pump model 2212-M04C49/C50/C51



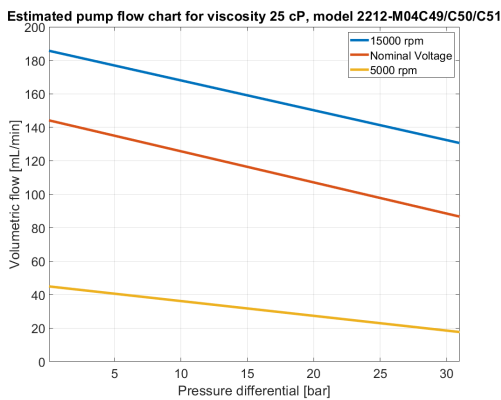
(b) Estimated maximum pressure differential with respect to fluid viscosity for pump model 2212-M04X01/X03/X04

Figure 5.4: Maximum pressure differential values interpolated among the working fluid viscosity range

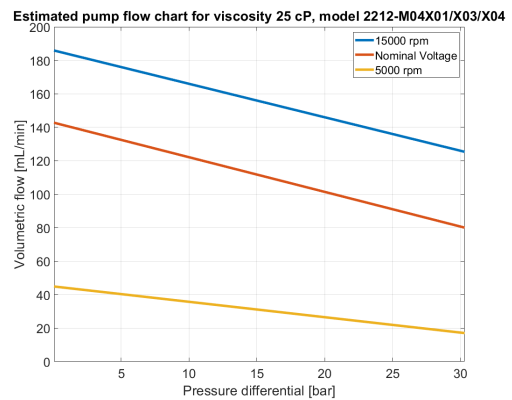
Once the maximum pressure differential has been obtained for the viscosity range reported by the data sheet, the behaviour of each pump based on the rotating speed is interpolated in order to verify what type of voltage/current/rotational speed are needed for the pump to operate correctly during the mission: a different operating point will also need different input power, which needs to be correctly estimated. By choosing two points on each line of the graphs, the slope coefficient m and the offset of the line q can be estimated for each operating line, obtaining the relation between fluid flow rate and pressure in analytical terms:

$$Flowrate[mL/min] = m \cdot Pressure[psid] + q \quad (5.7)$$

The values of m and q have been obtained for each of the three operating lines of the pump given by the minimum, nominal and maximum speed and these values have been interpolated as well among the viscosity range by using the MATLAB function "pchip" also adopted for the maximum pressure differential interpolation. The procedure of interpolation of each graph is shown in Appendix C. The final graphs representing the operating lines of each pump for a viscosity value of 25 cP are shown in Figure 5.5.



(a) Estimated maximum pressure differential with respect to fluid viscosity for pump model 2212-M04C49/C50/C51



(b) Estimated maximum pressure differential with respect to fluid viscosity for pump model 2212-M04X01/X03/X04

Figure 5.5: Maximum pressure differential values interpolated among the working fluid viscosity range

It has been estimated that the total (for all of the four thrusters) volumetric flow rate is around 94.967 mL/min , while the pressure requirement at the chamber is 2 MPa . To satisfy the feed pressure requirement of 3.2 MPa to coincide with the literature data, meaning that to keep a final low pressurization in the tank

a value of at least 3 MPa of pressure differential need to be delivered by the pump. It can be seen how for a constant volumetric flow rate of around 100mL/min, both the pumps are capable of providing up to 30 bar of pressure differential: pump model 2212-M04C49/C50/C51 can provide a slightly higher pressure differential of 31 bar, while pump model 2212-M04X01/X03/X04 can reach the value of 30.34 bar. Since the performance are very similar, the decision between which candidate to be chosen will be made taking into account other characteristics such as weight, dimensions but most importantly power: since power available for a CubeSat system is as critical as volume, the total power needed to correctly operate the pump needs to be as low as possible. These considerations will be thoroughly detailed in the following section of the thesis.

5.2.2. Pump power usage estimation

The data-sheet from each pump also provides information regarding the power input necessary to work at a given speed. Table 5.2 and Table 5.3 display the power requirement for model 2212-M04C49/C50/C51 and 2212-M04X01/X03/X04 respectively.

Table 5.2: Pump models, with nominal voltages, speed constant and max continuous current values for pump 2212-M04C49/C50/C51 [29]

	Nominal Voltage	Speed Constant	Max Continuous Current
C49	12 V	981 RPM/V	3.21 A
C50	24 V	416 RPM/V	1.40 A
C51	48 V	211 RPM/V	0.69 A

Table 5.3: Pump models, with nominal voltages, speed constant and max continuous current values for pump 2212-M04X01/X03/X04 [30]

	Nominal Voltage	Speed Constant	Max Continuous Current
X01	12 V	1050 RPM/V	2.71 A
X03	24 V	549 RPM/V	1.40 A
X04	48 V	274 RPM/V	0.72 A

It can be seen that there are indeed three models which differ by the nominal voltage input: from this point onwards, only the model adopting a nominal voltage of 12 V is considered for both candidates. By using the values from Table 5.2, the nominal rpm and the power at maximum current input can be found:

$$rpm_{nomC} = V_{nomC} \cdot SC = 11772 \text{ rpm} \quad (5.8)$$

$$P_{nomC} = V_{nomC} \cdot I = 38.52 \text{ W} \quad (5.9)$$

where V_{nom} is the nominal voltage of the pump, SC is the speed constant and I is the current. Applying the same procedure for the other candidate using data from Table 5.3 results in:

$$rpm_{nomX} = V_{nomX} \cdot SC = 12600 \text{ rpm} \quad (5.10)$$

$$P_{nomX} = V_{nomX} \cdot I = 32.52 \text{ W} \quad (5.11)$$

Between the two pumps, it can be noted that pump model C requires more nominal input power compared to pump model X: this is most probably due to the different pressure differential that can be reached by the two components, since the former can provide up to 31 bar of pressure differential, while the latter only up to 30.3 bar. Since the difference performance-wise is similar at viscosity levels of 25 cP, it is decided that pump model 2212-M04X01X03X04 is the chosen candidate to be adopted in the propulsion system, due to the lower power requirement.

The power requirement obtained earlier is only applicable when working at nominal voltage conditions and maximum continuous current, and is indicative of a single operating point of the pump. Since the

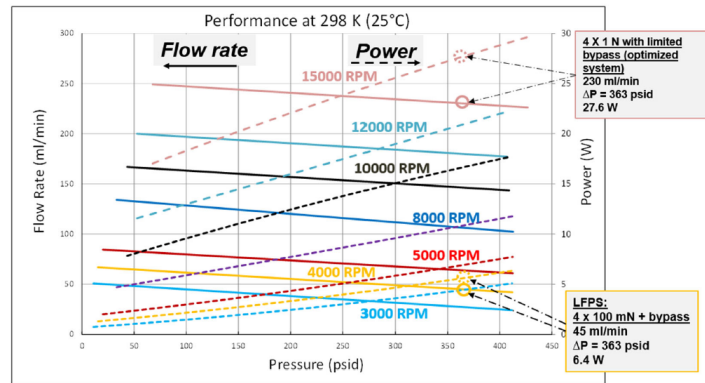


Figure 5.6: Lunar Flashlight pump performance and power requirement at different speeds [11]

pressurant in the tank will expand, the pressure at which the propellant will exit the tank will decrease over time, requiring more ΔP from the pump and therefore a newer operating point.

Throughout the missions, the pump will work at different operating points due to the lowering pressure inside the tank. At BOL, the propellant will exit the tank at high pressure and therefore the pump can produce a lower value of ΔP such that at the exit of the pump the fluid pressure will still be around 3.2 MPa. The power needed to operate at this condition will surely be lower than the power at end of the transfer and also dependent on the pressurization of the tank, which will be detailed in the next section. Since this value will mark the lowest pump power requirement, the attention is shifted towards the behaviour of the pump at end of the transfer: in this case, the propellant tank will almost be empty and at low pressure, therefore the pump needs to provide most of the ΔP . It is convenient to design the system in this way in order to keep the pressurization of the tank as low as possible, requiring less thickness from the tank structure. Since the maximum pressure differential of the pump is 30.34 bar, it is decided that the lowest pressure of the tank needs to be higher than at least 2 bar.

$$P_{min} > 2 \text{ bar}$$

To identify the power requirement at the end of the transfer conditions, the correct values of voltage and current need to be extrapolated from the interpolated graph shown in Figure 5.5 (b): the volumetric flow of the propellant is 94.967 mL/min and the pressure differential is chosen to be the maximum available, to simulate the lowest propellant pressure case. It can be noted how for this operating case, the nominal speed (voltage) of the pump will not suffice and an higher voltage will need to be applied in order to correctly generate the ΔP for the volumetric flow: since the operating point is below the maximum allowable speed of the pump, this point is not out of range. During interpolation, it has been noted how for high pump speed the slope of the lines is constant, with the only difference shown in the offset which increases linearly with the speed (voltage). For these reasons, the line corresponding to an higher speed of the pump can be easily found by generating a line which passes through the operating point at end of the transfer: in this way the speed and voltage of the pump in that conditions are known, and the maximum power needed by the pump can be estimated.

While the voltage is shown to control the speed of the rotor of the pump, via the speed constant provided in the data sheet, there is only a single value provided for the current which is the maximum continuous current that is allowed to flow. Since no information is provided regarding how current influences the performance of the pump, it is reasonable that this parameter may affect the position of the operating point once the speed (voltage) is fixed: the further it is among the line, the more current is needed, until reaching the maximum available pressure differential which is characterized by the max continuous current. This linear behaviour is confirmed in the analysis of the mission Lunar Flashlight, which also plans to adopt a pump-fed propulsion system for its CubeSat mission to the Moon by employing a different pump from Flightworks, Inc. In Figure 5.6 it can be noted how following a line of constant speed corresponds to a linearly increasing power requirement at high speeds, suggests that the linear approximation for the current usage is applicable to the pump adopted for the Mars mission too.

Following these considerations, Equation (5.7) can be inverted to find the offset at the operating point at end of the transfer conditions and estimate the speed at which the pump will need to operate in

that case, obtaining the corresponding voltage and, given that the maximum current is circulating since the end of the transfer conditions operating point is at the maximum available pressure differential, the power requirement can be estimated. Doing this procedure leads to the operating point conditions at end of the transfer shown in Table 5.4

Table 5.4: Pump operating conditions at the end of the transfer conditions.

Property	Value	Unit
\dot{V}	94.967	mL/min
ΔP	30.34	bar
Speed	13609	rpm
Voltage	12.96	V
Power	35.12	W

5.2.3. Pump dimensions

Other than its performance, the selected pump has been chosen since it is highly compatible with a different range of fluids, while also being compact and lightweight- Most of the other pumps, from the same and other different customers, were not capable of providing the correct volumetric flow rate/pressure differential, and those that could had much bigger dimensions compared to the one selected here, and weighing more. The mass of the pump is 175 g.

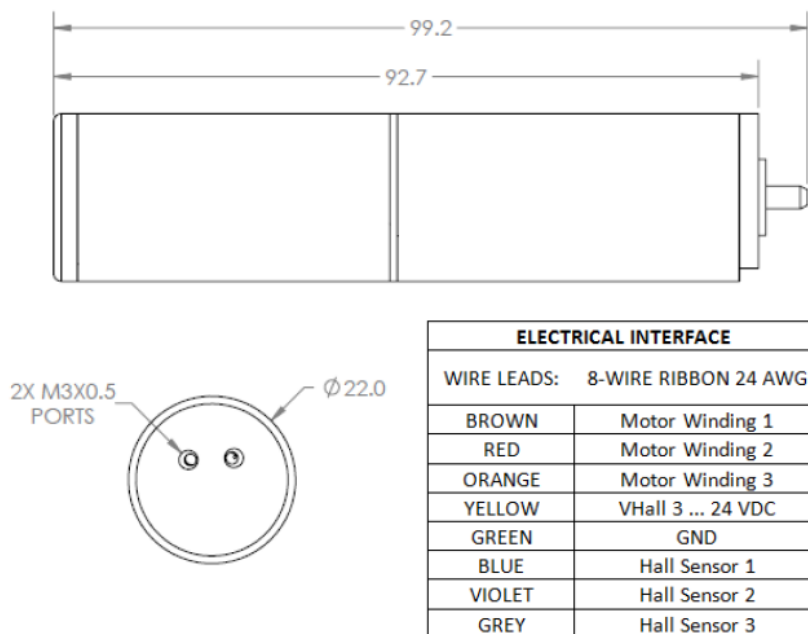


Figure 5.7: Pump model 2212-M04X01 dimensions in mm [30].

Unfortunately, no data is available regarding the minimum feed pressure required to the pump to operate correctly and avoid cavitation. Therefore, it is assumed that the minimum value of the tank pressure of 2 bar is enough to not generate cavitation during operating conditions.

5.3. Tank design

This section of the chapter will highlight the main choices undertaken during the design of the tank. The maximum pressure level needs to be considered, since at BOL the pressurant will not have expanded and the tank needs to withstand an higher level of pressure compared to the end of the transfer conditions. The design includes the research for a tank shape that better fits inside the CubeSat volume,

as well as the decision on which material is able to withstand the internal pressure of the tank without causing the tank body to add too much weight to the propulsion system.

5.3.1. Pressurization level

In a typical blow-down system the propellant tank is filled with both the propellant and the pressurant gas. An important parameter for a blow-down system dimensioning is the blow-down ratio, which is defined as the ratio between the final and initial volume occupied by the pressurant gas. By assuming that all of the propellant will be used, the blow down ratio B_R is found with:

$$B_R = \frac{V_g^{(f)}}{V_g^{(i)}} = \frac{V_t}{V_g^{(i)}} \quad (5.12)$$

where the apex (f) refers to the pressurant final condition and (i) to the initial conditions. It is assumed that the final volume of the pressurant will coincide with the total volume of the tank, once all of the propellant is expelled.

It is clear that having pressurant inside the propellant tank will determine an increase of the tank itself, due to allocating both pressurant and propellant in the same space: the volume increase, by initially assuming only propellant and pressurant will be present inside the tank, is found with:

$$V_t = V_p + V_g = V_p + \frac{V_t}{B_R} \quad (5.13)$$

$$V_t = V_p \left(\frac{B_R}{B_R - 1} \right) \quad (5.14)$$

As expected from Equation (5.14), when increasing the blow-down ratio, the increase of the tank volume with respect to the ideal tank containing only propellant volume is lower, since less pressurant will be present inside the tank. This consideration may direct towards the choice of a very high blow down ratio, but choosing a value too high will negatively effect the pressure that the tank will need to sustain at BOL. In order to evaluate the maximum operating pressure of the tank which will be acting at BOL, a regression has to be made from the final operating pressures: starting from the end of the transfer conditions, it is possible to determine what are the initial properties of the gas at the beginning of operations. When considering the expansion of the gas, there are a few options on which approximations to use to describe the expansions of the gas:

- Isothermal expansion: if the gas expansion is slow and the tank is subject to heat exchange, the process can be approximated by an expansion of the pressurant with its temperature remaining constant throughout the process.
- Isentropic expansion: if the gas expansion is fast and there is no heat exchange with the tank, the process can be approximated as if there was no heating within the system.
- Polytropic expansion: a polytropic expansion is a process which happens in between the previous two cases.

Since the tank is projected to take most of the propulsion system volume, together with the fact that there are going to be several activations of the propulsion system in which the expansion will slowly decrease the amount of propellant mass each time, it is decided to treat the expansion of the pressurant as isothermal. By using the ideal gas law, together with the minimum required feed pressure, the mass of propellant gas is obtained with:

$$M_g^{(f)} = \rho_g^{(f)} V_t = \frac{P_{min} V_t}{R_g T_g^{(f)}} \quad (5.15)$$

The same can be done for the initial conditions:

$$M_g^{(i)} = \rho_g^{(i)} V_g^{(i)} = \frac{P_g^{(i)} V_g^{(i)}}{R_g T_g^{(i)}} \quad (5.16)$$

By assuming isothermal expansion, the initial and final temperature of the pressurant are the same. Therefore, the ratio between the initial to final pressure of the pressurant tank is found with:

$$\frac{P_g^{(i)}}{P_{min}} = \frac{V_t}{V_g^{(i)}} = B_R \quad (5.17)$$

The pressurant chosen for this application is gaseous N_2 at initial 293 K of temperature. The following graph shows the relation between the initial to final pressure ratio, with respect to the blow-down ratio of the system:

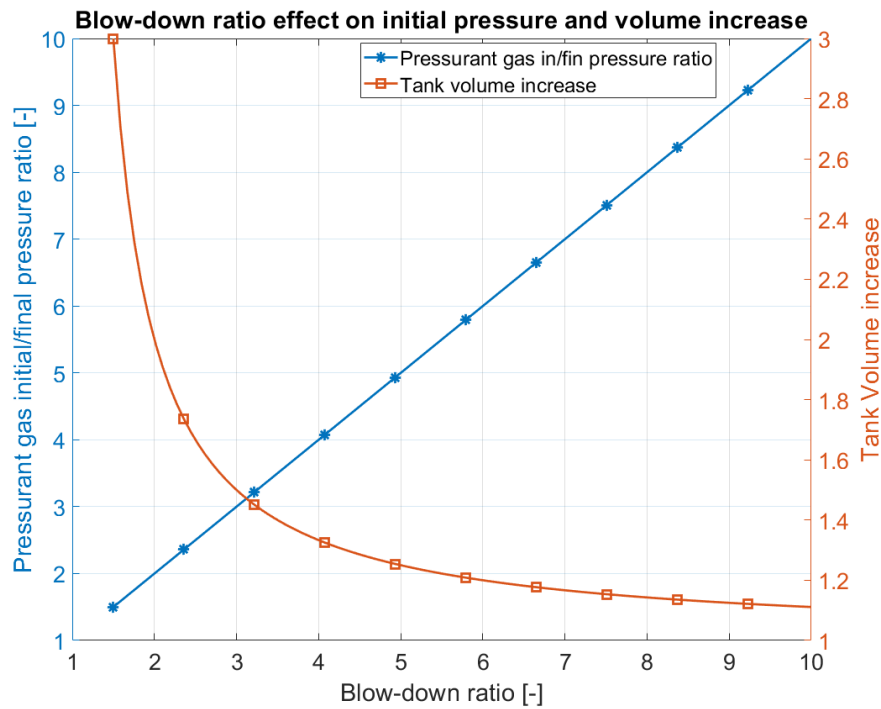


Figure 5.8: Initial to final pressure ratio of pressurant gas and internal tank volume increase for blow-down ratio varying between 1 to 10.

It can be seen from Figure 5.8 that in order to minimize the internal volume of the tank comprehensive of both propellant and pressurant, the blow down ratio shall be as high as possible. On the other hand, this will lead to an increase in the pressurant gas initial pressure, once its final conditions are fixed: if the initial volume of pressurant gas is too small, its pressure will need to be very high in order to make sure that after full expansion, the final pressure condition is met and the pressure does not become too low. High initial pressure of the pressurant will result in having to increment the thickness of the tank, that will need to be able to withstand high pressures, increasing its volume and mass.

Since no minimum required feed pressure value is available for the pump, the value of minimum tank pressure obtained from the previous section of $P_{min} = 2 \text{ bar}$ is used as an end of the transfer requirement for the tank pressure: the previous consideration will be used in order to inversely derive the tank initial pressure requirement, in order to make sure that, after full emptying, the minimum value of 2 bar is achieved and the pressure does not decrease even lower. Given from Figure 5.8 the tank volume does not decrease considerably for blow-down ratios values higher than 7, it is decided that a preliminary value for the blow-down ratio is 7. This means that the total internal volume of the tank comprehending propellant and pressurant is:

$$V_t = V_p \left(\frac{B_R}{B_R - 1} \right) = 1.167 V_p \quad (5.18)$$

Considering a 5 % increase due to PMD that will likely be present in a further design of the tank, the total internal tank volume will adjust at:

$$V_t = 1.217 V_p = 13.72 \text{ dm}^3 \quad (5.19)$$

The initial tank pressure will therefore be:

$$P_g^{(i)} = P_{min} B_R = 14 \text{ bar} \quad (5.20)$$

The density of gaseous Nitrogen at 298 K and at a pressure of 14 bar is found through NIST database [1], and verified with the gas constant equation by using a gas constant of $R_{N_2} = 297 \text{ J/kg/K}$ [82]. The density value at these conditions amounts to $\rho_{N_2} = 15.866 \text{ kg/m}^3$. The volume of pressurant is $V_{N_2} = 0.167 V_p = 1.883 \text{ dm}^3$, meaning that the total weight of pressurant is $M_{N_2} = \rho_{N_2} V_{N_2} = 0.03 \text{ kg}$.

The MEOP is chosen to be at 1.25 times more than the initial gas pressure to have a slight margin when calculating the thickness for the tank structure:

$$MEOP = 1.25 \cdot P_g^{(i)} = 17.5 \text{ bar} \quad (5.21)$$

5.3.2. Tank shape

Given the amount of total impulse to be provided by this propulsion system, the shape of the tanks is a critical parameter that will affect most of total volume occupied on the CubeSat by the propulsion system, and the amount of volume available to allocate the rest of the subsystems. The mass of the tank is influenced too: given different shapes, the stresses that the tank will need to withstand will require different minimum thickness, and therefore the mass of the tank will also vary based on the shape of the tank. Since for this initial iteration the spacecraft initial mass is 30 kg and the propellant mass is already over 16 kg, the tank can not be too heavy or there will be no available mass budget for the rest of the subsystem.

Cylindrical tank with emi-spherical caps One of the most commonly used shapes for propellant tanks is a cylindrical one, with two emi-spherical caps at the end. This particular shape is able to withstand very high pressure with minimum thickness for both the cylindrical and spherical caps. On the other hand, due to the large amount of propellant mass (and volume) to be carried on-board, using a conventional cylinder with emi-spherical caps is not convenient, since it would occupy most of the available volume. The total length occupied by a cylindrical tank of volume V with emi-spherical shells of radius R_t is given by Equation (5.22):

$$L_{tot} = \frac{V}{\pi R_t^2} + \frac{2}{3} R_t + 2 t_{sphcap} \quad (5.22)$$

The thickness of the cylindrical and spherical cap are respectively:

$$t_{cyl} = \frac{MEOP \cdot R_t}{\sigma} SF \quad (5.23)$$

$$t_{sphcap} = \frac{MEOP \cdot R_t}{2\sigma} SF \quad (5.24)$$

where the MEOP is the maximum expected operating pressure, R_t is the radius of the tank, σ is the yield stress of the material and SF is the safety factor to be applied, chosen to be 1.5 for this case. The titanium alloy Ti-6Al-4V is used as material for the tank, with a yield strength of $\sigma = 880 \text{ MPa}$ and a density of $\rho_t = 4430 \text{ kg/m}^3$.

The mass of the tank is found by evaluating the external volume, subtracting the internal volume to obtain the volume of the shell, and multiplying by the tank material density:

$$V_{out} = \pi(R_t + t_{cyl})^2 L_{cyl} + \frac{4}{3} \pi(R_t + t_{sphcap})^3 \quad (5.25)$$

$$V_{in} = \pi R_t^2 L_{cyl} + \frac{4}{3} \pi R_t^3 \quad (5.26)$$

$$M_t = \rho_t (V_{out} - V_{in}) \quad (5.27)$$

The available range of the inner radius is varied between 90 to 98 mm: the values of mass and total height for this tank shape are shown in Figure 5.9.

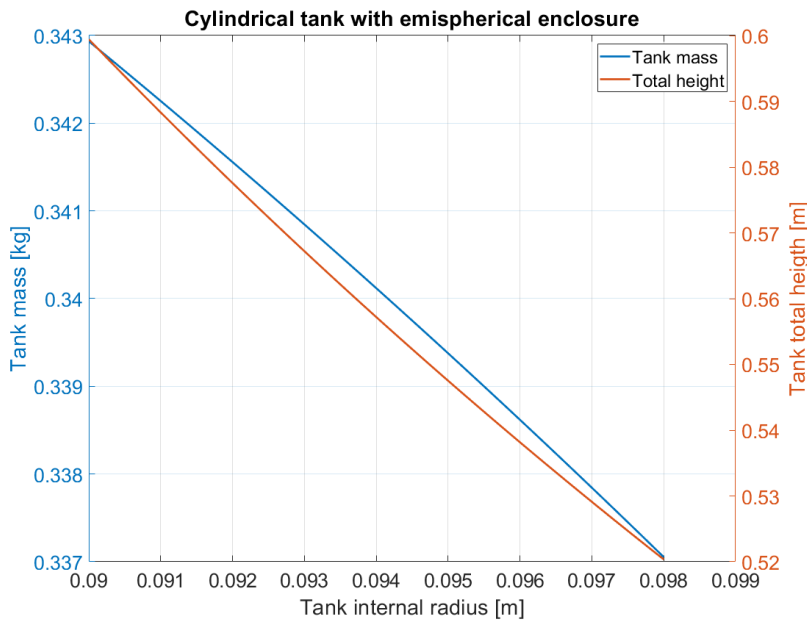


Figure 5.9: Mass and height of cylindrical tank with emispherical enclosure on internal radius R_t .

Considering the maximum available tank radius of 98 mm, the total height of the tank amounts to $L_{tot} = 52 \text{ cm}$, while its mass is $M_t = 0.337 \text{ kg}$.

Circular cross-section with plate enclosure Having a circular cross section with two circular plates that enclose the inner volume is the most efficient way to contain as much volume as possible for a circular cross-section, since the section is not reduced in the semi-spherical parts of the caps. Therefore, it is analysed as one of the possibilities for containing the propellant for this missions. The use of cylindrical tanks is very common in space-applications, since they are easy to manufacture and require small thicknesses due to the constant and low distribution of stresses on its circumference. Having circular caps is not optimal in terms of thickness requirement, since the distribution of stresses among a circular shape help minimize the amount of thickness required to withstand internal pressure. A flat cap requires much more thickness to withstand the same amount of pressure, as it will be shown in this section. While in the previous case the thickness of the spherical caps could be ignored for the approximate total length calculation of the tank, it is not negligible for this application; the total length of a tank with circular cross section and flat caps is found with:

$$L_{tot} = \frac{V}{\pi R_t^2} + 2t_{cap} \tag{5.28}$$

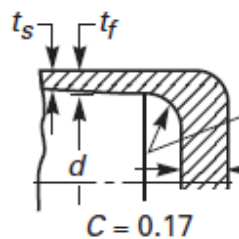


Figure 5.10: Integrally forged flat head [75]

The thickness for the cylindrical part of the tank, due to internal pressure loadings, is found with Equation (5.24), while for the circular plates to enclose the cylinder, the thickness is found with [82]:

$$t_{cap} = \sqrt{\frac{C \cdot MEOP \cdot D_t^2}{\sigma}} SF \quad (5.29)$$

Here, the coefficient C depends on how the cap is integrated within the pressure vessel. For integrally forged shells this amounts to a value of $C=0.17$, as can be seen from Figure 5.10. The mass of the cylindrical tank is obtained with:

$$M_t = \rho_t (V_{out} - V_{in}) \quad (5.30)$$

$$M_t = \rho_t [(\pi(R_t + t_{cyl})^2(h_{cyl} + 2t_{cap}) - \pi R_t^2 h_{cyl})] \quad (5.31)$$

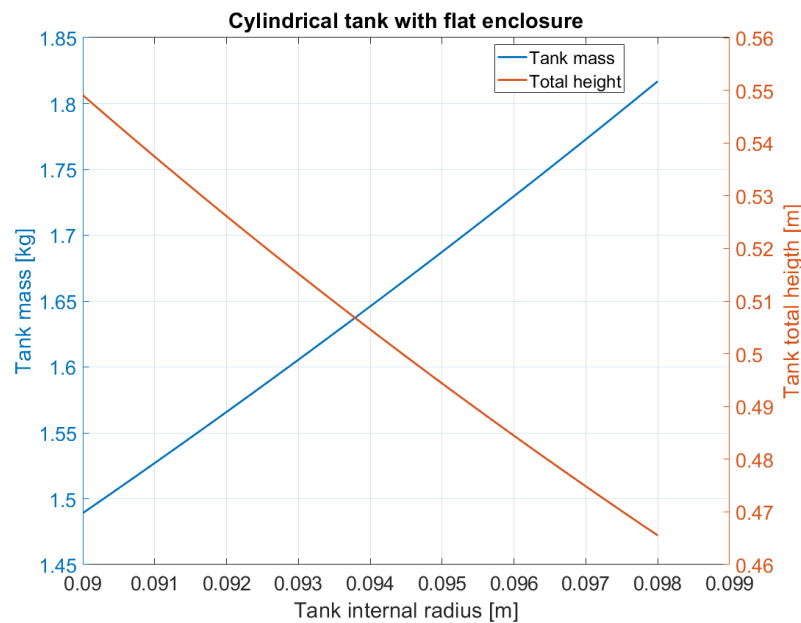


Figure 5.11: Tank mass and total height based on internal radius R_t .

As it can be seen from Figure 5.11, by adopting the solution of a cylindrical tank with flat enclosure it is possible to reduce the total height of the tank (considering the thickness of the two flat caps) with respect to the hemi-spherical caps case. Of course, this causes an increase in the total mass of the tank since the additional material required to withstand the pressure in the caps is considerably higher than the stress in the spherical caps. For the internal radius value of 98 mm, the total height can be as low as 46 cm. This result will be compared with another available option for the tank shape.

Rectangular cross-section Another option to be investigated is a shape that is not commonly seen particularly in space applications because of the non-optimal distribution of stresses: in a perpendicular cross-section pressure vessel, the stresses are different on each point since there are both membrane and bending stresses acting at the same time. In this case it worth analysing this option, since being allowed to use the whole square section instead of a circular one will optimize the amount of volume taken by the tank. Such a solution has already been proposed in other study cases such as [10] and [26]. The latter, from TU Delft, has been found suitable for application to smaller satellites. Due to the particular shape of the tank, the section can be schematized as shown in Figure 5.12. In this particular application, the smaller side H will represent the base of the tank (2×2 U), while the longer side h will represent the internal height: from [75], the stresses can be found by analyzing only one fourth of the section itself, thanks to its symmetry properties.

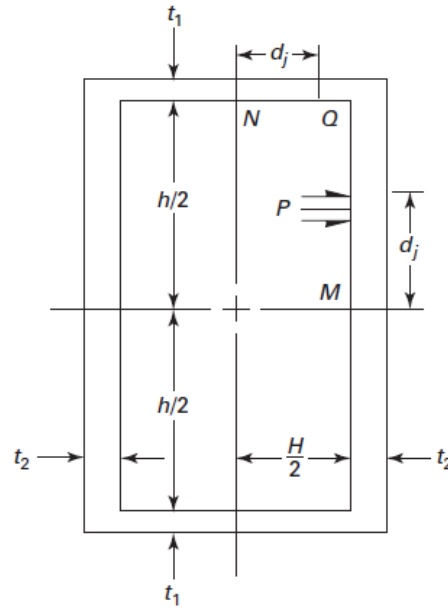


Figure 5.12: Sketch of pressure vessel of non-circular cross section

The points in which the highest stresses may reside are the ones denoted by N , M , and Q in Figure 5.12, which correspond to the mid-point of each side of the section, and the corner. The following equations are reported from [75], providing an estimate of the stresses acting on each of these points. The membrane stress are found by using Equation (5.32) and Equation (5.33), respectively for the short and long-side plates:

$$S_m = \frac{MEOP \cdot h}{2t_1} \quad (5.32)$$

$$S_M = \frac{MEOP \cdot H}{2t_2} \quad (5.33)$$

where t_1 and t_2 are the thicknesses of side of length h and H respectively, as shown from figure 5.12. The bending stress acting on each of the three points is calculated with Equations (5.34) - (5.36):

$$S_{bN} = \frac{MEOP \cdot c}{12I_1} \left[-1.5H^2 + h^2 \left(\frac{1 + \alpha^2 K}{1 + K} \right) \right] \quad (5.34)$$

$$S_{bQ} = \frac{Ph^2 c}{12I_1} \left(\frac{1 + \alpha^2 K}{1 + K} \right) \quad (5.35)$$

$$S_{bM} = \frac{MEOP \cdot h^2 c}{12I_2} \left[-1.5 + \left(\frac{1 + \alpha^2 K}{1 + K} \right) \right] \quad (5.36)$$

in which $c = t/2$ is the distance from neutral axis of cross section, $I = t^3/12$ is the moment of inertia, $\alpha = H/h$ is the rectangular vessel parameter and $K = (I_2/I_1)\alpha$ is the vessel parameter. Finally, the total stress acting on points N and M , the mid-points of each side of the vessel, can be found by combining the previously calculated stresses:

$$S_{Ntot} = S_m + S_{bN} \quad (5.37)$$

$$S_{Mtot} = S_M + S_{bM} \quad (5.38)$$

$$S_{Qtot} = S_m + S_{bQ} \quad (5.39)$$

For the MEOP value of 17.5 bar and a short-side length of $H = 17.5$ cm and a long-side length of $h = 44.83$ cm, the following stresses in point N , M and Q are obtained:

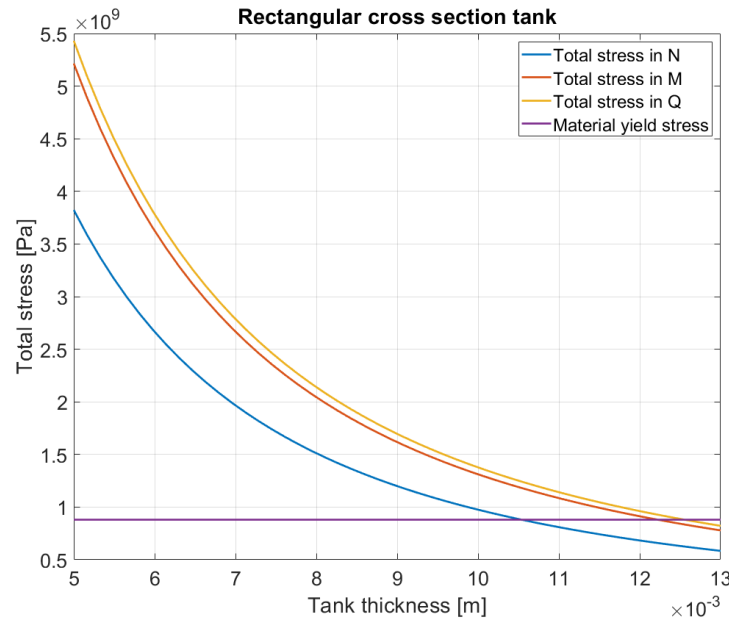


Figure 5.13: Total stresses in point N (mid-line of short side of the tank), point M (mid-line of long side of the tank) and maximum yield stress of tank material.

As can be seen from Figure 5.13, the stresses on each mid-line point will be different based on the thickness of that side. Given the different dimensions of the two sides of the tank, there are going to be two different thickness limits for each side in order to be able to withstand the internal pressure. The thickness of the short side needs to be minimum $t_1 > 10.5$ mm, while the thickness of the long side needs to be at least $t_2 > 12.5$ mm. Such values are much higher than the previous case, since non-circular sections are not optimal to withstand high pressures.

The mass of this prismatic tank can be found with:

$$M = \rho_t (V_{out} - V_{in}) \quad (5.40)$$

$$M_t = \rho_t [(h + 2t_1)(H + 2t_2)^2 - hH^2] = 22.34 \text{ kg} \quad (5.41)$$

The total length is given by $L_{tot} = h + 2t_1 = 46.93$ cm, but the mass is definitely too high to be considered a feasible application for a Cubesat mission. It is envisioned that further work could be done in this topic, by either choosing a different shape for the prismatic tank or by reinforcing the internal parts of the tank to make it withstand internal pressure without only relying on the structure of the walls.

5.3.3. Conclusions

This section of the chapter described the evaluation of the most optimal shape of the tank, as well as the amount of volume, mass and pressure of the gas pressurant at the initial state of operations (BOL). The conditions of the pressurant at BOL are crucial to the whole mission, since on the one hand the tank needs to withstand the maximum amount of pressure which occurs at BOL conditions, while at full expansion of the pressurant there needs to be enough residual pressure to satisfy the end of the transfer minimum pressure requirement set in the previous section. Otherwise, the sum of the pressurized propellant and the maximum pressure differential of the pump will not satisfy the 3.2 MPa feed pressure requirement. Between the three options, the cylindrical tank with flat enclosures seems the most efficient in terms of volume, without adding too much weight to the propulsion system. The prismatic tank mass is too high to be considered applicable to this mission, while the cylindrical tank with semi-spherical caps helps saving around 1.5 kg with respect to the flat caps one, at the cost of a total height of 52 cm, compared with 46 cm of the flat caps one. Since the maximum volume considered is 24 U, corresponding to a maximum available height of 60 cm for all of the subsystems and payload, for the initial spacecraft mass of $M_0 = 30$ kg the cylindrical tank with flat caps seems to be the most promising option in terms of volume saving, at the cost of the mass budget. Below, in Table

5.5, a detailed summary of the volume, mass and dimensions of the propellant pressurization system is highlighted:

Table 5.5: Tank, propellant and pressurant volume and mass budget.

Property	Value	Unit
Propellant volume V_p	11.2734	dm^3
Propellant density ρ_p	1.47	kg/dm^3
Propellant mass M_p	16.5720	kg
Pressurant volume (GN2) V_{N_2}	1.883	dm^3
Pressurant density (at 298 K) ρ_{N_2}	15.866	kg/dm^3
Pressurant mass M_{N_2}	0.03	kg
PMD volume V_{PMD}	0.564	dm^3
Tank internal volume V_{T-in}	13.72	dm^3
Tank internal radius R_{T-in}	98	mm
Tank internal height h_{T-in}	454.721	mm
Tank circumference thickness t_{cyl}	0.292	mm
Tank external radius R_{T-out}	98.29	mm
Tank cap thickness t_{cap}	5.405	mm
Tank external height h_{T-out}	465.5	mm
Tank density (Ti-6Al-4V) ρ_T	4.430	kg/dm^3
Total tank volume V_{T-out}	14.130	dm^3
Tank structure volume V_{t-s}	0.4101	dm^3
Tank mass	1.817	kg

5.4. Feed system

The feed system is to be designed by taking into account the pressure drops that will happen throughout the system. There will be several components that will ensure the correct functioning of providing the thruster the propellant at the correct pressure rate: these components will also cause some pressure losses to the flow which need to be estimated.

5.4.1. Preliminary design

This section will focus on the preliminary design of the feed system for the propulsion system: a sketch of the feed system will be generated and for the main components a research will be performed to find a COTS solution that could fit the needs of the mission, needing to keep mass and volume as low as possible while also satisfying the requirements of the mission. Afterwards, an early estimation of the pressure drops occurring along the feed system will be included, for both the COTS component (if possible), the feeding lines and the injector plate.

The tank will need a fill and drain valve to allow for filling the tank with propellant and pressurant. It is expected that at least a pressure and a temperature sensor will be present in order to help with the estimation of propellant and pressurant left at any time of the mission. Before the propellant is fed to the pump, two other components are inserted: a filter, which is needed in order to avoid impurities inside the flow that may lower the performance of the system and cause the occurrence of malfunctions, and a latch valve that effectively de-couples the tank from the pump. The pump will be placed after these two components, and two other pressure and temperature sensor are placed right after the pump, together with a flow-meter: in this way, it is possible to verify whether the pump is working at the correct operating point by measuring the volumetric flow and the pressure of the propellant exiting the pump. Afterwards, the main feeding line will split into three different lines which respectively carry 2/5, 2/5 and 1/5 of the total volumetric flow. The latter line goes directly to the thruster located in the center of the array, while the other two lines get split again by using a tee junction into four lines which carry 1/5

of the volumetric flow each: in this way the flow is evenly divided between 5 lines, since the thrusters will also be designed equally and the operating conditions are expected to be the same. This option would fix the mass flow given the nozzle throat diameter of the thruster: any difference in the operating conditions, once the nozzle throat diameter is fixed, could generate differences in the mass flow division in-between thrusters. This issue can be solved by adopting active flow control through a flow-control valve, or integrated within the thruster valves: this option would nullify the errors that may be caused by different operating level conditions due to different pressure drops in the feeding lines, for example, but at the cost of higher mass and power. It is decided to not investigate further this option, since it would case an increase in mass and power requirements for each of the five thruster, but is left as a recommendation for the choice of a thruster valve, preferring a component which might also provide active flow control for the thruster.

Each thruster will be able to provide up to 1.2 N of thrust for a total of 6 N, as required from PROP-02 in Table 3.16. Before reaching the thruster, the propellant will go through a thruster valve that will be open only when the thrusters will need to be active. With this design, it is possible to correctly split the propellant line into 5 for each thrusters, while allowing closed-loop control over the pump by checking the volumetric flow and pressure of the propellant, being able to control the voltage and current over the pump to modify its operating point.

The fill & drain valve, together with the pressure and temperature sensors and flow-meter are expected to be found as COTS in a later stage of the design of the system: for this early level, a COTS choice is made for the other three components that would fit the needs of the mission. These are the filter, a latch valve and a thruster valve.

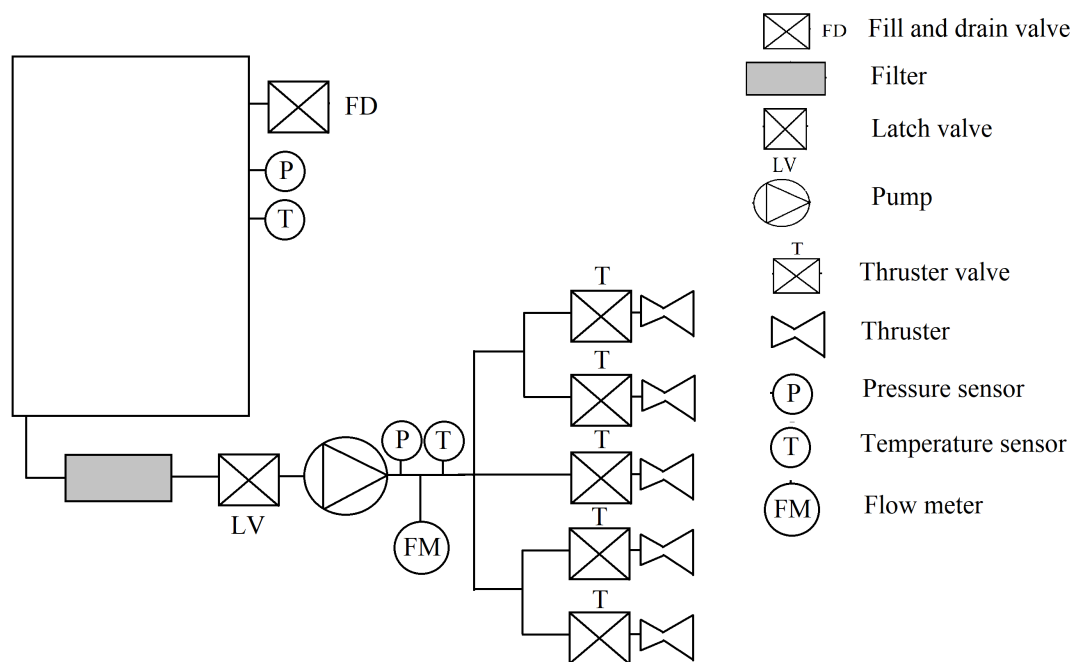


Figure 5.14: Propulsion system sketch.

Filter A filter is needed in a propulsion system in order to make sure to filtrate the flow from impurities. It is put before the latch valve and the pump in order to avoid malfunctions caused by the presence of foreign matter. It is also required to use a filter before the pump, from the pump manufacturer data-sheet [30].

A fitting component is found within the VACCO F1D10807-02 filter [73]. Its MEOP is 300 psi, which correspond to 20.7 bar: since the filter is going to be placed before the pump, the maximum pressure that it will experience will be 14 bar from the initial BOL pressurization level. The total diameter is 14 mm and the total length from inlet to outlet is 97.5 mm, making it a good choice for this application where as low volume as possible needs to be wasted. The weight is 0.053 lb, 0.025 kg.

thruster. The proof and burst pressure are 1500 and 2500 psi, respectively. It weights 85 grams, the maximum power requirement is < 4 W, and the external diameter is 27.7 mm, while the total length is 75 mm.

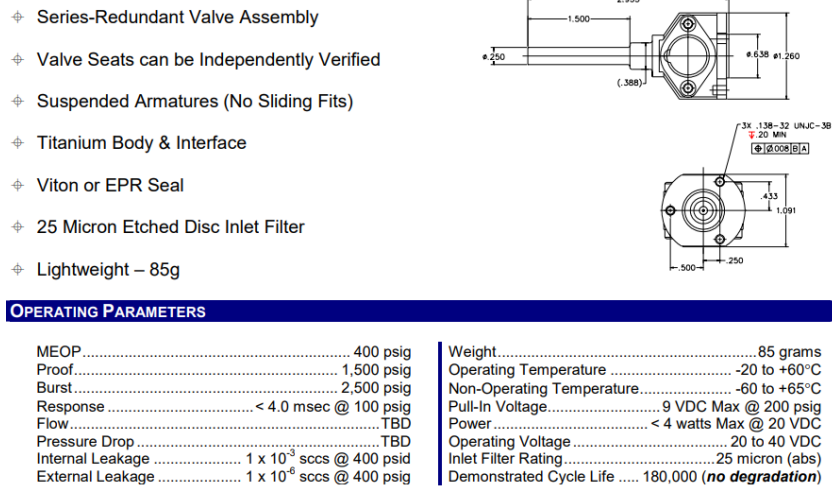


Figure 5.17: VACCO V0D10898-01 thruster valve data sheet [72]

5.4.2. Feed system pressure drop estimation

This section of the thesis is reserved to the estimation of the pressure drops that will occur along the feed lines and the COTS components of the propulsion system. While in the former case the value of viscosity μ is present in the equation and influences the results, the same is not found within the data-sheets of the components chosen for this application. The majority of them only provided the pressure drop values according to a fixed (or a range) flow of other fluids like water or hydrazine: just upscaling those values to the mass/volumetric flow of this application would only provide pressure drop values that would refer to that specific fluid shown in the data sheet. In the research pursued for the COTS components, a reference from Busek listed findings on the pressure drop correlation between water and AF-M315E through orifice calibration [67]. The results are only provided for volumetric flow rates between 9 to 12 mL/min, and show a pressure drop increase of a factor 2.2x with respect to the pressure drop occurring for water in the same conditions, as shown from Figure 5.18.

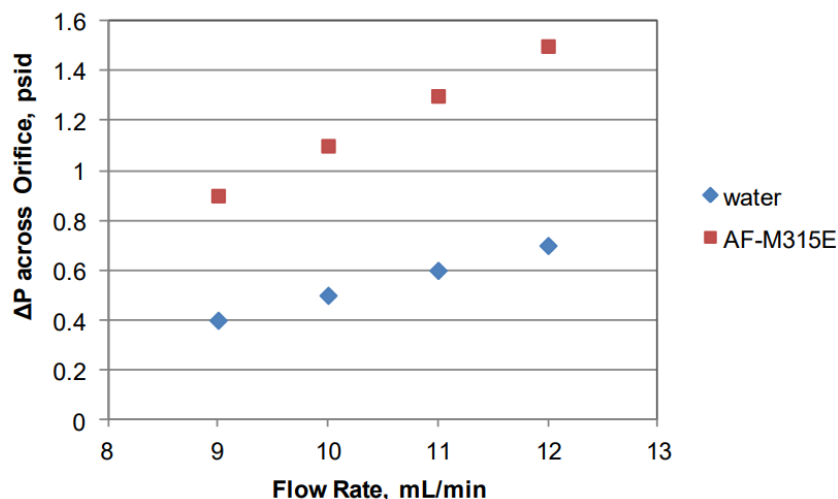


Figure 5.18: Pressure drop occurring for water and AF-M315E orifice calibration [67]

As listed in Table 5.1, the volumetric flows of AF-M315E in this application are 19 mL/min per thruster, for a total volumetric flow of 95 mL/min. Therefore this pressure drop factor can be applied when

estimating the pressure drops of the thruster valve and orifice, since the volumetric flow is comparable to the tested 9 to 12 mL/min. It is decided that the same value is adopted even for the case of the filter where the flow is still not divided, since it is expected that the pressure drop will not be high in this component and because the volumetric flow is still low and comparable to the ones tested, maintaining the linear trend shown in Figure 5.18. Since in [67] a factor of $2.2x$ is used to estimate the pressure drop across the valve after obtaining the pressure drop value from water, the same increase factor in pressure drop estimation will be used in the cases in which only a pressure drop related to the mass flow of water (or similar) is provided by data sheets. To properly adopt this correction factor which is valid for the same volumetric flow of water and AF-M315E, it needs to be reminded that such condition does not mean that the mass flows will be the same. This is important since most of the data sheets, as it will be seen below, provide information about the pressure drop based on the mass flow. If the pressure drop is based on the volumetric flow, then the same volumetric flow of AF-M315E can be used in the graph to obtain the approximated pressure drop. Due to the different densities of AF-M315E ($\rho_p = 1470 \text{ kg/m}^3$) and water ($\rho_{H_2O} = 1000 \text{ kg/m}^3$), having the same volumetric flow does not mean that the mass flow is the same:

$$\dot{V}_{H_2O} = \frac{\dot{m}_{H_2O}}{\rho_{H_2O}}; \dot{V}_p = \frac{\dot{m}_p}{\rho_p}; \dot{V}_{H_2O} = \dot{V}_p \Leftrightarrow \dot{m}_{H_2O} = \frac{\dot{m}_p}{1.47} \quad (5.42)$$

Hence, in cases where the pressure drop is provided in terms of mass flow of water (or similar), the correct mass flow of water will need to be adopted.

Tubing and connections The pressure losses for an incompressible laminar flow of density ρ , velocity v in a tube of length and diameter L_t and D_t is found with Equation (5.43):

$$\Delta P_t = f \frac{1}{2} \rho v^2 \frac{L_t}{D_t} \quad (5.43)$$

in which f is the friction factor defined by Equation (5.44):

$$f = \frac{64}{Re} \quad (5.44)$$

Given the fluid viscosity μ , the Reynolds number is calculated with Equation (5.45):

$$Re = \frac{\rho v D_t}{\mu} \quad (5.45)$$

Equations (5.43) - (5.45) can be combined to obtain the expression highlighted in Equation (5.46) for the pressure drop ΔP_t in a tube:

$$\Delta P_t = \frac{128\mu\dot{V}}{\pi D_t^3} \cdot \left(\frac{L_t}{D_t} \right) \quad (5.46)$$

The expression from Equation (5.46) is left with the ratio (L_t/D_t) apart from the rest since this value can be used to approximate the pressure drop in other components of the feed systems for which it is not possible to define an adequate length or diameter. For example, for pipe bends and tee junctions the L_t/D_t ratio can be approximated as shown in Figure 5.19:

Bends	L_{eq}/D
180 bend, $R = 5D$	28
90 bend, $R=5D$	16
90 bend, $R=1,5D$	20
45 bend, $R = 1,5 D$	16
Tee, flow straight through	20
Tee, flow through side outlet	65

Figure 5.19: L/D ratio for different tubing components [82]

To have a first estimate of the tube length, it is expected that at least 400 mm of tubing will be used for the main line of propellant which passes through the filter, latching valve and pump. To do this, it is also expected that five 90 bends and two 180 bends are implemented, together with the 3-way splitter. Afterwards, the lines are split into three, as explained earlier: while one of the lines feeds the propellant directly into one thruster, the other two head in the direction of the four thrusters, splitting again to reach each thruster valve. Estimating that the segment after the first split is of length 50 mm, together with the latest, it is possible to evaluate the pressure drop along the whole tubing line, considering that a tee junction and a 90 bend are implemented in this segment. The pressure drop is estimated through Equation (5.46) with a varying tube diameter and the results are shown below:

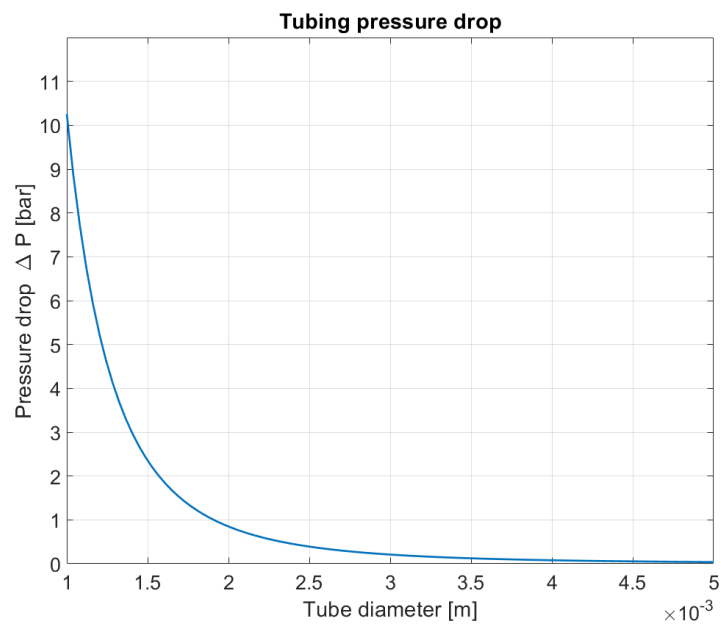


Figure 5.20: Tubing pressure drop estimation for varying tube diameter D_t

As it can be seen from Figure 5.20, the pressure drop can become very high if the diameter of the tubing is too small. For this reason, it is decided to use an internal tube diameter of at least 2 mm. Since most of the components are from US companies and therefore adhere to the imperial measuring system, it is decided to look for tubing manufacturers that provide standardized tubing diameters in US metrics. Company Swagelok provides an high number of choices of stainless steel tubing at different outer diameters and thicknesses [62]. Given the pressure drop estimation, the tube components that better fit in this application are model SS-T4-S-065-6ME, with an external diameter of 1/4 inches (6.35 mm) and a tube wall thickness of 0.065 inches (1.651 mm), for an internal diameter of 3.048 mm. The weight per unit length is 0.19 kg/m and having a working pressure of 10200 psi (703 bar). It is therefore possible to evaluate the total mass of the tubing system: the total length is expected to be around 800 mm total, considering the initial feeding line of 400 mm and the four lines division of a total of 100 mm each, resulting in a total weight of 152 g.

For the chosen model of tubing, the pressure drop among the whole line is $\Delta P_t = 0.21$ bar. For the feeding line that goes straight into the thruster and is not split, the difference is of 0.024 bar, therefore it is considered negligible and it can be assumed that the flow pressure will reach each thruster and the same operating conditions.

Filter and thruster valve The data-sheet from the chosen filter from VACCO model F1D10807-02 highlighted in Figure 5.15 indicates a pressure drop of 1.50 psid with 0.0539 lb/s (24.44 g/s) of N_2H_4 , hydrazine. The pressure drop among an orifice or a fluid system components generally increases with the mass flow squared, therefore it is possible to estimate the pressure drop occurring to the total flow of the system by adapting the data-sheet value to the one occurring in this application. Since the ΔP is based on N_2H_4 , hydrazine, the correction factor will be used: the viscosity of hydrazine at 25° is 0.9

cP and its density is 1000 kg/m^3 [43], both very close to the reference values of water (viscosity is 1 cP), therefore it is decided to increase the resulting pressure drop by the correction factor of $2.2x$. The total mass flow of propellant through the filter is $\dot{m}_{tot} = 2.3267 \text{ g/s}$, which corresponds to a mass flow of water of $\dot{m}_{H_2O} = 1.583 \text{ g/s}$ for a resulting pressure drop over the filter of:

$$\Delta P_{filter} = 2.2 \left(\frac{\dot{m}_{H_2O}}{\dot{m}_{N_2H_4}} \right)^2 \Delta P_{N_2H_4} = 0.0138 \text{ psi} = 0.001 \text{ bar} \quad (5.47)$$

The data sheet from the latch valve does not allow for an easy estimation of the pressure drop, so it is left as a further design detail. On the other hand, the thruster valve from VACCO model V0D10898-01 provides the pressure drop value for a range of mass flow of water, as shown from Figure 5.21.

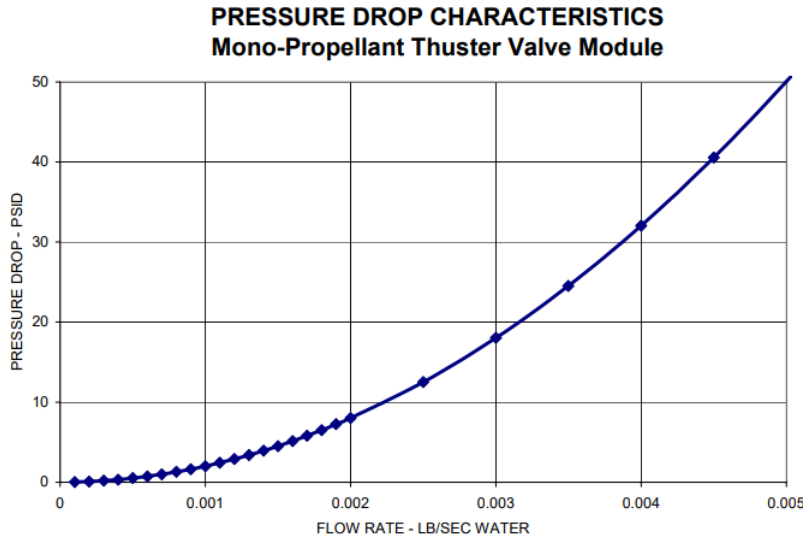


Figure 5.21: Thruster valve pressure drop graph [72]

In this case, the pressure drop occurring for a mass flow rate of $\dot{m}_{thruster} = 0.46535 \text{ g/s}$, corresponding to a mass flow of water of $\dot{m}_{H_2O} = 0.3166 \text{ g/s}$ (0.0007 lb/s) can be identified on the graph, and the pressure drop associated to that value can be multiplied by a factor of $2.2x$ to estimate the effect on the AF-M315E flow. This provides a pressure drop over the thruster valve of $\Delta P_{thruster\ valve} = 2.2 \cdot 1.5 \text{ psi} = 0.23 \text{ bar}$.

5.4.3. Injector design

The injector is to be designed by taking into account the pressure drop that will need to be present in order to effectively de-couple the feed system from the combustion chamber. The pressure drop value is usually chosen to be 20% of the chamber pressure [82]: in this case, since the chamber pressure is expected to be at 2 MPa , the pressure drop at the injector is fixed at 4 bar . Since the equation for the pressure drop occurring over an orifice does not take into account viscosity effects, the pressure drop used in the calculations will be divided by a factor $2.2x$: in this way, the orifice will be sized for a flow of water of viscosity 1 cP that would experience a lower pressure drop, while when using AF-M315E the pressure drop will increase and reach the desired 4 bar. If this is not accounted for, and the design is continued by adopting the original 4 bar of pressure drop across the orifice, due to viscosity the pressure drop across the orifice could result in higher losses.

Once the pressure drop requirement at the injector is chosen, the following equation can be used in order to find its dimensions:

$$\dot{V}_{thruster} = C_{d-inj} A_{inj} \sqrt{\frac{2\Delta P_{inj}/2.2}{\rho}} \quad (5.48)$$

where C_{d-inj} is the discharge coefficient that characterizes the injector. Assuming a single injector hole, the area and diameter of the injector are:

Table 5.6: Injector design values.

Property	Value	Unit
$\dot{V}_{thruster}$	19	mL/min
C_{d-inj}	0.7	-
ΔP_{inj}	4	bar
ρ	1.47	kg/dm ³
A_{inj}	0.0288	mm ²
D_{inj}	0.191	mm

5.4.4. Conclusion

This section of the thesis has highlighted the design of the feed system for the propulsion system: since the tank already makes up most of the mass and volume available on the 24U CubeSat, tubing and components needed to be sized and chosen in order to minimize pressure losses while being compact enough to fit inside the available volume. An early design sketch of the feed system is provided, with the main components of the system and the feed line separations. Afterwards, 3 COTS components have been chosen as adequate for this particular application: since this design is early level, it is expected that there may be components that may better satisfy the needs of the mission, with a lower mass, volume or power requirement: in any case, a choice for the most important parts of the system has been provided to show the feasibility of the mission. The pressure drop occurring across the feed system has been estimated through equations where possible, in the case of tubing and tubing components, but also recurring to data-sheet graphs if available. In the latter case most of the data available is applied to fluid with low viscosity such as water or hydrazine, therefore a correction factor has been applied to resemble the behaviour of AF-M315E higher viscosity.

Below in Table 5.7 an summary of the mass and pressure drop of the main feeding system components is highlighted:

Table 5.7: Feeding system mass and pressure drop estimation.

Property	Value	Unit
Tubing outer diameter	6.35	mm
Tubing thickness	1.651	mm
Tubing internal diameter	3.048	mm
Tubing length	800	mm
Tubing weight	152	g
Filter mass	25	g
Latch valve mass	160	g
Latch valve power	< 28	W
Thruster valve mass	85	g
Thruster valve power	<4	W
Injector diameter	0.191	mm
ΔP_{tubing}	0.21	bar
ΔP_{filter}	0.001	bar
$\Delta P_{latchvalve}$	TBD	bar
$\Delta P_{thruster valve}$	0.23	bar
ΔP_{inj}	4	bar
Total $\Delta P_{feedsystem}$	4.44	bar

5.5. Thruster design

This section is dedicated to the specific design of the thruster dimension and material that will ensure the correct decomposition of the propellant and provide the correct performance levels required by the mission. The first part is dedicated towards the analysis and design considerations for a catalyst bed that correctly decomposes AF-M315E: this includes the choice of correct bed length and diameter, together with the analysis on the shape, dimension and material of the pellets that compose the catalyst bed. Afterwards, the combustion chamber and nozzle are designed, including their dimensions and material.

5.5.1. Catalyst bed

The mass flow through the thruster is constrained by the chamber thermochemical parameters and the throat area. Since all of the chamber conditions have already been determined in Chapter 4, in Table 4.6, with a chamber pressure of $P_c = 2 \text{ MPa}$ and a chamber temperature of $T_c = 2166 \text{ K}$, the following equation can be used to obtain the throat area (and diameter):

$$\dot{m} = \frac{\Gamma P_c A_t}{\sqrt{RT_c}} \quad (5.49)$$

resulting in a throat diameter of $D_t = 0.639 \text{ mm}$ and throat area of $A_t = 0.32105 \text{ mm}^2$. Once the throat area is fixed, the attention is shifted towards the catalyst bed design.

The catalyst bed is an integral part of the monopropellant propulsion system: after passing through the injector, the propellant flow is spread uniformly on the catalyst bed, in which it starts reacting with the bed material and its temperature increases. The propellant flow experiences a transition phase from liquid to gaseous in which its thermochemical properties and composition vary, until the propellant has completely reacted over the catalyst bed and the resulting gas can be accelerated through the convergent-divergent nozzle.

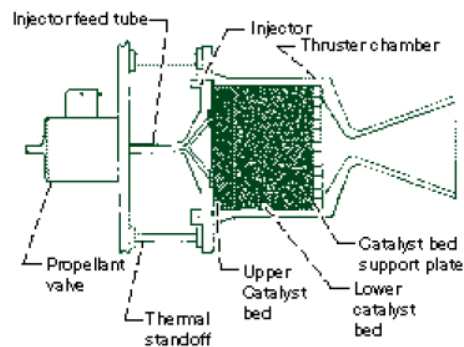


Figure 5.22: Monopropellant thruster sketch, with catalyst bed highlighted [82]

Typical catalyst beds can be either monolithic, consisting of a single extruded body with several holes in which the propellant is able to flow, or a granulated pellet bed, in which the bed is composed of several small bodies with which the propellant interacts flows throughout during its residence time in the chamber. Of the two, the most common ones adopted for monopropellant is the latter: for typical hydrazine or hydrogen peroxide monopropellants, multiple research has been performed in order to carefully determine the material composition that allows for the most efficient propellant decomposition and the minimization of the pressure drop along the bed [32]. Most of these case studies, however, rely on the complete knowledge of the propellant composition and reaction behaviour, which is not the case for the newly developed propellants based either on ADN or HAN. Therefore, a mathematical model could not be created to simulate the exact phase variation and pressure drop of the propellant among the bed. However, a classical analysis of the pellet sized is hereby highlighted, which will help in an early estimation of the correct pellet bed size.

A model is hereby presented to provide an high-level design of the dimension and shape for a granulated catalytic bed. One of the most important parameters that serve to identify the level of ordering

of the pellets inside the granulated bed, which in return will be crucial in estimating the pressure drop along the catalytic bed, is the void fraction ϵ , or porosity. It is defined as the ratio between the volume of void inside the bed and the total volume of the bed [15]. Inside granular beds, there is the possibility of modelling and predict the overall ordering of the pellets inside the bed, and therefore to estimate the void fraction among the radial coordinate. One model useful for this purpose was devised by Bey and Eigenberger [9]: it allows for an estimate of the void fraction profile, as well as the average void fraction on the cross section of the bed, based on the geometry of the pellets. Using this model, it is possible to define the geometry and dimensions of the pellets based on the needs. It has been recently updated and generalized by adopting non-dimensional coordinates that no longer depend on the actual dimensions of the particles and the bed, but on the ratio between the dimensions of the pellets and the bed [47].

The non-dimensional coordinates that will be used in this analysis are the ratio between the diameter of the bed and the diameter of the pellets \tilde{D} , and the ratio between the current radius and the total radius of the bed \tilde{r} , ranging from 0 to 1:

$$\tilde{D} = \frac{D_{bed}}{D_{pellet}} \quad \tilde{r} = \frac{r_{coord}}{r_{bed}}$$

The model divides that the catalyst bed cross section can be divided into two concentric regions defined by the sign of the non-dimensional radial function r' :

$$r' = \frac{\tilde{D}(1 - \tilde{r})}{2r_{min}} - 1 \quad (5.50)$$

which ranges between negative and positive values among the non-dimensional radial coordinate \tilde{r} . The core region is defined for values where r' is positive, while the wall region is defined from its negative values. The constant r_{min} is only dependant on the ratio \tilde{D} :

$$r_{min} = \frac{1}{2} \left(\tilde{D} - \sqrt{\tilde{D}(\tilde{D} - 2)} \right) \quad (5.51)$$

The void fraction profile is highly dependant on the region of the catalyst bed (either core or wall), and on the geometry of the pellets. Two geometry are the most analysed for pellets, which are the spherical and cylindrical shape. For pellets with spherical geometry, the void fraction profile is approximated by:

$$\begin{cases} \epsilon_{loc,wall} = \epsilon_{min} + (1 - \epsilon_{min})r'^2 & r' < 0 \\ \epsilon_{loc,core} = \epsilon_0 + (\epsilon_{min} - \epsilon_0) \exp\left(-\frac{r'}{c}\right) \cos\left(\frac{\pi}{b}r'\right) & r' \geq 0 \end{cases} \quad (5.52)$$

where ϵ_{min} , ϵ_0 , b and c are constant values that are dependent on the geometry and the dimensions of the pellets. Some of the experimented values of such constants are shown in Table 5.8:

Table 5.8: Spherical and cylindrical pellets constants ϵ_{min} , ϵ_0 , b and c investigated by Bey and Eigenberger [47].

shape	D_p [mm]	L_p [mm]	ϵ_{min}	ϵ_0	b	c
sphere	4.5 ± 2.0	–	0.27	0.39	0.876	10
	6.3 ± 1.0	–	0.24	0.39		
	7.5 ± 1.0	–	0.24	0.395		
	9.8 ± 1.0	–	0.24	0.41		
	14 ± 1.5	–	0.24	0.41		
cylinder	4.5	4.5	0.275	0.365	0.876	2
	6	6	0.275	0.375		
	12	12	0.3	0.42		
	6	5–20	0.275	0.365		

The mean void fraction $\bar{\epsilon}$ among the whole cross section of the bed, for spherical pellets, is approximated by:

$$\bar{\epsilon}_{sphere} = 0.375 + 0.34 \frac{1}{\tilde{D}} \quad (5.53)$$

Cylindrical pellets behaviour can be estimated by using similar equations to the spherical case; the radial function r' is defined with an additional term a_0 :

$$r' = a_0 \frac{\tilde{D}(1 - \tilde{r})}{2r_{min}} - 1 \quad (5.54)$$

$$a_0 = 1.8 - \frac{2}{\tilde{D}} \quad (5.55)$$

The void fraction profile when using cylindrical pellets is approximated by:

$$\begin{cases} \epsilon_{loc,wall} = \epsilon_{min} + (1 - \epsilon_{min})r'^4 & r' < 0 \\ \epsilon_{loc,core} = \epsilon_0 + (\epsilon_{min} - \epsilon_0) \exp\left(-\frac{r'}{c}\right) \cos\left(\frac{\pi}{b}r'\right) & r' \geq 0 \end{cases} \quad (5.56)$$

while the mean void fraction $\bar{\epsilon}$ can be approximated by:

$$\bar{\epsilon}_{cylinder} = 0.36 + 0.1 \frac{D_{ps}}{D_b} + 0.7 \left(\frac{D_{ps}}{D_b}\right)^2 \quad (5.57)$$

where D_{ps} is the value of the diameter of a sphere with equal volume to the cylindrical pellet, which is found as follows, by geometric relations:

$$D_{ps} = \sqrt[3]{\frac{3}{2}D_p^2 L_p} \quad (5.58)$$

In both the two analysed geometries, the average void fraction $\bar{\epsilon}$ found by Equations (5.53) and (5.57) decreases with increasing \tilde{D} . This means that if the diameter of the pellets is much smaller with respect to the diameter of the bed, the pellets will arrange themselves by covering more of the available cross section.

The evaluation of the profiles of void fraction among the catalyst bed radius is crucial to understand and make a trade-off on the choice for the geometry and the dimensions of the pellets. It is important for a catalyst bed to not cause the flow of propellant to choose preferential paths and not completely react during the passage in the catalyst bed: since the pressure drop in the catalyst bed is dependant on the void fraction of the profile, the latter shall be as much constant as possible in order to not provide preferential paths in the catalyst bed. Using Equations (5.52) and (5.56), it is possible to plot the void fraction profiles among the non-dimensional coordinate \tilde{r} for different ratios of diameter bed to pellet \tilde{D} : the results are shown in Figure 5.23.

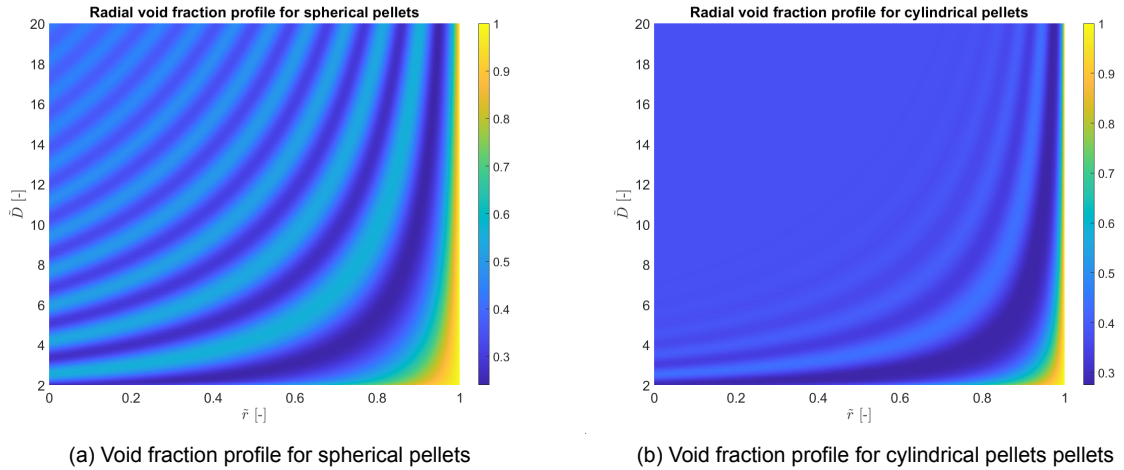


Figure 5.23: Plots of void fraction profile for : (a) spherical pellets, using $\epsilon_{min} = 0.24$, $\epsilon_0 = 0.41$, $b = 0.876$, $c = 10$ and for (b) cylindrical pellets, using $\epsilon_{min} = 0.275$, $\epsilon_0 = 0.375$, $b = 0.876$, $c = 2$

The plots show that for spherical pellets, once the diameters of the catalyst bed and the pellets are fixed, obtaining a value of \tilde{D} , the local void fraction $\epsilon(\tilde{r})$ varies significantly among the non-dimensional radial coordinate \tilde{r} . In the cylindrical pellets case, instead, for a high enough value of \tilde{D} , the oscillations in the void fraction profile that are so accentuated in the core region for the spherical pellets case are not present: this results in a more smoothed profile of the porosity in the central region of the catalytic bed. As it was hinted earlier, these results are important during the design of the catalytic bed since the pressure drop among the catalyst is also dependent on the void fraction of the bed. The relation is known as Ergun equation, and combines the pressure losses both kinetic and viscous, applicable to many types of flows [16]:

$$\frac{\Delta P}{L} = \frac{150\mu(1-\epsilon)^2}{D_s^2 \epsilon^3} u_0 + \frac{1.75\rho(1-\epsilon)}{D_s \epsilon^3} u_0^2 \quad (5.59)$$

where μ is the viscosity of the fluid, ρ is its density, L is the length of the catalytic bed, u_0 is the velocity of the fluid and D_s is the Sauter mean diameter of the pellet, which corresponds to the diameter of a sphere with the same volume/surface area ratio of the considered particle. In the cylinder case, it is found with:

$$D_s = 6 \frac{V_p}{A_p} = 6 \frac{\frac{\pi}{4} D_p^2 L_p}{\frac{\pi}{2} D_p^2 + \pi D_p L_p} \quad (5.60)$$

Equation (5.59) displays the double nature of pressure losses that occur when a fluid passes through the catalytic bed: the first term is representative of the viscous losses since the term μ , corresponding to the viscosity of the fluid, is present; the second term, instead, is related to the kinetic losses, due to the velocity of the fluid u_0 being squared. It can now be noted that the local void fraction might cause high difference in pressure drops among the cross section of the catalytic beds: as explained before, this has to be limited otherwise the propellant might flow only through some preferential paths and the catalytic reactions might not be homogeneous and complete. Therefore, it is envisioned to prefer cylindrical pellets with small diameter with respect to the bed diameter, which is expressed by a large value of \tilde{D} , since as shown from Figure 5.23-(b), the oscillations in void fraction among the radius are the lowest. While the previous considerations are correct, the trend of the pressure losses with varying void fraction pushes the choice into the opposite direction: Equation (5.59) displays that for smaller pellets, which means larger \tilde{D} and lower void fraction $\bar{\epsilon}$, the ΔP increases significantly: the dimensions of the pellets will be needed to be carefully chosen taking into consideration both the positive and negative effects that having a larger or lower overall void fraction will result into.

Due to the previous considerations, it is decided to consider pellets which have the same length and diameter L_p and D_p , to be consistent with the previous investigation and choose a diameter ratio of 7:

in this way, the oscillations of the void fraction radially is minimized with respect to bigger pellets, and the pressure drop expectedly does not increase much due to the pellets not being too small. Equation (5.59) can not be used in this case to estimate the pressure drop, since it is not known how the AF-M315E reacts to catalyst decomposition and what are its viscosity and density values along the catalyst bed.

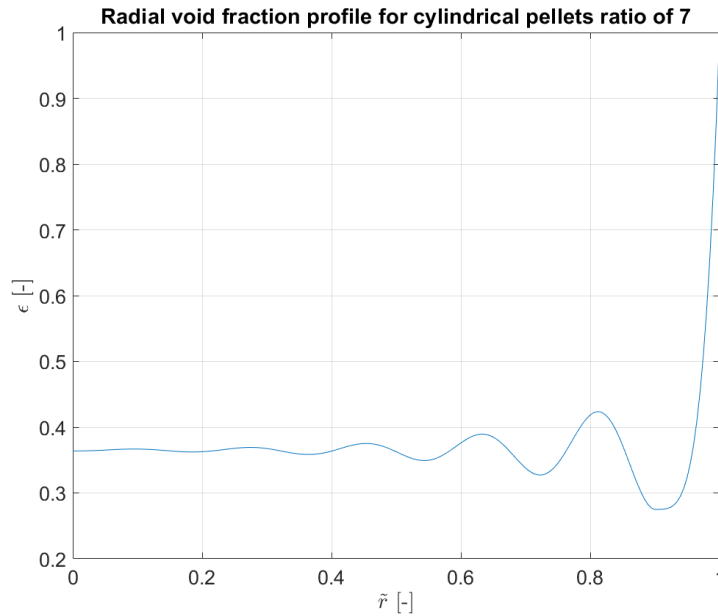


Figure 5.24: Radial void fraction ϵ_{loc} for cylindrical pellets of diameter ratio 7. Cylinder length set equal to diameter.

An important parameter for catalyst bed design is the bed load G , defined as the ratio between the mass flow rate through the catalyst bed:

$$G = \frac{\dot{m}}{A_c} \tag{5.61}$$

A catalyst bed load too high might lead to malfunctioning or destruction of the catalyst bed, reducing its operational life. For H_2O_2 and N_2H_4 thrusters, [23] has shown how for a mass flow rate below 2 g/s , the catalyst bed loading for the operating points of existing thruster is below $20 \text{ kg/m}^2/\text{s}$, as can be seen in Figure 5.25.

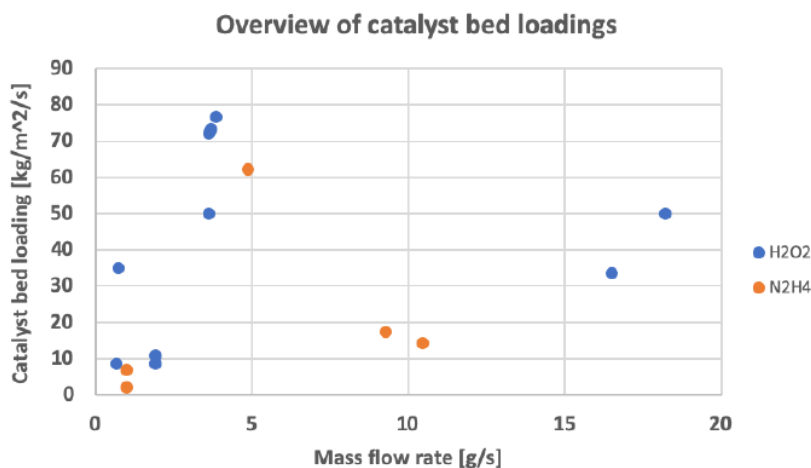


Figure 5.25: Catalyst bed loading for state-of-the-art H_2O_2 and N_2H_4 thrusters [23]

In [31], a catalytic bed made from platinum barium pellets was adopted for a HAN thruster: the nominal mass flow was 1.04 g/s and the catalytic bed diameter was 10 mm , resulting in a catalyst bed load of $13.24 \text{ kg/m}^2/\text{s}$. The diameter of the chamber is decided to be fixed in order to comply with these values of bed load: the value of $G_{cat} = 15 \text{ kg/m}^2/\text{s}$ is chosen, remaining below $20 \text{ kg/m}^2/\text{s}$. The chamber cross-sectional area can be found with Equation (5.62):

$$A_c = \frac{\dot{m}}{G_{cat}} \quad (5.62)$$

resulting in a chamber cross section of $A_c = 31.023 \text{ mm}^2$ and a chamber diameter of $D_c = 6.285 \text{ mm}$. With this value of chamber area, the contraction ratio defined as the ratio between the chamber cross-sectional area and the nozzle throat area is:

$$\varepsilon_c = \frac{A_c}{A_t} = 96.63 \quad (5.63)$$

The value for the contraction ratio is very high, due to the small throat area of the thruster: the design for the MARIO thruster employed a contraction ratio of 50. Nevertheless, simulations from RPA did not show any significant change by varying the contraction ratio up to 100: hence, the value of $\varepsilon_c = 96.63$ is adopted. Since the chamber diameter is fixed, the dimensions of the pellets can be found: $L_p = D_p = D_c/7 = 0.8978 \text{ mm}$, and the corresponding average radial void fraction value is $\bar{\varepsilon}_{cylinder} = 0.395$.

Material In recent years, several laboratory tests have been performed in order to verify the capabilities of catalytic decomposition of AF-M315E. The GPIM mission, adopting the GR-1 thrusters on which this design is based off, adopted LCH-240 catalyst [42]. This catalyst composition from Aerojet Rocketdyne, together with the models LCH-240(A) and LCH-241, have proved to withstand the high temperatures of AF-M315E decomposition and to be able of a total run time of 11.5 hours total [39]. The GR-1 maximum continuous burn time is of 20 minutes [41], which makes it similar to the 10 minutes burn time t_b adopted in the preliminary mission analysis of Chapter 3, therefore it is decided to adopt the same material for this preliminary catalyst bed sizing. The GR-1 thruster required 10 W of catalyst bed preheat power due to the high temperatures at which the AF-M315E starts the decomposition process: in latest research, the development of a successor of the thruster named "GR-1A" has brought light on the possibility of reducing this value by 30% [42], hence requiring a pre-heat power of 7 W : the latter value will be used for the pre-heat power requirement of the catalyst bed.

The LCH-240 catalyst adopts cylindrical catalyst pellets of hafnium oxide with 5% iridium: the granules range from values of 0.025 in (0.635 mm) up to 0.050 in (1.27 cm) [52]. These dimensions fit the preliminary design dimensions of the catalyst pellets L_p and D_p , 0.8978 mm , therefore it is recommended to adopt the same material composition for this application.

Other references have tested the application of different metallic materials for the pellets, such as aluminium oxide, tungstated zirconia or silicon carbide, all coated with 25% iridium [76]. Between these 3 materials, the silicon carbide based pellets performed the best by suffering no damage, while the others experience destruction which could lead to mission failure: the total duty cycle lasted for 3680 seconds, corresponding to 61 minutes.

Pressure drop Few literature is available regarding the pressure drop of AF-M315E in particular over a catalyst bed: hence, it is decided to base the estimation of pressure drop on literature analysing the decomposition of HAN-Methanol based fuel, since AF-M315E is based on HAN. In [27] a simulation is performed based on a chamber pressure of 1.19 MPa lower than this application case, but with a much higher mass flow rate of 70 g/s . Nevertheless, as it can be seen from Figure 5.26, for a porosity value of 0.4, which is close to the $\bar{\varepsilon}_{cylinder}$ value found for the pellets of this application, the pressure drops from 1.4 MPa to 1.2 MPa , resulting in a 14.3% of pressure decrease over the bed.

A second reference performed experiments using HAN-Methanol and a catalytic bed of platinum Barium, for a pressure of 9 bar , a thrust of 1.5 N and a mass flow of 1.04 g/s [31]. Experiments were performed at different pre-heating temperatures, with 350° providing the most efficient results in terms of decomposition rate.

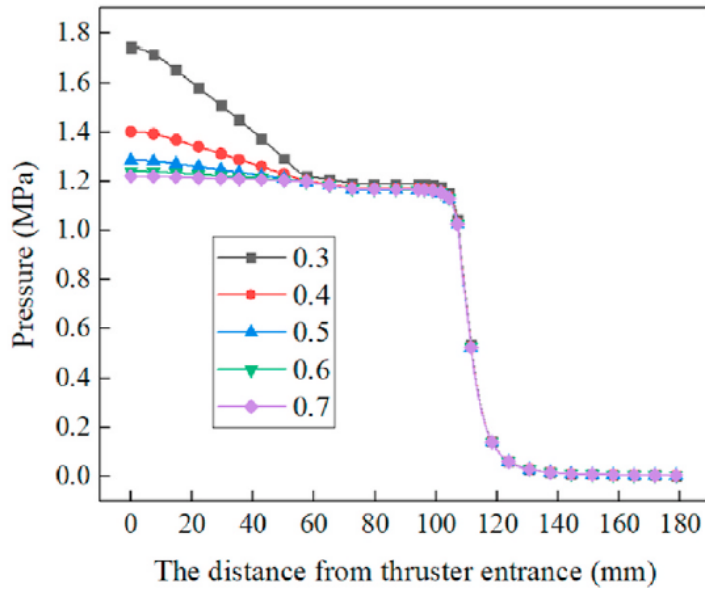


Figure 5.26: Pressure profile simulation of HAN-Methanol propellant over catalyst bed for different bed porosity values [27]

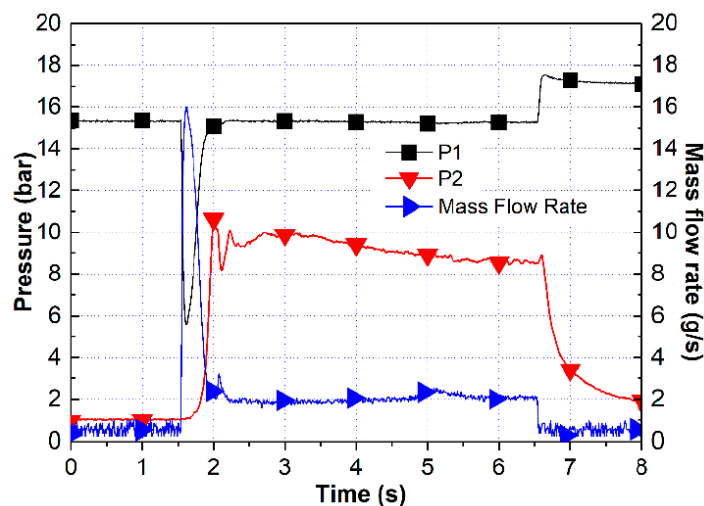


Figure 5.27: Pressure profile simulation of HAN-Methanol propellant over platinum barium pellets, with pre-heating to 350° [31]

As can be seen from Figure 5.27, the pressure drops from a value of 15 *bar* to 10 *bar*, finally dropping to 9 *bar*, probably due to degradation in the catalyst bed. Considering the early stages of the experiment, the pressure drop is of around 5 *bar*.

No other information was found about the pressure drop along a catalyst bed for AF-M315E or other HAN-based propellants, and the ones mentioned earlier provide only case studies in which the operating conditions are much different in terms of mass flow rate and chamber pressure. Hence, a typical value for the pressure drop is used as an expected pressure drop value: 20% of the chamber pressure, which amounts to 4 *bar* [82]. Given the previous references, it might correctly estimate the pressure drop over this catalyst bed application case.

5.5.2. Combustion chamber and nozzle

Once the throat area is found, the values adopted in Chapter 4 for the propellant simulations can be used to dimension the nozzle: the values used are $\varepsilon_E = 200$ for the exit area ratio and 15° for the divergent semi-half angle of the thruster. The concept of characteristic length (L^*) is adopted to

complete the design of the combustion chamber: it is the ideal length of a chamber that does not possess a contraction section. It is defined in Equation (5.64):

$$L^* = \frac{V_c}{A_t} \quad (5.64)$$

and can be used to find the required chamber volume. For mono-propellant systems it is expected that the chamber characteristic length L^* may vary between 0.5 to 2 m, with a tendency towards the uppermost limit [82]: since there are no values for any AF-M315E thruster, the value of $L^* = 1.5 \text{ m}$ is used from [37] which uses an ADN-based propellant. The chamber volume comprehends both the cylindrical part and the contraction, up to the throat area. By geometrical considerations, summing the volume of the cylinder and the contraction frustum, it can be found with Equation (5.65):

$$V_c = A_c L_1 + \frac{1}{3} L_{con} A_c \left(1 + \frac{A_t}{A_c} + \sqrt{\frac{A_t}{A_c}} \right) \quad (5.65)$$

where A_c is the circular cross section of the cylinder part of the combustion chamber, while L_1 and L_{con} are the respective length of the cylindrical part and the contraction part. Finally, another equation can be used to complete the set to constrain the chamber dimensions: the contraction angle β is set to 30° a typical value obtained from [82].

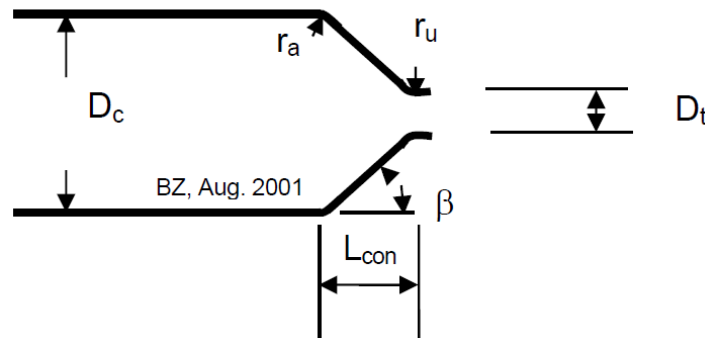


Figure 5.28: Chamber cylindrical and convergent part sketch [82]

This means that a further relation between the chamber diameter and throat diameter can be expressed as Equation (5.66):

$$(R_c - R_t) = L_c \tan \beta \quad (5.66)$$

For the divergent part of the conical nozzle, the following equation is adopted to obtain the nozzle divergent length, in which R_u is the throat longitudinal radius which range between $0.5R_t$ to $1.5R_t$ [82]. An intermediate value of $R_u = R_t$ is used, remembering that during propellant simulations the expansion half angle has been set to $\theta = 15^\circ$:

$$L_N = \frac{(\sqrt{\varepsilon_E} - 1) \cdot R_t + R_u \cdot (1/\cos \theta - 1)}{\tan \theta} \quad (5.67)$$

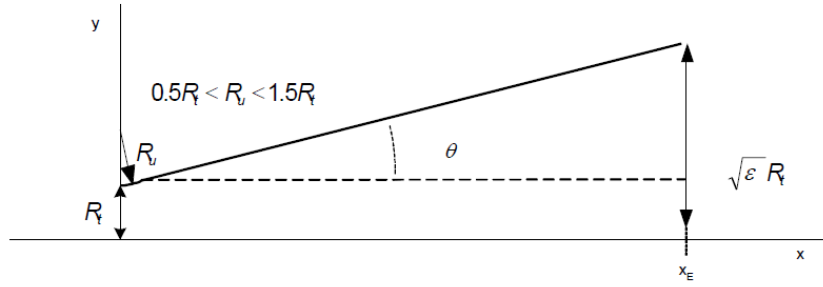


Figure 5.29: Conical nozzle sketch [82]

Using Equations (5.49), Equation (5.62) and Equations (5.64) - (5.67), the chamber cylindrical part and the convergent-divergent nozzle are fully constrained. The material to be adopted for the chamber design needs to be able to withstand the high temperatures in the chamber, which will be just below 2200 K . For a temperature this high, the material of choice is rhenium, which has already been considered as a candidate material to withstand high chamber temperature [47]. It has a density of $\rho_c = 20800\text{ kg/m}^3$ and a yield strength of $\sigma_c = 290\text{ MPa}$ [8]. The total mass of the thruster consisting of chamber section and nozzle can be found with the thin shell approximation method: for a given surface area S , the mass M of a body of thickness t and density ρ can be found with Equation (5.68):

$$M = \rho S t \quad (5.68)$$

A common approximation adopted for early chamber and nozzle dimensioning is to define the overall chamber and nozzle thickness equal to the one of the cylindrical chamber wall [82], evaluated in Equation (5.69):

$$t_c = \frac{MEOP \cdot D_c}{2\sigma_c} SF \quad (5.69)$$

where a safety factor of $SF = 5$ is chosen for this application. This approximation is used since from Equation (5.69) the pressure and diameter throughout the contraction part of the chamber and the nozzle will vary continuously, meaning that a different value of thickness can be used to withstand the pressure in each point. Since the cylindrical chamber is the part of the thruster which experiences the highest pressure, it is decided to use it to dimension the whole thruster. The thruster can be divided into three section: initial cylinder, (1) contraction (2) and expansion part (3); the surface area of each part of the thruster are obtained, by geometry, with Equation (5.70) - (5.72):

$$S_1 = 2\pi R_c L_1 \quad (5.70)$$

$$S_2 = \pi(R_c + R_t) \frac{L_{con}}{\cos \beta} \quad (5.71)$$

$$S_3 = \pi(R_t + R_e) \frac{L_N}{\cos \theta} \quad (5.72)$$

Once all of the three surface areas of the thruster are calculated, they are summed ($S_{tot} = S_1 + S_2 + S_3$) and the thruster mass is found with Equation (5.68). An overview of the dimensioning of the thruster, comprehending the masses and dimensions of the chamber and nozzle is highlighted in Table 5.9. The total thruster mass, comprehending of catalyst bed, catalyst bed holder and heater, and other components is taken by comparison with 0.5 N thruster from [48]: the thruster (without valves) adopting AF-M315E weighs around 80 g . It is therefore expected that for a 1.2 N thruster the mass can be estimated to be 200 g : a similar value is obtained by taking as reference 1 N hydrazine thruster from [7], in which a thruster comprehensive of thruster valve weighs 280 g .

Table 5.9: Thruster (chamber + nozzle) dimensions.

Property	Value	Unit
Throat diameter D_t	0.64	mm
Exit area ratio ε_E	200	-
Nozzle exit diameter	9.04	mm
Contraction ratio ε_c	96.63	-
Chamber diameter	6.285	mm
Characteristic length L^*	1.5	m
Chamber volume (total) V_c	481.578	mm ³
Contraction angle β	30	deg
Chamber cylinder length L_1	13.71	mm
Chamber contraction length L_{con}	4.889	mm
Total chamber length $L_{chamber}$	18.6	mm
Nozzle expansion half-angle	15	deg
Nozzle divergent length L_N	15.721	mm
Chamber + nozzle combined length $L_{thruster}$	34.32	mm
Chamber and nozzle thickness t_n	0.108	mm
Single thruster shell mass	1.3	g
Estimated thruster mass (without valve)	200	g

5.5.3. Conclusion

This section of the thesis work has detailed the design of the combustion chamber and nozzle both in dimension and mass, in order to satisfy the propulsion system requirement. Given the required mass flow of propellant through the thruster, the throat area has been sized and from this value all of the other important parameters could be derived, since in Chapter 4 most of the simulations were performed with fixed area ratios and angles, normalized around the throat area. Other than the dimensions, a candidate material has been found, able to sustain the high temperatures that will be present in the combustion chamber and nozzle: rhenium. The adequate amount of thickness to withstand the pressures along the chamber has been determined, which determines the mass of each thruster. A detailed research has been performed on the catalyst bed shape and materials that might better help with the decomposition of the HAN-based propellant AF-M315E. Due to the lack of literature available, the considerations have been directed on the generic dimensions and shape of the pellets that might help with the decomposition of any propellant, since a proper model could not be found for the pressure drop estimation along the bed, since the composition of the propellant is not known properly and not enough literature has been produced on this topic. Since some literature was found about the materials that could better withstand the high temperatures of AF-M315E throughout its decomposition, some candidate materials for the pellets have been analysed and an early design solution has been recommended.

5.6. Preliminary design

The preliminary design for a propulsion system satisfying the mission and propulsion system requirements defined in Table 3.15 and Table 3.16 has been concluded, taking an estimated guess of initial spacecraft mass of $M_0 = 30$ kg.

5.6.1. Pressure budget

As stated at the beginning of the chapter, the propulsion system components need to provide the propellant flow to the chamber environment at the correct pressure in order to guarantee the performance parameters estimated in Chapter 4. The overall pressure drops, caused by the flow passing through the feeding lines and components, injector and catalyst bed have been estimated, amounting to:

$$\Delta P_{tot} = \Delta P_{feed} + \Delta P_{inj} + \Delta P_{cat} = 8.44 \text{ bar} \quad (5.73)$$

The pressurization level of the tank plus the working range of the pump chosen for the design need to compensate the pressure drop ΔP_{tot} , to make sure that the propellant reaches the chamber conditions at the design value of $P_c = 2 \text{ MPa}$. The initial pressurization value of the tank is of 14 bar , while at the end of the transfer conditions when all the propellant is expelled amounts to 2 bar . As can be seen by Figure 5.5 - (b), the COTS pump model is able to generate a pressure increase up to 30.34 bar for a volumetric flow level of 94.967 mL/min , which is the total amount of propellant volumetric flow comprehensive of the five thrusters. The total pressure that the system is able to provide at end of the transfer conditions, in which the propellant tank is empty and only filled with pressurant, is:

$$P_{feedEOT} = 32.34 \text{ bar} \quad (5.74)$$

The value of $P_{feedEOT}$ is comparable with the GR-1 thruster feed pressure at 1.2 N , representative of state-of-the-art AF-M315E (ASCENT) thruster. The pressure budget reached at end of the transfer, for which the feed pressure maximum level is the lowest possible, is:

$$P_{budgetEOT} = P_{feedEOT} - \Delta P_{tot} = 23.9 \text{ bar} \quad (5.75)$$

The value of $P_{budgetEOT}$ ensures that the propulsion system, designed as it is, is able to provide even at the end of the transfer conditions the correct amount of propellant flow at the chamber pressure values required by the propellant simulations made in Chapter 4, ensuring the correct performance of the propellant. At BOL conditions, the tank is pressurized at 14 bar , therefore the pump will need to work at a lower power operating point to generate the correct amount of pressure differential to ensure a chamber pressure of $P_c = 2 \text{ MPa}$.

5.6.2. Power budget

The power budget is obtained by taking into account the main components of the system chosen until now: the pump, the valves and the catalyst bed heater. Further design can estimate the amount of power required for an eventual tank heater, if needed. Since the catalyst bed heaters need to be active only before the activation of the valves, they are not accounted for in the peak power budget.

Table 5.10: Propulsion system power budget.

Component	Part	Power [W]
Pump	FlightWorks Inc. 2212-M04X01	35.12 (max)
Latch valve	VACCO V8E10580-01	28 (max)
Thruster valve (x5)	VACCO V0D10898-01	20 (max)
Catalyst bed heater (x5)	assuming GR-1A configuration	35
Peak power budget when thrusting	-	83.12 (max)

The power budget of the propulsion system is still very high, mainly due to the presence of several thruster, which increase the total power budget since they require a thruster valve and a catalyst bed heater each. On the other hand, the propulsion system needs to be active only for the manoeuvres around the perigee of Earth and Mars, much less than an electrical propulsion system and therefore requiring less energy compared to an electric-propelled deep-space mission. The latch valve from VACCO shows a maximum power value of 28 W which needs to be investigated more in detail, since it is a maximum value and the operating power conditions for this mission are not known. The pump power has been taken as the maximum expected, when the propellant tank is almost empty and therefore the pump needs to provide the highest amount of ΔP . Other thruster valve options may help save some power such as a microvalve from Busek, tested for a 0.5 N thruster based on AF-M315E [67]: due to its piezoelectric technology, it only requires 0.5 W for activation to correctly gauge the flow of AF-M315E inside the thruster. If proven applicable for higher ranges of thrust, it can help save up to 15 W of power for the thruster valves. This value is still lower when compared to the chemical-electrical propulsion system developed for MARIO, in which the peak power for the electrical propulsion system manoeuvres reach a value of 111 W [37]. This might lead to a lower mass budget for the electric propulsion system, which amounts to 4 kg for the MARIO mission.

5.6.3. Mass budget

In Table 5.11, a recap of the inert and wet mass of the propulsion system is shown: the main components only have been considered, since they represent the highest contributor to the propulsion system mass. A final margin of 5% on the inert mass is added, in order to take into account other components, such as the fill & drain valve or the tank PMD, that will be chosen or designed further into the project. The pressurant and propellant mass are already increased due to the 10% margin adopted for the Δv_{miss} .

Table 5.11: Preliminary propulsion system mass budget.

Component	Material/Part	Mass [g]
Tank	Ti-6Al-4V	1817
Pump	FlightWorks Inc. 2212-M04X01	175
Filter	VACCO F1D10807-02	25
Latch valve	VACCO V8E10580-01	160
Thruster valve (x5)	VACCO V0D10898-01	425
Tubing	Swagelok SS-T4-S-065-6ME	152
Thruster (x5)	Rhenium	1000
Total inert mass	only considering main components	3754
Total inert mass (margined 5%)	only considering main components	3941
Pressurant mass	(GN ₂)	30
Propellant mass	AF-M315E (ASCENT)	16582.9
Propulsion system wet mass	-	20555

The total margined mass of the propulsion system is 20.55 kg total, which makes up for over 2/3 of the total mass of the satellite on which the mission was based off, taken from Chapter 3. This means that 9.45 kg are left to the remaining 4 units of the 24U Cubesat for the remaining subsystems and payload. For MARIO, the sum of the mass of Structure, electrical power system, communications and attitude control system allocated in 5 Cubesat units amounted to 12 kg [38]: if the same mass is considered for this mission, the satellite would reach over 33 kg of total mass. From this stage, two options are available:

- It can be assumed that 9.45 kg are enough to successfully allocate the rest of the spacecraft subsystems and payload. In this way, the rest of the spacecraft mass is left to be optimized in order to match the initial estimated spacecraft mass of 30 kg.
- The design is iterated again for several initial satellite masses M_0 between 25 and 35 kg: the procedure shown in Chapter 3 can be repeated, with the known value of specific impulse of AF-M315E at the operating conditions fixed throughout the thesis work: in this way, a new Δv budget is obtained and margined for the cases of 25 and 35 kg, generating a different requirement for propellant mass, which will affect the pressurant mass and tank dimensions. Since the results from Chapter 3 have shown that the optimal Δv value is found at maximum thrust level of 6 N, the design of the thruster and the choices made for the pump, feeding lines and components can be kept the same, leaving only room to the spacecraft tank to slightly vary in shape and mass. In this way, the effect of the initial spacecraft mass can be measured and a different solution might provide an higher overall mass budget available for the rest of the subsystems and payload.

The latter option is investigated, analyzing what could the mass and volume budget be for a propulsion system design equal to the preliminary one, except for the tank dimensions, but taking into account an initial spacecraft mass of 25 and 35 kg. While for an initial spacecraft mass of 30 kg the best option due to volume limitations has been to adopt a tank with flat caps, it may happen that for other values of initial spacecraft mass M_0 , which will require different amount of propellant mass M_p , other options might be available and leave and higher mass/volume budget for the mission. This option is investigated in the next section of the chapter.

5.7. Design finalization

This section of the thesis is meant to serve as a wrap up of the detailed design of the propulsion system performed in this chapter. A preliminary design has been presented in the previous chapter: now, the design is iterated for different initial spacecraft mass values by freezing parts of the propulsion system components in order to gauge the influence of initial spacecraft mass on the system, and to find a solution which might better fit inside the CubeSat volume and provide a slightly higher mass margin for the rest of the subsystems and payload. The final propulsion system design obtained by this iteration is highlighted in this section, providing the power and mass budget, together with the trajectory analysis for the specific case and a CAD drawing of the final propulsion system.

5.7.1. Effects of initial spacecraft mass M_0

The propulsion system requirement PROP-01 on the Δv derived in Chapter 3 at the beginning of the thesis work has been obtained by making an assumption on the initial spacecraft mass, M_0 , and assuming an average Δv obtained from the trajectory analysis between the range of 240 s to 300 s for the specific impulse, since the optimal propellant configuration was still unknown. Once the propellant choice has been fixed to AF-M315E, the requirement PROP-01 has been defined after the initial satellite mass $M_0 = 30 \text{ kg}$ and the correct specific impulse value I_{sp} . The same design process can be done for an initial spacecraft mass of 25 and 35 kg, in order to be representative of the range taken into account at the beginning of the thesis work. The choices made for the components of the propulsion system such as COTS valves, pump and filter are fixed, together with the dimensions of tubing and the thruster, since it has been seen in Chapter 3 that the optimal Δv solution is found for the maximum available thrust level of 6 N. This means that the only part of the propulsion system subject to change is the amount of propellant mass to be carried on-board, which influences the dimensions and shape of the tank. The trajectory analysis is performed again for the initial satellite mass values of 25 and 35 kg, but using the propellant specific impulse of AF-M315E at the conditions described in Chapter 4. Afterwards, the propellant mass and volume budget is derived and, based on the shape of the tank and its dimensions, a mass and volume budget accounting for the rest of the propulsion system components is generated. The choice of adopting a prismatic tank is not included, since for the the initial satellite masses considered, it weighs too much and exceeds by far the maximum amount of mass to be carried on board. In order to occupy the available volume as efficiently as possible, a tank radius of $0.098 \text{ m} = 98 \text{ mm}$ is considered, for both the emi-spherical caps case and the flat caps case. In this way, it can be seen how having a different initial spacecraft mass affects the final result and in which cases a different tank shape might lead to a better optimization in terms of mass and/or volume. It is expected that the mass budget increases with the initial satellite mass, since the mass available to the spacecraft after subtracting the propellant mass is obtained with Equation (5.76):

$$M_{sys} = M_0 - M_p = M_0 \exp\left(-\frac{\Delta v}{I_{sp}g_0}\right) \quad (5.76)$$

which for a constant specific impulse I_{sp} and a constant Δv (only slight changes are present in the Δv from Chapter 3) increases linearly with the initial satellite mass. The tank design will be performed by using the real Δv obtained by each configuration, therefore the result might slightly differ from this linear dependence. The tank dimension, mass and mass budget obtained by performing the design again with the correct estimated I_{sp} of the propellant for initial satellite masses of 25 – 30 – 35 kg are highlighted in Table 5.12.

The value of M_{sys} is comprehensive of the propulsion system components, therefore while most of the COTS components are fixed, a different shape of tank affects the mass budget left available for the rest of the subsystems and payload. The latter, which will be called M_{budget} , is shown in Figure 5.30 for varying range of initial satellite masses.

Table 5.12: Mass and tank dimensions iteration based on the Δv obtained with the I_{sp} from Chapter 4. Tank radius of 98 mm.

Parameters / Initial satellite mass M_0	25	30	35
Earth escape Δv_E [m/s]	876.6	916.8	945.7
Mars capture Δv_M [m/s]	943.29	967.7	990.4
Total Δv_{miss} (margined) [m/s]	2001.88	2072.90	2129.70
Propellant mass M_P [kg]	13.4975	16.57196	19.675258
Tank volume V_t (margined) [dm ³]	11.1745	13.7198	16.289
Tank mass M_t (flat cap) [kg]	1.749	1.817	1.885
Total tank height H_t (flat cap) [mm]	381.2	465.5	550.7
Available mass M_{budget} (flat cap) [kg]	7.6022	9.4563	11.2816
Tank mass M_t (emi-spherical cap) [kg]	0.2697	0.3371	0.4051
Total tank height H_t (emi-spherical cap) [mm]	436.0	520.3	605.5
Available mass M_{budget} (emi-spherical cap) [kg]	9.1271	11.0102	12.8355

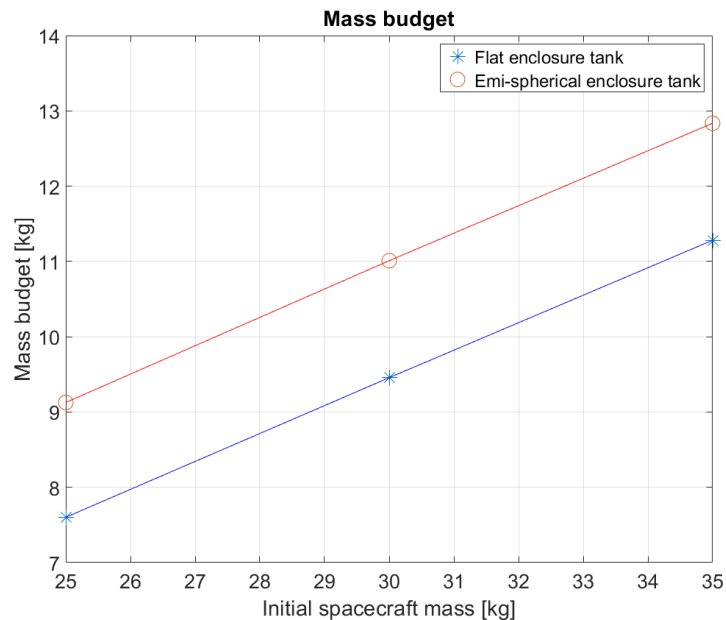


Figure 5.30: Mass budget available for the spacecraft subsystems and payload for initial spacecraft mass values of 25, 30 and 35 kg, choosing a cylindrical tank with emi-spherical or flat enclosure. A fit of the values is presented.

As can be seen from Figure 5.30, the value of M_{budget} increases as expected with the initial spacecraft mass. Furthermore, if a cylindrical tank with emi-spherical enclosures is chosen, the mass budget available for the same initial mass is higher than the one obtained with a cylindrical tank with flat enclosures, since the mass of the latter is higher. On the other hand, the total height of the tank is affected by this choice, as it has been seen from the preliminary design: choosing flat enclosures will save more volume compared to the other option, as it can be seen from Figure 5.31. The value of V_{budget} has been estimated by evaluating the total height of the tank and multiplying the amount of height left in a 24 U CubeSat by the 2x2 U section. To account for the presence of the components below the tank, an additional 2 cm and 4 cm were added to the tank height for the emi-spherical enclosure and flat enclosure, respectively: the components can more easily fit below the emi-spherical enclosure without requiring additional volume, while for the flat-enclosure tank the diameter of the components add to the overall volume intake.

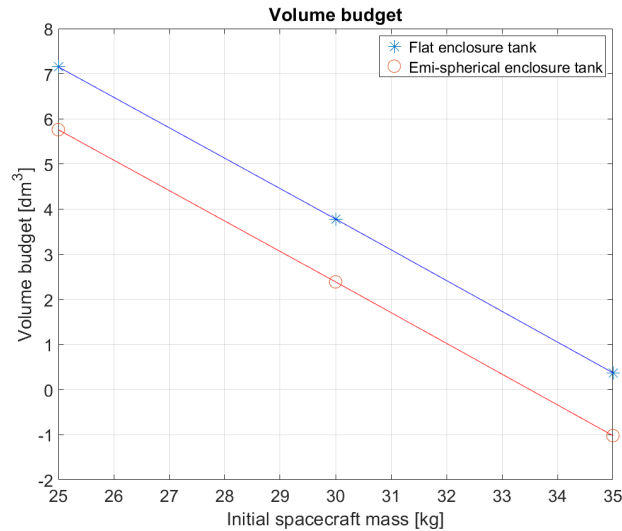


Figure 5.31: Volume budget available for the spacecraft subsystems and payload for initial spacecraft mass values of 25, 30 and 35 kg, choosing a cylindrical tank with emi-spherical or flat enclosure. A fit of the values is presented.

Figure 5.31 shows an expected trend: adopting a flat-enclosure tank allow for an higher volume saving, compared to the emis-pherical enclosure tanks, given the same initial satellite mass. The two graphs from Figure 5.30 and Figure 5.31 can be used for a generic Mars mission that wants to employ AF-M315E as propellant: for example, if the mass budget for the rest of the subsystem needs to be at least \bar{M}_{budget} , the graph from Figure 5.30 can be used to estimate the initial spacecraft mass for the two cases of tank shape. The latter can be used to then estimate the height of the tank corresponding to that option, checking whether the volume budget for the rest of the subsystems and payload fits inside the available volume.

The MARIO mission required 12 kg for the main subsystems to be allocated [37]: it can be seen from Figure 5.30 that for such a value of mass budget, only adopting a tank with emi-spherical enclosures allows for such a high value of M_{budget} , with an initial satellite mass of around 32.5 kg. This initial mass value corresponds to an available volume budget below 1 U, which is deemed to low for a feasible mission. It is decided that for a final representative design, a mass budget value of \bar{M}_{budget} of 10 kg might be representative of the rest of the spacecraft mass. In the case of the emi-spherical tank, this means that an initial mass of 28 kg suffices, leaving a volume budget of slightly less than 4 U. In the case a flat-enclosure tank is chosen, an initial mass of around 31.5 kg is needed, leaving an available volume below 2.5 U. Therefore, for this specific case, it is decided to assume an initial satellite mass of 28 kg, adopting an emi-spherical tank.

The following sections will verify that the design satisfies the mission and propulsion system requirements, providing the mass budget of $\bar{M}_{budget} = 10$ kg for the rest of subsystems and payload, and a CAD drawing of the propulsion system is presented.

5.7.2. Trajectory analysis

This section is reserved to showcase the trajectory analysis results for the final design case: the mission is started adopting a spacecraft initial mass of $M_0 = 28$ kg, the thruster and propellant configuration ensure a specific impulse value of $I_{sp} = 262.865$ s and the same hypothesis regarding the trajectory simulations and the starting orbit defined in Chapter 3, Table 3.15, are adopted: between each manoeuvre, a waiting time of $\Delta t_b = t_b$ needs to be waited before activating the thrusters again. The optimal thrust level for the manoeuvres is the maximum available, 6 N, while a different value of manoeuvre burn time t_b has been found for the Earth escape manoeuvres and Mars stabilization, respectively. For the Earth escape manoeuvres, the spacecraft uses the thrusters to raise the orbit at first, based on its true anomaly value in order to maximize the manoeuvring time around the perigee, and when the orbit becomes open the strategy adopted is to fire thrusters as soon as possible. Regarding the Mars stabilization, the value of θ_{man} at which to start the manoeuvres and the burn time t_b have been found, generating an optimal Δv for Mars stabilization, given the initial conditions provided by Earth escape.

Below, the trajectory analysis and mass budget are shown for the two phases of the interplanetary trip.

Earth escape The result from the thrust and manoeuvre time $T - t_b$ combinations for an initial spacecraft mass of $M_0 = 28 \text{ kg}$ and propellant specific impulse $I_{sp} = 262.865 \text{ s}$ are shown in Figure 5.32.

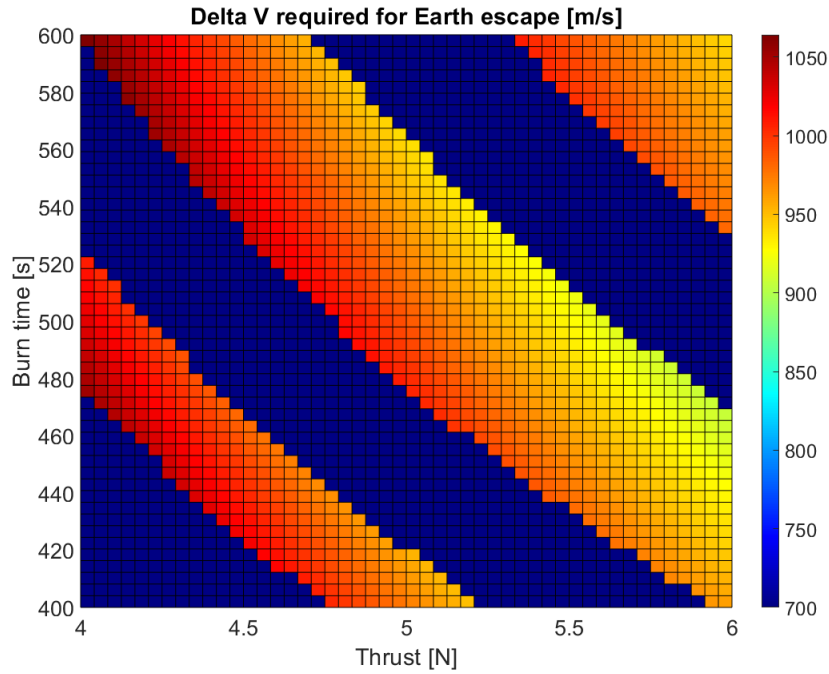


Figure 5.32: Earth escape optimization for an initial spacecraft mass of $M_0 = 28 \text{ kg}$ and propellant specific impulse $I_{sp} = 262.865 \text{ s}$

As expected, the optimum value is found for a thrust level of 6 N , coherently with the results of Chapter 3 for the initial spacecraft mass range of $25 - 35 \text{ kg}$. The manoeuvre time t_b for which the optimum is found is 465.3 s . The trajectory followed by the satellite under such circumstances is shown in Figure 5.33, in which the sphere of influence of the Earth is also depicted. Table 5.13 displays the mission parameters for the Earth orbit raising and escape phase of the mission. The value of t_{SOIE} is the amount of hours since the beginning of the first orbit raising manoeuvre until the edges of the Earth’s sphere of influence are reached.

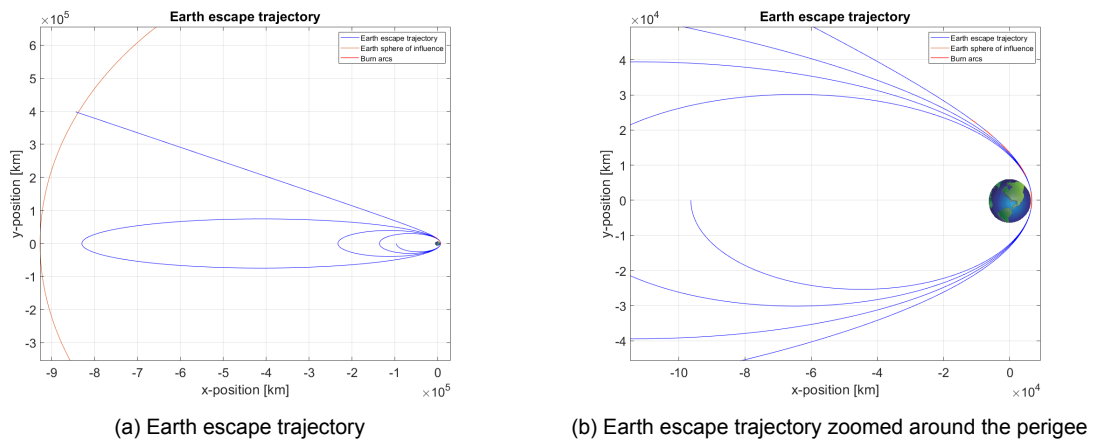


Figure 5.33: Successful Earth escape trajectory

Table 5.13: Mission parameters for Earth orbit raising and escape.

Parameter	Value	Unit
Initial spacecraft mass M_0	28	kg
Thrust T	6	N
Specific impulse	262.865	s
Single manoeuvre burn time t_b	465.3	s
Orbit raising manoeuvres	4	-
Manoeuvres along hyperbolic orbit	4	-
Total burn time t_{bEtot}	3557.5	s
Ideal Δv required for Earth escape	749.2	m/s
Real Δv required for Earth escape	903.68	m/s
Propellant mass used M_{PE}	8.2775	kg
Final mass at Earth escape	19.7225	kg
Final specific orbit energy E_{escape}	4.3322	km^2/s^2
Time needed to reach the edges of Earth's SOI t_{SOIE}	991	h

From Table 5.13 it can be noted how mission requirements MISS-E02 and MISS-E03 are satisfied: the orbit raising manoeuvres are 4, less than 6, causing a total number of passes between the Van Allen belts, after the operation start, to amount to 9. The final orbit specific energy reached is $4.3322 km^2/s^2$, complying with MISS-E03, allowing for a direct transfer towards Mars. The final mass at Earth escape, to be used as the initial mass at the Martian sphere of influence entrance, is $19.7225 kg$.

Mars stabilization After the interplanetary trip in the heliocentric system of reference, the spacecraft enters the Martian sphere of influence. Once close enough to the planet, the thrusters are activated again to brake and lower the velocity of the spacecraft, reducing the specific orbit energy. The initial spacecraft mass considered is now $M_{0M} = 19.7225 kg$ and the minimum Δv is researched as done previously in Chapter 3, by checking the feasibility of the Mars capture by varying the manoeuvre burn time t_b and the true anomaly θ_{man} at which to start the manoeuvres. The results are shown in Figure 5.34.

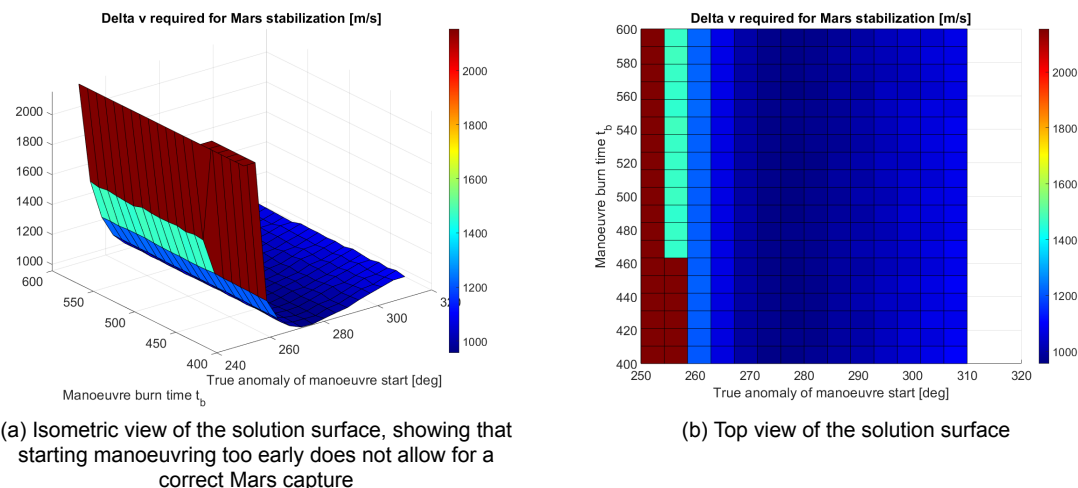


Figure 5.34: Mars capture Δv budget for an initial spacecraft mass (at Mars) of $M_{0M} = 19.7225 kg$ and a propellant specific impulse value of $I_{sp} = 262.865 s$

The optimum is found for a manoeuvre time of $t_b = 526.3 s$ and a true anomaly start of the manoeuvres of $\theta_{man} = 275.7 deg$. The trajectory followed by the spacecraft under these circumstances is shown in

Figure 5.35 and Figure 5.36.

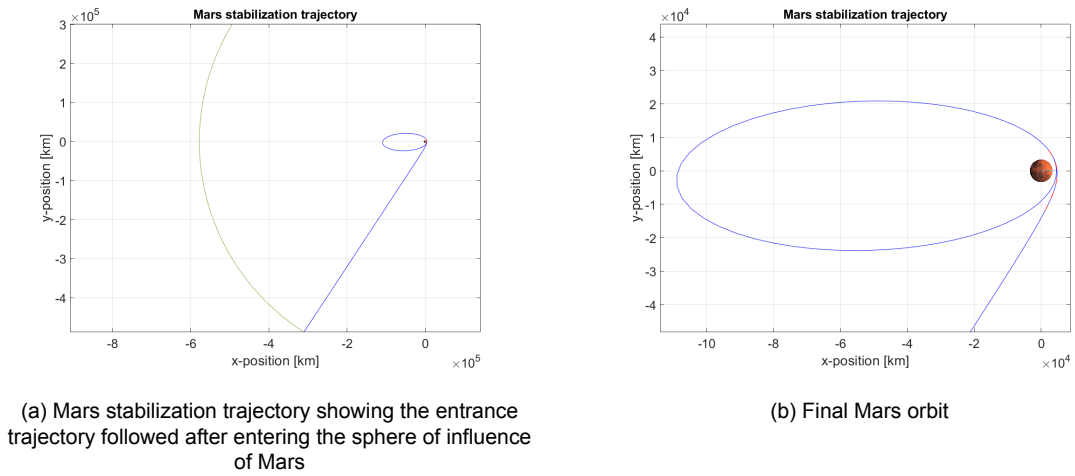


Figure 5.35: Successful Mars stabilization trajectory

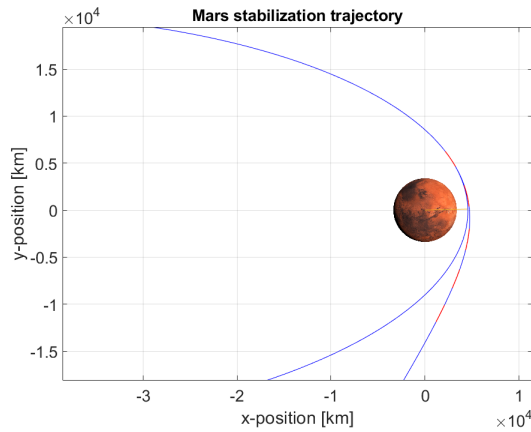


Figure 5.36: Zoomed-in particular of the final orbit, showing the burn arcs in red.

Table 5.14 highlights the mission parameters for the Mars capture for the analysed case. It can be noted how mission requirements MISS-M01 and MISS-M02 are satisfied: the final orbit energy eccentricity after stabilization is $e_M = 0.9196$, lower than 0.92. The peri-apsis distance of the orbit is $r_{pM} = a_M \cdot (1 - e_M) = 4567.34 \text{ km}$, lower than 5000 km. The ideal Δv value for Mars capture is computed by using the targeted final eccentricity value of 0.92 and semi-major axis of the orbit obtained in Chapter 3 with Equation (3.29). The t_{SOIM} value represents the time elapsed from the entrance in the Martian sphere of influence until the last manoeuvre is performed.

The total Δv required for both phases of the mission is

$$\Delta v_{tot} = \Delta v_E + \Delta v_M = 1860.30 \text{ m/s} \quad (5.77)$$

which, after taking a margin of 10%, reaches the value of:

$$\Delta v_{miss} = 1.1 \cdot \Delta v_{tot} = 2046.34 \quad (5.78)$$

Table 5.14: Mission parameters for Mars capture.

Parameter	Value	Unit
Initial spacecraft mass at Mars M_{0M}	19.7225	kg
Thrust T	6	N
Specific impulse	262.865	s
Burn time t_b	526.3	s
Mars stabilization manoeuvres	5	-
Total burn time t_{bMtot}	2627.1	s
True anomaly of manoeuvre start θ_{man}	275.7	deg
Final specific orbit energy E_{escape}	-0.377	km ² /s ²
Final orbit eccentricity e_M	0.9196	-
Final orbit semi-major axis a_M	56809.32	km
Ideal Δv required for Mars capture	858.15	m/s
Real Δv required for Mars capture	956.61	m/s
Propellant mass used M_{pM}	6.1127	kg
Final mass at Mars	13.61	kg
Minimum distance from Mars d_{min}	1180.6	km
Time elapsed from entering Mars SOI t_{SOIM}	59.76	h

This value of Δv_{miss} is used for the dimensioning of the propellant tank and estimation of the pressurant volume and mass, with the same procedure of Chapter 3. The total time required for the interplanetary transfer is:

$$t_{transfer} = t_{SOIE} + T_{sun} + t_{SOIM} = 301.8 d = 0.827 y \quad (5.79)$$

which is much lower than the transfer time obtained for an electrical propulsion system reaching Mars. The transfer time for the MARIO mission is 1472.69 d [37].

5.7.3. Final design dimensioning and CAD drawing

The propellant mass required to achieve Δv_{miss} with an initial satellite mass of 28 kg is:

$$M_p = M_0 \left[1 - \exp\left(-\frac{\Delta v_{miss}}{I_{sp} g_0}\right) \right] = 15.337 kg \quad (5.80)$$

Assuming the propellant density of AF-M315E, $\rho_p = 1.47 kg/dm^3$, the propellant volume is:

$$V_p = \frac{M_p}{\rho_p} = 10.433 dm^3 \quad (5.81)$$

The propellant volume value is used to estimate the total volume of the tank, which to be consistent with the considerations of Chapter 5.3, where the PMD volume and pressurant volume are taken into account to ensure the correct pressurization level of the system, is multiplied by a factor of 1.217:

$$V_t = 1.217 V_p = 12.6977 dm^3 \quad (5.82)$$

The initial tank pressure will be 14 bar, since with the blow-down ratio of $B_R = 7$ the end of the transfer pressurization level of 2 bar is obtained. The latter has shown to be high enough, when summed to the pressure differential provided by the pump, to still provide the correct pressure budget to the mass flow. The density of gaseous Nitrogen at 298 K and at a pressure of 14 bar is found through NIST database [1], and verified with the gas constant equation by using a gas constant of $R_{N_2} = 297 J/kg/K$ [82]. The density value at these conditions amounts to $\rho_{N_2} = 15.866 kg/m^3$. The volume of pressurant is $V_{N_2} = 0.167 V_p = 1.742 dm^3$, meaning that the total weight of pressurant is $M_{N_2} = \rho_{N_2} V_{N_2} = 0.028 kg$.

A cylindrical tank with emi-spherical enclosures is adopted, made by Ti-6Al-4V, with a yield strength of $\sigma = 880 \text{ MPa}$ and a density of $\rho_t = 4430 \text{ kg/m}^3$. Assuming a tank radius of $R_t = 0.098 \text{ m} = 98 \text{ mm}$, the dimensioning is obtained by means of Equations (5.22) - (5.25) and shown in Table 5.15:

Table 5.15: Pressurant, propellant and pressurant volume and mass budget for the final design, considering an initial spacecraft mass of $M_0 = 28 \text{ kg}$.

Property	Value	Unit
Propellant volume V_p	10.433	dm^3
Propellant density ρ_p	1.47	kg/dm^3
Propellant mass M_p	15.337	kg
Pressurant volume (GN2) V_{N_2}	1.742	dm^3
Pressurant density (at 298 K) ρ_{N_2}	15.866	kg/dm^3
Pressurant mass M_{N_2}	0.028	kg
PMD volume V_{PMD}	0.564	dm^3
Tank internal volume V_{T-in}	12.6977	dm^3
Tank internal radius R_{T-in}	98	mm
Tank cylinder height L_{T-cyl}	290.17	mm
Tank circumference thickness t_{cyl}	0.29	mm
Tank external radius R_{T-out}	98.29	mm
Tank cap thickness t_{sphcap}	0.146	mm
Tank external height h_{T-out}	486.47	mm
Tank density (Ti-6Al-4V) ρ_T	4.430	kg/dm^3
Total tank volume V_{T-out}	12.76767	dm^3
Tank structure volume V_{t-s}	0.07	dm^3
Tank mass	0.31	kg

A CAD drawing with the main components is shown in Figure 5.37, Figure 5.38 and Figure 5.39. It comprises of: propellant and pressurant tank, filter, latch valve, pump, tubing, thruster valve and thruster. The propellant flows through the filter at first (in light blue), then the latch valve (in grey) and finally through the pump (in black). After reaching the pump, the propellant feed lines are split into three: one is directed towards the central thruster, while the other two, carrying 2/5 of the total propellant mass flow, are split again by using a tee junction and are directed towards the other 4 thrusters at the corner of a square.

Volume budget The height increase between the propellant tank and the junction between the feed lines and the thruster valves is of 40 mm , obtained from the CAD model, meaning that the total height of the propulsion system, excluding the thruster valve and thruster assembly that are expected to sit outside the spacecraft, amounts to 526.47 mm , leaving an available volume of $V_{budget} = 3 \text{ U}$, if a 24 U CubeSat is considered: for Figure 5.31, an increase of 20 mm only was considered to estimate the available volume, yielding an higher value of the volume budget left. the configuration shown in the CAD model is not optimal: the components of the feed system could fit in a more compact shape if the volume at the sides of the bottom emi-spherical cap is used to allocate them. Further improvements to the components configuration are possible, leaving room for increased volume budget for the rest of the subsystems and payload to be positioned at the top of the tank.

Pressure budget From the CAD model, the correct amount of feed lines length is obtained: $L_{feed} = 530 \text{ mm}$, which for the linear mass of 0.19 kg/m for the Swagelok SS-T4-S-065-6ME tubing, amounts to a tubing mass of 100.7 g . Taking into account the pressure losses inside the components and localized in the junctions, the pressure drop is estimated to not vary much from the preliminary design, as shown by Table 5.16. The difference of pressure drop between the central thrusters and the other four is of



Figure 5.37: Isometric view of the CAD model

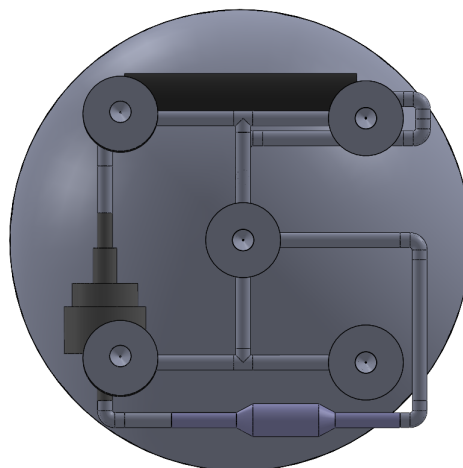


Figure 5.38: Bottom view of the CAD model

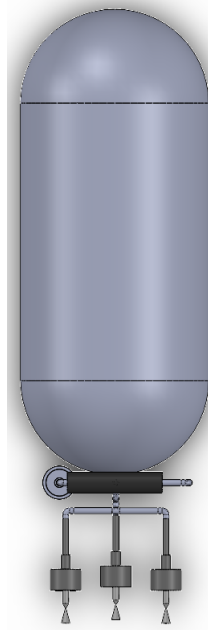


Figure 5.39: Front view of the CAD model

0.022 *bar*, therefore ensuring an equal thruster chamber pressure and performance parameters. The total pressure drop is found in Equation (5.83):

$$\Delta P_{tot} = \Delta P_{feed} + \Delta P_{inj} + \Delta P_{cat} = 8.45 \text{ bar} \quad (5.83)$$

As stated earlier in the chapter, the sum of the pump ΔP and pressurization left in the tank at the end of the transfer is:

$$P_{feedEOT} = P_{pressEOT} + \Delta P_{pump} = 32.34 \text{ bar} \quad (5.84)$$

The pressure budget reached at end of the transfer, for which the feed pressure maximum level is the lowest possible, is:

$$P_{budgetEOT} = P_{feedEOT} - \Delta P_{tot} = 23.89 \text{ bar} \quad (5.85)$$

which means that the pressure chamber level of $P_c = 2 \text{ MPa}$ can be reached even at the latest stages of the transfer. This was to be expected, since the design parameters for the sizing of the tank have not changed: by keeping the same increase for the propellant tank with respect to the propellant volume ($V_t = 1.217V_p$ as derived in Chapter 5.3), the same blow-down ratio is maintained, even if the overall dimensions change due to the different amount of propellant to be carried on-board, since the initial spacecraft mass is different. Nevertheless, the CAD model has provided an exact value for the tubing length, providing a better estimation of the pressure drop along the feed lines: as expected, these pressure drops are low, and do not compromise the mission. A summary of the pressure drop and the dimensions of the feed lines is shown in Table 5.16.

Mass budget Having completed the design of the tank and the tubing, the propulsion system mass budget is summarized in Table 5.17.

Table 5.17 shows that for an initial satellite mass of $M_0 = 28 \text{ kg}$, the total propulsion system wet mass, margined, amounts to $M_{pSYS} = 17.67 \text{ kg}$. This leaves a mass budget of $M_{budget} = 10.33 \text{ kg}$ left for the rest of subsystems and payload, complying with the minimum mass budget value of $\bar{M}_{budget} = 10 \text{ kg}$ set earlier in the chapter.

Table 5.16: Final design of feeding system mass and pressure drop estimation.

Property	Value	Unit
Tubing outer diameter	6.35	mm
Tubing thickness	1.651	mm
Tubing internal diameter	3.048	mm
Tubing length	530	mm
Tubing weight	100.7	g
Injector diameter	0.191	mm
ΔP_{tubing}	0.218	bar
ΔP_{filter}	0.001	bar
$\Delta P_{latchvalve}$	TBD	bar
$\Delta P_{thruster valve}$	0.23	bar
ΔP_{inj}	4	bar
Total $\Delta P_{feedsystem}$	4.45	bar

Table 5.17: Final propulsion system design mass budget.

Component	Material/Part	Mass [g]
Tank	Ti-6Al-4V	310
Pump	FlightWorks Inc. 2212-M04X01	175
Filter	VACCO F1D10807-02	25
Latch valve	VACCO V8E10580-01	160
Thruster valve (x5)	VACCO V0D10898-01	425
Tubing	Swagelok SS-T4-S-065-6ME	100.7
Thruster (x5)	Rhenium	1000
Total inert mass	only considering main components	2195.7
Total inert mass (margin 5%)	only considering main components	2305.49
Pressurant mass	(GN ₂)	28
Propellant mass	AF-M315E (ASCENT)	15337
Propulsion system wet mass	-	17670
Mass budget M_{budget}	Payload and subsystems	10330

Power budget The power budget is the same as for the preliminary design, shown in Table 5.18.

Table 5.18: Final design propulsion system power budget.

Component	Part	Power [W]
Pump	FlightWorks Inc. 2212-M04X01	35.12 (max)
Latch valve	VACCO V8E10580-01	28 (max)
Thruster valve (x5)	VACCO V0D10898-01	20 (max)
Catalyst bed heater (x5)	assuming GR-1A configuration	35
Peak power budget when thrusting	-	83.12 (max)

5.7.4. Conclusion

In this section of the chapter, the variation of the mass and volume budget depending on the initial spacecraft mass value M_0 have been estimated. The design of the feeding lines dimensions, components such as valves, filter and pump have been kept equal to the preliminary design adopted for an initial spacecraft mass of 30 kg, since the optimal Δv for the Earth escape manoeuvre has shown to be linked to the maximum available thrust level of 6 N. By maintaining the same thrust value, as well as the specific impulse I_{sp} of the propellant, the mass flow to be fed to the thrusters remains the same: this will generate the same results as for the preliminary design, and therefore only the effects on the tank shape and dimensions are taken into account. Performing the design of the tank for cases of initial spacecraft masses of 25 and 35 kg has shown that adopting a cylindrical tank with semi-spherical caps might be leave a feasible amount of mass/volume budget for lower amount of initial spacecraft mass, since the propellant to be carried on board is lower. This leads to the consideration that for masses lower than 30 kg, it might be convenient to sacrifice a bit of volume budget that could be obtained by adopting a cylindrical tank with flat enclosures in order to obtain an higher mass budget for the rest of the subsystems and payload. A mass budget value of $\bar{M}_{budget} = 10 \text{ kg}$ has been set, and performing the design of the propulsion system tank with semi-spherical caps for an initial spacecraft mass of 28 kg showed to satisfy this requirement. Therefore, the option is investigated by performing the trajectory analysis, obtaining the Δv budget for the mission and the corresponding propellant mass and volume required. After the tank has been sized to correctly pressurize the propellant, the sum of the margined propulsion system mass amounts to 17.67 kg, leaving a mass budget of $M_{budget} = 10.33 \text{ kg}$. The CAD model of the propulsion system has been presented: further optimization is foreseen in the configuration of the components. The volume available below the tank could be adopted in order to fit the components and save some volume which is otherwise occupied by the propulsion system. The overall tank height is 486.47 mm and the height of the components up to the thruster assembly is of 40 mm, resulting in a total height of the propulsion system of 526.47 mm. This leaves a volume budget of around 3 U: if the components are arranged more efficiently, it is believed that up to 4 U of volume budget can be available to the rest of subsystems and payload.

5.8. Conclusion

This chapter of the thesis work has been dedicated to the detailed design of the propulsion system. After the choice of adopting AF-M315E as propellant, in section 5.1 the mass flow to be fed to the thrusters has been found, given the maximum available thrust level of 6 N that showed optimal Δv budget results from Chapter 3. The state-of-the-art GR-1 thruster adopting AF-M315E as propellant in the mission GPIM has been used to obtain an estimate of the feed pressure level to ensure the functioning of the thrusters at the correct operating points. Due to volume limitations inside the CubeSat, both blow-down systems and regulated were not appealing, and the decision of adopting a pump-fed system is made. In section 5.2, the research for a COTS pump that satisfies the requirements of the propulsion system is shown: two candidate pumps are found, and the final choice is made by using pump model 2212-M04X01X03X04 from Flightworks Inc.

In section 5.3 the design of the tank is proposed for an initial satellite mass value of $M_0 = 30 \text{ kg}$. The correct amount of pressurant is obtained, such that the sum of pump pressure and pressurant satisfies the feed pressure level found in section 5.1. A trade-off between three different shapes for the tank is

performed, and for the case of $M_0 = 30 \text{ kg}$, the optimal solution is found within a cylindrical tank with flat enclosures, since a cylindrical tank with semi-spherical enclosures would require too much volume. In section 5.4, the rest of the components are designed or obtained from COTS. The propulsion system is sketched in Figure 5.14, while COTS solutions for a filter, latch valve, tubing system and thruster valve are proposed. The injector is also designed at this stage, and an estimated pressure drop across all of the feeding lines is obtained.

In section 5.5 the design of the catalyst bed and thruster is performed. The catalyst bed is designed in order to correctly match with literature data for the catalyst bed load G for thrusters of the same mass flow and thrust range, while the catalyst bed pellets are designed based on considerations on the void fraction ε . The latter values are confirmed to be feasible since the dimensions fall within the range of the pellets adopted by the catalyst LCH-240 [52]. The thruster is dimensioned based on the performance values found in Chapter 4, to ensure that the correct specific impulse is obtained.

In section 5.6, the preliminary design obtained for an initial spacecraft mass of $M_0 = 30 \text{ kg}$ is highlighted, showing the pressure, volume and mass budget. The mass budget is deemed to low, below 9.45 kg is left for the rest of subsystems and payload, and therefore it is decided to investigate what the best design could be for the initial spacecraft mass value of 25 and 35 kg that were considered at the beginning of the thesis work. This is done by freezing the design of the propulsion system, except for the tank, since the results from Chapter 3 have shown that the optimum Δv is still obtained with a thrust level of 6 N .

In section 5.7, the mass and volume budget left for an initial spacecraft mass of 25 and 35 kg are reported, showing what the effects of choosing a cylindrical tank with semi-spherical or flat enclosures on the mass and volume budget. It is decided to aim for a minimum mass budget level of \bar{M}_{budget} of at least 10 kg : from Figure 5.30, this value is obtained for a spacecraft mass of at least 27.5 kg using a tank with semi-spherical caps, therefore the option of an initial spacecraft mass of $M_0 = 28 \text{ kg}$ is investigated. The trajectory analysis is performed again for this initial spacecraft mass value, obtaining the Δv budget and checking that the mission requirements are indeed satisfied. The propellant, pressurant and tank mass and volume are dimensioned and a CAD design of the model is shown in Figure 5.37, Figure 5.38 and Figure 5.39. A better estimation of the tubing length is obtained from the CAD model, allowing for a further check on the pressure budget. Finally, the mass budget is found to be $M_{budget} = 10.33 \text{ kg}$, satisfying the need of leaving at least 10 kg for the rest of subsystems and payload. At the current configuration stage, the amount of volume left in the 24 U CubeSat is 3 U, but it is envisioned that the components could be placed more efficiently (near the bottom semi-spherical cap of the tank) in order to save further volume.

As expected, the amount of propellant required a deep-space mission to Mars highly constrains the volume and mass left available for the other subsystems, due to the high Δv requirement of such a mission. Compared to electrical propulsion system, the mass and volume occupied are much higher due to the low specific impulse I_{sp} of chemical propellants compared to their electric counterparts. On the other hand, the availability of high levels of thrust allows for the reduction of travel time, which amounts to years when looking at electric-propelled deep-space mission, to 301.8 days, as shown in Equation (5.79). Other than mass and volume, though, having a high thrust requirement comes at the cost of high power requirements which are generally much lower than the electrical propulsion systems. Since most thrusters for CubeSat generate around 0.5 to 1.5 N of thrust, requiring up to 6 N of thrust implies the adoption of several thrusters, multiplying the generally low power requirement for valves and catalyst bed heaters for each thruster needed: nevertheless, the total power budget of the system hereby presented amounts to 83.12 W, significantly lower than the 111 W budget for MARIO [37]. Due to the volume limitations, adopting a pump-fed system in order to reduce the impact of pressurization further increases the power burden on the system, but leaves more flexibility for the allocation of the rest of the subsystems and payload.

6

Conclusions

The last chapter of the thesis wraps up the work performed in the previous chapters, answering to the initial research questions, providing the lessons learned throughout the project and suggesting recommendations for future work and insights to whomever would pursue deeper research in the field.

6.1. Research objective

The aim the thesis work has been to reply to several research question, for which a research objective has been established in the beginning:

"Designing a chemical propulsion system to be employed for a deep-space Mars mission".

The research objective has been split into different research questions, listed below, to which the thesis work has been directed:

1. *What are the Cubesat mission requirements that will most benefit from the application of chemical propulsion?*

The application of chemical propulsion allows CubeSat missions to change the orbit of reference at which they are deployed at, allowing for independence in the mission design, not having to rely only on launches which treat them as secondary payloads. Chemical propulsion provide high-thrust high-impulsive manoeuvres, which allow fast manoeuvring and transfers: this allows a CubeSat to move from its parking orbit around Earth and reach the ends of the Earth's sphere of influence, autonomously directing itself towards other celestial bodies. In Chapter 2, the possibility of applying high levels of thrust (in the range of 4-6 N) to a CubeSat weighing from 25-35 kg, has been investigated: it has been found that even with limiting burn times of 10 minutes per manoeuvre, it is possible for a CubeSat around a SSGTO orbit to leave the Earth's sphere of influence, direct itself towards the martian sphere of influence and stabilize around Mars. While requiring a very high level of Δv as expected, the application of a fully chemical propelled trip from Earth to Mars with a Cubesat of 24 units of volume is promising and is analysed in the thesis work. Mission in which the requirements pose constraints on the operational life of the satellite will surely benefit from chemical propulsion, since they allow for high-thrust manoeuvres that drastically reduce the transfer time.

What is(are) the best propellant(s) option(s) that are more efficient for the Cubesat mission?

Several mono-propellant options have been analysed during the thesis work: the most promising propellant candidates are the new "green" propellants that are less toxic than hydrazine and allow for an easier and safer ground handling. The two main propellant families are based on EIL (energetic ionic liquids) which are ADN and HAN: both EIL, when mixed with other chemical components, have been proved to generate exhaust gases that provide high specific impulse level to a propulsion system. In terms of efficiency, the volume required to store the propellant inside the CubeSat is crucial since the volume availability is restricted: for this reason, another parameter to

take into account during the trade-off is the volumetric specific impulse level ρI_{sp} , which combines the conversion of mass into impulse with the density of the propellant, providing an estimation on the volume impact on the propulsion system. The comparison has been performed based on literature data and thermochemical simulations: out of all the 5 propellants considered, the AF-M315E (ASCENT) option has been found as the most performing in terms of TRL, heritage and specific impulse and volume performance.

What is the architecture of the propulsion system that can better satisfy the mission requirements?

Due to the limited amount of volume available for an high Δv budget mission, the classic blow-down and regulated pressure-fed system do not suit this application due to the high increase in volume requirement that they would bring, together with lower reliability and highly pressurized systems (for regulated systems) and a decreasing thrust level (for a blow-down system). An efficient alternative has been found in the adoption of a pump-fed system, which is becoming more popular in recent years for CubeSat propulsion systems: adopting a pump to provide most of the ΔP to reach the required pressure in chamber affects the power usage of the propulsion system, but COTS pump are able to provide high ΔP system to propellant mass/volumetric flows of currently developed thrusters, for viscosity ranges of the ADN and HAN propellants. In this way, a compact solution has been found, without impacting severely on the total volume of the propulsion system; depending on the mass budget required for the rest of subsystems and payload, a different tank shape might be preferable. In order to correctly operate the system, the pump needs a filter, a latch valve to de-couple the pump from the tank, and five thruster valves (one for each thruster) for which COTS promising candidates have been proposed. Based on the amount of mass budget estimated to be carried on-board, accounting for the other subsystems and payload, a different shape of tank might better meet the needs of the mission.

6.2. Recommendations and future work

During the propulsion system design, several criticalities have been found for this application which may be better tackled if further time was available, which will be highlighted below:

1. The preliminary mission analysis has been performed based on the approximation of circular orbits of the planets: while this provides with an early estimation of the required energy of the orbit to leave Earth and reach Mars, these energy values are not fixed and are determined based on the position of Earth and Mars around the Sun, which change throughout the years. If one wanted to obtain a better Δv estimation for the transfer, the exact orbit energy requirements can be used for a given launch window that minimizes Δv .
2. A better estimation of the Δt_b can be used, if further information about the propellant and state-of-the-art propulsion system is known: in this application, while for several thruster the value of longest burn time t_b was available, there was little to no information regarding the amount of time that have to be waited before restarting the engine. Knowing this value could lead to a drastic decrease in the Δv budget since it diminishes the amount of time spent manoeuvring along the hyperbolic orbit of escape/stabilization.
3. If further information is obtained regarding the AF-M315E propellant, the proper RPA (or CEA) simulation can be used to estimate the thermochemical performance: in this case, the data found from literature did not coincide with the performance parameters of most of the literature, therefore the approach of adopting ideal rocket theory equation was used. If further information is known about the propellant, more precise simulations, as well as thermochemical behaviour throughout a catalyst bed can be estimated and, in the latter case, a proper pressure drop can be found for given pellet geometry.
4. Mission Lunar Flashlight adopts a recirculation path of the flow before and after the pump [5]: this allows for a correct closed-loop control of the mass flow and pressure increase, by making sure that the pump is correctly tuned to the operating point without having any propellant reach the thrusters at a different mass flow and pressure value. Accounting for this increases the tubing complexity and therefore the option was not analysed in this application, but could be adopted in this case too.

5. No data has been found regarding the NPSH level of the pump, therefore it has been estimated that a pressure of 2 *bar* is enough to no produce any cavitation in the pump: if in the future pumps that provide higher ΔP to the mass flow are available as COTS, and the NPSH level is known to be very low, the pressurization requirement of the tank might drop considerably and other shapes such as a rectangular prismatic tank may be the best option to save volume while not weighing too much. While in this case the pressurization level was too high for a prismatic tank, if the BOL pressurization requirement is low enough such shapes could benefit both mass and volume of the overall propulsion system.

Bibliography

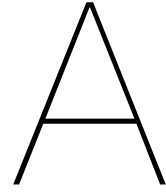
- [1] Nist chemistry webbook - nitrogen. <https://webbook.nist.gov/cgi/cbook.cgi?ID=7727-37-9>. Accessed: 09-21-2021.
- [2] Flightworks, inc. website: space applications. [flightworksinc](http://flightworksinc.com). Accessed: 25-11-2020.
- [3] Daniela Ivette Aguilar. Testing of a 1n af-m315e thruster. 2018.
- [4] Rachid Amrousse, Toshiyuki Katsumi, Nobuyuki Azuma, and Keiichi Hori. Hydroxylammonium nitrate (han)-based green propellant as alternative energy resource for potential hydrazine substitution: From lab scale to pilot plant scale-up. *Combustion and Flame*, 176:334–348, 2017.
- [5] Dawn Andrews, Grayson Huggins, E Glenn Lightsey, Nathan Cheek, Nathan Daniel Lee, Ali Talaksi, Sterling Peet, Lacey Littleton, Sahaj Patel, Daniel Cavender, et al. Design of a green monopropellant propulsion system for the lunar flashlight cubesat mission. 2020.
- [6] K Anflo and B Crowe. In-space demonstration of an adn-based propulsion system. In *47th AIAA/ASME/SAE/ASEE Joint Propulsion Conference & Exhibit*, page 5832, 2011.
- [7] ArianeGroup. Chemical monopropellant thruster family. <https://www.space-propulsion.com/brochures/hydrazine-thrusters/hydrazine-thrusters.pdf>. Accessed on 08-01-2022.
- [8] Steven P Berg and Joshua L Rovey. Assessment of multimode spacecraft micropropulsion systems. *Journal of Spacecraft and Rockets*, 54(3):592–601, 2017.
- [9] Oliver Bey and Gerhart Eigenberger. Fluid flow through catalyst filled tubes. *Chemical Engineering Science*, 52(8):1365–1376, 1997.
- [10] AE Blach, VS Hoa, CK Kwok, and AKW Ahmed. Rectangular pressure vessels of finite length. 1990.
- [11] Christopher M Bostwick, Russell W Barie, Jose Torres, Eric Besnard, and Daniel Cavender. Development and qualification of green propellant micropump for microsat and cubesat propulsion systems. In *AIAA Propulsion and Energy 2021 Forum*, page 3733, 2021.
- [12] Charles D Brown. *Spacecraft propulsion*. Aiaa, 1996.
- [13] Laura M Burke, Robert D Falck, and Melissa L McGuire. Interplanetary mission design handbook: Earth-to-mars mission opportunities 2026 to 2045. 2010.
- [14] Busek. Green monopropellant thruster bgt-x5. <https://www.busek.com/bgtx5>, 2021.
- [15] A Kayode Coker. *Fortran programs for chemical process design, analysis, and simulation*. Elsevier, 1995.
- [16] A Kayode Coker. *Ludwig's applied process design for chemical and petrochemical plants*. gulf professional publishing, 2014.
- [17] TU Delft. "flight and orbital mechanics" lecture slides. https://ocw.tudelft.nl/wp-content/uploads/AE2104-Orbital-Mechanics-Slides_11_12.pdf. Accessed: 25-11-2020.
- [18] Eleonora Dimas, Gary Holland, Robert Masse, Scott Dawley, Nicholas Brown, Robert Holmes, Donald Tzeng, Jaime Neidert, Greg Drake, Adam Brand, et al. Environmentally sustainable liquid gas generator formulations program. Technical report, Aerojet Rocketdyne Redmond United States, 2019.

- [19] Bradford ECAPS. Ecaps hpgp thrusters. <https://www.ecaps.space/products-overview-ecaps.php>. Accessed: 17-09-2021.
- [20] ESA. Mars express operations. https://www.esa.int/Enabling_Support/Operations/Mars_Express_operations. Accessed: 02-09-2021.
- [21] Mark Fokema and James Torkelson. Thermally stable catalyst and process for the decomposition of liquid propellants, August 9 2007. US Patent App. 11/457,985.
- [22] AJ Fortini, JR Babcock, and MJ Wright. Self-adjusting catalyst for propellant decomposition. *United States patent US 20080064913A1*, 2008.
- [23] Thim Franken, Ferran Valencia-Bel, Botchu Vara Siva Jyoti, and Barry Zandbergen. Design of a 1-n monopropellant thruster for testing of new hydrogen peroxide decomposition technologies. In *Aerospace Europe Conference*, 2020.
- [24] Dominic Freudenmann and Helmut K Ciezki. Adn and han-based monopropellants—a minireview on compatibility and chemical stability in aqueous media. *Propellants, Explosives, Pyrotechnics*, 44(9):1084–1089, 2019.
- [25] Amir S Gohardani, Johann Stanojev, Alain Demairé, Kjell Anflo, Mathias Persson, Niklas Wingborg, and Christer Nilsson. Green space propulsion: Opportunities and prospects. *Progress in Aerospace Sciences*, 71:128–149, 2014.
- [26] I Granero. Design and structural analysis of the propellant tank for a water resistojet. 2015.
- [27] Jiang-wen Guan, Guo-xiu Li, Hong-meng Li, Tao Zhang, Jun Chen, and Yong-jin Gu. Effect of catalytic bed porosity and mass flow rate on decomposition and combustion processes of a han-based monopropellant thruster. *Vacuum*, 194:110566, 2021.
- [28] Keiichi Hori, Toshiyuki Katsumi, Shujiro Sawai, Nobuyuki Azuma, Keigo Hatai, and Junichi Nakatsuka. Han-based green propellant, shp163—its r&d and test in space. *Propellants, Explosives, Pyrotechnics*, 44(9):1080–1083, 2019.
- [29] Flightworks Inc. M-series (magnetic drive gear pumps) models 2222-m04c49/c50/c51. [http://products.flightworksinc.com/Asset/Product%20Data%20Sheet%20\(2222-M04C49.C50.C51\).pdf](http://products.flightworksinc.com/Asset/Product%20Data%20Sheet%20(2222-M04C49.C50.C51).pdf), . Accessed on 28-11-2021.
- [30] Flightworks Inc. M-series (magnetic drive gear pumps) models 2222-m04x01/x03/x04. [https://products.flightworksinc.com/Asset/Product%20Data%20Sheet%20\(2212-M04X01.X03.X04\).pdf](https://products.flightworksinc.com/Asset/Product%20Data%20Sheet%20(2212-M04X01.X03.X04).pdf), . Accessed on 28-11-2021.
- [31] Shinjae Kang and Sejin Kwon. Preparation and performance evaluation of platinum barium hexaaluminate catalyst for green propellant hydroxylamine nitrate thrusters. *Materials*, 14(11):2828, 2021.
- [32] R-J Koopmans, JS Shrimpton, GT Roberts, and AJ Musker. Dependence of pellet shape and size on pressure drop in h₂ o₂ thrusters. *Journal of Propulsion and Power*, 30(3):775–789, 2014.
- [33] Kristina Lemmer. Propulsion for cubesats. *Acta Astronautica*, 134:231–243, 2017.
- [34] Stephen Longhurst. Delta-v requirements for interplanetary micro-spacecraft.
- [35] K Mani, Francesco Topputo, Angelo Cervone, et al. Chemical propulsion system design for a 16u interplanetary cubesat. In *69th International Astronautical Congress (IAC 2018)*, pages 1–15. International Astronautical Federation, IAF, 2018.
- [36] Karthik V Mani, Angelo Cervone, and Francesco Topputo. Combined chemical–electric propulsion for a stand-alone mars cubesat. *Journal of Spacecraft and Rockets*, 56(6):1816–1830, 2019.
- [37] Karthik Venkatesh Mani. Combined chemical–electric propulsion design and hybrid trajectories for stand-alone deep-space cubesats. 2020.

- [38] Karthik Venkatesh Mani, Alvaro Sanz Casado, Vittorio Franzese, Angelo Cervone, and Francesco Topputo. Systems design of mario: Stand-alone 16u cubesat from earth to mars. In *70th International Astronautical Congress, Washington DC*, pages 1–17, 2019.
- [39] R Masse, J Overly, M Allen, and R Spores. A new state-of-the-art in af-m315e thruster technologies. In *48th AIAA/ASME/SAE/ASEE Joint Propulsion Conference & Exhibit*, page 4335, 2012.
- [40] Robert Masse, May Allen, Ronald Spores, and Elizabeth A Driscoll. Af-m315e propulsion system advances and improvements. In *52nd AIAA/SAE/ASEE Joint Propulsion Conference*, page 4577, 2016.
- [41] Robert K Masse, Ronald A Spores, May Allen, Scott Kimbrel, and Chris McLean. Enabling high performance green propulsion for smallsats. 2015.
- [42] Robert K Masse, Ronald Spores, and May Allen. Af-m315e advanced green propulsion—gpim and beyond. In *AIAA Propulsion and Energy 2020 Forum*, page 3517, 2020.
- [43] Gary R Maxwell. Hydrazine. *Synthetic Nitrogen Products: A Practical Guide to the Products and Processes*, pages 337–346, 2004.
- [44] Alex McGee. Hot-fire testing of an af-m315e 1-newton thruster. 2017.
- [45] Christopher H McLean. Green propellant infusion mission: Program construct, technology development, and mission results. In *AIAA Propulsion and Energy 2020 Forum*, page 3810, 2020.
- [46] Michele Negri. Replacement of hydrazine: overview and first results of the h2020 project rheform. 2015.
- [47] Michele Negri, Marius Wilhelm, Christian Hendrich, Niklas Wingborg, Linus Gediminas, Leif Adelöw, Corentin Maleix, Pierre Chabernaud, Rachid Brahmi, Romain Beauchet, et al. New technologies for ammonium dinitramide based monopropellant thrusters—the project rheform. *Acta Astronautica*, 143:105–117, 2018.
- [48] AES Nousseir, A Pasini, and A Cervone. Modular impulsive green-monopropellant propulsion system for micro/nano satellites high-thrust orbital maneuvers (mimps-g). In *Proceedings of the International Astronautical Congress, CyberSpace Edition*, pages 12–14, 2020.
- [49] Ahmed ES Nousseir, Angelo Cervone, and Angelo Pasini. Review of state-of-the-art green monopropellants: For propulsion systems analysts and designers. *Aerospace*, 8(1):20, 2021.
- [50] Mathias Persson, Kjell Anflo, and Pete Friedhoff. Flight heritage of ammonium dinitramide (adn) based high performance green propulsion (hpgp) systems. *Propellants, Explosives, Pyrotechnics*, 44(9):1073–1079, 2019.
- [51] Staffan Persson, Sytze Veldman, and Per Bodin. Prisma—a formation flying project in implementation phase. *Acta Astronautica*, 65(9-10):1360–1374, 2009.
- [52] Jonathan Polaha. Internal resistive heating of catalyst bed for monopropellant catalyst, July 7 2011. US Patent App. 12/948,558.
- [53] Digital Solid State Propulsion. Dssp caps-3 data sheet. <https://static1.squarespace.com/static/59de9c9c18b27ddf3bac610a/t/5a3a9c5d9140b78b7a1768e9/1513790563886/Brochure+Inlet+CAPS+3+Website.pdf>, . Accessed: 21-09-2021.
- [54] Digital Solid State Propulsion. Cubesat delta-v motor data sheet. https://static1.squarespace.com/static/59de9c9c18b27ddf3bac610a/t/5b9989a98985830bc3e07838/1536788908562/CDM-1+Brochure+Metric_r2.pdf, . Accessed on 21-09-2021.
- [55] Industrial Solid Propulsion. Industrial solid propulsion product portfolio. http://www.specificimpulse.com/images/ISP_Portfolio.pdf, . Accessed: 21-09-2021.

- [56] Asad Rahman, Jitkai Chin, Feroz Kabir, and Yew Mun Hung. Characterization and thrust measurements from electrolytic decomposition of ammonium dinitramide (adn) based liquid monopropellant flp-103 in mems thrusters. *Chinese Journal of Chemical Engineering*, 26(9):1992–2002, 2018.
- [57] Aerojet Rocketdyne. *Modular Propulsion Systems Data Sheet*. Accessed: 2-12-2019.
- [58] Robert L Sackheim and Robert K Masse. Green propulsion advancement: challenging the maturity of monopropellant hydrazine. *Journal of Propulsion and Power*, 30(2):265–276, 2014.
- [59] Ronald A Spores. Green propellant infusion mission propulsion system development. In *49th AIAA/ASME/SAE/ASEE Joint Propulsion Conference*, page 3849. 2013.
- [60] Ronald A Spores. Gpim af-m315e propulsion system. In *51st AIAA/SAE/ASEE Joint Propulsion Conference*, page 3753, 2015.
- [61] George P Sutton and Oscar Biblarz. *Rocket propulsion elements*. John Wiley & Sons, 2016.
- [62] Swagelok. Swagelok stainless steel seamless tubing and tube support systems. <https://www.swagelok.com/downloads/webcatalogs/en/ms-01-181.pdf>. Accessed on 12-12-2021.
- [63] Hyperion Technologies. Pm200 data sheet. https://hyperiontechnologies.nl/wp-content/uploads/2019/11/HT_PM200.pdf, . Accessed: 14-10-2021.
- [64] Hyperion Technologies. Pm400 data sheet. https://hyperiontechnologies.nl/wp-content/uploads/2016/08/HT-PM400.10-V1.0_Flyer.pdf, . Accessed: 14-10-2021.
- [65] Jason Thrasher, Shae Williams, Phillip Takahashi, and John Sousa. Pulsed plasma thruster development using a novel han-based green electric monopropellant. In *52nd AIAA/SAE/ASEE Joint Propulsion Conference*, page 4846, 2016.
- [66] Francesco Topputo and Edward Belbruno. Earth–mars transfers with ballistic capture. *Celestial Mechanics and Dynamical Astronomy*, 121(4):329–346, 2015.
- [67] Michael Tsay, John Frongillo, Derek Lafko, and Jurg Zwahlen. Development status and 1u cubesat application of busek’s 0.5 n green monopropellant thruster. 2014.
- [68] Michael Tsay, Charlie Feng, Lenny Paritsky, Jurg Zwahlen, Derek Lafko, and Mike Robin. Complete em system development for busek’s 1u cubesat green propulsion module. In *52nd AIAA/SAE/ASEE Joint Propulsion Conference*, page 4905, 2016.
- [69] Akshay Reddy Tummala and Atri Dutta. An overview of cube-satellite propulsion technologies and trends. *Aerospace*, 4(4):58, 2017.
- [70] Tethers Unlimited. Hydros data sheet. <https://www.tethers.com/wp-content/uploads/2019/09/2019-HYDROS.pdf>. Accessed: 14-10-2021.
- [71] HIKARU Uramachi, DAIJIRO Shiraiwa, TSUTOMU Takai, NOBUHIKO Tanaka, TAKAO Kaneko, and KATSUMI Furukawa. Green propulsion systems for satellites—development of thrusters and propulsion systems using low-toxicity propellants. *Mitsubishi Heavy Ind. Tech. Rev*, 56:1–7, 2019.
- [72] VACCO. Vacco liquid propellant thrusters catalog. https://www.vacco.com/images/uploads/pdfs/liquid_propellant_thrusters.pdf, . Accessed on 12-12-2021.
- [73] VACCO. Vacco filtration catalog. https://www.vacco.com/images/uploads/pdfs/VACCO_Filtration_Catalog_042121_FINAL_with_bookmarks_web.pdf, . Accessed on 12-12-2021.
- [74] VACCO. Vacco valves catalog. https://www.vacco.com/images/uploads/pdfs/latch_valves_high_pressure.pdf, . Accessed on 12-12-2021.

- [75] A Safety Valves. Asme boiler and pressure vessel code: Section viii, ". *Pressure Vessels, " construction.*
- [76] Alejandro Andre Vazquez. Development of an iridium-ceramic substrate catalyst bed for the decomposition of ionic green liquid monopropellants. 2019.
- [77] Karel F Wakker. Fundamentals of astrodynamics. 2015.
- [78] N Wingborg, M Johansson, and L Bodin. Initial development of a laboratory rocket thruster for adn-based liquid monopropellants—foi-r-2123—se. *Weapons and Protection—FOI: Tumba, Sweden*, 2006.
- [79] Niklas Wingborg, C Eldsäter, and Henrik Skifs. Formulation and characterization of adn-based liquid monopropellants. In *ESA Special Publication*, volume 557, 2004.
- [80] Niklas Wingborg, Anders Larsson, Mattias Elfsberg, and Patrik Appelgren. Characterization and ignition of adn-based liquid monopropellants. In *41st AIAA/ASME/SAE/ASEE Joint Propulsion Conference & Exhibit*, page 4468, 2005.
- [81] Malte Wurdak, Friedolin Strauss, Lukas Werling, Helmut K Ciezki, Dirk Greuel, Robert Lechler, Niklas Wingborg, Dov Hasan, and Carsten Scharlemann. Determination of fluid properties of the green propellant flp-106 and related material and component testing with regard to applications in space missions. In *Space Propulsion Conference, Bordeaux, France*, 2012.
- [82] B.T.C. Zandbergen. *Thermal Rocket Propulsion Reader*. AE4S01, version 2.06. TU Delft, 21 August 2017. ISBN 9780198520115.
- [83] Kevin Zondervan, Jerry Fuller, Darren Rowen, Brian Hardy, Chris Kobel, Shin-Hsing Chen, Phillip Morrison, Timothy Smith, and Alison Kremer. Cubesat solid rocket motor propulsion systems providing delta-vs greater than 500 m/s. 2014.



Earth escape single variable simulations

As a first approach to the problem, the burn time t_b variable has been kept fixed, while the values of thrust have been varied between a range of possible choices: in this way the problem is solved by only varying the thrust, and showing how different thrust levels affect the Δv to be budgeted for Earth escape. The previously strategies for choosing when to start a new manoeuvre will be implemented to find the optimal true anomaly at which to activate the propulsion system. If done correctly, the Δv requirement shall approach the ideal Δv budget calculated in Equation (3.12).

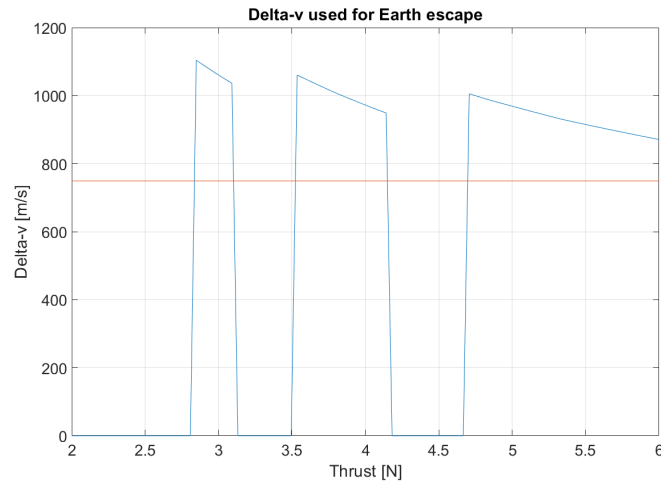
One result sample is shown below: the initial mass of the satellite, the specific impulse of the propellant and the burn time are kept fixed, and the thrust range is varied between 2 and 6 N. The values of the constants are fixed as follows:

- $M_0 = 25 \text{ kg}$
- $I_{sp} = 240 \text{ s}$
- $t_b = 600 \text{ s}$

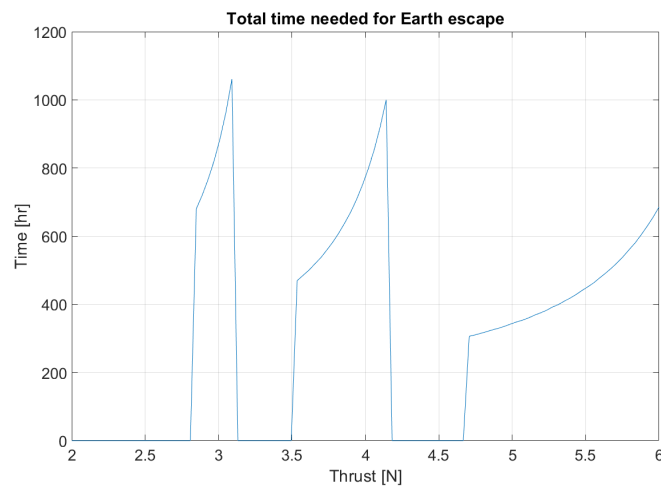
Figure A.1 (a) shows the Δv budget for the Earth escape, given the initial constants: the blue line represent the values of thrust at which the Earth escape is successful, while the ideal value of the Δv budget calculated in Equation (3.12) is shown with an orange line across the graph. A few insights on the problem are given from this first graph:

- Not all values of thrust allow for the Earth escape procedure, which is considered successful if the constraints are satisfied, both related to the orbiting time around Earth, the maximum distance from Earth and the final energy reached by the hyperbolic orbit once at the edges of the sphere of influence. The thrust values at which the Earth escape is not successful, given the fixed input of $t_b = 600 \text{ s}$, are not shown and for both the graphs in Figure A.1 the respective y-value is set to 0.
- The thrust values for which Earth escape is not achieved separate the Δv budget line into different sections. It can be seen that each part of the graph is characterized by a different number of manoeuvres required to bring the energy of the orbit to a positive value: in fact, the first region of successful thrust levels around 3 N is characterized by 4 different manoeuvres around the perigee to increase the energy of the orbit, with a fifth one to make the orbit hyperbolic. The second and third region, below and after 4.5 N, are characterized by 3 and 2 orbit raisings, respectively, plus an additional one to make the orbit hyperbolic. It can also be noted that for each region of successful escape, the function is monotonically decreasing, which means that for a fixed wanted number of sequences around the perigee, it is more convenient to move towards the right edge of the function, which locally minimizes the Δv budget.
- The ideal value calculated in Equation (3.12) is not reached by any value of thrust used in the simulation range: this is due to the fact that the simulation procedure is not based on ideal calculation between orbits but integrates the equation of motion shown in Equation (3.13). While the gravity losses are small when orbiting around Earth since the satellite is manoeuvring near

the perigee in a sort of symmetric motion about the x-axis of the orbit, they become much more relevant in the second phase of Earth escape: due to the constraint of Δt_b , the satellite needs to wait before starting the propulsion system again. This causes the satellite to be farther away from the Earth when a new manoeuvre is executed along the hyperbolic orbit, having a lower impact on the velocity of the satellite when a boost is performed, therefore needing more Δv and propellant mass.



(a) Δv budget needed for the Earth escape



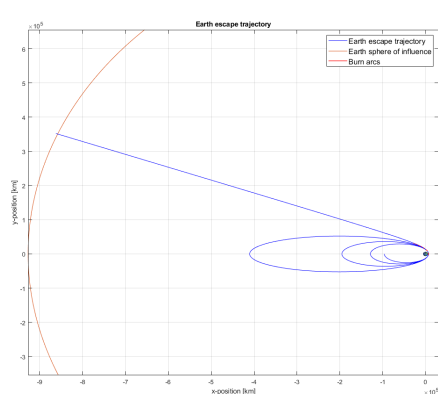
(b) Time needed to reach the sphere of influence of Earth

Figure A.1: Results of Earth escape simulation using the constant input values of $M_0 = 25$ kg, $I_{sp} = 240$ s, $t_b = 600$ s

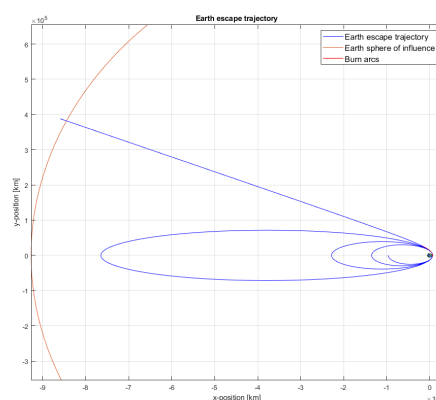
Figure A.1 (b) shows the time, in hours, required to achieve Earth escape from the parking SSGTO which is described by the Keplerian parameters in Table 2.1, starting from the standard true anomaly $\theta = \pi$ rad. From this graph, it can be noted that:

- The values for which the Earth escape is not successful have been put to 0, dividing once again the results into three different regions, each one representative of a different number of orbit raising manoeuvres before reaching the hyperbolic orbit, as described previously.
- In contrast to the previous graph, each region of successful Earth escape is characterized by a monotonically increasing line, which means that given a fixed number of orbit raising, it is more time-convenient to be on the left edge of the graph. This shows that going for a lower value of Δv budget by having a higher value of thrust of the propulsion system, will increase the time needed to escape Earth's sphere of influence.

The most striking difference from the graphs shown in Figure A.1 is the different behaviour of the Δv budget and the total time needed to escape Earth's sphere of influence: for a given region, the first is monotonically increasing and the second is monotonically decreasing. This is caused by the fact that each region, as stated previously, is characterized by a different number of orbit raising manoeuvres around Earth, becoming lower as thrust increases. For the thrust values at the left and right edge of a solution region, the number of orbit raising manoeuvres around Earth is the same, but what makes a crucial difference is the possibility of expelling more propellant since a higher level of thrust is available. This means that the leftmost solution of one region is characterized by a series of orbit raises in which the last one before the hyperbolic transition is far from Earth's sphere of influence, while the orbit raising procedure for the rightmost solution will be characterized by having the final orbit of raising strategy much closer to the sphere of influence of Earth. Figure A.2 displays the two different trajectories that the satellite will follow for two different thrust levels of the same solution region, respectively 3.6 and 4.1 N.



(a) Thrust level of 3.6 N

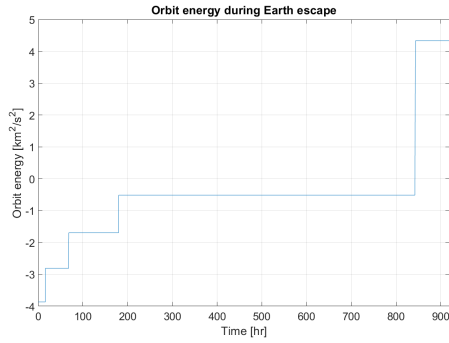


(b) Thrust level of 4.1 N

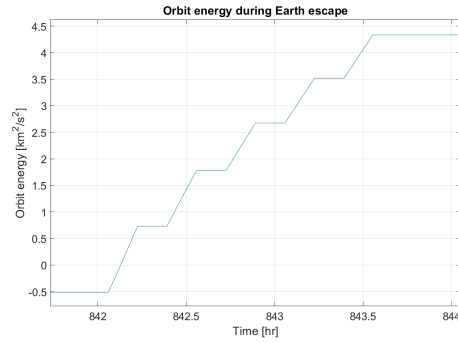
Figure A.2: Earth escape trajectories using the constant input values of $M_0 = 25$ kg, $I_{sp} = 240$ s, $t_b = 600$ s

In Figure A.2 (a) the satellite flies towards Earth for the last time with an high enough energy of the orbit that will allow the next manoeuvre to enter the hyperbolic escape phase, which means that escape velocity has been reached by a small amount and the rest of the impulse shall be given by the propulsion system in this second phase, which is less efficient than the first one since the satellite will be moving farther away from Earth. On the other hand, Figure A.2 (b) shows that for an higher level of thrust (still in the same region of solutions), the last orbit after the raisings is much closer to the sphere of influence, which means that the satellite would need only a small boost to be able to start the hyperbolic phase of the escape. When coming near Earth, a full manoeuvre lasting t_b is performed, which is much more efficient than the previously described one, since it will be made around the perigee, and not when moving away from it.

This behaviour shows how it is much more important to be able to perform manoeuvres around Earth, if possible, because the effects of gravity losses will be much higher when moving farther away from Earth: the hyperbolic phase of the Earth escape is the most critical of the two, since the satellite needs to reach an high enough orbit specific energy (calculated in Equation (3.9)), and to be able to make sure that the propulsion system works in the most efficient way possible it is needed to manoeuvre as much as possible when in the first phase of orbiting around Earth. There will be surely need to perform later manoeuvres during the second phase since the parameters of a propulsion system for CubeSats do not allow for a faster Earth escape, but the lesson learned from this study is that the propulsion system parameters and the burn time of each manoeuvre must be carefully designed to achieve Earth escape in the most efficient way, operating as much as possible around Earth with a closed orbit.



(a) Orbit energy during Earth escape



(b) Zoomed-in values of orbit energy when starting the second phase of Earth escape

Figure A.3: Orbit energy variation during Earth escape manoeuvres, using the the constant input values of $M_0 = 25$ kg, $I_{sp} = 240$ s, $t_b = 600$ s

As can be seen from Figure A.3, the value of the orbit energy increases together with each manoeuvre executed by the propulsion system: in Figure A.3 (a), it is highlighted how the energy increases from negative values to higher ones, corresponding to the first phase of orbit raising. The long delay between the last manoeuvre executed in this strategy is due to the high eccentricity of the last orbit around Earth, which has been showed in Figure A.2 (b). Afterwards, the energy seems to steeply increase from a negative value to a positive value, characteristic of hyperbolic orbits. Figure A.3 (b) shows how this effect is caused not by a single manoeuvre, but due to a sequence of manoeuvres which are delayed from each other by the time-delay value of Δt_b , as designed. It can also be noted in this last picture that the energy value increases by lower values each time a manoeuvre is performed: this is because the first manoeuvres in the second phase of Earth escape are made closer to the Earth, while the following others are performed later in the space of Earth influence and affect less the energy increase of the orbit.

B

Mars stabilization budget estimation

This appendix is reserved to showcase the ideal Δv budget estimation for the Mars stabilization phase of the mission.

Since the peri-apsis of the hyperbolic orbit followed by the satellite when it enters the Martian sphere of influence is fixed by its "infinite velocity" value, one value for the initial eccentricity or peri-apsis of the orbit needs to be fixed. It has been chosen to fix the value for the peri-apsis, assuming that its value will almost remain constant during the braking phase compared to the eccentricity value of the orbit, that will diminish during each braking manoeuvre. The initial orbit eccentricity can be found with:

$$e_M^{(i)} = 1 - \frac{r_{pM}}{a_M^{(i)}} \quad (\text{B.1})$$

where the apex (i) stands for initial conditions. Assuming an impulsive manoeuvre around the peri-apsis of the orbit, the peri-apsis distance itself will not vary considerably and can be kept constant and equal to the peri-apsis of the initial hyperbolic orbit. Depending on the final orbit eccentricity target $e_M^{(f)}$, the semi-major axis of the target orbit is found with:

$$a_M^{(f)} = \frac{r_{pM}}{1 - e_M^{(f)}} \quad (\text{B.2})$$

where the apex (f) stands for final orbit conditions. Once all of the parameters of the initial hyperbolic orbit and final target orbit are set, the velocities at the perigee can easily be calculated and the ideal Δv is obtained with the following relations:

$$v_{perM}^{(f)} = \sqrt{\frac{\mu_m [1 + e_M^{(f)}]}{a_M^{(f)} [1 - e_M^{(f)}]}} \quad (\text{B.3})$$

to obtain the perigee velocity at the final target orbit, where μ_m is the gravitational parameter of Mars. The velocity at the peri-apsis of the initial hyperbolic orbit is found with:

$$v_{pM}^{(i)} = \sqrt{v_{escM}^2 + v_{\infty M}^2} \quad (\text{B.4})$$

$$v_{escM} = \sqrt{2 \frac{\mu_M}{r_{pM}}} \quad (\text{B.5})$$

The ideal Δv needed to brake at the peri-apsis in order to transform the hyperbolic initial orbit to an elliptical orbit of arbitrary eccentricity $e_M^{(f)}$ is:

$$\Delta v_M = v_{pM}^{(i)} - v_{perM}^{(f)} \quad (\text{B.6})$$

All of the previous relations can be used in order to estimate the ideal Δv needed to brake from an hyperbolic orbit using a single instantaneous braking manoeuvre around the peri-apsis of the orbit.

Since the semi-major axis of the initial orbit is fixed, these Δv budget values will depend on the initial hyperbolic orbit peri-apsis r_{pM} and on the final orbit eccentricity $e_M^{(f)}$. The values of ideal Δv to stabilize around Mars, with starting conditions defined by the infinite velocity $v_{\infty M}$ are shown in the figure below, by varying the chosen initial peri-apsis of the initial hyperbolic orbit. Furthermore, the results are shown for different final eccentricities of the target orbit $e_M^{(f)}$ in Figure B.1.

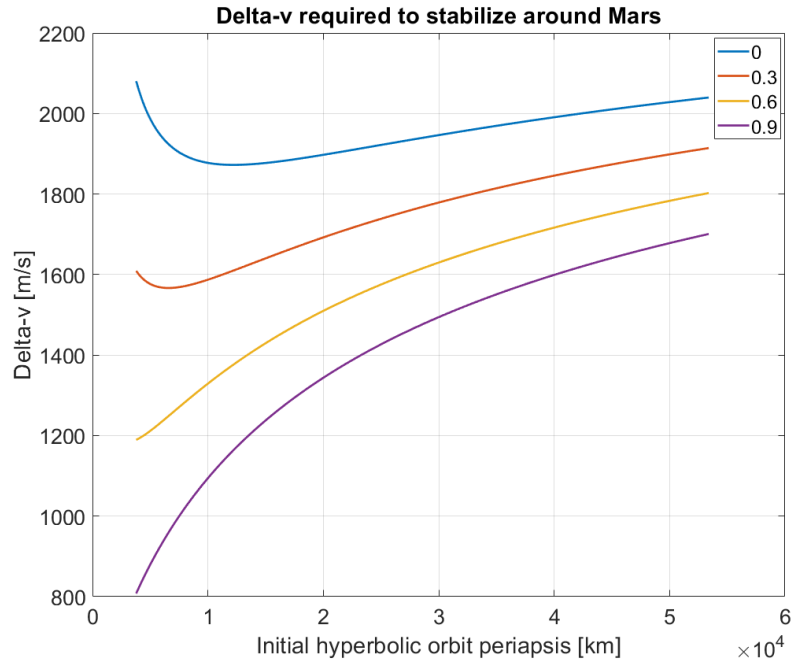
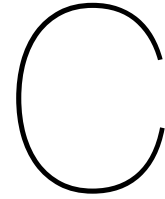


Figure B.1: Ideal Δv budget required to stabilize around Mars, entering the sphere of influence with the hyperbolic orbit parameters defined in Chapter 3.4. On the x-axis the initial periapsis of the orbit is varied. Values are shown for final target orbit eccentricities of 0, 0.3, 0.6, 0.9.

Figure B.1 shows how the Δv budget varies for different final eccentricities of the orbit: it is clear that for higher eccentricity values of the final orbit, the total budget required is lower, since the orbit has to vary its energy until it changes its shape from open to closed in all of the cases but then an additional amount is needed to bring the shape of the orbit closer to a circular one, which corresponds to the eccentricity value of 0. Furthermore, it can be seen how a different initial periapsis of the hyperbolic orbit affects the results, since for the same value of final orbit eccentricity, the Δv budget varies too. For the case of this mission, it has been estimated that even an high eccentric orbit could be enough to satisfy the mission requirements, therefore the case of final orbit eccentricity close to 0.9 is investigated. Furthermore, the results obtained for the case where the eccentricity value is 0.9 match the ones obtained in the analysis performed in [66], where a comparison between the Δv budget required for an Hohmann transfer is compared with the ballistic capture method.

Table B.1: Output Δv results for Mars capture [km/s], used for validation with [66], by using as input values: $M_0 = 30$ kg, $I_{sp} = 240$ s, $t_b = 20$ s and $T = 500$ N. The infinite velocity $v_{\infty M}$ values at Mars for the H1-H4 cases are: 3.388 (H1), 2.090 (H2), 3.163 (H3), 1.881 (H4) [km/s]

Periapsis distance [$10^5 km$]	0.05	0.1	0.2	0.3	0.4	0.5	0.75	1	1.25	1.5	1.75	2	2.25	2.5
H1	1.3018	1.6233	1.9460	2.1346	2.2679	2.3587	2.5200	2.6181	2.6927	2.7453	2.7786	2.8104	2.8454	2.8698
H2	0.5889	0.7486	0.9282	1.0382	1.1260	1.1930	1.3018	1.3904	1.4479	1.4868	1.5247	1.5626	1.5825	1.6030
H3	1.1811	1.4646	1.7717	1.9424	2.0647	2.1501	2.3010	2.3902	2.4586	2.5248	2.5705	2.5982	2.6251	2.6577
H4	0.4935	0.6151	0.7781	0.8826	0.9668	1.0102	1.1356	1.2012	1.2472	1.2914	1.3302	1.3654	1.3827	1.4008



Candidate pumps data-sheet performance graph interpolation

This Appendix is reserved to showcase the procedure undergone to recreate the mathematical equations of the data-sheet of the pump candidates crucial for the pressurization system of the mission, which are pump models 2212-M04C49/C50/C51 and 2212-M04X01/X03/X04 from Flightworks, Inc. The data-sheets of both pumps provide the operating values and lines for minimum, nominal and maximum speed at different fluid viscosities: 1, 2, 16 and 70 cP. The propellant chosen in the previous chapter is AF-M315E (ASCENT) characterized by a fluid viscosity of 25 cP: since the data-sheet graphs do not provide the operating lines of the pumps at this viscosity, the latter have been interpolated between the operating fluid viscosity range in order to estimate the behaviour at the fluid viscosity of interest for the mission.

Since each pump shows a different maximum pressure differential level depending on the viscosity, while the maximum allowable flow rate stays constant, the former needs to be interpolated in order to be able to generate the graphs for each viscosity in the range between 1 to 70 cP.

Table C.1: Pump models maximum pressure differential for four different fluid viscosities, in psi.

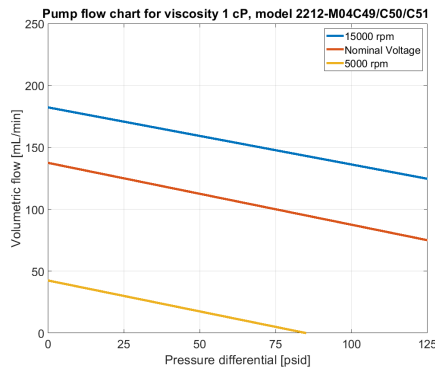
Pump model	ΔP_{max} @1 cP	ΔP_{max} @2 cP	ΔP_{max} @16 cP	ΔP_{max} @70 cP
M04C49/C50/C51	125	250	450	300
M04X01/X03/X04	125	250	440	325

Interpolation of data in Table C.1 through the MATLAB function "pchip" provides the trends shown in Figure 5.4.

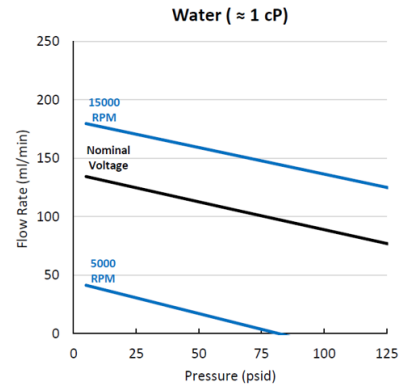
Once the maximum pressure differential for each viscosity value is known, the three lines corresponding to the maximum, nominal and minimum speed of the pump can be extrapolated and an interpolation can be performed such that the performance for every different viscosity is obtained. Each line can be expressed as follows:

$$Flowrate[mL/min] = m \cdot Pressure[psid] + q$$

It takes only two points on each line to fully constrain the values of the slope m and offset q . This process has been performed for each operating line in the four different graphs available at 1, 2, 16 and 70 cP. The following are the representations of the results obtained with the approximation of pump model 2212-M04C49/C50/C51 operating lines, shown in Figure C.1, Figure C.2, Figure C.3 and Figure C.4.

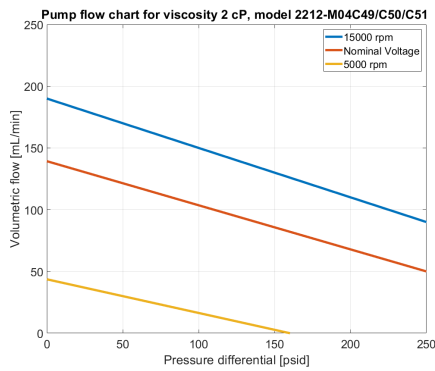


(a) Mathematically reproduced graph

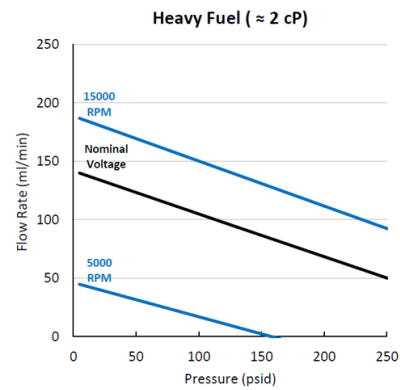


(b) Data-sheet graph

Figure C.1: Extrapolated and real operating graph of pump 2212-M04C49/C50/C51 for a fluid of viscosity 1 cP [29]

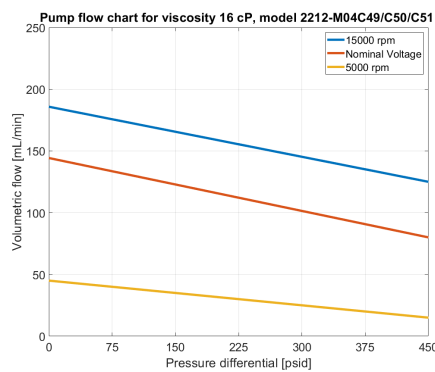


(a) Mathematically reproduced graph

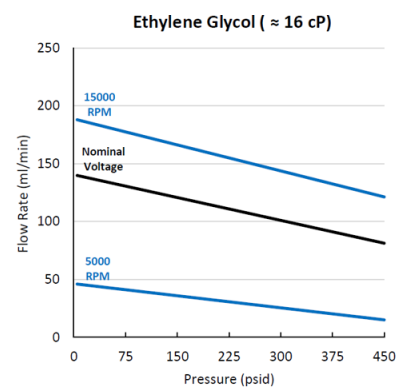


(b) Data-sheet graph

Figure C.2: Extrapolated and real operating graph of pump 2212-M04C49/C50/C51 for a fluid of viscosity 2 cP [29]

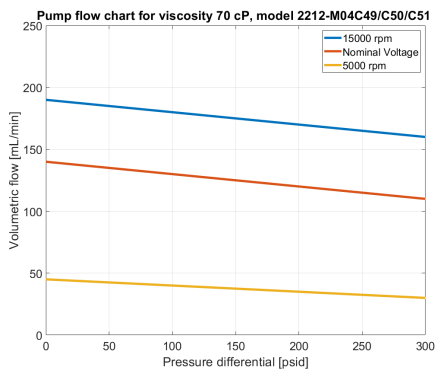


(a) Mathematically reproduced graph

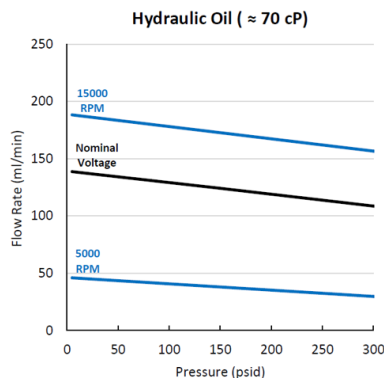


(b) Data-sheet graph

Figure C.3: Extrapolated and real operating graph of pump 2212-M04C49/C50/C51 for a fluid of viscosity 1 cP [29]



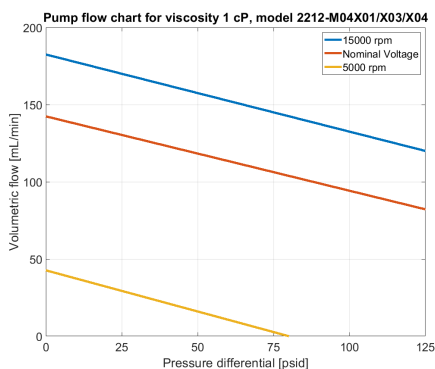
(a) Mathematically reproduced graph



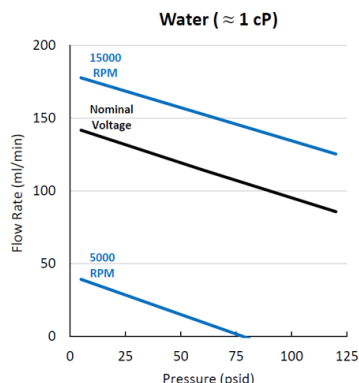
(b) Data-sheet graph

Figure C.4: Extrapolated and real operating graph of pump 2212-M04C49/C50/C51 for a fluid of viscosity 1 cP [29]

The same process is repeated for pump model 2212-M04X01/X03/X04: the comparison is shown in Figure C.5, Figure C.6, Figure C.7 and Figure C.8.

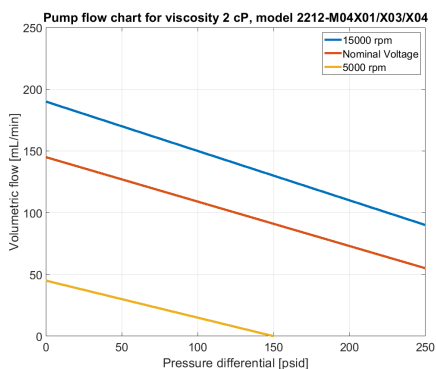


(a) Mathematically reproduced graph

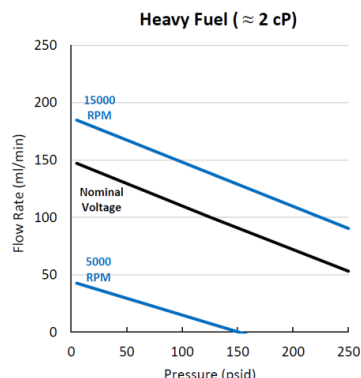


(b) Data-sheet graph

Figure C.5: Extrapolated and real operating graph of pump 2212-M04X01/X03/X04 for a fluid of viscosity 1 cP [30]

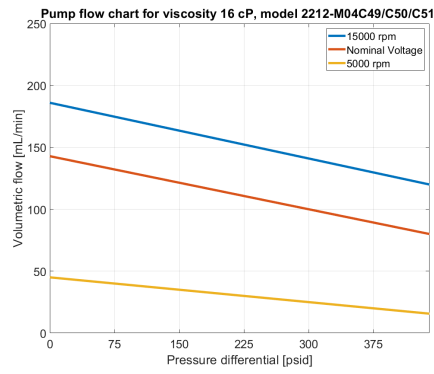


(a) Mathematically reproduced graph

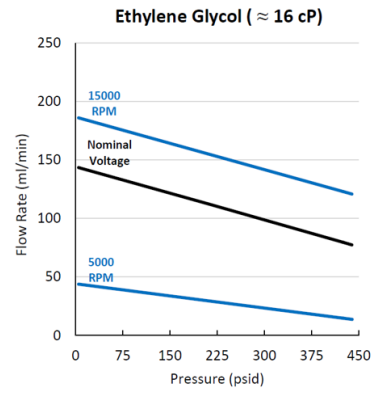


(b) Data-sheet graph

Figure C.6: Extrapolated and real operating graph of pump 2212-M04X01/X03/X04 for a fluid of viscosity 2 cP [30]

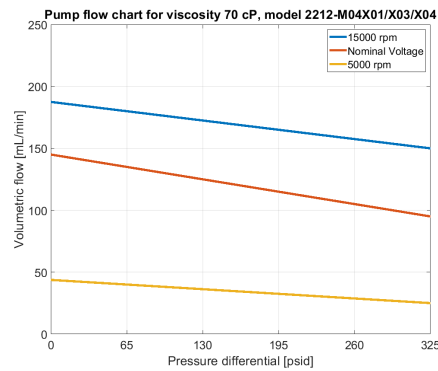


(a) Mathematically reproduced graph

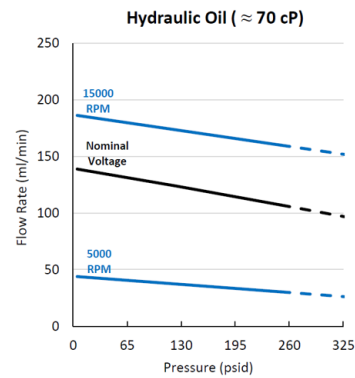


(b) Data-sheet graph

Figure C.7: Extrapolated and real operating graph of pump 2212-M04X01/X03/X04 for a fluid of viscosity 16 cP [30]



(a) Mathematically reproduced graph



(b) Data-sheet graph

Figure C.8: Extrapolated and real operating graph of pump 2212-M04X01/X03/X04 for a fluid of viscosity 70 cP [30]

Once each of the lines has been approximated, each of the values of slope m and offset q are interpolated among the viscosity range in order to estimate the performance of each pump at the fluid viscosity value of interest, which is 25 cP for AF-M315E (ASCENT). The results are shown in Figure 5.5.